THE UNIVERSITY OF TEXAS AT AUSTIN
CENTER FOR TRANSPORTATION RESEARCH

TECHNICAL REPORT 0-7113-1
TxDOT PROJECT NUMBER 0-7113

The Service and Ultimate Behavior of Bent-to-Column Joints in TxDOT Substructures

Hwa-Ching Wang
Terence J. Briscoe
Pavel Kraus
Juan E. Castano
Seda Mursel
Yongjae Yu
Hansol Jang
Elias Saqan
Jarrod Zaborac
Zachary D. Webb
Anca C. Ferche
Oguzhan Bayrak

July 2025

Published February 2026

https://library.ctr.utexas.edu/ctr-publications/0-7113-1.pdf

Technical Report Documentation Page

1. Report No. FHWA/TX-26/0-7113-1	2. Government Accession No.	3. Recipient's Catalog No.
4. Title and Subtitle The Service and Ultimate Behavior of Bent-to-Column Joints in TxDOT Substructures		5. Report Date Submitted: July 2025 6. Performing Organization Code
7. Author(s) Hwa-Ching Wang, Terence J. Briscoe, Pavel Kraus, Juan E. Castano, Seda Mursel, Yongjae Yu, Hansol Jang, Elias Saqan, Jarrod Zaborac, Zachary D. Webb, Anca C. Ferche, Oguzhan Bayrak		8. Performing Organization Report No. 0-7113-1
9. Performing Organization Name and Address Center for Transportation Research The University of Texas at Austin 3925 W. Braker Lane, 4th Floor Austin, TX 78759		10. Work Unit No. (TRAIS) 11. Contract or Grant No. 0-7113
12. Sponsoring Agency Name and Address Texas Department of Transportation Research and Technology Implementation Division 125 E. 11th Street Austin, TX 78701		13. Type of Report and Period Covered Technical Report September 2021 – July 2025 14. Sponsoring Agency Code

15. Supplementary Notes
Project performed in cooperation with the Texas Department of Transportation and the Federal Highway Administration.

16. Abstract

This research examined the service and ultimate behavior of bridge bent-to-column connections in Texas Department of Transportation (TxDOT) substructures to develop design recommendations for improved structural resilience under extreme events, including flooding, vehicular collision, and loss of column. A three-phase approach was employed. First, analytical studies, including plastic collapse mechanism and nonlinear dynamic analyses, were conducted on typical multi-column bents to quantify the vulnerability of poorly detailed connections and establish the foundation for a capacity-based plastic design approach and an analysis procedure for loss-of-column scenarios. Second, a large-scale experimental program tested thirteen full-scale bent-to-column specimens under lateral loads simulating vehicular collisions. The program explored various reinforcement anchorage types (straight, hooked, and headed bars) and levels of joint confinement. Third, the test results were used to validate nonlinear finite element models that further explained the observed behavior.

Experimental findings revealed that TxDOT's standard connection details, though designed as pinned, are capable of moment transfer without shear failure; the column achieved their nominal moment capacity with reinforcement yielding at the face, exhibiting ductile behavior. Enhanced anchorage (hooked or headed bars) and transverse joint confinement (hoops) were shown to improve moment capacity, post-yield performance, and damage control under service loads. The study also found that current code provisions for development length are conservative for these applications. Finite element analyses accurately captured the response and identified the embedment lengths required to develop reinforcement yield strength.

This research concludes that adopting a capacity-based plastic design philosophy is essential for resilient multi-column bents and connections subjected to extreme events. The findings offer actionable design guidance, including step-by-step procedures and a worked example, enabling bridge engineers to design safer, more robust substructures in future TxDOT projects.

17. Key Words Reinforced Concrete, Bridge Substructures, Bent-to-Column Joints, Capacity Design, Plastic Hinge, Extreme Events, Vehicular Collision, Loss of Column, Development Length, Joint Confinement	18. Distribution Statement No restrictions. This document is available to the public through the National Technical Information Service, Alexandria, Virginia 22312; www.ntis.gov.

19. Security Classif. (of report) Unclassified	20. Security Classif. (of this page) Unclassified	21. No. of pages 168	22. Price

Form DOT F 1700.7 (8-72) Reproduction of completed page authorized

THE UNIVERSITY OF TEXAS AT AUSTIN
CENTER FOR TRANSPORTATION RESEARCH

The Service and Ultimate Behavior of Bent-to-Column Joints in TxDOT Substructures

Hwa-Ching Wang, Ph. D., PE
Terence J. Briscoe
Juan E. Castano
Pavel Kraus
Seda Mursel
Yongjae Yu, Ph. D.
Jarrod Zaborac, Ph. D.
Zachary D. Webb
Hansol Jang, Ph. D.
Elias Saqan Ph. D., PE
Anca Ferche, Ph. D.
Oguzhan Bayrak Ph. D., PE

CTR Technical Report:	0-7113-1
Report Date:	Submitted: July 2025
Project:	0-7113
Project Title:	Investigate the strength of struts crossing cold joints
Sponsoring Agency:	Texas Department of Transportation
Performing Agency:	Center for Transportation Research at The University of Texas at Austin

Project performed in cooperation with the Texas Department of Transportation and the Federal Highway Administration.
Center for Transportation Research
The University of Texas at Austin
3925 W. Braker Lane, 4th floor
Austin, TX 78759

http://ctr.utexas.edu/

Disclaimers

Author's Disclaimer: The contents of this report reflect the views of the authors, who are responsible for the facts and the accuracy of the data presented herein. The contents do not necessarily reflect the official view or policies of the Federal Highway Administration or the Texas Department of Transportation (TxDOT). This report does not constitute a standard, specification, or regulation.

Patent Disclaimer: There was no invention or discovery conceived or first actually reduced to practice in the course of or under this contract, including any art, method, process, machine manufacture, design or composition of matter, or any new useful improvement thereof, or any variety of plant, which is or may be patentable under the patent laws of the United States of America or any foreign country.

Engineering Disclaimer

NOT INTENDED FOR CONSTRUCTION, BIDDING, OR PERMIT PURPOSES.

Project Engineer: Oguzhan Bayrak
Professional Engineer License State and Number: Texas No. 106598
P.E. Designation: Research Supervisor

Acknowledgments

The authors express appreciation to Texas Department of Transportation (TxDOT) for providing funds and supports to conduct this research study. The contributions of the project manager Katelyn Kasberg (RTI Division) and other members of the Project Monitoring Committee – Anthony Felderhoff, Courtney Holle, Gregory Sanders, Laura Ortiz, Sandip Tamrakar, and Seth Cole – facilitated great improvements to the outcome of this project.

Table of Contents

List of Tables

List of Figures

Chapter 1. Introduction

Bridge substructures in Texas commonly rely on bent-to-column joints to transfer loads safely and effectively from superstructures to supporting columns. Ensuring the reliable performance of these joints is essential for maintaining the integrity and serviceability of transportation infrastructure. This chapter introduces the context, goals, scope, and organization of the research project 0-7113 focused on evaluating and improving the service and ultimate behavior of TxDOT bent-to-column joints.

1.1. Overview

In multi-column bents, the bent-to-column joints serve as critical structural components that transmit forces from the superstructure into the supporting columns. Historically, TxDOT standard designs assume these connections primarily carry axial loads with low eccentricities, enabling the use of relatively simple joint details. However, evidence from extreme loading events—including vehicular and vessel collisions, flooding, and loss of a support—has demonstrated that these assumptions may not always be conservative. Under such conditions, bent-to-column joints can experience significant moment and shear demands that exceed their original design capacity. Failure modes such as joint shear failure and inadequate anchorage of column longitudinal reinforcement can compromise overall structural performance. This research addresses these challenges by systematically evaluating the behavior of bent-to-column connections under service and ultimate load levels, and proposing design improvements tailored to extreme event demands.

1.2. Project Objective

The primary objective of this research project is to evaluate the service-level and ultimate performance of bent-to-column joints in TxDOT bridge substructures and to develop practical, mechanically-based detailing recommendations that improve their resilience under extreme events. The project aims to ensure that joint failures are prevented before the yielding of adjacent members, promoting ductile behavior and consistent with capacity-based plastic design principles. Recommendations developed through this study are intended to support TxDOT's efforts to update and enhance standard joint details for improved serviceability, safety, and lifesaving under extreme events.

1.3. Project Scope

To fulfill this objective, the research included the following key tasks:

- Conduct a comprehensive literature review of extreme loading demands, existing design standards, joint detailing strategies, and retrofitting methods applicable to bent-to-column connections.
- Analyze confinement and anchorage requirements for TxDOT bent-to-column joints through detailed design evaluation and analytical modeling.
- Develop structural models of multi-column bents subjected to extreme loading scenarios, including flooding, vehicular impacts, severe scour, and support loss.
- Design and fabricate large-scale test specimens with representative joint details for both in-plane and out-of-plane loading directions.
- Perform monotonic lateral loading tests to evaluate joint behavior, including load-displacement response, cracking patterns, reinforcement strain development, and anchorage performance.
- Analyze experimental results to identify key factors affecting joint performance and propose refined detailing strategies aimed at ensuring ductile behavior and avoiding premature failures.
- Develop design recommendations for bent-to-column connections, especially under extreme events.

1.4. Organization

This report is structured as follows:

Chapter 2 reviews relevant literature on extreme events, strut-and-tie modeling for joint design, anchorage methods, and existing detailing practices, identifying gaps and design challenges.

Chapter 3 summarizes the results of structural analyses on multi-column bents under various extreme events and establishes the foundation of capacity-based plastic design concept and static/dynamic approaches.

Chapter 4 presents a large-scale experimental program, including test setups, instrumentation, loading procedures, experimental results for both in-plane and out-of-plane directions, and supporting finite element analyses.

Chapter 5 provides design guidelines for bent-to-column joints, developed based on the results and findings from Chapters 3 and 4.

Chapter 6 offers an overall summary and conclusions of the research, including recommendations for future work and practical implementation.

Chapter 7 summarizes the value of research.

Chapter 2. Literature Review

In Texas, column bents are widely used as substructures of bridges. As shown in Figure 2-1, a column bent consists of a bent cap, one or multiple columns, and bent-to-column joints. The bent-to-column joints play an important role as they transfer the loads from the superstructure to the columns. From a design viewpoint, a bent-to-column joint should not fail before its adjoining members exhaust their ultimate capacity. In other words, failure modes related to bent-to-column joints including joint shear failure and bond failure of column bars should be avoided. It is preferred to have a flexural failure at the end of the column instead of a failure in the joint in order to guarantee ductility.

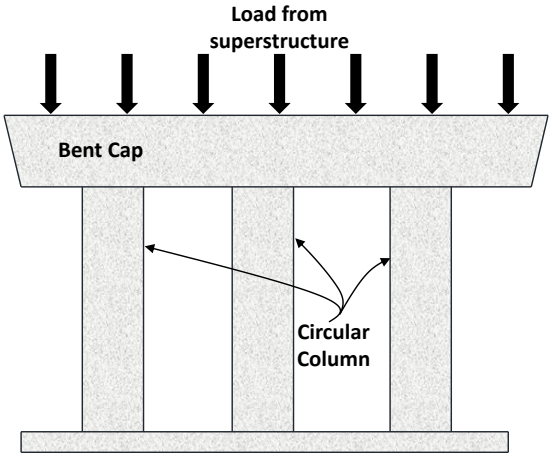

Figure 2-1. Example of multi-column bent

Joint failure modes and behavior have been under-studied in Texas because the column bents are rarely designed to carry high moment demands, primarily due to the fact that the columns supporting a bent cap are subjected to axial loads with low eccentricities. For example, the TxDOT bent cap analysis program CAP 18 (1975) assumes that the bent cap is a continuous beam supported by knife-edge supports. Therefore, moments are not transferred from the bent cap to the columns. With this assumption, the bent-to-column joints are not critical, and therefore, TxDOT has long used simple details of bent-to-column joints for bent caps with multiple columns.

In recent years, however, with the occurrence of various extreme loading events, it has become apparent that such simple details provided in the current TxDOT standard designs may be insufficient. Multi-column bents can potentially be exposed to floods, vehicular collisions, and loss of support. In these situations, bent-to-column joints are no longer transferring only axial loads, but rather, joint flexural and shear behavior become essential. Column reinforcing bars on the tension side are required to develop the yield strength and the joint needs to be well-confined to prevent premature failure. The current TxDOT standard drawings of bent-to-column joints do not consider these mechanisms and plausibly require improvement.

With this regard, a comprehensive review was conducted about available strategies aimed at enhancing bent-to-column joint design, along with relevant code provisions applicable to extreme events. The findings are summarized in this chapter. The specific extreme events considered in this research project are discussed in a dedicated subchapter. Additionally, common detailing techniques for bent-to-column joint confinement are examined, including methods for anchoring column reinforcing bars. Retrofitting approaches for improving joint performance are also reviewed.

2.1. Extreme Events and Design

Significant research effort has been devoted in recent years to studying the effects of extreme events on bridges due to increasing occurrences of events such as vehicle collision accidents, vessel collisions, floods, hurricanes, and scouring. The design under such events is typically more complex compared to traditional design. The TxDOT Bridge Design Manual assumes bent-to-column connections as simply supported, without considering the transfer of moments through those connections (the standard analysis option in the TxDOT bent cap analysis program CAP 18 (1975)). Extreme events, however, usually require load redistribution with transfer of moments through bent-to-column connections that makes those connections no longer pin supports. Additionally, bent-to-column connections shall be designed to sustain large plastic deformation owing to dynamic load re-distribution.

2.1.1. Vehicular Collisions

Vehicle collisions with bridge piers are one of the main extreme events resulting in severe damages and even partial or total collapse of bridges. Studies conducted by Wardhana and Hadipriono (2003) and Cook (2014) have shown that vehicular collisions are the second leading cause of bridge failures after hydraulic causes. Accidents involving vehicle collisions can severely affect the structural members of the bridges including pier, bent cap, foundation system, and superstructure. For example, shear failure in a bent-to-column joint occurred after a tractor trailer hit a bridge located in Colorado due to the force from the impact, as shown in Figure 2-2. Therefore, vehicular collision as an extreme event needs to be taken into account while designing the bent-to-column connections.

Figure 2-2. Failure of a pier located in bent cap connection caused by truck impact in Colorado (Gallegos and McPhee, 2007)

For bridges to resist vehicle collision loads, the column, as well as the connection need to be examined for resistance to such demands. The Equivalent Static Force (ESF) approach is provided in several design codes and reports to design structures against vehicle impacts. An ESF of 600-kip vehicular collision force needs to be resisted by piers and connections in design by TxDOT guidelines in accordance with AASHTO-LRFD (2024) design provisions. Abdelkarim and ElGawady (2017) showed that the constant 600-kip force can be unconservative when the column collided by a vehicle with a kinetic energy higher than 1800 kip-ft, which corresponds to a high-speed vehicle with a velocity greater than 75 mph or a tractor-trailer or a fully-loaded semi-truck with a weight heavier than 30 kips.

Other previous research conducted on vehicular collision with bridges focused mainly on the effects on the piers. In a study conducted by Heng et al. (2021), numerical simulations of vehicle collision with bridge pier were performed. Based on the finite element (FE) model developed for a heavy truck collision with a bridge pier, bending moment values were determined through the height of the pier corresponding to three instants, including the impact at 0.01 seconds, 0.025 seconds, and 0.245 seconds. According to the dynamic behavior of the truck, the process was divided into stages. The first instant corresponded to the head impact stage, the second to the engine impact stage, and the last to the trailer impact stage. Large moment values were observed at the top of the column at the last two instants specified. Similarly, Wu et al. (2020) investigated dynamic responses of bridge piers under vehicle collision impact with several cases including different pier heights, different vehicle velocities, etc., and high bending moment and shear values were observed at the top of the column in some cases under dynamic analysis. Therefore, it is concluded that the bent-to-column connection needs to be designed to carry bending moments and shear under collision.

2.1.2. Vessel Collisions

In recent years, more frequent usage of navigable waterways, larger ship sizes, and use of narrow waterways led to concerns of vessel collisions with bridges. Similar to vehicle collisions, vessel collisions with bridges may also lead to the collapse of bridge structures. However, this is an understudied area in the literature.

The behavior of a bridge under barge impact was examined in a study conducted by Fan et al. (2020). The FE model developed showed that the damage is located at the impact zone, and both ends of the column in a flexure-dominated manner when subjected to different impact velocities.

In order to design the columns and connections considering vessel effects, the same ESF method is followed as vehicle collision. In this approach, the dynamic amplification is indirectly accounted for, and larger moment demands than that derived from static analysis are anticipated. Therefore, the detailing of bent-to-column joints needs to be improved to sustain large moment demands that possibly occur under such impacts.

2.1.3. Severe Scouring

Scour is also one of the main reasons of bridge failures in the United States. It has been reported that more than half of the bridge failures were induced by hydraulic causes including scour between 1950 and 1991. The majority of flood caused failures were also attributed to scour. Static, as well as dynamic, characteristics of the bridges changes due to the scour effect, and it may cause excessive deflections and increased maximum actions in structural members. Due to the removal of streambed materials by scour, capacity and stability of overall bridge could be affected. The performance of a bridge under scour effects are complicated as it depends on several factors including impact levels, scour development, and its changed characteristics as discussed in Shang et al. (2018). Extensive research has been conducted to characterize the behavior of scour. Klinga and Alipour (2015) investigated the response of the bridges supported on pile-group foundation under scour effects. Pushover analysis was conducted to obtain lateral displacement values through the height of the column and pile group. Four different soil types were analyzed, and the simulation results showed that as the scour depth increases, the lateral resistance of the structure reduces. Furthermore, with increasing scour depth, the top displacement also increased. It is plausible that scour can result in increased moment and ductility demands on the column-to-bent connection. Thus, those effects should be considered and improved detailed connections at the column to bent cap could be necessary.

2.1.4. Strut-and-Tie Models for Bent-to-Column Connections

Because transferring moments through joints is required under extreme loading events, diagonal compressive forces develop as a result of the transmitted moments. Williams et al. (2012) developed a strut-and-tie model for a cantilever bent cap and demonstrated that corner connections transmitting moments are subjected to significant diagonal compressive forces, as illustrated in

Figure 2-3. In these connection regions, reinforcing bars are typically detailed with bends to enable force transfer and provide anchorage. As described by Klein et al. (2008), such a connection node can be modeled as a "curved-bar node," which represents the bend region of a continuous reinforcing bar where two tension forces and one compression force meet in a CTT node configuration. For example, Node A in Figure 2-3 can be designed as a curved-bar node. Designing curved-bar nodes requires careful consideration of the bend radius at the exterior corner to ensure adequate anchorage. The experimental study by Wang et al. (2020) found that inadequate proportioning of the curved-bar node can lead to premature failure in the diagonal compression zone or reduced ductility of the joint.

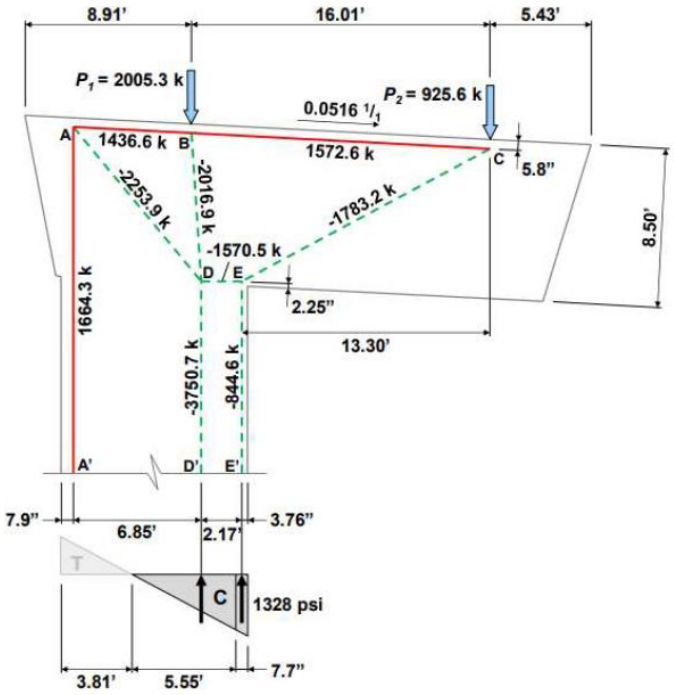

Figure 2-3. Strut-and-Tie model for bent-to-column connection under moment (Williams et al., 2012)

Unlike traditional joint design methods that treat joint shear as an independent design demand requiring separate reinforcement, the force-transfer approach incorporates joint shear directly into the equilibrium analysis. This integration can reduce excessive reinforcement congestion within the joint region, making detailing more efficient. The force-transfer design approach offers an effective strategy for detailing joints subjected to extreme loading conditions, as is common in seismic applications.

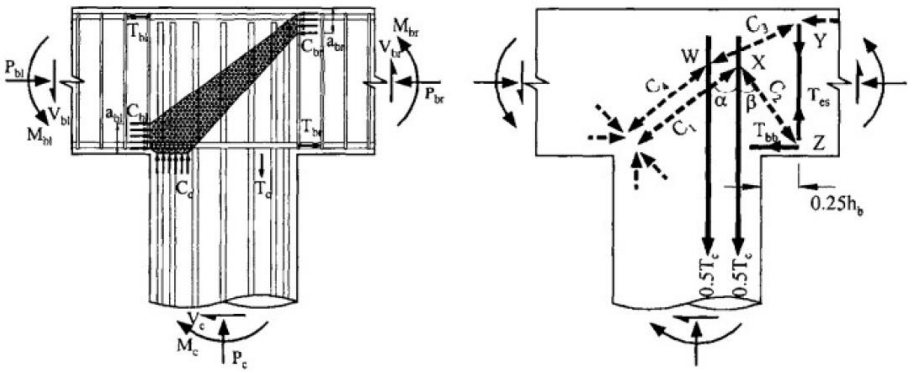

Figure 2-4. Idealized joint strut and external strut force transfer mechanism (Sritharan, 1999, 2001)

Moreover, seismic performance can be improved by ensuring the joint region sufficiently anchors the column's longitudinal reinforcement. Prestressing the cap beam enables a broader and deeper compression strut, which can effectively develop and anchor the column bars within the joint core. Previous investigations, such as those by Sritharan et al. (1999), examined T-shaped bent-to-column joints and found that under seismic loading, compressive forces are diagonally transferred into the columns. Follow-up research by Sritharan et al. (2001) involved designing and testing bent-to-column connections to assess seismic behavior and validate external strut-force transfer design strategies, as illustrated in Figure 2-4, where tension and compression paths are represented by solid and dashed lines, respectively, in accordance with the strut-and-tie framework.

These studies evaluated two types of specimens: joints with prestressed cap beams and joints without prestressing, both tested under cyclic loading. For the prestressed cases, minimal reinforcement was used in the T- and knee joints to control cracking and limit damage during seismic events. This detailing allowed the adjacent columns to develop higher plastic moment capacities. In contrast, joints without cap beam prestressing were designed to address greater tension demands within the joint region, as depicted in Figure 2-5. Such non-prestressed joints were expected to experience higher internal stresses and potential shear cracking.

For these non-prestressed designs, reinforcement layout followed the external force-transfer approach based on strut-and-tie principles. For example, in a T-joint, roughly half of the column's tensile force, T_c, is resisted by a compression strut in the cap beam outside the joint (C_2). To maintain equilibrium, the vertical components of struts C_1 and C_2 were balanced, and the remaining forces were resolved at nodal points. Reinforcement was detailed based on these calculated forces. Column bar anchorage lengths met minimum requirements, designed using a uniform bond stress of $14\sqrt{f_c'\,(psi)}$, applicable to both prestressed and non-prestressed configurations.

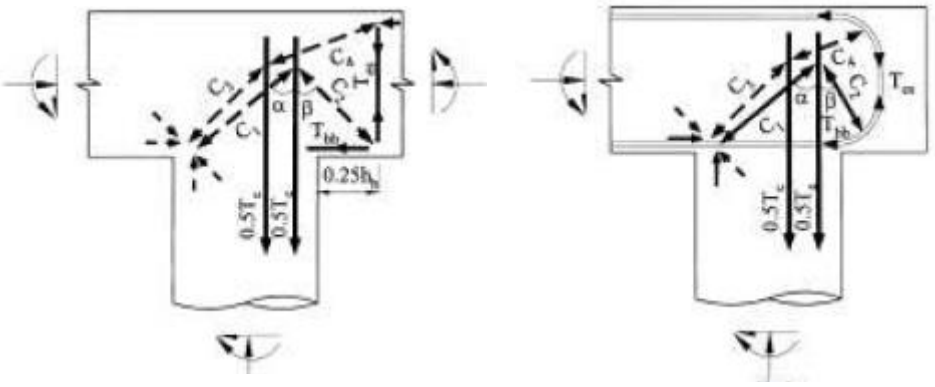

(a) T-joint (b) knee joint

Figure 2-5. External strut-force transfer model for joints without cap beam prestressing

Overall, these studies concluded that adopting a force-transfer design approach can significantly reduce reinforcement congestion in joints. Prestressed cap beams further reduced reinforcement needs compared to non-prestressed designs. Both types of joints demonstrated satisfactory, ductile performance under simulated seismic loading. However, further investigation is warranted to optimize reinforcement detailing in T-joints, as the full capacity of interior columns was not consistently developed relative to exterior columns at the knee joint. Additionally, cap beam prestressing was shown to improve seismic behavior by increasing energy dissipation capacity.

2.2. Detailing Methods of Bent-to-Column Joint Confinement

Confinement in bent-to-column connections is crucial as it can improve serviceability and prevent joint failure. It has been common practice to use continuation of the column transverse reinforcement through the joint. However, a great amount of transverse reinforcement to well-confine the joint makes construction difficult. Vertical hairpins, hoops, and crossties are among the methods that provide joint confinement.

Hanson et al. (1967) showed that hoops are required for a beam-column joint to provide adequate confinement. Hoshikuma et al. (1997) investigated the effectiveness of hoops on providing confinement and the authors showed that an increase in the volumetric ratio of hoop reinforcement improves confinement. Hoshikuma et al. (1997) also investigated the effectiveness of the cross ties on confinement. Two specimens of equal size with rectangular hoops were designed only with a difference of the inclusion of the cross ties to compare this effect as shown in Figure 2-6. The specimen with cross ties showed significantly enhanced performance compared to the specimen without cross ties. This study maintained that cross ties can effectively increase the ductility, and to achieve effective confinement, rectangular hoop alone was insufficient for a specimen with an aspect ratio of 4.0.

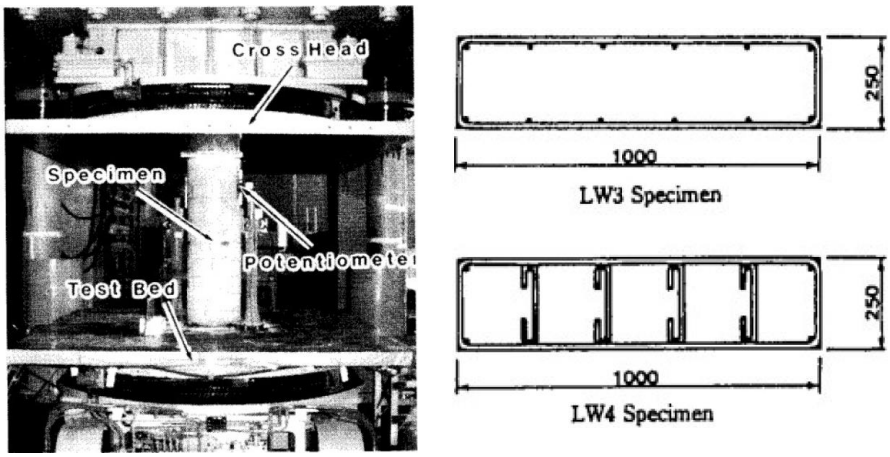

(a) Test setup (b) Cross-section

Figure 2-6. Experimental setup and cross-section of specimens used in Hoshikuma et al (1997)

Headed reinforcement has been shown to be effective in reducing the congestion as well as providing confinement. Studies showed that reduction in the development length is possible depending on a number of factors including the size of the head, the connection between the bar and the plate, and the location in the structure. Thus, it is crucial to design the end plate. If it is too small, the development of yield forces in the bar leads to crushing of concrete, which can potentially cause slipping or pullout. If the plate is too large, however, the constructability benefit can be eliminated due to the increasing congestion. Moreover, headed bars can be used to provide passive lateral confinement as demonstrated in tests conducted by Haroun et al. (1994). When the headed bars were placed in transverse direction as shown in Figure 2-7, the confinement was improved as explained in a study by Ying (2001).

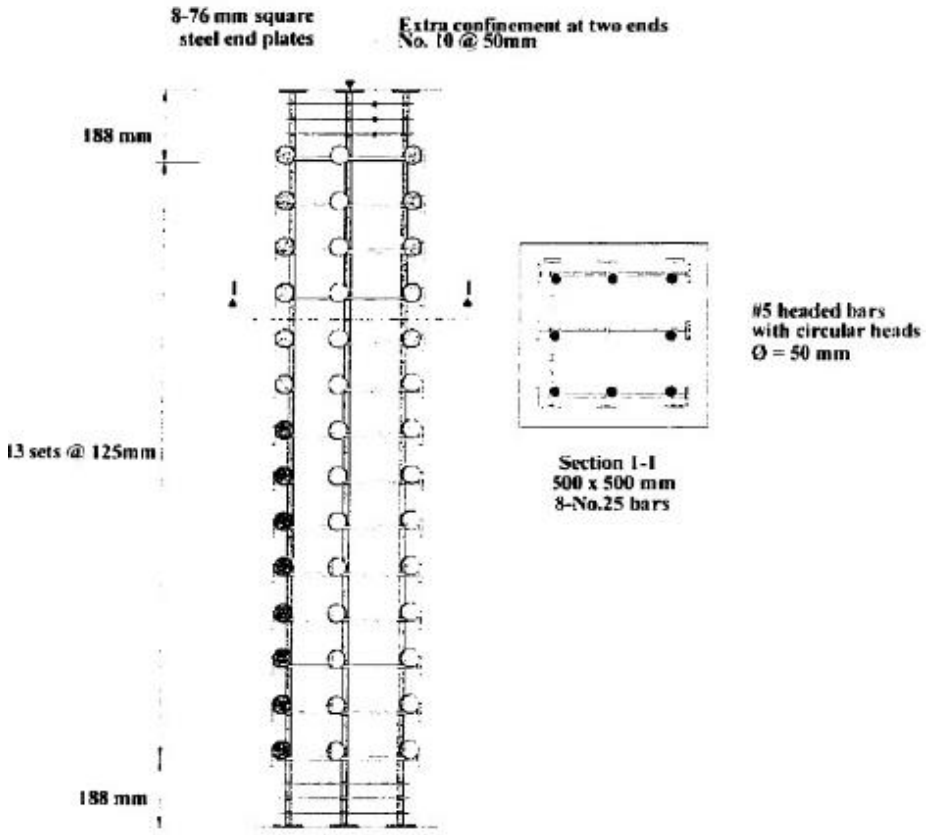

Figure 2-7. Headed bars used as a confining steel (Ying (2001))

Naito et al. (2001) investigated the bridge beam-column connection for seismic performance and analyzed different joint confinement techniques. Based on the study performed, the authors showed that joint spiral improved the confinement and decreased the principal tensile strain. Yet, it was concluded that for such small improvement in confinement, it is difficult to construct. Moreover, two similar specimens were tested to see the confinement effect of different techniques including spiral reinforcement and headed bars as illustrated in Figure 2-8. The observations indicated that the joint with headed reinforcement was better confined than the joint with spiral confinement as joint cracking occurred much earlier in spirally reinforced specimen.

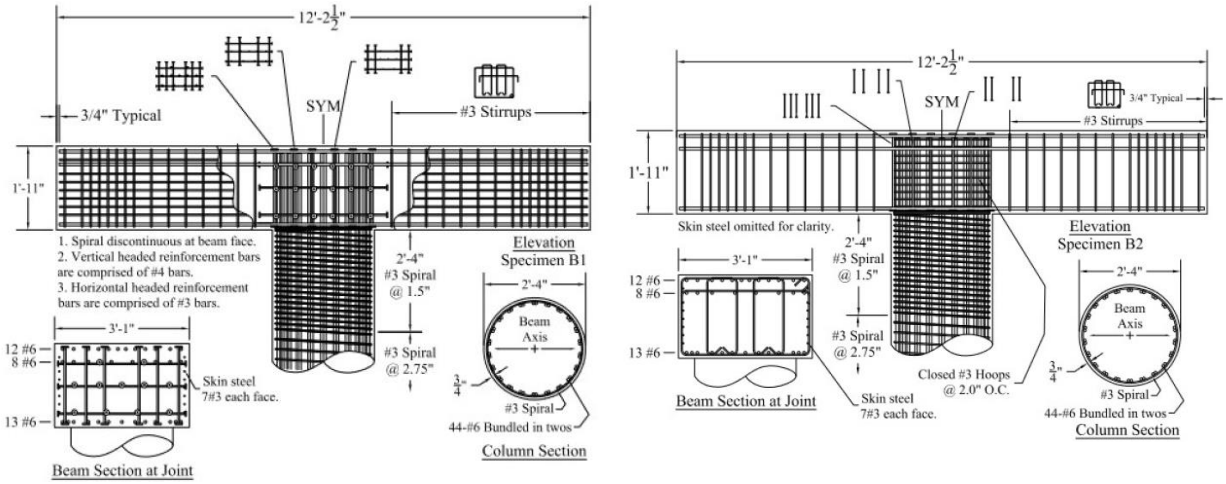

(a) Headed bars (b) Spiral reinforcement

Figure 2-8. Rebar layout for the specimens tested by Naito et al., 2001

Ingham et al. (1998) investigated bent-to-column joints in bridges after the bridge bents based on a pre-1970 design performed poorly during the 1989 Loma Prieta earthquake. Four different specimens were tested including: an as-built unit, a repaired unit, a retrofitted unit, and a redesigned unit under cyclic loading as shown in Figure 2-9. The as-built joint was designed with light vertical and horizontal joint reinforcement consistent with the detailing procedures and had limited anchorage length for column longitudinal bars. For the repaired joint, the concrete and transverse reinforcement was replaced completely, and additional vertical joint reinforcement was included; in addition, the embedment depth of the longitudinal column reinforcement was increased. For the retrofitted joint, an as-built specimen was encased by a concrete jacket that resulted in an increased joint width. The redesigned joint was prestressed to provide confinement with the largest embedment length for the longitudinal column reinforcement. The experimental test results with cyclic loading showed that extensive damages were observed in the as-built joint, which was attributed to the inadequate embedment length of the reinforcement, as opposed to the other three specimens. More ductile behavior was observed for the rest of the specimens with higher capacities.

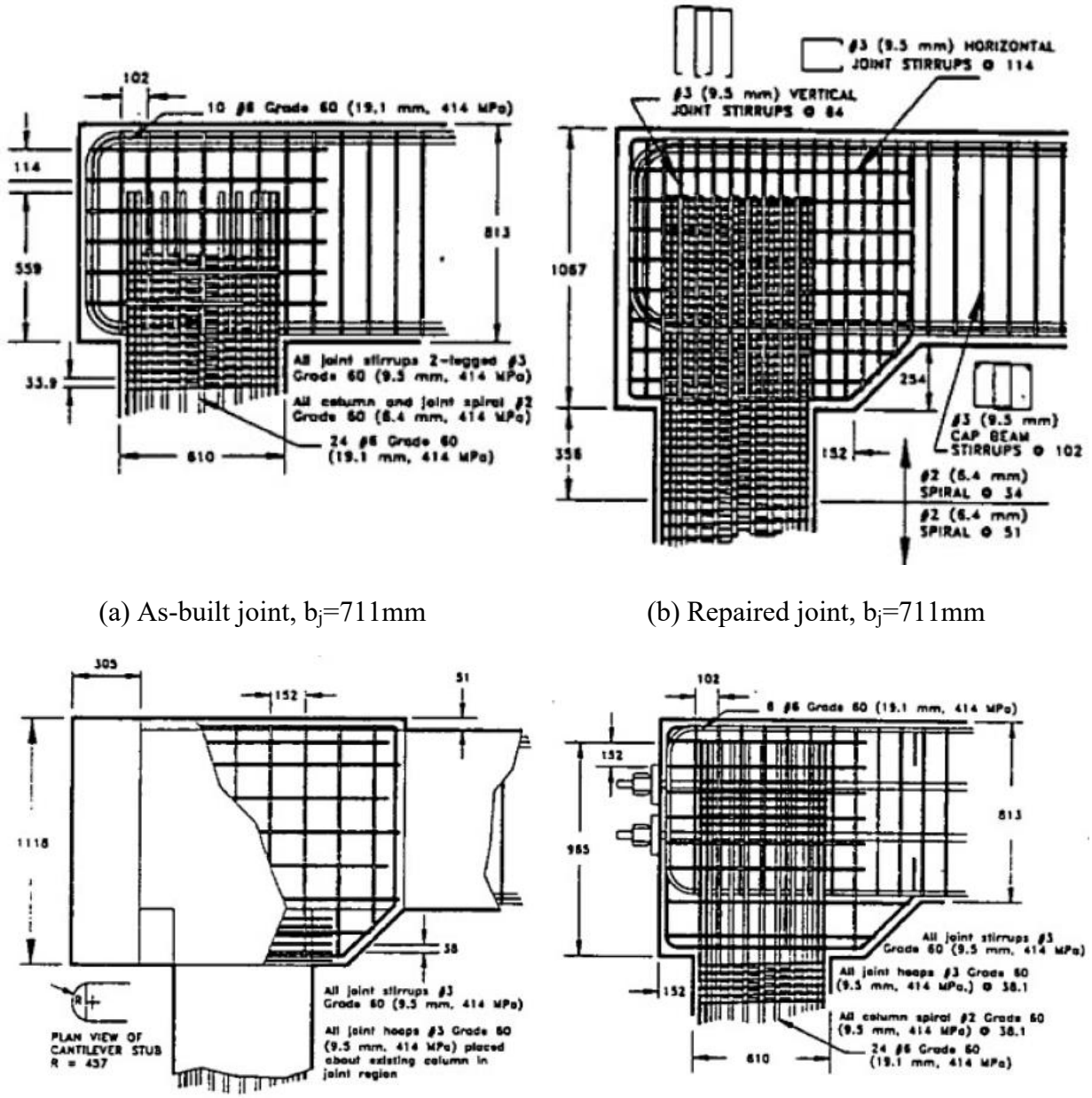

(a) As-built joint, b_j=711mm

(b) Repaired joint, b_j=711mm

(c) Retrofitted joint, b_j=864mm

(d) redesigned joint, b_j=711mm

Figure 2-9. Bent-to-Column connection details of four specimens subjected to cyclic loading (Ingham et al., 1998)

Larosche et al. (2014) also investigated the pile to bent cap connections subjected to simulated seismic loading. An assembly of three prestressed piles with a cast-in place bent cap using three different connections were constructed. The interior connection, Connection A, was designed using only minimum reinforcement based on SCDOT provisions with increased pile embedment depth that SCDOT requires. Exterior connections, however, were designed using two proposed methods including increase in the amount of bent cap reinforcement and increase in the dimension

of the cap to avoid bent cap failure during reverse cyclic loading. To provide sufficient confinement the dimension of the bent cap at the exterior end of the standard detail was increased from 560 mm (~22 in.) to 0.9 m (~35 in.) at Connection C. The bent cap reinforcement, however, was increased at Connection A by adding bars to the standard detail, Connection B, including the additional square spiral, four-leg stirrups and bundling of additional skin and bottom mat reinforcement U-bars as shown in Figure 2-10.

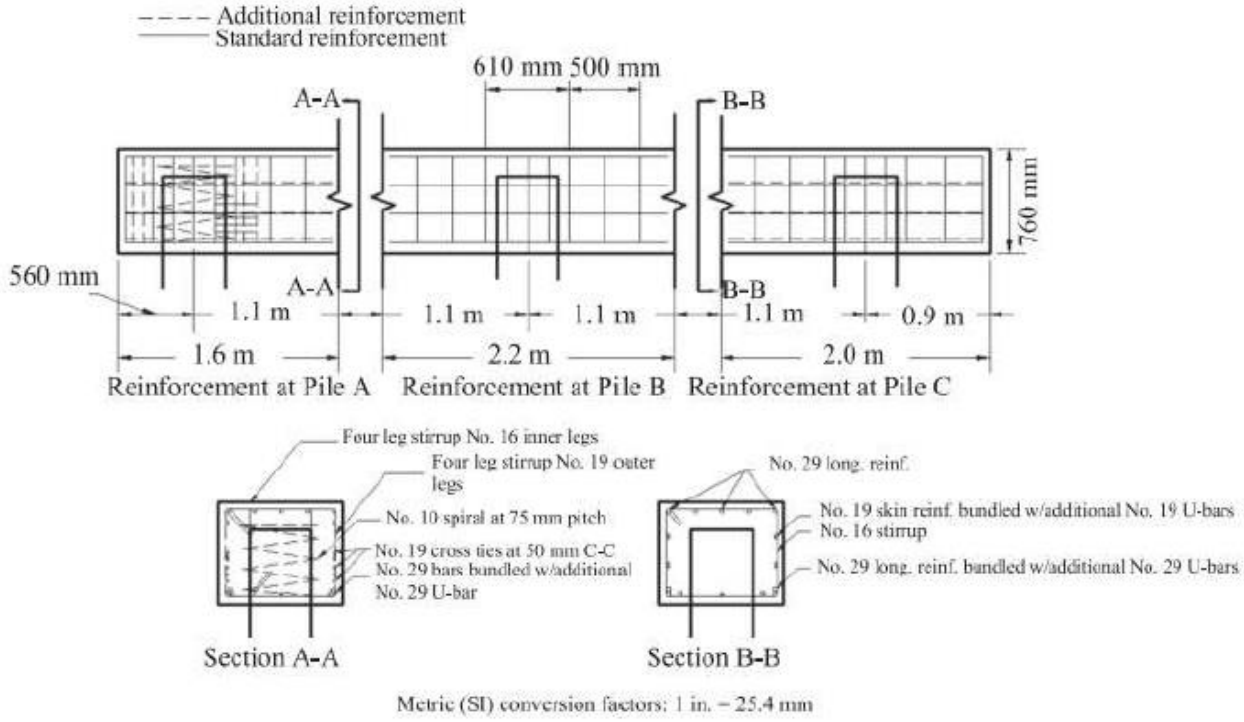

Figure 2-10. Reinforcement detail in the pile to bent cap connections (Larosche et al., 2014)

The specimen was subjected to a displacement history based on a numerical analysis performed in SAP2000. It was concluded that the increased pile embedment depth showed satisfactory performance based on the performance of the interior connection where damage occurred was limited to minor spalling in the perimeter of connection. Both exterior joint designs also performed well, yet, the exterior joint with dense reinforcement showed better pile confinement as final measurements recorded confining stresses of 400 psi in Connection C, and 500 psi in Connection A. The heavily reinforced connection showed superior performance in limiting strand slip that could be proven by the difference in the crack widths as the damages were presented in Figure 2-11. Overall, the specimen had higher displacement ductility capacity than the maximum specified by SCDOT, and both designs were recommended for implementation by the authors.

Detailing methods of pile cap connections were also investigated in a study by Joen and Park (1990) to improve the energy dissipating capacity under seismic loads. A number of connection details differed in the properties of the piles including embedment length, spiral reinforcements, dowel bars were tested to achieve a moment-resisting connection as shown in Figure 2-12. The least

damage among all specimens was observed in the connection when the end of the pile is roughened and is embedded in the cast-in-place cap. The connection type with dowel bars was not recommended, due to the concentration of damage observed. Also, spiral reinforcements were suggested to assist the transfer of lateral forces.

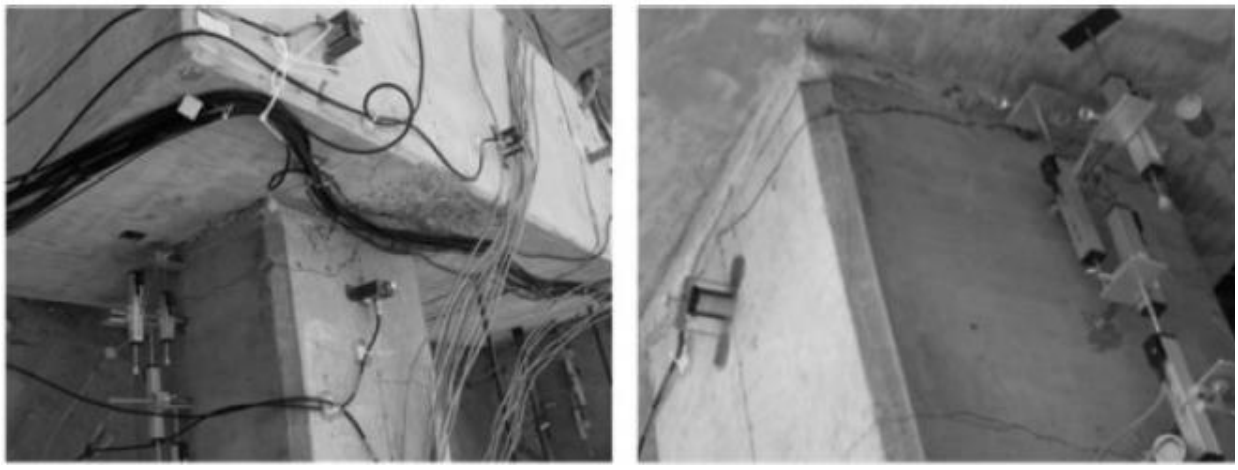

(a) Heavily reinforced connection

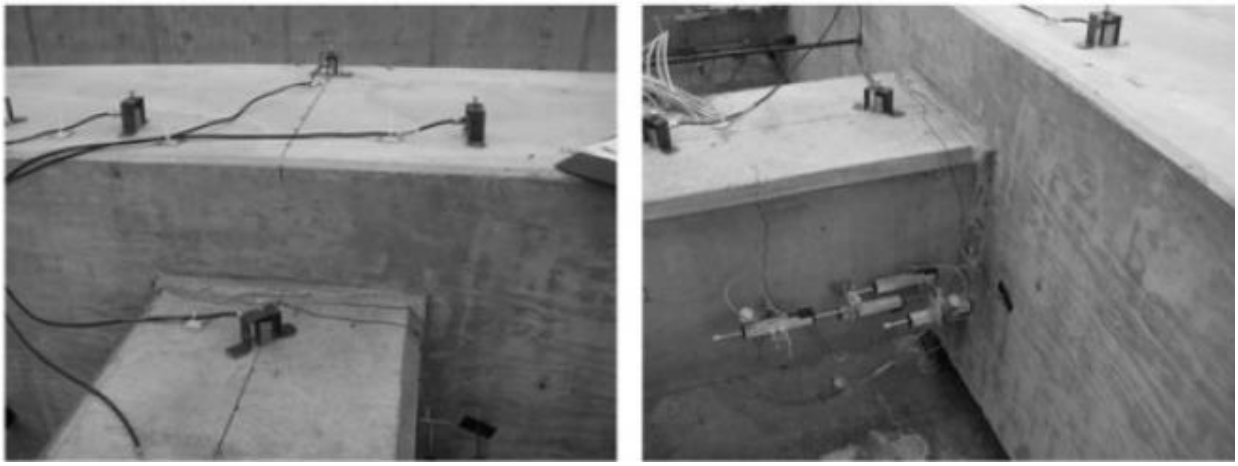

(b) Connection with increased overhang

Figure 2-11. Damages in the connection with different conditions

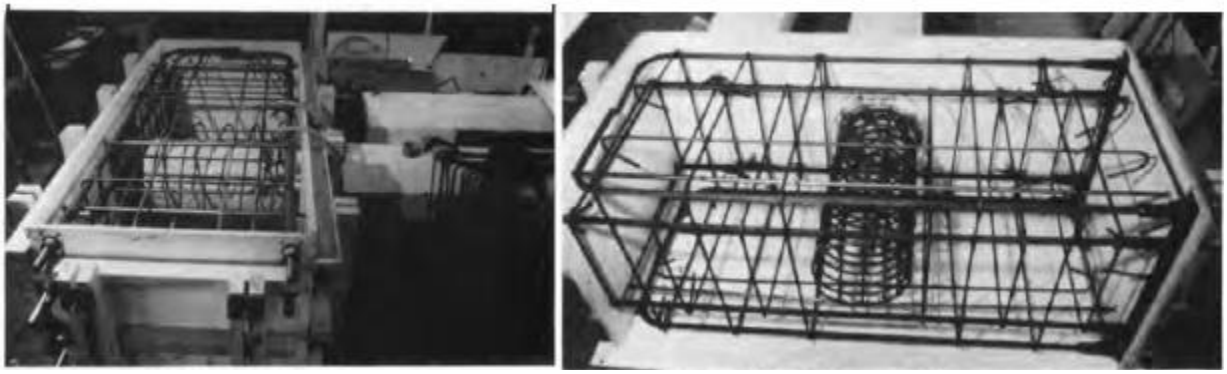

Figure 2-12. Details of some specimens tested (Joen and Park, 1990)

The effect of confinement on the response of the column-beam connections was also analyzed by Roeder et al. (2001). Eight joint details, with or without confining reinforcement using different anchorage methods were tested as shown in Figure 2-13. Large inelastic deformations were tolerated by all the specimens during tests under cyclic loading and the maximum displacement achieved for all specimens was similar. It was concluded, thereafter, that confinement did not significantly affect overall behavior of the connections.

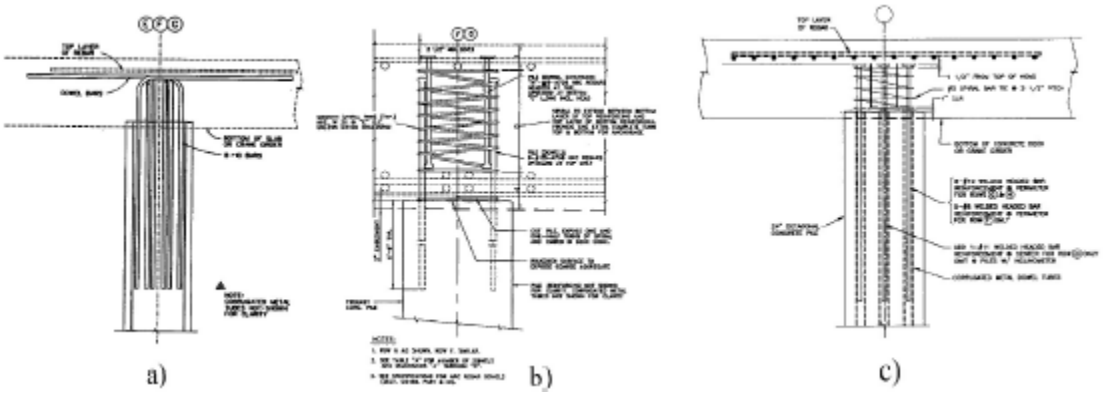

Figure 2-13, Some specimen details tested (Roeder et al. 2001)

2.3. Anchorage of Reinforcement

This section presents widely accepted and state-of-the-art techniques of anchoring longitudinal reinforcement in concrete joints. Bar anchorage plays an essential role to guarantee that the reinforcing bars develop the yield strength, and thereby the full flexural capacity of the moment frame can be developed. Plastic hinging can be expected without unwanted bond or anchorage failures. To date, strategies of anchorage can be primarily categorized into three types: straight bars, hooked bars, and headed bars. The anchorage of straight bars and hooked bars are discussed and followed by the anchorage of headed bars in this chapter.

2.3.1. Straight Bars

The anchorage of straight bars has been widely used; current TxDOT standard bent-to-column joints also employ this type. Straight bar anchorage, compared to the other two types, is the easiest method; however, the required development length is the longest. Past studies revealed that bond deterioration potentially reduces the effectiveness of straight bar anchorage because the anchorage capacity relies only on bond to the surrounding concrete. The downsides restrict the application of straight bars as anchorage in bent-to-column joints, where available length is relatively limited.

Research found that the bond strength is related to factors including concrete strength, side cover to the bars being developed, spacing between bars to develop, and the bar diameter. Also, if bars being developed are confined with transverse reinforcement, the development length can be reduced. Other important factors, on the other hand, include coating conditions and concrete placement. To guarantee sufficient anchorage capacity for straight bars in tension, design codes introduce simplified equations that incorporate the key factors to design the development length. Primary design expressions included in major design codes are reviewed in this section.

2.3.1.1. Code Provisions in the U.S.

2.3.1.1.1. AASHTO LRFD 2020

In accordance with Section 5.10.8.2 of AASHTO LRFD (2024), the development length for straight bars in tension (l_d) is determined by a basic development length (l_{db}) multiplied with five modification factors (λ_{rl}, λ_{cf}, λ_{rc}, λ_{er}, and λ), as shown in Equation 2-1 and Equation 2-2.

$$l_d = l_{db}\left(\frac{\lambda_{rl}\lambda_{cf}\lambda_{rc}\lambda_{er}}{\lambda}\right) \qquad \textit{Equation 2-1}$$

$$l_{db} = 2.4 d_b \frac{f_y}{\sqrt{f'_c}} \qquad \textit{Equation 2-2}$$

where f_y is specified minimum yield strength of reinforcement (ksi), f'_c is compressive strength of concrete for use in design (ksi), and d_b is nominal diameter of reinforcing bar (in.). Among the five modification factors, λ, concrete density factor, applies when the concrete is lightweight. The other four modification factors reflect the conditions of bars being developed. Two of the four modification factors increase the required development length as summarized in Table 2-1. The factor λ_{rl}, reflects the fact that bond strength is compromised due to thick concrete below the bars. The factor λ_{cf}, coating factor, reflects that coated bars have lower bond ability with surrounded concrete.

Table 2-1. AASHTO LRFD Modification factors that increase the development length of reinforcement in tension

Modification factor that increases l_d	Condition	Value of factor
λ_{rl} Reinforcement location factor	For horizontal reinforcement, more than 12.0 in. of fresh concrete is cast below	1.3
	For horizontal reinforcement, no more than 12.0 in. of fresh concrete is cast below and f'_c is greater than 10.0 ksi	1.3
λ_{cf} Coating factor	For epoxy-coated bars with cover less than $3d_b$ or with clear spacing between bars less than $6d_b$	1.5
	For epoxy-coated bars not covered above	1.2

Note: The product $\lambda_{rl} \times \lambda_{cf}$ need not be taken greater than 1.7.

Other than the factors that increase the development length, the other two factors, λ_{rc} and λ_{er}, decrease the development length, as summarized in Table 2-2. The former one reflects better bond condition if bars are well confined. It is believed that sufficiently thick cover concrete and concrete between bars can control bond splitting cracks. Also, presence of bars across the plane of splitting also controls the splitting cracks, resulting in shorter development length. The latter one, named excess reinforcement factor, requires shorter development length if more reinforcement is provided than needed.

Table 2-2. AASHTO LRFD Modification factors that decrease the development length of reinforcement in tension

Modification factor that decreases l_d	Design expression
λ_{rc} Confinement factor	$0.4 \le \lambda_{rc} = \frac{d_b}{c_b + k_{tr}} \le 1.0$ $k_{tr} = \frac{40A_{tr}}{sn}$ where: c_b = the smaller of distance from center of bar being developed to the nearest edge of concrete and one-half the center-to-center spacing of the bars k_{tr} = transverse reinforcement index A_{tr} = total cross-sectional area of all transverse reinforcement crossing potential plane of splitting s = maximum center-to-center spacing of transverse reinforcement n = number of bars being developed
λ_{er} Excess reinforcement	$\lambda_{er} = \frac{\text{Required } A_s}{\text{Provided } A_s}$

2.3.1.1.2. AASHTO LRFD 2024

The 10th Edition of the AASHTO LRFD Bridge Design Specifications introduces a significant update to the calculation of development length for reinforcing bars in tension. Moving away from separate provisions for different anchorage types, the new article provides a single, unified

equation. This mechanics-based approach is applicable to straight bars, hooked bars, and headed bars, unifying the design process by incorporating a term, F_h, that accounts for the force contribution from a hook or a head. For a straight bar, this term is simply taken as zero, allowing the same fundamental equation to be used for all anchorage conditions, as shown in Equation 2-3 and Equation 2-4.

$$l_d = l_{db}\lambda_{rl}\lambda_{cf}\lambda_{rc} \qquad \textit{Equation 2-3}$$

$$l_{db} = 0.17 d_b \left[\frac{\lambda_{er} f_y - \frac{F_h}{A_b}}{1.97\lambda f'^{0.25}_c}\right]^2 \qquad \textit{Equation 2-4}$$

where l_{db} is basic development length (in.); λ_{rl} is reinforcement location factor; λ_{cf} is coating factor; λ_{rc} is reinforcement confinement factor; d_b is nominal diameter of reinforcing bar or wire (in.); f_y is specified minimum yield strength of reinforcement (ksi); F_h is force developed by hooks or heads (kip); A_b is nominal area of reinforcing bar or wire (in.^{2}); f'_c is compressive strength of concrete for use in design (ksi); λ_{er} is excess reinforcement factor; λ is concrete density modification factor, as specified in AASHTO LRFD Article 5.4.2.8.

The modification factors applied to the basic development length, λ_{rl} (location) and λ_{cf} (coating) are conceptually similar to those in the previous edition. However, the reinforcement confinement factor, λ_{rc}, has been significantly revised, as shown in Table 2-3. The new form of the reinforcement confinement factor includes confinement index and modulus ratio.

Table 2-3 Modification factors to the development length of AASHTO LRFD 10th edition

Modification factor that	Design expression
λ_{rc} Reinforcement Confinement Factor	$\lambda_{rc} = \frac{d_b c_b}{(c_b(1-\beta_t) + 1.67 n_s k_{tr})^2}$ $k_{tr} = \frac{A_{tr}}{sn}$ where: c_b = the smaller of the distance from center of bar or wire being developed to the nearest concrete surface and one-half the center-to-center spacing of the bars or wires being developed (in.) β_t = ratio of unfactored compressive stress due to permanent loads (taken as a negative value) transverse to the plane of splitting to the modulus of rupture, as determined by Article 5.4.2.6 ($-1 \le \beta_t \le 0$) n_s = modular ratio, E_s/E_c k_{tr} = transverse reinforcement index A_{tr} = total cross-sectional area of all transverse reinforcement which is within the spacing s and which crosses the potential plane of splitting through the reinforcement being developed (in.^{2}) s = maximum center-to-center spacing of transverse reinforcement within ℓ_d (in.) n = number of bars or wires developed along plane of splitting
λ_{rl} Reinforce location factor	For horizontal reinforcement, placed such that more than 12.0 in. of fresh concrete is cast below the reinforcement, The factor is taken as 1.3
λ_{cf} Coating factor	• 1.3 for horizontal reinforcement, placed such that more than 12.0 in. of fresh concrete is cast below the reinforcement. • 1.5 for epoxy-coated or zinc and epoxy dual-coated bars with cover less than $3d_b$ or with clear spacing between bars less than $6d_b$ • 1.2 for epoxy-coated or zinc and epoxy dual-coated bars not covered above, epoxy-coated or zinc and epoxy dual-coated hooked bars designed with Article 5.10.8.2.4, and epoxy-coated or zinc and epoxy dual-coated headed bars designed with Article 5.10.8.2.7. • 1.0 for uncoated or zinc-coated (galvanized) bars. • The product $\lambda_{rl} \times \lambda_{cf}$ need not be taken greater than 1.7.
λ_{er} Excess reinforcement	$\lambda_{er} = \frac{\text{Required } A_s}{\text{Provided } A_s}$

2.3.1.1.3. ACI 318-25 (2025)

The development length of straight bars in tension required in ACI 318-25 is determined in a similar way to the that in AASHTO LRFD. That is, the basic development length should be

modified according to conditions of bars being developed and transverse confinement. Nevertheless, ACI 318-25 simplified equations for designers' convenience.

The general equation, in accordance with Section 25.4.2.4 of ACI 318-25, can be expressed as Equation 2-5.

$$l_d = \left(\frac{3}{40} \frac{f_y}{\lambda \sqrt{f'_c}} \frac{\psi_t \psi_e \psi_s \psi_g}{\left(\frac{c_b + k_{tr}}{d_b} \right)} \right) d_b \qquad \textit{Equation 2-5}$$

where k_{tr} has the same definition as AASHTO LRFD and the term $\left(\frac{c_b+k_{tr}}{d_b}\right)$ shall not be taken larger than 2.5. It should be noted that the input units of Equation 2-5 are in in.-lbf system, which is different from that of AASHTO LRFD (2024). The other factors are summarized in Table 2-4. It can be observed in Table 2-4 that ACI 318-25 (2025) also considers coating conditions and the casting position. The factor for the casting position is simpler in ACI 318-15 (2025), compared to that of AASHTO LRFD (2020), which requires modification for compressive strength of concrete higher than 10 ksi even though fresh concrete below the horizontal bars being developed less than 12 in. Additionally, ACI 318-25 (2025) has modification factors for reinforcement grade as research (Orangun et al. (1977)) showed that the required development length does not increase proportionally with increases in yield strength. Also, the size factor reflects the fact that smaller bars have favorable performance.

Table 2-4. ACI 318-19 Modification factors for development of deformed bars in tension

Modification factor	Condition	Value of factor
λ Light weight	Light weight concrete	0.75
	Normal weight concrete	1.0
ψ_g Reinforcement grade	Grade 40 or Grade 60	1.0
	Grade 80	1.15
	Grade 100	1.3
ψ_e Epoxy*	Coated reinforcement with clear cover less than $3d_b$ or clear spacing less than $6d_b$	1.5
	Coated reinforcement for all other equations	1.2
	Uncoated reinforcement	1.0
ψ_s Size	No. 7 and larger bars	1.0
	No. 6 and smaller bars	0.8
ψ_t Casting position	More than 12 in. of fresh concrete below horizontal reinforcement	1.3
	Other	1.0

Note: The product $\psi_e\psi_t$ need not to be greater than 1.7

Detailed coating condition in accordance with Table 25.4.2.5 of ACI 318-19

Other than the general equation, the provision considers practical bars spacing design and transverse reinforcement and provides simplified equations. In accordance with ACI 318-19

Section 25.4.2.3, development length can be calculated based on conditions of spacing and cover, as well as bar size as summarized in Table 2-5. It should also be noted that ACI 318-19 does not allow development length to be shortened if excess reinforcement is provided.

Table 2-5. ACI 318-25 Simplified equations of development length for deformed bars in tension

Spacing and cover	No. 6 and smaller bars	No. 7 and larger bars
1. Clear spacing not less than d_b, clear cover not less than d_b, and transverse reinforcement satisfying code minimum 2. Clear spacing not less than $2d_b$ and clear cover not less than d_b	$\left(\frac{f_y\psi_t\psi_e\psi_g}{25\lambda\sqrt{f'_c}}\right)d_b$	$\left(\frac{f_y\psi_t\psi_e\psi_g}{20\lambda\sqrt{f'_c}}\right)d_b$
Other cases	$\left(\frac{3f_y\psi_t\psi_e\psi_g}{50\lambda\sqrt{f'_c}}\right)d_b$	$\left(\frac{3f_y\psi_t\psi_e\psi_g}{40\lambda\sqrt{f'_c}}\right)d_b$

2.3.1.2. Other Code Provisions

2.3.1.2.1. Canadian Standards Association

In the Canadian CSA A23.4 Code "Design of concrete structures" (2019), the development length of deformed bars in tension is calculated in a similar manner to ACI 318-19 (2019): a basic development length equation modified with four factors that reflect bar conditions. CSA (2019) also provides simplified basic development length equations based on clear spacing and the existence of code-complying transverse reinforcement.

The general development equation can be expressed as Equation 2-6.

$$l_d = 1.15\frac{k_1k_2k_3k_4}{(d_{cs}+K_{tr})}\frac{f_y}{\sqrt{f'_c}}A_b \qquad \textit{Equation 2-6}$$

in which

$$K_{tr} = \frac{A_{tr}f_{yt}}{10.5sn} \qquad \textit{Equation 2-7}$$

where k_1 is bar location factor; k_2 is coating factor; k_3 is concrete density factor; k_4 is bar size factor; A_b (mm^2) is the area of individual bar being developed; d_{cs} (mm) relates to clear cover and bar spacing; f_{yt} (MPa) is the yield strength of transverse reinforcement. The value of each factor and d_{cs} are summarized in Table 2-6. It should be noted that metric units are used in CSA.

Table 2-6. CSA modification factors for development length of deformed bars in tension

Modification factor	Condition	Value of factor
k_1 Bar location factor	More than 300 mm of fresh concrete below horizontal reinforcement	1.3
	Other cases	1.0
k_2 Coating factor	Epoxy-coated reinforcement with clear cover less than $3d_b$ or clear spacing less than $6d_b$	1.5
	Epoxy-coated reinforcement for all other equations	1.2
	Uncoated reinforcement	1.0
k_3 Concrete density factor	Low-density concrete	1.3
	Semi-low-density concrete	1.2
	Normal density concrete	1.0
k_4 Bar size factor	25M and larger bars	1.0
	20M and smaller bars	0.8
d_{cs} Concrete cover	The smaller of a) the distance of closest edge of concrete to center of bar being developed; b) two-third of center-to-center spacing of bars being developed.	

Note: The product $\psi_e\psi_t$ need not to be greater than 1.7
Detailed coating condition in accordance with Table 25.4.2.5 of ACI 318-19

Similar to ACI 318-19, CSA 23.4 also provides simplified development length equations based on commonly designed concrete cover and bar spacing in practice, as summarized in Table 2-7. The modification factors in the equations are the same and summarized in Table 2-6. In addition, excess reinforcement factor, $A_{s,required}/ A_{s,provided}$, is allowed.

Table 2-7. CSA simplified development length equations

Conditions	Minimum development length
1. Member containing code-complying minimum transverse reinforcement 2. Slabs, walls, shells, or folded plates having clear spacing of greater than $2d_b$ between bars being developed	$0.45k_1k_2k_3k_4\frac{f_y}{\sqrt{f'_c}}d_b$
Other cases	$0.6k_1k_2k_3k_4\frac{f_y}{\sqrt{f'_c}}d_b$

2.3.1.2.2. Fib Model Code for Concrete Structure 2010

The *fib* Model Code, published in Europe, uses a more analytical method to calculate design anchorage length for straight bars. Indeed, other anchorage types are applicable. Generally, the method requires that the design bond strength times the anchorage length be greater than the stress

to be developed. In accordance with Section 6.1.3.4 of fib Model Code, the design anchorage length can be expressed as Equation 2-8. It should be noted the symbols in the equations may not be the same as the original fib Model Code. In addition, metric unit system is used in fib Model Code.

$$l_d = \frac{f_{sd}}{4\mu} d_b \geq \max\left\{0.3\frac{f_{sd}}{4\mu} d_b, 10d_b,\ 100\ \text{mm}\right\} \qquad \textit{Equation 2-8}$$

In Equation 2-8, f_{sd} is design bar stress, and μ is design bond strength. The design bar stress, according to the code, is basically determined by the bar yield strength multiplied by excess reinforcement factor. In addition, if the bar is anchored with other anchorage than straight bars, the design bar stress can be further reduced.

For the design bond strength, the *fib* Model Code provides an empirical equation based on database analysis. The equation considers factors including the coating, the casting position, the bar size, the bar grade, the confinement condition, and arrangement of transverse reinforcement. Moreover, the equation takes compression stress perpendicular to the potential splitting failure stress into account. For more information, it can be referenced in Section 6.1.3.2 through 6.1.3.4 of the *fib* Model Code.

2.3.2. Hooked Bars

The force transfer mechanism of hooked bars consists of the bond stresses along the straight portion and the bearing stresses inside the bar bend. This anchorage technique reduces the required development length, compared to straight anchorage, if the bar bend and the tail extension are well designed. For the seismic design of joints, hooked anchorage was shown to be effective in activating a more efficient shear resistance mechanism. On account of these advantages, hooked bars are commonly used in beam-column joints, footings, and additional applications. Hooked bars are also promising to facilitate anchorage in bent-to-column joints designed for extreme loading events. The geometry of hooked bars, however, inevitably causes congestions, especially in heavily-reinforced joints. In this section, major studies on hooked anchorage in beam-column joints are reviewed. Also, design expressions suggested in major design codes are reviewed.

2.3.2.1. Studies on Anchorage of Hooked Bars in Joints

2.3.2.1.1. Marques and Jirsa (1975)

Early systematic experimental investigations into hooked anchorage in beam-column joints dates back to the 1970s in Texas. Marques and Jirsa (1975) conducted an extensive experimental program to study the anchorage behavior of hooked bars in beam-column joints. The authors tested 32 specimens simulating exterior beam-column joints with anchorage of hooked bars, as shown in Figure 2-14. Variables including column axial load, column reinforcement, side concrete cover,

degrees of confinement, bar size, and hook bent angle. After successfully identifying contribution of each factor to the anchorage strength, the study concluded that the embedment length was essential when determining the anchorage strength. Level of axial load, on the contrary, did not have significant effect. Concrete cover, when sufficient, did not appear to cause influence and tie spacing in the joint should be relatively small to the bend diameter of the anchored bar. Based on the findings, the authors provided an equation to calculate the anchorage strength. The method separated contribution of the hook from that of the straight portion. In other words, the anchorage strength was the summation of the strength provided by the hook and by the straight portion.

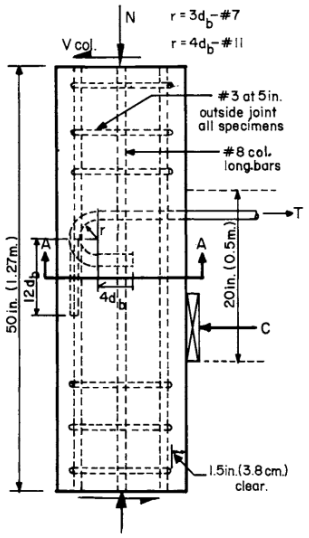

Figure 2-14. Test setup used in Marques and Jirsa (1975)

2.3.2.1.2. Pinc et al. (1977)

Two years later, Pinc et al. (1977) extended the experimental program by Marques and Jirsa (1975) and tested 16 specimens simulating exterior beam-column joints. The study further investigated the effect of embedment length and lightweight concrete. The purpose was to expand the dataset and develop a simple relationship between anchorage strength and embedment length of hooked bars. To be specific, the anchorage strength contributed by the hook and the straight portion could be no longer considered separately.

The study in the end proposed a general equation for calculating anchorage strength of hooked bars with one single embedment length, l_{dh}, as shown in Equation 2-9. The equation took the effects of bar size and lightweight concrete into consideration. The equation then became the basis of design development length for hooked bars.

$$f_u = 50\psi\Omega\frac{l_{dh}}{d_b}\sqrt{f'_c} \qquad \textit{Equation 2-9}$$

In Equation 2-9, f_u is anchorage strength; ψ reflects bar size and confinement conditions; Ω is the factor of lightweight concrete.

2.3.2.1.3. Hamad et al. (1993)

Not until the year of 1993 was the anchorage behavior of epoxy-coated hooked bars investigated. Hamad et al. tested 25 specimens simulating exterior beam-column joints with coated hooked bars. Variables included bar size, concrete strength, concrete cover, hook geometry, and amount of transverse reinforcement. The results were compared to those of Marques and Jirsa (1975) and Pinc et al. (1977).

The study revealed that epoxy-coated hooked bars have an anchorage strength consistently lower than uncoated hooked bars. Furthermore, the relative anchorage strength between uncoated hooked bars and coated hooked bars was independent of other investigated factors. Based on this observation, a modification factor of 1.2 was introduced to enlarge the required development length for epoxy-coated hooked bars.

2.3.2.1.4. Sperry et al. (2017)

Sperry et al. (2017) noted that design expressions for development length of hooked bar in ACI 318-14 and AASHTO LRFD 2012 were based on a relatively small number of tests conducted in 1970s. This experimental study, in order to expand the knowledge domain, widened the range of key factors that affected the anchorage strength of hooked bars in beam-column joints. One of the highlights was high strength steel and high strength concrete. Other variables included number of hooked bars, bar size, bar spacing, embedment length, bend geometry, and degrees of confinement. In total, 337 specimens simulating beam-column joints were tested. The testing frame, as shown in Figure 2-15, was also similar to early studies.

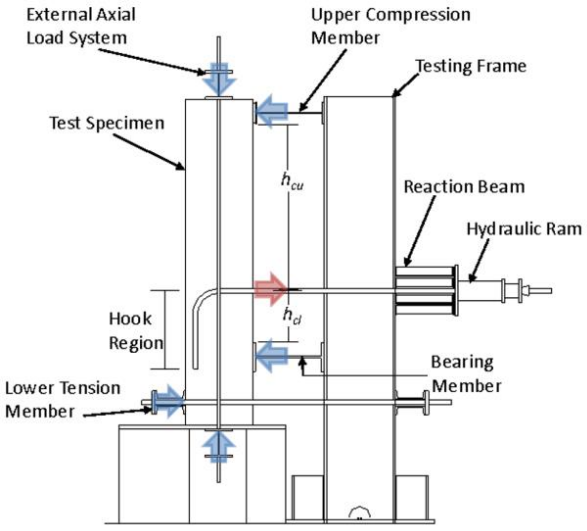

Figure 2-15. Testing frame used in Sperry et al. (2017)

The study concluded that provisions of ACI 318-14 for development length tended to be less conservative when bar size and concrete strength increased. When the bar diameter of hooked bars

increased, a failure of side cover was observed more often. Furthermore, ACI 318-14 overestimated the effect of confining reinforcement on the anchorage strength of hooked bars in tension. The observations opened discussion for revising the code provisions.

2.3.2.1.5. Sperry et al. (2018)

Under the same large-scale experimental program, Sperry et al. (2018) did not stop but further investigated the effect of confinement on anchorage strength of hooked bars in tension. The investigated parameters included hook bend angle, concrete clear cover, and orientation of confining reinforcement. It was found that hooked bars with 90- and 180- degree bend had comparable anchorage strength, which echoed the study by Marque and Jirsa (1975). Another important finding was that confining reinforcement oriented parallell to the straight portion of hooked bars had better anchorage strength. In addition, thick concrete cover (greater than $3.5d_b$) did not further increase the anchorage strength.

2.3.2.1.6. Ajaam et al. (2018)

In the same year, Ajaam et al. (2018) evaluated a database, as part of a large study, consisting of 245 specimens of simulated beam-column joint with closely spaced hooked bars. The purpose was to bridge a knowledge gap that ACI code provisions were developed using test data lacking specimens with closely spaced hooked bars. Indeed, the test data was generated with specimens containing only two longitudinal bars in one layer. In this study, the authors selected specimens reinforced with three to six layers in a single layer and specimens with two layers of hooked bars. In addition, bar size ranged from No. 5 to No. 11 bars.

The study concluded that the development length required in ACI 318-14 overestimated the anchorage strength of hooked bars especially when they were closely spaced or were in large size. Based on the observations, the study suggested that modification to the design development length take place for hooked bar with a center-to-center spacing smaller than $6d_b$. Furthermore, ties or stirrups parallel to the straight portion should be provided to avoid penalty of using longer required development length.

2.3.2.2. Relevant Code Provisions

2.3.2.2.1. ACI 318-19 (2019)

ACI 318 committee made plenty revisions to the development length of hooked bars in the current version ACI 318-19. Instead of referring to the studies in the 1970s, the new provisions are based on Sperry et al. (2017, 2018) and Ajaam et al. (2018) as mentioned above. The equation for development length of hooked bars in tension is shown in Equation 2-10.

$$l_{dh} = \left(\frac{f_y \psi_e \psi_r \psi_o \psi_c}{55\lambda\sqrt{f'_c}}\right) d_b^{1.5} \qquad \textit{Equation 2-10}$$

In which the modification factors are summarized in Table 2-8.

Table 2-8. ACI 318-19 modification factors for development of hooked bars in tension

Modification factor	Condition	Value of factor
λ Light weight	Light weight concrete	0.75
	Normal weight concrete	1.0
ψ_e Epoxy	Coated* reinforcement	1.2
	Uncoated or galvanized reinforcement	1.0
ψ_r Confining reinforcement	For No. 11 and smaller bars with $A_{th} \geq 0.4A_{hs}$ or $s \geq 6d_b$	1.0
	Other	1.6
ψ_o Location	For No. 11 and smaller diameter hooked bars: 1) Terminating inside column core with side cover ≥ 2.5 in. or 2) With side cover normal to plane of hook ≥6db	1.0
	Other	1.25
ψ_c Concrete strength	For $f'_c < 6000$ psi	$f'_c/15000+0.6$
	For $f'_c \geq 6000$ psi	1.0

Note:
1) Detailed coating condition in accordance with Table 25.4.2.5 of ACI 318-19.
2) s is minimum center-to-center spacing of hooked bars
3) A_{th} is total area of confining reinforcement
4) A_{hs} is total area of hooked bars being developed at a critical section

The equation considers different effects compared to the approach used in ACI 318-14 (2014). First, large bar diameters increase the required development length in a non-linear relationship. Further, the new equation takes the confining condition and bar spacing into account. For closely spaced hooked bars and under-confined hooks, a longer development length is required. The epoxy factor, however, remained unchanged.

2.3.2.2.2. AASHTO LRFD (2020)

Provisions of development length for hooked bars in tension in AASHTO LRFD (2020) are based on the analysis of NCHRP Report 603 and the method in ACI 318-14. The basic equation can be expressed as shown in Equation 2-11.

$$l_{dh} = \frac{38.0 d_b}{60.0}\left(\frac{f_y}{\sqrt{f'_c}}\right)\left(\frac{\lambda_{rc}\lambda_{cw}\lambda_{er}}{\lambda}\right) \qquad \textit{Equation 2-11}$$

in which the modification factors are summarized in Table 2-9

Table 2-9. AASHTO LRFD (2020) Modification factors for hooked bars in tension

Modification factor	Condition	Value of factor
λ_{rc} Reinforcement confinement factor	1) For No. 11 bar and smaller hooks with side cover normal to plane of the hook greater than 2.5 in. and for 90-degree hook with cover on the bar extension greater than 2.0 in. 2) For 90-degree hooks of No. 11 and smaller bars enclosed within ties or stirrups perpendicular to the bar being developed, spaced less than $3d_b$ along the l_{dh}; or enclosed within ties or stirrups parallel to the bar being developed along the bar extension, spaced not greater than $3d_b$. Both cases require the first tie of stirrup within $2d_b$ of the outside of the bend. 3) For 180-degree hooks of No. 11 and smaller bars enclosed within ties or stirrups perpendicular to the bar being developed, spaced less than $3d_b$ along the l_{dh}; the first tie of stirrup within $2d_b$ of the outside of the bend.	0.8
λ_{cw} Coating factor	For epoxy-coated reinforcement	1.2
λ_{er} Excess reinforcement factor	For anchorage or development where full yield strength is not required or provided reinforcement is in excess of required by analysis.	$\frac{\text{Required } A_s}{\text{Provided } A_s}$

It can be seen that the required development length of AASHTO LRFD (2020) for hooked bars in tension is similar to that of ACI 318-14. There exist basic equations and modification factors. However, AASHTO LRFD (2020) does not include the modification factor of concrete cover. Instead, concrete cover is required to be greater than 2.5 in.; otherwise, the factor λ_{rc} should not be applied.

2.3.2.2.3. Canadian Standard Association

Not explicitly stated, the method of calculating development length in CSA 23.4 for hooked bars in tension is similar to ACI 318-14 and AASHTO LRFD (2020). To be specific, CSA requires an equation of basic development length, l_{dh}, for hooked bars in tension with a yield strength of 400 MPa, as shown in Equation 2-12.

$$l_{dh} = 100\frac{d_b}{\sqrt{f'_c}} \qquad \textit{Equation 2-12}$$

Then required development length should be calculated by multiplying the basic development length to modification factors according to applicable conditions. The modification factors are summarized in Table 2-10.

Table 2-10. CSA modification factor of development length for hooked bars in tension

Condition	Value of factor
For bars with f_y other than 400MPa	$f_y/400$
For 35 M or smaller bars where the side cover is greater than 60 mm, and for 90-degree hooks where the cover on the bar extension is greater than 50 mm	0.7
For 35M or smaller bars where the hook is enclosed vertically or horizontally within three ties or stirrups spaced at least smaller of one hook diameter and $3d_b$	0.8
Anchorage of development for f_y is not required for reinforcement exceeding that required by analysis.	$\frac{\text{Required } A_s}{\text{Provided } A_s}$
For structural low-density concrete	1.3
For epoxy-coated reinforcement	1.2

2.3.2.2.4. fib Model Code for Concrete structure 2010

In *fib* Model Code, design of the development length for hooked bars can be determined with two steps. Firstly, design bar stress, f_{sd}, can be calculated by Equation 2-13.

$$f_{sd} = \alpha_1 f_{yd} - (F_h/A_s) \qquad \textit{Equation 2-13}$$

where α_1 is excess reinforcement ratio, F_h represents the force developed by the hook, and A_s is the cross-sectional area of the bar being considered. For a hook with a standard bend, the value F_h can be taken as Equation 2-14.

$$F_h = 60 f_{bd} A_s \qquad \textit{Equation 2-14}$$

where f_{bd} general design bond strength (see Section 6.1.3 of *fib* Model Code for more details). With determined values of f_{bd}, the required development length can be then determined using Equation 2-8.

2.3.3. Headed Bars (Mechanical Anchorage)

Headed bars provide an alternative approach to develop longitudinal reinforcement within beam-column joints or bent-to-column joints. Like hooked bars, the anchorage strength of headed bars consists of bearing strength of the head and the bond strength of the straight portion. The contribution of the head has potential to largely reduce needed development length of the reinforcement. Moreover, headed bars have no bar bends or extensions, occupying less space in the joints where they are anchored, and thereby congestion can be reduced. The attributes make headed bars promising to fully develop bar stress in such joints as a replacement of hooked bars. The application of headed bars can date back to nuclear construction for large bars in the 1960s to 1970s. As time goes by, the use of headed bars and number of studies are growing rapidly, along with the increasing use of high-strength material. In this section, studies of the anchorage of hooked bars are reviewed. Current design code provisions for headed bars are also included.

2.3.3.1. Applications in Beam-Column Joints

2.3.3.1.1. Park et al. (2003)

In the year of 2003, when design recommendations for headed bars were not well-established, Park et al. (2003) conducted a series of tests to investigate the effects of key parameters on the anchorage strength of headed bars. The parameters included bar diameters, head plate configurations, types of welding, compressive strength, and embedment length. The study also aimed to evaluate existing design recommendations such as ASTM A970-98 and ACI 349.

To accomplish the objectives, the authors developed 58 pull-out tests and 13 beam-like specimens. Four different shapes of heads were used, including square heads, rectangular heads, circular heads, and ecliptic heads. Welding methods of friction welding and general welding are also included as parameters. To fabricate a specimen, the authors pre-embedded a headed bar into concrete specimen supported on steel frames. A steel beam was used to provide self-reaction for the hydraulic cylinder to pull-out the headed bar. In the meantime, a load cell was used to measure the test load. The test setup is shown in Figure 2-16.

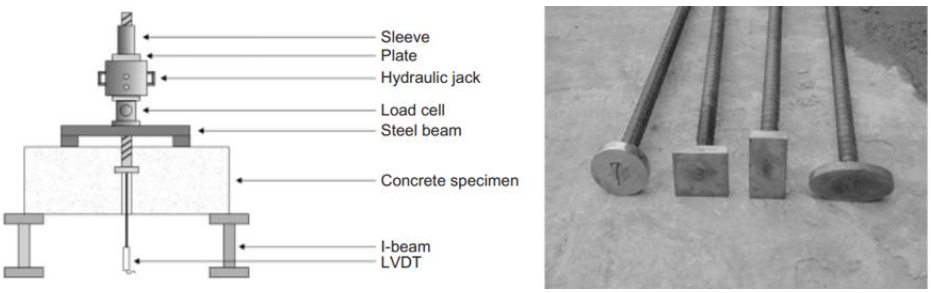

Figure 2-16. Test setup and specimens used in Park et. al (2003)

Test results revealed that headed bars had three primary failure modes: yielding or fracture of bars, concrete breakout, and pull-through failure. All the considered parameters more or less had effects on the anchorage capacity, and the existing design recommendations predicted the anchorage capacity with a safety margin. In addition, the angle of failed concrete cones was related to the configuration of the head, and circular heads seemed to provide higher efficiency than other shapes did. The author recommended that these factors should be taken into account in practice. This study opened discussions about these factors for more investigations.

2.3.3.1.2. Chun et al. (2007)

Not long after Park el al. (2003), Chun et al. (2007) investigated mechanical anchorage in exterior beam-column joints subjected to cyclic loading. Unlike the previously introduced studies, Chun et al. (2007) used actual specimens of beam-column joints rather than simulated ones. One of the primary objectives of the study was to evaluate design recommendations of ACI 352R-02 for RC beam-column joints reinforced with headed bars under load reversal. In addition, there was limited

experimental data to support the use of large-headed bars, multiple layers of reinforcement, or closely distributed reinforcement. Further, existing standards and provisions suggested that relatively large head sizes (nine times larger than the bar size) be used, which were thought to be impractical. The study was aimed to expand the knowledge domain of using headed bars, especially in beam-column joints under cyclic loads.

The authors developed two types of specimens: exterior beam-column joints and knee joints as shown in Figure 2-17. The specimens were tested under a displacement-controlled load intensified along with the number of cycles. Tests showed that bond deterioration occurred in the straight portion of headed bars as load increased. However, the deterioration did not inhibit the joint from developing flexural yielding. More importantly, a head with a bearing area three to four times the bar area was able to provide sufficient anchorage, substantially relaxing the previous requirement, namely nine times the bar area. Further, multiple layers of closely spaced headed bars that were designed using ACI 352R-02 performed well in the specimens. The study successfully expanded the application of headed bars in a more practical way in beam-column joints.

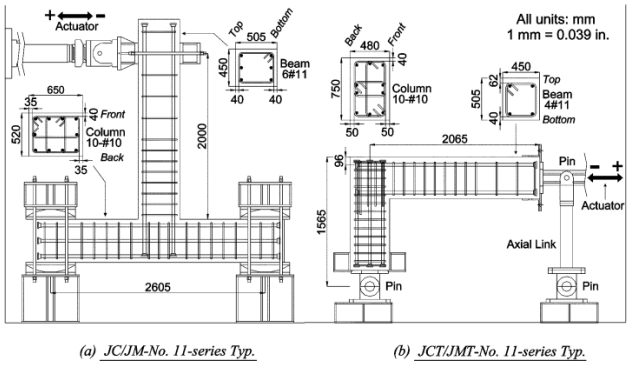

Figure 2-17. Test setup used in Chun et al. (2007)

2.3.3.1.3. Kang et al. (2010, 2011)

After Chun et al. (2007) suggested that requirements for using of headed bars be relaxed, Kang et al. (2010) further investigated more possible configurations and key parameters that affected the design of headed bars. In the study, the authors conducted pull-out tests and specimens of exterior beam-column joint under cyclic loads.

The experimental program had two phases. The first phase was to study headed bars with small heads. The effects of head shapes and head attaching techniques were also investigated. The test setup, as shown in Figure 2-18, was designed to apply cyclic lateral load and create flexural stresses into the headed longitudinal reinforcement. Before the actual cyclic tests, the authors conducted pull-out tests to investigate the load-slip behavior.

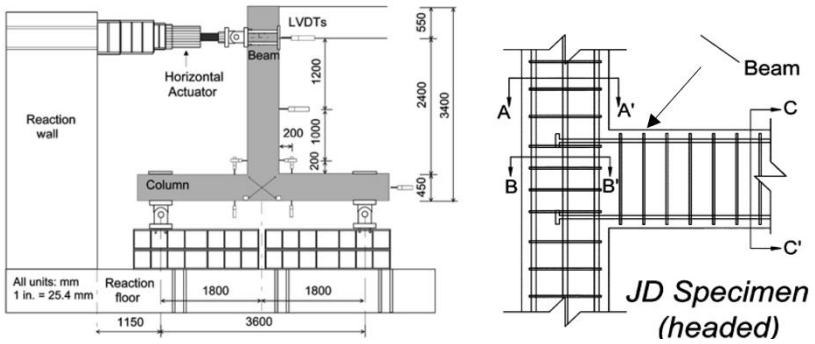

Figure 2-18. Test setup used in Kang et al. (2010)

Test results provided insights into the relationship between anchorage strength, head size, and embedment length. It was found that larger heads, unsurprisingly, exhibited higher anchorage strengths. Nevertheless, if the embedment length was long enough, small head sizes (at least 2.6 times the bar area) did not cause concrete breakout. With the observation, the authors recommended that anchorage of headed bars in exterior beam-column joints should be designed with a development length of 15db and a head size of 3 times bar area to guarantee ductile behavior.

Kang et al. (2011), with the same test setup, further investigated the behavior of closely spaced headed bars anchored in exterior beam-column joints. The study concluded that a clear bar spacing of approximately $2d_b$ could be allowed for headed bars under cyclic loading. The conclusion from both studies increased the use of headed bars with small heads and small bar spacing, which were not permitted in old versions of ACI 318 or ASTM A 970.

2.3.3.1.4. Chimire et al. (2019)

After the work of Kang et al. (2010, 2011), Ghimire et al. (2019) extended the coverage of headed bar study into high-strength material. In an extensive experimental program, Ghimire et al. (2019) tested more than two hundred specimens of simulated exterior beam-column joints (see Figure 2-19). Investigated parameters in the study included concrete compressive strength, embedment length, bar size, head size, bar spacing, and degrees of confinement. An important highlight was that the concrete compressive strength reached as high as approximately 16 ksi, and the highest bar anchorage stress was approximately 153 ksi.

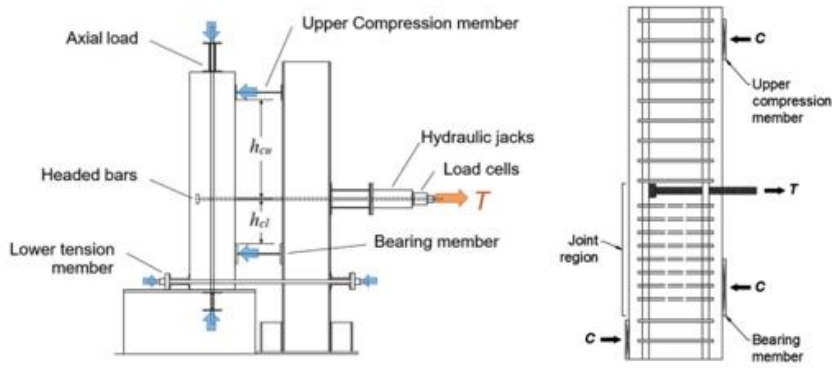

Figure 2-19. Specimen and test setup in Ghimire et al. (2019)

The failure modes observed include concrete breakout and side face blowout. In addition, back face blowouts were observed when closely spaced headed bars were used and no confining reinforcement was provided within the joint region. Test data also revealed that the current code requirements for headed bar spacing could be safely reduced.

A comparison between the test bar stresses at failure and the calculated anchorage strength based on ACI 318-14 (2014) indicated that the code-based estimation tended to be significantly conservative. However, the conservatism decreased when bar size or concrete compressive strength increased. As such, the code provisions were recommended to be modified to reflect the effects of concrete compressive strength, bar size, and confinement conditions. Further, concrete compressive strength was not found to contribute as much as previously believed. With the suggestions stated, the authors further conducted a parametric analysis in order to determine the degree of contribution of each parameter to the anchorage strength of headed bars. The study culminated with the development of an empirical equation for estimating the anchorage strength of headed bars, T_h, as shown in Equation 2-15.

$$T_h = \left(781 f_{cm}^{0.24} l_{eh}^{1.03} d_b^{0.35} + 48800 \frac{A_{tt}}{n} d_b^{0.88}\right)\left(0.0622 \frac{c_{ch}}{d_b} + 0.5428\right) \qquad \textit{Equation 2-15}$$

where f_{cm} is measured concrete compressive strength; l_{eh} is embedment length measured to the joint face to bearing face of the head; A_{tt} is total area of effective confinement within joint region; c_{ch} is center-to-center bar spacing. The equation became the basis for the code provisions for headed bars in ACI 318-19 (2019).

2.3.3.2. Applications in Beam-to-Column Joints

2.3.3.2.1. Matsumoto et al. (2001) and Brenes et al. (2006)

In early 2000s, TxDOT launched research projects to develop precast bent cap systems. There were two primary studies conducted by Matsumoto et al. (2001) and Brenes et al. (2006) at The University of Texas at Austin. Although the objects of the two projects were to develop precast

bent cap systems suitable for Texas, both projects investigated the anchorage strength of headed bars as connectors between a bent cap and a column, as well.

Pull-out test results conducted by Matsumoto et al. (2001) showed that regardless of straight bars or headed bars, the anchorage strength allowed the longitudinal column reinforcement to develop 1.25 times the yield stress when the embedment length was $13d_b$. When the embedment length was 8.5db, the headed bars developed 20% higher strength and larger ductility than the straight bars did. Based on the test results, the authors recommended a minimum embedment length of 13 times the bar diameter.

On the other hand, pull-out test results by Brenes et al. (2006) suggested that the minimum embedment length, $l_{e,min}$, should be calculated using Equation 2-16 regardless of the type of connectors.

$$l_{e,min} = \max\left\{\frac{\beta f_y d_b}{180\gamma\sqrt{f'_c}}, 8d_b, 12\text{ in.}\right\} \qquad \textit{Equation 2-16}$$

In Equation 2-16, β is the modification factor for duct material; and γ is the modification for group effect.

2.3.3.2.2. Papadopoulos et al. (2018)

Papadopoulos et al. (2018) tested three full-scale slab-column connections reinforced with headed bars (Figure 2-20) with the objective of investigating the effectiveness of headed bars in such connections under load reversals. In the study, head size was designed in accordance with ASTM A970, providing a bearing area of nine times the bar area, while bar size and embedment length varied.

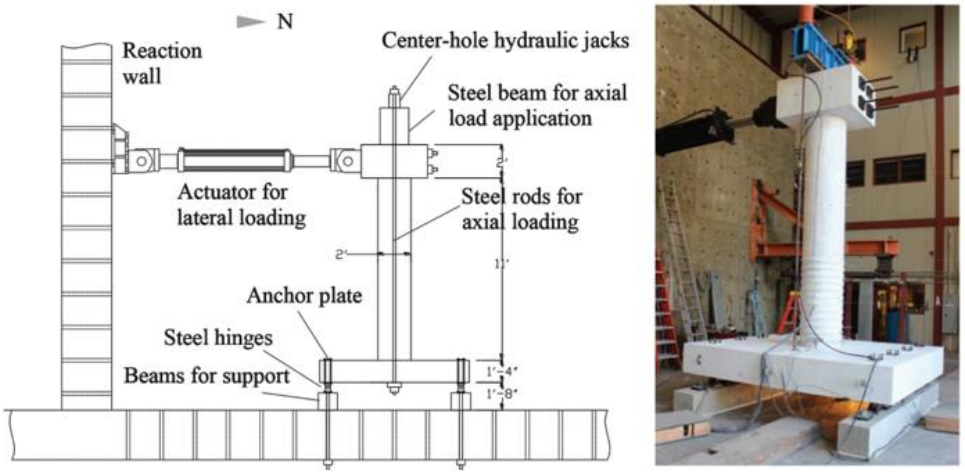

Figure 2-20. Specimen and test setup in Papadopoulos et al. (2018)

It was observed that a development length of $11d_b$ was adequate for the headed bar to develop satisfactory moment capacity and ductility of slab-column joints given a minimum of 2 in. of clear concrete cover. Finite element analyses further showed that a development length of $6.7d_b$ was sufficient if the concrete cover was between 4 in. to 6.5 in. During the tests, however, punching cracks on the back face were observed and additional tests would have been required to verify the design.

2.3.3.3. Standards and Code Provisions

2.3.3.3.1. ASTM A970-18

ASTM A970 "Standard Specification for Headed Steel Bars for Concrete Reinforcement" includes methods of producing headed bars, dimension requirements, and testing methods. The newest version of ASTM A970-18 was published in 2018. Important production and test methods are summarized here.

The standard provides three major fabrication methods for producing headed bars: welding, forging, and threading. For the overall geometry of the head, the purchaser has to specify the head diameter (for round heads), height, width, and thickness as illustrated in Figure 2-21. Alternative shapes are permitted if the purchaser agrees. Unlike older version of ASTM A970, which enforces the minimum head area relative to the bar diameter, ASTM A970-18 provides the purchaser with more flexibility.

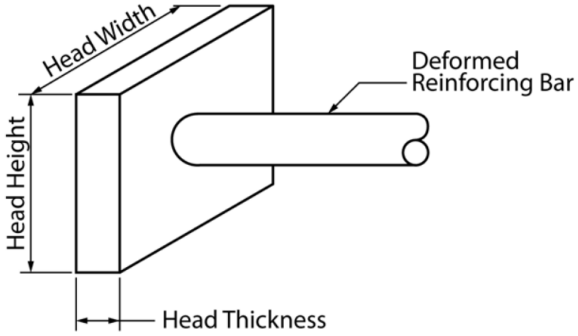

Figure 2-21. Schematic headed bars in ASTM A970-18

Regardless of the method and geometry specified by the purchaser, the performance of the headed bar should be tested by tensile testing and bend testing. Tensile testing requires the headed bar specimen to be at least 10 in. long with the head placed and well-supported in the tensile testing machine. The test tensile properties should conform to either of the following classes: a) developing the minimum specified tensile strength, or b) developing the minimum specified tensile strength and elongation. For bend testing, the headed bar needs to be bent at least 90 degrees without partial or total fracture of the bar, the head, and the head-to-bar connection.

2.3.3.3.2. ACI 318-25

In accordance with Section 25.4.4 of ACI 318-25 (2025), it is permitted to use headed reinforcement if the bar, the head, the arrangement of bars, and concrete conform to requirements on the material and geometry. First of all, the bar needs to be produced according to ASTM A970. The bar should not be larger than No. 11 and concrete should not be lightweight due to lack of experimental data. For the head, the bearing area is required not to be smaller than four times the bar area. There are also requirements for bar spacing and clear cover. Center-to-center spacing between bars has to be at least $3d_b$, and concrete clear cover for the bar should be at least $2d_b$.

With all requirements satisfied, headed bars should also fully develop the yield stress at a critical section by providing sufficient development length l_{dt}. According to Section 25.4.4.2, the value of l_{dt} can be calculated using Equation 2-17.

$$l_{dt} = \frac{f_y \psi_e \psi_p \psi_o \psi_c}{75\sqrt{f'_c}} d^{1.5} \qquad \textit{Equation 2-17}$$

In which the modification factors (ψ_e, ψ_p, ψ_o, and ψ_c) are summarized in Table 2-11. The calculated l_{dt} shall not be less than $8d_b$ or 6 in.

Table 2-11. ACI 318-19 modification factors for the development of hooked bars in tension

Modification factor	Condition	Value of factor
ψ_e Epoxy	Coated* reinforcement	1.2
	Uncoated or galvanized reinforcement	1.0
ψ_p Parallel tie reinforcement	For No. 11 and smaller bars with $A_{tt} \geq 0.3A_{hs}$ or $s \geq 6d_b$	1.0
	Other	1.6
ψ_o Location	For No. 11 and smaller diameter hooked bars: 1) Terminating inside column core with side cover ≥ 2.5 in. or 2) With side cover normal to plane of hook ≥6db	1.0
	Other	1.25
ψ_c Concrete strength	For $f'_c < 6000$ psi	$f'_c/15000+0.6$
	For $f'_c \geq 6000$ psi	1.0

Note:

- Detailed coating condition in accordance with Table 25.4.2.5 of ACI 318-19.
- A_{th} is total area of confining reinforcement parallel to bars being developed.

2.3.3.3.3. AASHTO LRFD (2020)

For the headed bars, current AASHTO LRFD (2020) allows the use of mechanical anchorage. It is also allowed to consider both the mechanical device and the embedment length when designing for developing bar stress.

2.3.3.3.4. Canadian Standards Association

Similar to AASHTO LRFD (2020), mechanical anchorage, including headed bar and headed studs, is allowed if tests demonstrate that is capable of developing the required strength. The development of reinforcement may consist of mechanical anchorage and embedment length. Nevertheless, standard details and design expressions are not included in CSA A23.3 (2019).

2.3.3.3.5. fib Model Code for Concrete Structures 2010

In the *fib* Model Code, headed anchorage is taken into consideration in three ways. The first one is to consider the head of headed bars a hook or a bend if the net projected area of the head equals that of a standard bend. Secondly, the capacity of the head has to be able to develop the bar without the contribution from bond along the straight portion. Otherwise, anchorage capacity of headed bars may be determined by test. Regardless of which one of the three conditions is considered, the embedment length should be long enough to avoid a highly-stressed region. Other than the three conditions, the *fib* Model Code does not provide further details, nor design expressions.

2.4. Retrofitting Strategies

In this chapter, general retrofitting techniques available for the bent-to-column connections are presented. The performance of RC joints has been considered as a significant factor as it affects the overall behavior of the structure. Moreover, bar slip occurs in RC joints due to inadequate anchorage of longitudinal bars or strain penetration. Therefore, strengthening the RC joints plays a crucial role for the global stability of the frames. Additionally, under extreme events, bent-to-column connections are vulnerable due to the increased moment and ductility demands. Yet, those effects on bent-to-column connections are not considered in current Texas design practice. In order to enhance the capacity of the bent-to-column joints, the retrofitting strategies that have been used include concrete jacketing of the joint region, strengthening with fiber-reinforced polymer (FRP) composite applications, steel jacketing of the connection, externally applied reinforcement, and prestressing. In the literature, an insufficient amount of research has been directed toward the retrofit for severe scouring or loss of supports due to the vehicular collision. Even though most of the techniques have been carried out for seismic retrofit, they can also be applicable to improve the performance of bent-to-column connections under the extreme events.

2.4.1. Application for RC Jacketing

Concrete jacketing is one of the most common strengthening methods for structural elements including RC joints. New concrete with new longitudinal and transverse reinforcement is placed in a new joint region by encasing the existing joint area. The required reinforcement to satisfy the load path mechanism is put in the jacket and it is connected to the existing section using dowels. Prior to jacketing, the surface of the existing joint should be roughened for bonding. In a field application in Tennessee, a bent cap in a bridge was retrofitted using concrete jacketing as shown in Figure 2-22.

Figure 2-22. Concrete encasement of a bent cap in Tennessee (Wright et al. (2011))

As the joint region becomes larger, the development length increases and the critical section for moment capacity shifts to the edge of the jacket. Additionally, as the thickness of the joint increases, the joint stress values decrease. One of the main disadvantages of the RC jacketing is that it increases the dimensions and mass that alters the dynamic properties. Moreover, changed dynamic properties can lead to increased demands in a location where it is not expected, so the structural analysis might be required to be conducted again.

The study performed by Thewalt and Stojadinovic (1995) tested an outrigger knee joint specimen with concrete jacketing as a retrofitting strategy. Two as-built specimens, one with a short and one with a long outrigger beam, were constructed and subjected to a horizontal loading quasi-static manner. Brittle failure was observed in both as-built specimens. At the end of the retrofitted specimen with a post-tensioned concrete jacket experiment, the joint region remained intact and only a few cracks appeared while the plastic hinge formed in the column. It was concluded RC jacketing to be an effective way, as the strength and ductility improved under the cyclic loading.

To overcome the increase in the size of the joint problem, a thin RC jacketing with small diameter reinforcement technique for beam-column joints is proposed by Karayannis et al. (2007) with two types of retrofit scheme including the light reinforcement and dense reinforcement jackets. It showed enhancement in the capacity, and energy dissipation in the experimental tests and the

cracking modes changed from brittle failure to ductile failure modes. Yet, it has been suggested as a successful repair technique for the jacketing with light reinforcement due to the damage level observed in retrofitted specimens, while for the jacketing with dense reinforcement, it could be a potential use of strengthening method.

2.4.2. Application for Steel Jacketing and External Steel Elements

To improve the strength and ductility of the joint, the region can be encased by placing steel plates around the joint region. The space between the plate and the existing joint region is generally filled with grout. Typically, steel parts are mechanically anchored to concrete to provide confinement. An example of the application of steel encasement in Missouri is depicted in Figure 2-23. Disadvantages of this type of arrangement include the potential for corrosion, and difficult installation of the heavy steel plates. However, construction time is much less compared to the RC jacketing application.

Figure 2-23. Steel jacketing application on a bent cap in Missouri (Wright et al. (2011))

Thewalt and Stojadinovic (1995) tested a specimen with the addition of steel plates connected by through-bolts to the beam and a curved steel plate on the exterior face of the joint resulted in improved ductility and high capacity as intended. The authors suggested that steel plate solution could be preferred to concrete jacket solution as it is easier to construct than the post-tensioned reinforced concrete upgrade.

Chen et al. (2005) investigated a typical column and bent cap assembly in the state of Alaska that includes large column reinforcement ratio. As this configuration likely leads to plastic hinge formation in the bent cap prior to formation in the column, the seismic performance needs to be improved. Therefore, a strengthening solution was proposed to ensure that bent cap and joint regions remain elastic while the column reaches its ultimate capacity. The retrofitting includes the use of a nail-jointed thin steel sheet wrapping the column for the desired ductility level and shear strength and steel plates in the bent cap at both sides of the column welded with two diagonal brace members in the joint region as shown in Figure 2-24. Using this scheme, under cyclic loading, a

ductile behavior was attained, and the steel plates in the joint region prevented the widening of the shear cracks in the joint region.

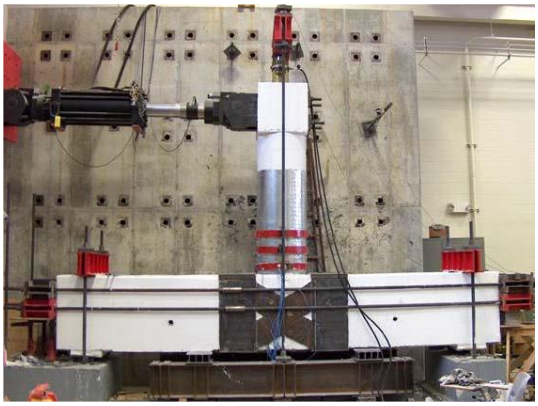

Figure 2-24. External steel element application to column and bent cap subassembly (Chen et al. (2005))

A study performed by McLean and Shattarat (2005) aimed to develop a retrofitting strategy for outrigger knee joint systems. Seven knee joint specimens were tested under seismic in-plane and out-of-plane loading. Shear cracks in joint region were observed in the as-built specimens under in-plane loading at a low displacement level. The retrofit solution consisted of an elbow-shaped steel jacket around the beam and the joint as shown in Figure 2-25. The retrofitted specimens exhibited more ductile behavior with a minimum ductility level, defined as the maximum achieved displacement divided by the yield displacement, of 5, as opposed to the as-built specimen with a ductility level in the range of 2.0 to 2.8, and enhanced energy dissipation. In the out-of-plane direction loading, twice the capacity of the as-built specimen was achieved due to the jacket.

To overcome one of the main deficiencies found in bent caps, i.e., insufficient shear reinforcement, externally applied shear reinforcement is one of the most common ways to increase the strength in the bent caps. In this technique, steel plates are placed on the top and bottom of the bent cap and they are connected using shear reinforcement as explained in Wright et al. (2011). By implementing external shear reinforcement, increased shear demand during earthquakes was expected to be resisted.

Figure 2-25. A specimen with elbow-shaped steel jacketing around the beam and joint (McLean and Shattarat (2005))

2.4.3. Application for FRP Composites

FRP composites have been increasingly utilized as a strengthening technique in RC joints as it offers several advantages over its alternatives, e.g., steel jacketing, concrete jacketing, etc., such as fast and easy installation, high strength-to-weight ratio, corrosion resistance, and no significant increase in member sizes. Yet, there are some drawbacks including the high cost of the material. Furthermore, to ensure a good bond between the concrete and the FRP composite, the surface of the concrete needs to be thoroughly cleaned. FRP application can enable the joint region to have improved shear capacity, flexural capacity, ductility, and confinement depending on the goal of the conducted study. Additionally, studies have shown that it is most effective in the joint region when the fibers are placed ±45-degree to the direction of principal planes so that the debonding of the FRP sheets are delayed and higher strains are reached.

Gergely et al. (2000) showed that the shear capacity of the RC joints can be increased by bonding carbon FRP (CFRP) sheets to the concrete surface and the overall damage control can be improved. In another study conducted by Pantelides et al. (2001a), deficiencies in the column bent cap assembly include insufficient confinement of the column lap-splice region, and plastic hinge region, inadequate shear strength of columns, lack of hoops in joint region, and insufficient anchorage of column longitudinal reinforcement to bent cap. CFRP composite, therefore, was applied to the column where the confinement is inadequate as shown in Figure 2-26. The FRP composite U-strap was also implemented to improve column bar anchorage into the joint and it prevented pullout of the longitudinal reinforcement from the joint, thus it was concluded that this technique could be a useful method as it improves the performance of the bent-to-column joints.

Moreover, ankle wrap concept was introduced to restore the joint shear strength. At the end of the tests conducted, displacement ductility of the retrofitted bent was 2.25 times of the as-built which was the aim of the study. Moreover, the maximum shear strain in the joints was approximately 4 times the strain observed in as-built specimen, and the principal tensile stress of the joint was 37% higher than the as-built joint.

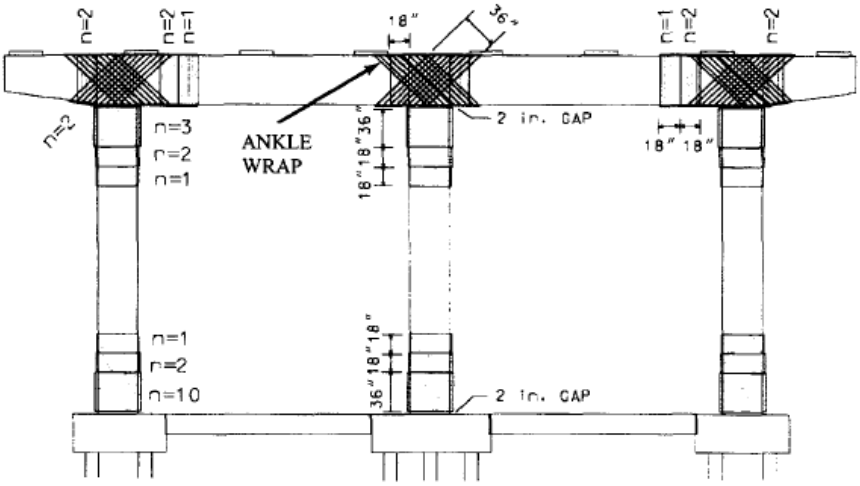

Figure 2-26. FRP composite layout in in the column and joints (Pantelides et al. (2001a))

Chen et al. (2005) also investigated the bent-to-column joints behavior using CFRP jacketing, and additionally, glass FRP (GFRP) anchors were used in an attempt to aid the development of mechanical bond between the CFRP sheets and concrete. They concluded that it provides adequate joint shear strength and the CFRP sheets prevent the cracks from further developing.

Another study by Silva et al. (2007) compared two testing units, one of them was strengthened using CFRP sheets after the onset of column shear failure was reached, while the second unit with a similar retrofitting scheme was strengthened prior to the testing. Unlike the first unit, in the second unit, GFRP anchors were also used in the joint region as illustrated in Figure 2-27 as this technique has shown to be effective in postponing the peeling of CFRP sheets. Overall, two units exhibited enhanced capacity and ductility, yet the second unit displayed more energy absorption with less pinching, and more ductile response. Importantly, retrofitting the undamaged joint was found to be successful in preventing joint shear failure.

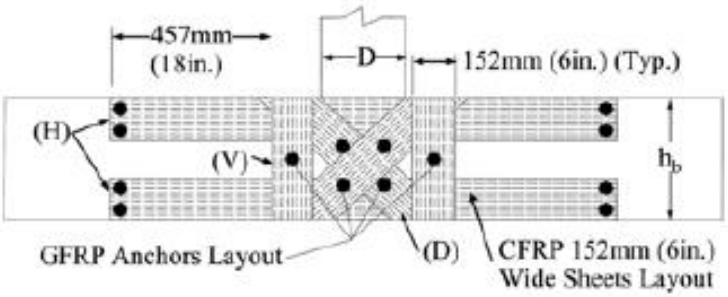

Figure 2-27 CFRP and GFRP anchor locations and application (Silva et al. (2007))

2.4.4. Strengthening Bent Caps using Prestressing

Applying an initial compressive strength in the bent caps is a way to enhance the capacity of the bent beams. As discussed in Priestley et al. (1996), prestressing tendons are placed in the ducts to improve the strength of the bent cap. Possible diagonal cracking in joint region is also reduced and anchorage strength of column longitudinal reinforcement is enhanced. Another way is to achieve that is to use posttensioned bars along both sides of the bent cap.

Several studies have also shown that prestressing can be a remedy of reinforcement congestion problem in joint region as well as improve the strength and stiffness of existing structure. Lowes and Moehle (1995) performed tests by retrofitting pre-1960's bridge connections. As-built specimen performed poorly with low ductility, and overall joint failure. The cap beam was widened, and post-tensioning rods were mounted. Even though no additional transverse reinforcement was placed, the joint was effectively confined owing to post-tensioning.

An experimental study conducted by Vasseghi et al. (2015) investigated the effectiveness of the longitudinal and transverse prestressing on the seismic performance. A specimen that is a portion of a bent with three columns was tested both as-built and as retrofitted with external prestressing along the cap beam, as well as transverse prestressing of one of the exterior joints as shown in

Figure 2-28. At the end of the test of the as-built specimen, the joint experienced severe damage along with slippage of column longitudinal reinforcement and concrete cracking on top of the cap beam was observed. No damage was observed at the exterior joint which is prestressed in both directions, and the associated column failed due to buckling and fracture of the longitudinal rebar after the plastic hinge formation. Due to prestressing of the cap beam along with transverse prestressing of an external joint, the strength as well as the ductility improved.

Figure 2-28. Retrofitted specimen with external prestressing along the cap and transverse prestressing at one external joint by Vasseghi et al. (2015)

2.4.5. Retrofit Scheme Proposed by Lubiewski et al. (2006)

The study conducted by Lubiewski et al. (2006) developed a retrofit strategy for the bent-to-column joints in Alaska bridges to increase the displacement ductility in an earthquake event in three phases. First, the longitudinal reinforcement in the column was reduced to a reinforcement ratio below 4% to avoid excessive amount of reinforcement in the joint area as suggested by Priestley et al. (1996). As such, the reinforcement ratio of the column longitudinal bars tested was reduced from 6.1% to 3.7% by cutting the bars. Second, to restore the flexure capacity of the bent cap, additional longitudinal reinforcement was added to the bent cap by increasing the width of the bent cap to install them. In the third phase, to ensure the composite action between the retrofit section and the existing section, headed bars were placed as shown in Figure 2-29. The experimental results showed that this retrofit scheme could reduce the damage in the bent cap and increase the ductility to the aimed level.

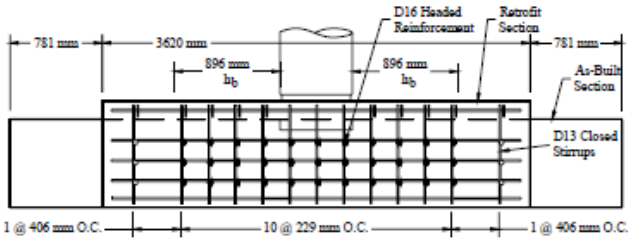

Figure 2-29. The reinforcement layout of the retrofitted specimen

2.5. Summary

In Texas, bent-to-column connection design has long used a very simple type of detail. The details do not include joint confinement or proper anchorage of column longitudinal reinforcing bars. Although the evaluation showed that the standard design had sufficient development length for developing the nominal flexural capacity, such a simple detailing technique appears to be questionable when sujected to various extreme events. It is imperative that the details be improved to accommodate potential high moments and shear demands.

To achieve the objective, relevant past studies categorized into four topics were reviewed and summarized in this chapter. Extreme events, including collisions and severe scouring, have frequently occurred in bent structures and affected the design of bent-to-column connections. It has been demonstrated experimentally and numerically that such extreme events substantially increase moment, shear, and ductility demands in bent-to-column connections.

Strategies that improve the detail of bent-to-column connections were reviewed, including joint confinement and bar anchorage. It has been acknowledged that appropriate joint confinement effectively improves behavior. Common approaches to confining the connections include crossties, spirals, and concrete jackets. It was also found that transverse headed reinforcing bars happened to improve joint confinement. All the mentioned methods were shown to be effective. However, in some cases where headed bars were used, joint confinement was not effective in improving the behavior. In addition to joint confinement design, types of bar anchorage were also reviewed. Widely accepted methods include straight bars, hooked bars, and headed bars. Representative studies and code provisions were included in the review.

Finally, commonly used retrofitting methods for bent-to-column connections were reviewed and presented. In the field, applications of sectional enlargement and steel jackets have been utilized and proven to be effective. FRP wrappings were also tested and found effective in absorbing energy from seismic loads and enhancing ductility. In addition to protecting the connections, external post-tensioning was found to strengthen multi-column bent structures.

Chapter 3. Structural Analysis for Extreme Events

In recent years, with the occurrence of various extreme loading events, it became evident that the details provided in the current TxDOT standard designs require further investigation. Multi-column bents can potentially be exposed to floods, vehicular collisions, and loss of support. In these situations, bent-to-column joints are no longer transferring only axial loads, and joint flexural and shear behavior become essential. Column bars in tension are likely required to develop their yield strength and the joint needs to be well-confined to prevent premature failure. The current TxDOT standard designs of bent-to-column joints do not consider these mechanisms and potentially require improvement.

Moreover, although the consideration of extreme loading events is mentioned in design codes and design manuals, existing methods are oversimplified and inconsistent. When designing for vehicular collision, the TxDOT bridge design manual suggests only shear forces in the impacted column to be considered, neglecting moment demand and transfer to other members. However, in AASHTO LRFD, flexural behavior is an important factor in design. Regarding loss of a support, both documents remain silent on detailed approaches of analysis or design. Following the literature review, this section presents the analysis of multi-column bents under extreme event analysis, and establishes the foundation of plastic design concept.

3.1. Overview

A framework was developed for the analysis of multi-column bents subjected to extreme events, organized as a workflow chart as shown in Figure 3-1. First, it should be determined if the multi-column bent is located in a flood-potential region or a vehicular collision-intense region. In the case of flood risk, it is recommended to consider lateral load induced by the stream (introduced in Section 3.3) and scouring. If the column is at risk of scouring, the designer may proceed to conduct analysis for the loss-of-a-support scenario (introduced in Section 3.5). If vehicular collision is considered, the designer is advised to follow the steps introduced in Section 3.4 to determine if the bent-to-column connection and the column have sufficient resistance.

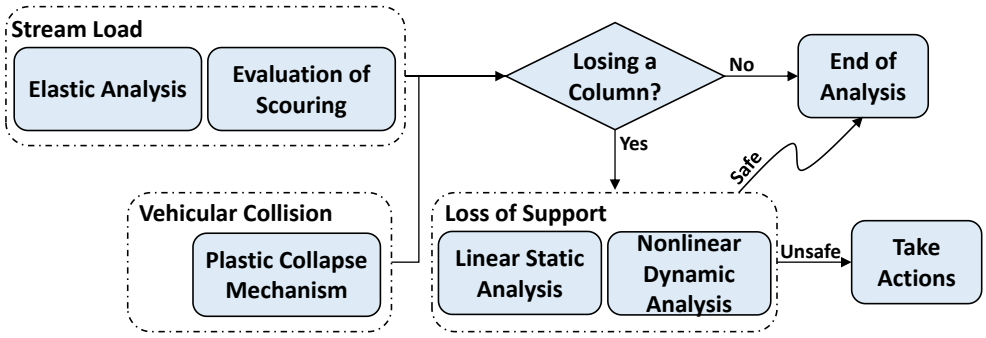

Figure 3-1. Framework of extreme event analysis

3.2. Configurations of Multi-Column Bents under Consideration

In theory, an infinite number of structural configurations of multi-column bents can be designed and constructed. However, it is not pragmatic, nor possible to exhaust all types of multi-column bents. As such, the research team identified, and analyzed representative configurations. Consulting with TxDOT, two commonly used configurations from the TxDOT Bridge Design Manual were studied.

The selected configurations included three-column bents with four girder lines [see Figure 3-2 (a)] and four-column bents with six girder lines [see Figure 3-2 (b)]. For each of the cases, the columns were evenly spaced, and so were the girder lines. As shown in the figure, the centerline of the first column is located at distance L_1 away from the edge and the column spacing is L_2. Similarly, the first girder line is located at L_{g1} away from the edge and the girder spacing is L_{g2}. The clear height of the multi-column bents under consideration is denoted as H.

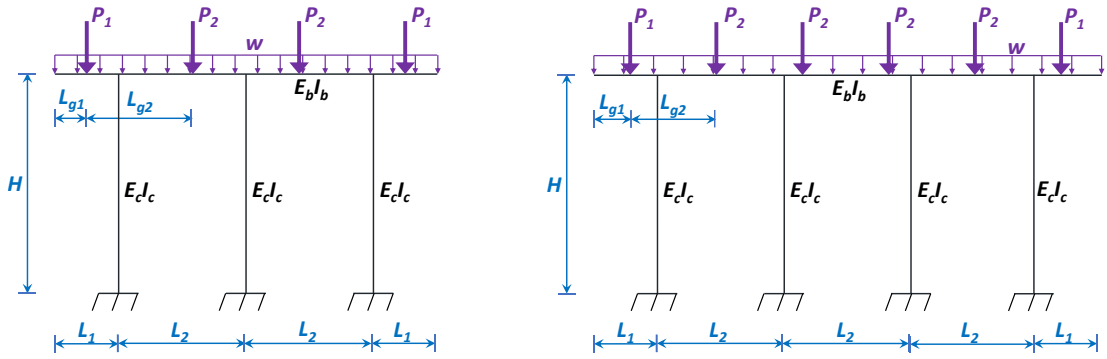

(a)Three-column bent model (b) Four-column bent model

Figure 3-2. Structural model of multi-column bents under consideration

All columns are assumed circular with the same cross-section; namely the same diameter (D_c) and the same reinforcement configuration. The bent is rectangular with cross-sectional dimensions of b and h. The bent longitudinal reinforcement consists of top and bottom rebars. The numbers of top reinforcing bars and of bottom reinforcing bars are not necessarily equal. With the assumed dimensions, the area of the columns and the bent (A_c and A_b) and the second moment of inertia the columns and the bent (I_c and I_b) can be determined. Moreover, the elastic moduli of concrete for the columns and the bent (E_c and E_b) are needed for the following analysis.

Loads, depending on the location, have two magnitudes, denoted as P_1 and P_2, shown in Figure 3-2. The load P_1 is applied to the exterior spans while the load P_2 is applied to the interior spans. This assumption was based upon the fact that symmetric load distribution is often used in structural design. In addition to girder loads, the self-weight of the bent is considered and assumed as an evenly distributed pattern load, w. The self-weight of the columns is neglected for simplicity.

Two types of boundary conditions are considered for the column-to-bent connections; one is pinned connection, and the other is rigid connection. The pinned connection is intended to simulate poorly detailed bent-to-column connections through which moments cannot transmitted. It should be noted that simple connection is also assumed in the CAP 18 software for bent cap design. On the other hand, rigid connection is assumed for well-detailed bent-to-column connections. All column bottoms are assumed fixed.

3.3. Structural Analysis for Stream Load

With the base structural models of multi-column bents, loads induced by floods are then superpositioned to determine demands to the each of the members. According to AASHTO LRFD, water load can be modeled as an evenly distributed pressure acting on the front face of the structure. The magnitude of the pressure can be calculated using Equation 3-1.

$$p = \frac{C_D V^2}{1000} \qquad \textit{Equation 3-1}$$

where p is pressure of flowing water (ksf); C_D is drag coefficient; and V is design velocity of water (ft/s). The calculated pressure is applied to the first column of the structure over a specified water depth (h), as shown in Figure 3-3. The magnitude (q) of the evenly distributed load is the pressure times the diameter of the column ($q=pD_c$). It should be noted that the debris raft effect suggested in AASHTO LRFD is not considered here.

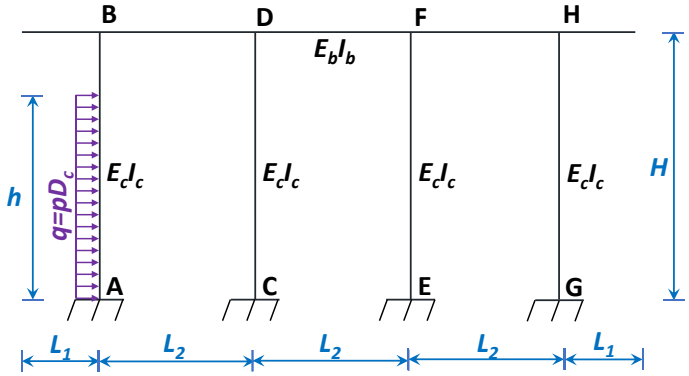

Figure 3-3. Flowing water load represented as distributed load on the first column

With all the structural properties and load information known, it is possible to construct an elastic structural matrix analysis for the structure in Figure 3-3, which can be generally expressed as Equation 3-2, in which $[P]$ is the generalized external force matrix; $[K]$ is the stiffness matrix; $[\Delta]$ is the generalized displacement matrix; and $[P^F]$ is the generalized fixed-end force matrix.

$$[P] = [K][\Delta] + [P^F] \qquad \textit{Equation 3-2}$$

For three-column bents with rigid connections, four degrees of freedom are identified, including rotations at node B, D, and F (θ_B, θ_D, θ_F) and the horizontal displacement of the bent cap (Δ_B). Per

the identified degrees of freedom, the stiffness matrix is a four-by-four matrix. The distributed load q, is transformed into a fixed-end moment (M_B^F) and a fixed-end force (R_B^F) acting at the node B. The final matrix form of three-column bents can be expressed as Equation 3-3.

$$\begin{bmatrix}0\\0\\0\\0\end{bmatrix}=\begin{bmatrix}\frac{4E_cI_c}{H}+\frac{4E_bI_b}{L_2} & \frac{2E_bI_b}{L_2} & 0 & \frac{-6E_cI_c}{H^2}\\ \frac{2E_bI_b}{L_2} & \frac{4E_cI_c}{H}+\frac{8E_bI_b}{L_2} & \frac{2E_bI_b}{L_2} & \frac{-6E_cI_c}{H^2}\\ 0 & \frac{2E_bI_b}{L_2} & \frac{4E_cI_c}{H}+\frac{4E_bI_b}{L_2} & \frac{-6E_cI_c}{H^2}\\ \frac{-6E_cI_c}{H^2} & \frac{-6E_cI_c}{H^2} & \frac{-6E_cI_c}{H^2} & \frac{36E_cI_c}{H^3}\end{bmatrix}\begin{bmatrix}\theta_B\\ \theta_D\\ \theta_F\\ \Delta_B\end{bmatrix}+\begin{bmatrix}M_B^F\\0\\0\\R_B^F\end{bmatrix} \quad \textit{Equation 3-3}$$

In Equation 3-3,

$$M_B^F=\frac{qh}{H^2}\left[\left(\frac{h}{2}\right)^2\left(H-\frac{h}{2}\right)+\frac{h^2}{12}\left(2H-\frac{3}{2}h\right)\right] \quad \textit{Equation 3-4}$$

$$R_B^F=\frac{-qh}{H^3}\left[\left(3H-\frac{h}{2}\right)\left(\frac{h}{2}\right)^2-\frac{h^2}{4}(h-H)\right] \quad \textit{Equation 3-5}$$

If the bent-to-columns connections are assumed to be pinned, the degree of freedoms can be reduced to one, the horizontal displacement of the bent cap (Δ_B), as moments at nodes B, D, and F are assumed zero. The structure can be treated as three cantilever beams deforming together. In this case, the matrix form of the structure is as shown in Equation 3-6 through Equation 3-8.

$$[0]=\left[\frac{9E_cI_c}{H^3}\right][\Delta_B]+[R_{B2}^F] \quad \textit{Equation 3-6}$$

where

$$R_{B2}^F=-\frac{M_A^F-\frac{1}{2}M_B^F+\frac{1}{2}qh^2}{H} \quad \textit{Equation 3-7}$$

$$M_A^F=-\frac{qh}{H^2}\left[\frac{h}{2}\left(H-\frac{h}{2}\right)^2+\frac{h^2}{12}\left(\frac{h}{2}-H\right)\right] \quad \textit{Equation 3-8}$$

For four-column bents with rigid connections, similar procedures of constructing the matrix form are applied. In this case, five degrees of freedoms are identified, including rotations at node B, D, F, and H (θ_B, θ_D, θ_F, and θ_H) and the horizontal displacement of the bent cap (Δ_B). The final matrix form of three-column bents can be expressed as Equation 3-9.

$$\begin{bmatrix}0\\0\\0\\0\\0\end{bmatrix}=\begin{bmatrix}\frac{4E_cI_c}{H}+\frac{4E_bI_b}{L_2} & \frac{2E_bI_b}{L_2} & 0 & 0 & \frac{-6E_cI_c}{H^2}\\ \frac{2E_bI_b}{L_2} & \frac{4E_cI_c}{H}+\frac{8E_bI_b}{L_2} & \frac{2E_bI_b}{L_2} & 0 & \frac{-6E_cI_c}{H^2}\\ 0 & \frac{2E_bI_b}{L_2} & \frac{4E_cI_c}{H}+\frac{8E_bI_b}{L_2} & \frac{2E_bI_b}{L_2} & \frac{-6E_cI_c}{H^2}\\ 0 & 0 & \frac{2E_bI_b}{L_2} & \frac{4E_cI_c}{H}+\frac{4E_bI_b}{L_2} & \frac{-6E_cI_c}{H^2}\\ \frac{-6E_cI_c}{H^2} & \frac{-6E_cI_c}{H^2} & \frac{-6E_cI_c}{H^2} & \frac{-6E_cI_c}{H^2} & \frac{48E_cI_c}{H^3}\end{bmatrix}\begin{bmatrix}\theta_B\\ \theta_D\\ \theta_F\\ \theta_H\\ \Delta_B\end{bmatrix}+\begin{bmatrix}M_B^F\\0\\0\\0\\R_B^F\end{bmatrix} \qquad \textit{Equation 3-9}$$

Similarly, if the columns have a pinned connection to the bent cap, the matrix form can be reduced as one degree of freedom with a stiffness equivalent to four cantilever beams, as shown in Equation 3-10.

$$[0]=\left[\frac{12E_cI_c}{H^3}\right][\Delta_B]+[R_{B2}^F] \qquad \textit{Equation 3-10}$$

Solving Equation 3-3, Equation 3-6, Equation 3-9 or Equation 3-10, depending on the structural configuration, delivers deflection and rotation at each node, namely the deformation matrix. Therefore, the moment and shear demands induced by flooding loads can be determined by applying the local structural matrix of the considered member. For the front column with rigid connections, the demands can be determined using Equation 3-11. For other columns with rigid connections, the demands can be determined using Equation 3-12. Notations are defined as shown in Figure 3-4.

$$\begin{bmatrix}V_{bot}\\M_{bot}\\V_{top}\\M_{top}\end{bmatrix}=\frac{E_cI_c}{H}\begin{bmatrix}\frac{12}{H^2} & \frac{-6}{H} & \frac{-12}{H^2} & \frac{-6}{H}\\ \frac{-6}{H} & 4 & \frac{6}{H} & 2\\ \frac{-12}{H^2} & \frac{6}{L} & \frac{12}{H^2} & \frac{6}{L}\\ \frac{-6}{H} & 2 & \frac{6}{H} & 4\end{bmatrix}\begin{bmatrix}0\\0\\\Delta_B\\\theta_B\end{bmatrix}+\begin{bmatrix}R_A^F\\M_A^F\\R_B^F\\M_B^F\end{bmatrix} \qquad \textit{Equation 3-11}$$

$$\begin{bmatrix}V_{bot}\\M_{bot}\\V_{top}\\M_{top}\end{bmatrix}=\frac{E_cI_c}{H}\begin{bmatrix}\frac{12}{H^2} & \frac{-6}{H} & \frac{-12}{H^2} & \frac{-6}{H}\\ \frac{-6}{H} & 4 & \frac{6}{H} & 2\\ \frac{-12}{H^2} & \frac{6}{H} & \frac{12}{H^2} & \frac{6}{H}\\ \frac{-6}{H} & 2 & \frac{6}{H} & 4\end{bmatrix}\begin{bmatrix}0\\0\\\Delta_B\\\theta_B\end{bmatrix} \qquad \textit{Equation 3-12}$$

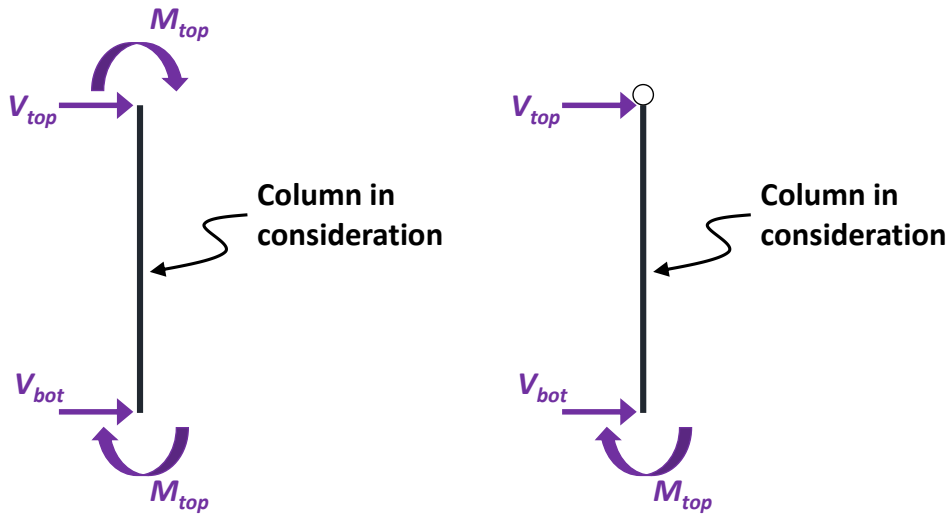

(a) Column with rigid connections (b) Column with a pin connection on top

Figure 3-4. Definition of notations of demands to a column

On the other hand, if the considered column has a pinned connection on the top, the demands are calculated using Equation 3-13, regardless of the front column or the other columns.

$$\begin{bmatrix} V_{bot} \\ M_{bot} \\ V_{top} \end{bmatrix} = \begin{bmatrix} \frac{-3E_cI_c}{H^3} \\ \frac{-6E_cI_c}{H^2} \\ \frac{3E_cI_c}{H^3} \end{bmatrix} [\Delta_B] \qquad \text{Equation 3-13}$$

It should be noted that gravity loads and girder loads are not included, as moments and shear at bent-to-column connections induced by those vertical loads are considered minor compared to the stream load. For simplicity, it is acceptable to only take lateral water load to calculate the demands. Moreover, compared to the other two extreme events considered in the current project, the stream load was found to cause negligible effects on multi-column bents, which will be discussed in Section 3.6.2.

3.4. Analysis of Vehicular Collision

Similar to the analysis for stream load, vehicular collision load is superpositioned onto the base multi-column bent structural model, as shown in Figure 3-5. The height and the magnitude of the lateral collision load are denoted as *h* and *P* for generality.

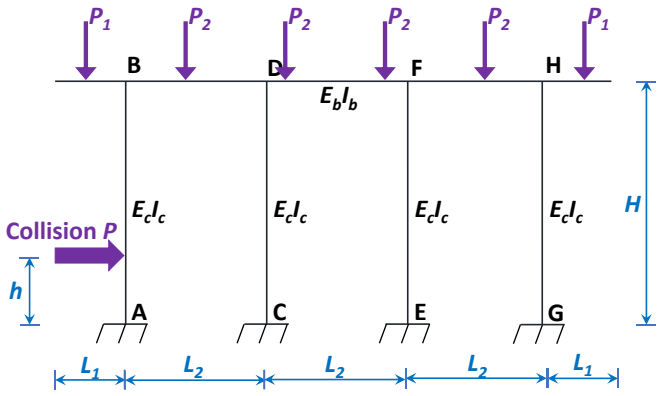

Figure 3-5. Structural model of multi-column bent under collision load

Unlike stream load, vehicular collisions generate considerable moments and shear forces at the point of collision and both ends of the impacted column. Elastic structural analysis is no longer valid because members are expected to exhibit nonlinear, plastic behavior. Also, applying elastic structural analysis solely will lead to impractical high demands for design. As such, it is recommended to employ the plastic design concept based on the upper bound theory of plasticity.

The step-by-step procedure of using the recommended approach is shown as the flowchart in Figure 3-6. After selecting a target multi-column bent, structural parameters and gravity loads have to be input first. The needed parameters are introduced in previous section. The following subsections will introduce the remainder of the steps in detail.

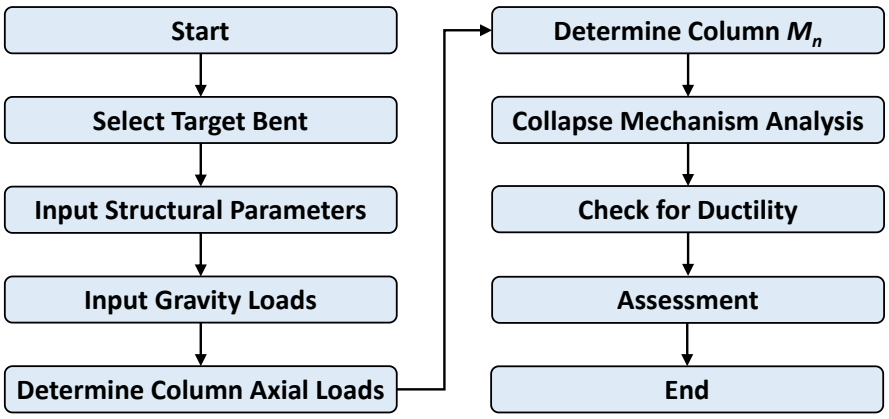

Figure 3-6. Flowchart of analysis for vehicular collision

3.4.1. Determine Column Axial Load

Column axial loads affect the plastic moment capacity of the columns, which is one of the essential design parameters for plastic design. The column axial loads in this case can be determined using elastic structural matrix analysis. The full stiffness matrix of the bents under consideration, however, includes too many degrees of freedom and can be overly complicated for decomposition.

It is suggested that the structure be simplified according to symmetry and equivalent boundary conditions. In other words, only half of the structure needs to be accounted for, and the columns can be considered a pinned rotational spring with a rotational stiffness of $4E_cI_c/H$. Furthermore, loads on the overhang can be transformed into a point load and a moment above the exterior column (namely exterior pinned rotational spring). After the simplification, three-column bents become a beam with one end fixed and the other end supported by a pinned rotational spring as shown in Figure 3-7(a); four-column bents become a beam with two pinned rotational springs and a "slider" support on the other end as shown in in Figure 3-7(b). The reaction at point A in the figure is the target column axial load.

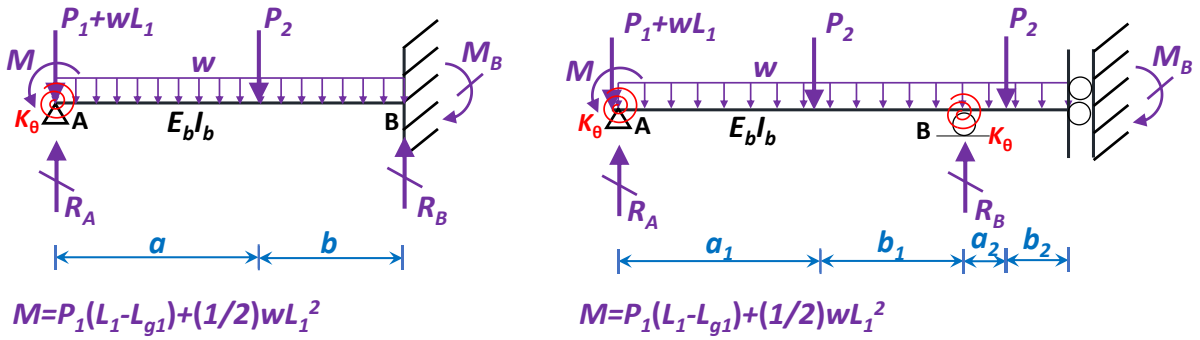

(a) Three-column bent (b) Four-column bent

Figure 3-7. Simplified structural model of multi-column bent

For the structural model for a three-column bent shown in Figure 3-7(a), only one degree of freedom, the rotation of Node A (θ_A), needs to be addressed. The stiffness matrix is therefore a one-by-one matrix, and the general matrix form of the structure can be expressed as Equation 3-14. The negative sign of the term M is to reflect that its direction is counterclockwise.

$$[-M] = \left[\frac{4E_bI_b}{L_2} + K_\theta\right][\theta_A] + [M_{AB}^F] \qquad \textit{Equation 3-14}$$

where K_θ=0 if pinned connection is used; K_θ =$4E_cI_c/H$ if rigid connection is used; M_{AB}^F is shown in Equation 3-15.

$$M_{AB}^F = -\frac{P_2ab^2}{L_2^2} - \frac{wL_2^2}{12} \qquad \textit{Equation 3-15}$$

Parameters *a* and *b* are related to girder line spacing and column spacing, as expressed in Equation 3-16 and Equation 3-17.

$$a = L_{g1} + L_{g2} - L_1 \qquad \textit{Equation 3-16}$$

$$b = L_1 + L_2 - L_{g1} - L_{g2} \qquad \textit{Equation 3-17}$$

Solving Equation 3-14 obtains the rotation at node A. One can therefore use the local stiffness matrix of the structure to determine the end shear at node A, as expressed in Equation 3-18. In the equation, definitions of the notations are shown in Figure 3-8.

$$\begin{bmatrix} V_A \\ M_A \\ V_B \\ M_B \end{bmatrix} = \frac{E_b I_b}{L_2} \begin{bmatrix} \frac{12}{L_2^2} & \frac{-6}{L_2} & \frac{-12}{L_2^2} & \frac{-6}{L_2} \\ \frac{-6}{L_2} & 4 & \frac{6}{L_2} & 2 \\ \frac{-12}{L_2^2} & \frac{6}{L_2} & \frac{12}{L_2^2} & \frac{6}{L_2} \\ \frac{-6}{L_2} & 2 & \frac{6}{L_2} & 4 \end{bmatrix} \begin{bmatrix} 0 \\ \theta_A \\ 0 \\ 0 \end{bmatrix} + \begin{bmatrix} R_{AB}^F \\ M_{AB}^F \\ R_{BA}^F \\ M_{BA}^F \end{bmatrix} \qquad \textit{Equation 3-18}$$

where

$$R_{AB}^F = \frac{P_2 b^2 (3a + b)}{L_2^3} + \frac{wL_2}{2} \qquad \textit{Equation 3-19}$$

$$M_{BA}^F = \frac{P_2 a^2 b}{L_2^2} + \frac{wL_2^2}{12} \qquad \textit{Equation 3-20}$$

$$R_{BA}^F = \frac{P_2 a^2 (a + 3b)}{L_2^3} + \frac{wL_2}{2} \qquad \textit{Equation 3-21}$$

$$M_{AB}^F = -\frac{P_2 ab^2}{L_2^2} - \frac{wL_2^2}{12} \qquad \textit{Equation 3-22}$$

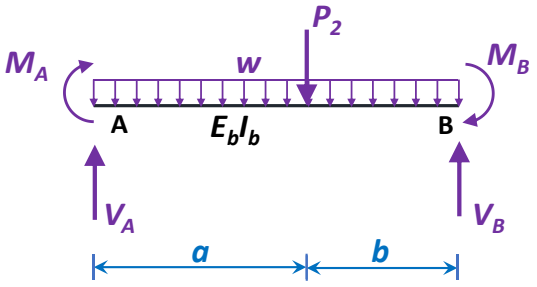

Figure 3-8. End forces of segment of bent cap

Therefore, the axial load of the first column (impacted column) P_A can be determined by adding the value of V_A and the external load acting at the node A, which is:

$$P_A = V_A + P_1 + wL_1 \qquad \textit{Equation 3-23}$$

On the other hand, if the structure under consideration is a four-column bent [see Figure 3-7(b)], three degrees of freedom should be addressed, including rotations at the nodes A and B (θ_A and θ_B) and deflection at the right end of the beam (Δ). Thus, the stiffness matrix is a three-by-three

matrix, and the general matrix form can be expressed as Equation 3-24. Again, the negative sign before the value of M is to correct the direction. Also, the value of K_θ is zero for pinned connections and $4E_cI_c/H$ for rigid connections.

$$\begin{bmatrix} -M \\ 0 \\ 0 \end{bmatrix} = \begin{bmatrix} \frac{4E_bI_b}{L_2} + K_\theta & \frac{2E_bI_b}{L_2} & 0 \\ \frac{2E_bI_b}{L_2} & \frac{12E_bI_b}{L_2} + K_\theta & \frac{-24E_bI_b}{L_2^2} \\ 0 & \frac{-24E_bI_b}{L_2^2} & \frac{96E_bI_b}{L_2^3} \end{bmatrix} \begin{bmatrix} \theta_A \\ \theta_B \\ \Delta \end{bmatrix} + \begin{bmatrix} M_{AB}^F \\ M_{BA}^F + M_{BC}^F \\ R_{CB}^F \end{bmatrix} \quad \textit{Equation 3-24}$$

where

$$M_{AB}^F = \frac{-P_2 a_1^2 b_1}{L_2^2} - \frac{wL_2^2}{12} \quad \textit{Equation 3-25}$$

$$M_{BA}^F = \frac{P_2 a_1^2 b_1}{L_2^2} + \frac{wL_2^2}{12} \quad \textit{Equation 3-26}$$

$$M_{CB}^F = \frac{-P_2 a_2 b_2^2}{(L_2/2)^2} - \frac{w(L_2/2)^2}{12} \quad \textit{Equation 3-27}$$

$$R_{CB}^F = \frac{P_2 a_2^2 (a_2 + 3b_2)}{(L_2/2)^3} \quad \textit{Equation 3-28}$$

Similarly, solving Equation 3-24 obtains the values of θ_A, θ_B, and Δ. These values are once again used to determine the end forces of the segment AB using the local stiffness matrix, as shown in Equation 3-29.

$$\begin{bmatrix} V_A \\ M_A \\ V_B \\ M_B \end{bmatrix} = \frac{E_bI_b}{L_2} \begin{bmatrix} \frac{12}{L_2^2} & \frac{-6}{L_2} & \frac{-12}{L_2^2} & \frac{-6}{L_2} \\ \frac{-6}{L_2} & 4 & \frac{6}{L_2} & 2 \\ \frac{-12}{L_2^2} & \frac{6}{L_2} & \frac{12}{L_2^2} & \frac{6}{L_2} \\ \frac{-6}{L_2} & 2 & \frac{6}{L_2} & 4 \end{bmatrix} \begin{bmatrix} 0 \\ \theta_A \\ 0 \\ \theta_B \end{bmatrix} + \begin{bmatrix} R_{AB}^F \\ M_{AB}^F \\ R_{BA}^F \\ M_{BA}^F \end{bmatrix} \quad \textit{Equation 3-29}$$

where

$$R_{AB}^F = \frac{P_2 b_1^2 (3a_1 + b_1)}{L_2^3} + \frac{wL_2}{2} \quad \textit{Equation 3-30}$$

$$R_{BA}^{F} = \frac{P_2 {a_2}^2 (a_2 + 3b_2)}{L_2^3} + \frac{wL_2}{2}$$ Equation 3-31

Finally, the axial load P_A in the first column can be determined using Equation 3-32.

$$P_A = V_A + P_1 + wL_1$$ Equation 3-32

3.4.2. Determine Column Flexural Capacity

With the determined axial load in the exterior column that is at risk of vehicular collision, one can determine the column's flexural capacity and shear capacity with known sectional properties, material, and reinforcement configuration. The *P-M* interaction diagram of the column can be constructed, and one can determine the flexural nominal capacity (M_n) corresponding to the axial load. The method is conceptually shown in Figure 3-9.

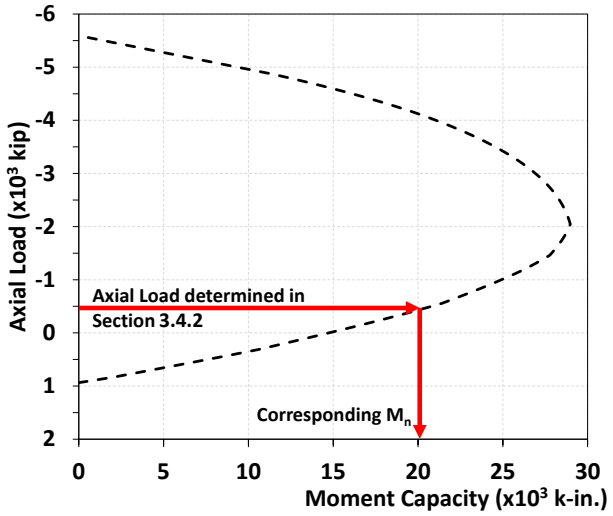

Figure 3-9. P-M interaction diagram for determining M_n

3.4.3. Collapse Mechanism Analysis

Collapse mechanism analysis is a method for determining the ultimate capacity of a structure on the basis of the upper bound theorem of plasticity. The method has prevailed in the field of earthquake engineering where plastic analysis and design are essential. As vehicular collision is also anticipated to cause plastic behavior of the impacted column, similar concepts of plasticity can be applied. According to the upper bound theorem of plasticity, given that a compatible of plastic deformation induced by enough number of plastic hinges, the structure will collapse if the rate of work done by the equivalent static lateral load of vehicular collision exceeds the internal plastic dissipation.

For multi-column bents with well-detailed joints, consider a structural model with n columns and rigid connections and with a clear column height H. Three collapse mechanisms can be identified given a load acting at a height of h, as shown in Figure 3-10 For the collapse mechanism shown in Figure 3-10 (a), a plastic hinge forms at each end of all columns with a rotation θ; the total internal plastic energy dissipation is the summation of plastic moment times the rotation in all columns and can be expressed as $2nM_p\theta$, where M_p is the plastic flexural capacity of the columns. It is recognized that the value of M_p can vary as axial loads are not necessarily equal in the columns. Nevertheless, the difference is not significant and is not considered in this derivation for simplicity. On the other hand, the work done by the lateral point load P equals the magnitude of the load times the displacement at the point and therefore has a value of $P\theta h$. Equating $2nM_p\theta$ to $P\theta h$ with appropriate arrangement delivers the expression of normalized plastic moment capacity needed to resist the external load with regard to the ratio of clear collision height to the distance between two end plastic hinges. The result can be expressed as Equation 3-33.

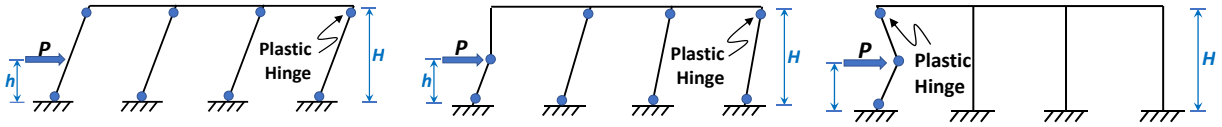

(a) Mechanism 1 (b) Mechanism 2 (c) Mechanism 3

Figure 3-10. Collapse mechanism of rigid-connected multi-column bent

$$\frac{M_p}{PH} = \left(\frac{h}{H}\right)\left(\frac{1}{2n}\right) \qquad \textit{Equation 3-33}$$

Similar formulation is applied to the collapse mechanism shown in Figure 3-10(b). In this case, given the rotation at the base of the impacted column equal to θ, the rotation at the hit point is also θ by geometry. The other plastic hinges, according to compatibility, have a rotation of $\theta h/H$. Therefore, the work done by the lateral load is then $P\theta h$ while the total internal energy dissipation is $2M_p/h+2(n\text{-}1)M_p/H$. Equating the work done by the lateral load to the total internal energy dissipation obtains the normalized required plastic moment capacity, as expressed in Equation 3-34.

$$\frac{M_P}{PH} = \left(\frac{h}{H}\right)\left[\frac{1}{2+2(n-1)\left(\frac{h}{H}\right)}\right] \qquad \textit{Equation 3-34}$$

The third collapse mechanism has all plastic hinges on the impacted column as shown in Figure 3-10(c), which is the prevalent failure mode in the field. Regarding the collapse mechanism, assuming that the rotation at the bottom plastic hinge is θ, the top plastic hinge and the plastic hinge at the hit point have rotations of $\frac{\theta h}{H-h}$ and $\frac{\theta H}{H-h}$ respectively per compatibility. In addition, the corresponding lateral displacement at the hit point is then θh. With the similar formulation, the

normalized required plastic moment capacity can be expressed as Equation 3-35. It should be noted that the expression is independent of number of columns as anticipated.

$$\frac{M_P}{PH} = \left(\frac{h}{H}\right)\left(1 - \frac{h}{H}\right)\left(\frac{1}{2}\right) \qquad \textit{Equation 3-35}$$

It is useful to plot the normalized moment capacity (M_p/PH) with regard to the height ratio (h/H) per Equation 3-33 through Equation 3-35, as shown in Figure 3-11. In the figure, each of the lines defines the failure envelop of the corresponding collapse mechanism. Taking the highest value of M_p/PH among the three curves forms an overall failure envelope; multi-column bents above the overall failure envelop have a sufficient moment capacity to resist the collision load. It can be seen from Figure 3-11(a) that when the height ratio is under 0.5, Mechanism 3 controls the failure mechanism otherwise Mechanism 2 does for three-column bents. On the other hand, from Figure 3-11(b), when the height ratio is under 0.667, Mechanism 3 controls the failure mechanism otherwise Mechanism 2 does for four-column bents. Mechanism 1, however, is always under the overall failure envelop, meaning the mechanism requires a much higher later load to develop, given the same values of M_p and the height ratio. The observation explains that Mechanism 3, single-column failure, is the most common failure mode as the collision point is hardly higher than 0.5 times the clear height of a multi-column bent.

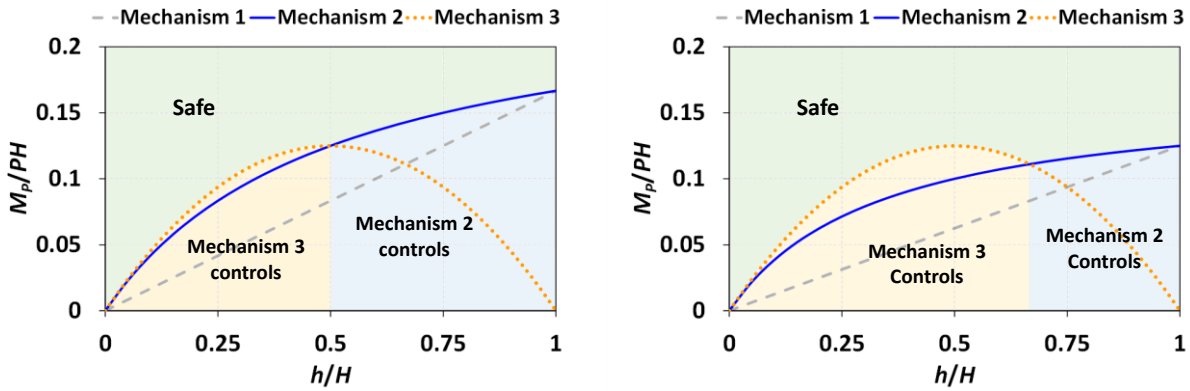

(a) Three-column bent (b) Four-column bent

Figure 3-11. Required moment capacity for resisting lateral load regarding height ratio

A key factor that the structure is able to form the failing mechanism is rotational deformability of the plastic hinges, especially the one under the largest rotation. For Mechanism 1, all plastic hinges are rotating by the same angle, indicating all the plastic hinges form at the same time. For Mechanism 2, plastic hinges at the bases and the connections rotate by θ while the plastic hinge at the collision point is $\theta h/H$. For Mechanism 3, the plastic hinge at the bottom rotates by the rotation at the bottom plastic hinge is θ, the top plastic hinge and the plastic hinge at the hit point have rotations of $\frac{\theta h}{H-h}$ and $\frac{\theta H}{H-h}$, as mentioned earlier. As the value of θ can be arbitrary, therefore, at any given θ, these plastic hinges need to be ensured the deformability, known as ductility. For example,

for Mechanism 3, the plastic hinge at the hit point has to take a rotation of $\frac{H}{H-h}$ times the rotation of the base plastic hinge, which is considered the ductility requirement.

The procedure of determining the required plastic moment capacity is the same as mentioned in the above for multi-column bents with poorly-detailed joints. The only difference to be considered is that moments are not transmitted through the bent-to-column connections. That is, no plastic hinges form on top of the columns; instead, regular hinges are placed to create pinned connections. With this regard, two major collapse mechanisms are identified for multi-column bents with poorly detailed joints as shown in Figure 3-12. Types of the mechanisms are labeled in alignment with the previous section; there is no Mechanism 2.

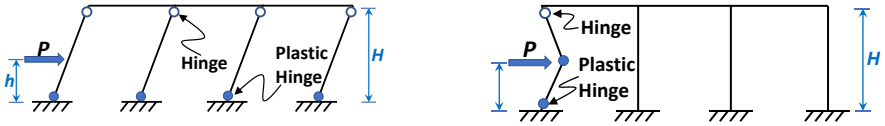

(a) Mechanism 1 (b) Mechanism 3

Figure 3-12. Collapse mechanism of pinned-connected multi-column bent

The first collapse mechanism, as shown in Figure 3-12 (a), is also a full collapse, having a plastic hinge on the bottom of each of the columns. The total internal plastic energy dissipation in this case is $nM_p\theta$, which is half the value of the case of well-detailed joints; the external work remains the same value as $P\theta h$, Similarly, equating the total internal plastic energy dissipation to the external work obtains an expression for normalized plastic moment capacity shown in Equation 3-36.

$$\frac{M_P}{PH} = \left(\frac{h}{H}\right)\left(\frac{1}{n}\right) \qquad \textit{Equation 3-36}$$

The other collapse mechanism is characterized as collapse of the impacted column, as shown in Figure 3-12 (b). Two plastic hinges are assigned to the first column at the bottom and the hit point. In this case, given that the rotation at the bottom plastic hinge is θ, the rotation at the hit point can be expressed as $\frac{\theta H}{H-h}$, and the lateral displacement is θh. Therefore, the total internal plastic dissipation is $M_P\theta\frac{2H-h}{H-h}$, and the external work done by the lateral force is $P\theta h$. Similarly, the normalized plastic moment capacity can be expressed Equation 3-37.

$$\frac{M_P}{PH} = \frac{h}{H}\left(\frac{1-h/H}{2-h/H}\right) \qquad \textit{Equation 3-37}$$

Figure 3-13 shows plots of the normalized required moment capacity M_p/PH with regard to the height ratio h/H per Equation 3-36 and Equation 3-37. Similarly, the highest value of M_p/PH between the two curves is taken as the failure envelop. Datapoints above the failure envelop are considered having sufficient moment capacity to resist collision load. It can be seen that

Mechanism 3 controls the failure mode if the height ratio is less than 0.5 for three-column bents, and if the height ratio is less than 0.667 for four-column bents. Mechanism 3 is also more prevalent for pinned columns in the field as rarely is the hit point higher than 0.5 time the clear height. The ductility requirement for the plastic hinges follows the same principle as mentioned earlier.

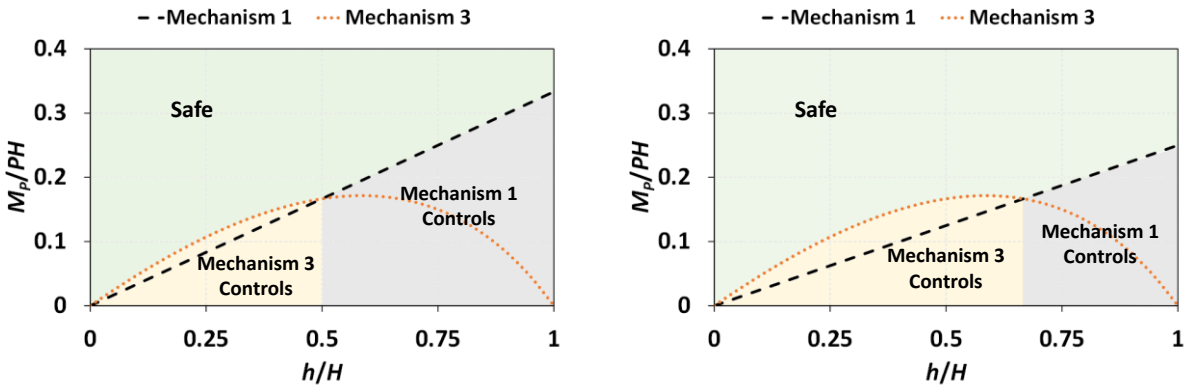

(a) Three-column bent (b) Four-column bent

Figure 3-13. Required moment capacity for resisting lateral load regarding height ratio

The required value of M_p/PH for pinned multi-column bents is generally higher than that for rigid-connected multi-column bents. The observation indicates that well-detailed column-to-bent joints are always preferable.

3.4.4. Check Shear Capacity and Bond Strength for Ductility

One of the basic assumptions behind the upper bound theorem of plasticity is that the material has sufficient deformability. The constitutive relationship of the material is analytically assumed as elastoplastic. When applying the assumption to columns in the current analysis, brittle failures such as shear failures and bond failures should be avoided. The avoidance of the brittle failures can be achieved from the viewpoint of capacity-based design. To be specific, shear and anchorage demands to the column are determined using the flexural capacity at the plastic hinges. The flexural capacity is usually amplified with an overstrength factor. The overstrength factor, per AASHTO LRFD, reflects factors including material strength in the long-term, reinforcement strain hardening, confinement, and higher concrete ultimate strain than expected.

Shear demands to plastic-hinging regions can be determined by taking the free body diagram of the impacted column as shown in Figure 3-14, per force equilibrium. For columns with a pinned connection to the bent cap, the shear demands to the top joint and the bottom can be calculated using equations shown in Figure 3-14(a). On the other hand, for columns with a rigid connection to the bent cap [see Figure 3-14(b)], the shear demands the top joint and the bottom can be calculated using equations shown in Figure 3-14(b).

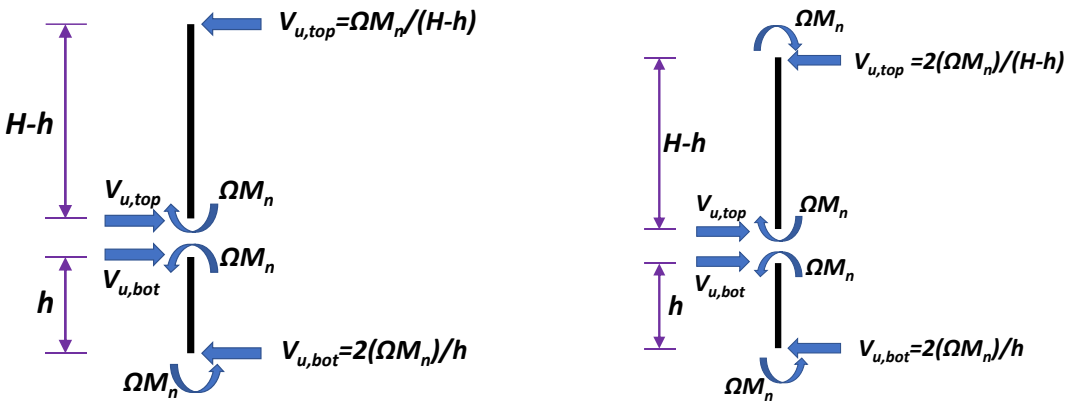

(a) Pinned connection on top (b) Rigid connection on top

Figure 3-14. Determination of shear demand to impacted column for ductility

After determining the shear demand, it is essential to examine if the shear capacity of all of the top connection, the bottom, and the hit point are sufficient to withstand the demands. The shear resistance of a column exhibiting excessive plastic deformation, suggested by Priestley et al. (1996), consists of contributions from concrete (V_c), transverse reinforcement (V_s), and compression strut mechanism (V_p), which can be generally expressed as Equation 3-38.

$$V_n = V_c + V_s + V_p \qquad \textit{Equation 3-38}$$

The contribution of concrete can be calculated using Equation 3-39.

$$V_c = k\sqrt{f'_c}A_e \qquad \textit{Equation 3-39}$$

where k ranges from 0.6 to 3.5 depending on the ductility factor; higher ductility factors lead to lower k-values. A_e is effective shear area, which can be taken as $0.8A_{gross}$. The contribution of transverse reinforcement for circular columns is given by

$$V_s = \frac{\pi}{2}\frac{A_h f_y D'}{s}\cot\theta \qquad \textit{Equation 3-40}$$

where A_h is the area of shear reinforcement; D' is the center-to-center core diameter; and s is the pitch spacing; and θ is the angle of the critical inclined flexure shear cracking, which can be taken as 35 degrees.

The last term V_p, resulting from a diagonal strut mechanism caused by axial compression as shown in Figure 3-15, is expressed as

$$V_p = P\tan\alpha \qquad \textit{Equation 3-41}$$

where α is the angle of the inclined strut resisting shear on the other or the bottom; P is the axial load. The α-value is determined based on the centerline of the strut connecting to the center of flexural compression area of the hit point and the top or the bottom of the column.

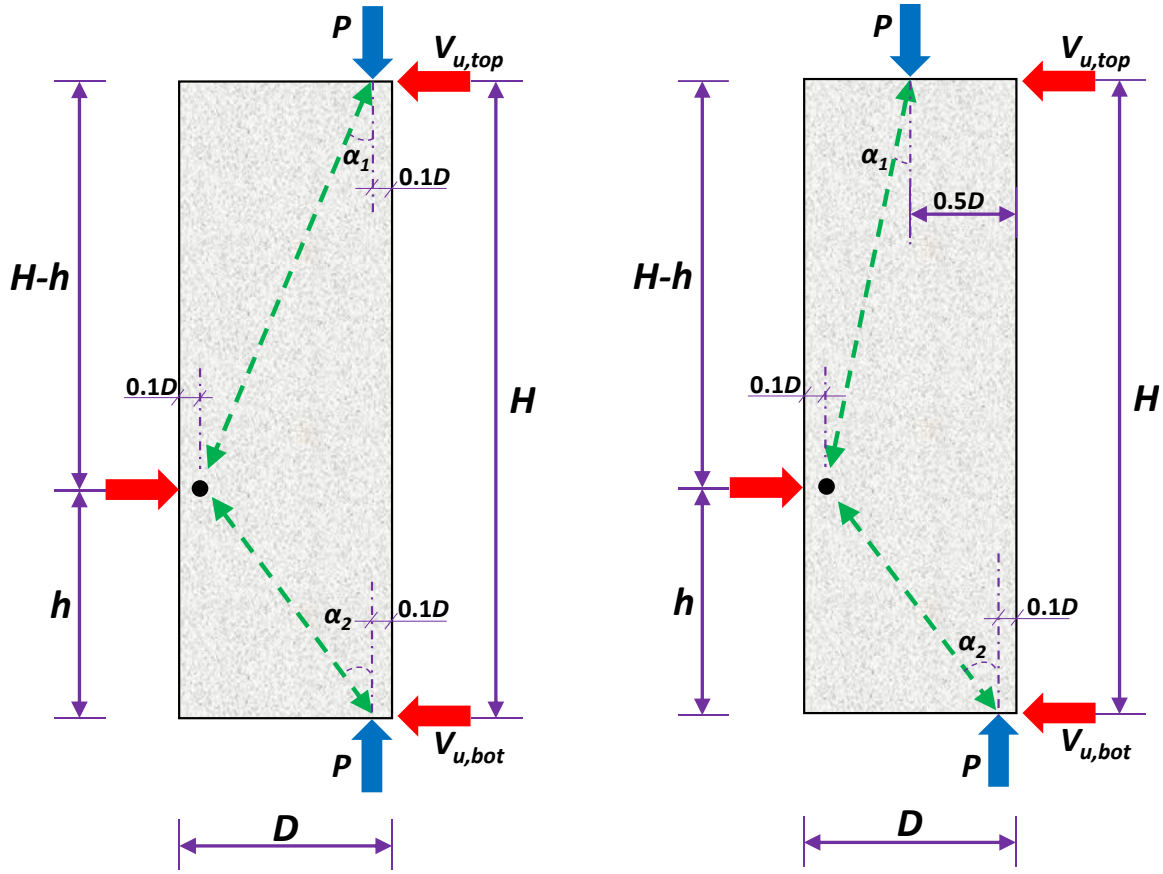

(a) Rigid connection on top (b) Pined connection on top

Figure 3-15. Contribution of axial load in terms of compression struts

Alternatively, AASHTO LRFD Article 5.7.3.3 prescribes the calculation of nominal shear resistance. Comparing the shear demand V_u to the shear capacity with a resistance factor ϕV_n, it is possible to determine whether the considered collapse mechanism can be achieved without premature brittle failures.

Moreover, to guarantee sufficient rotational deformability of plastic hinges, it is needed to provide enough transverse confining reinforcement according to code provisions within the plastic hinge regions, extending to the greater of the column diameter, one sixth of the clear height, and 18 in. The confining reinforcement ratio can be taken as

$$\rho_s = \frac{4A_{sp}}{d_c s} \geq 0.12\frac{f'_c}{f_{yh}} \qquad \text{Equation 3-42}$$

In addition, the anchorage of column longitudinal reinforcing bars should be checked and the shear strength in the joint needs to be guaranteed. An approach is to ensure that column longitudinal reinforcing bars are able to develop a stress of Ωf_y. The overstrength factor Ω can be applied here due to higher expected column reinforcing bar's strains. Based on the concept, the required development length for straight bars can be determined by replacing f_y with Ωf_y in Eq. 5.10.8.2.1 in AASHTO LRFD, which is shown as

$$l_d = 2.4 d_b \frac{\Omega f_y}{\sqrt{f'_c}} \left(\frac{\lambda_{rl} \lambda_{cf} \lambda_{fc}}{\lambda} \right) \qquad \textit{Equation 3-43}$$

For hooked bars, development length can be calculated as

$$l_d = \frac{38}{60} d_b \frac{\Omega f_y}{\sqrt{f'_c}} \left(\frac{\lambda_{rc} \lambda_{cw}}{\lambda} \right) \qquad \textit{Equation 3-44}$$

Per the new AASHTO LRFD 10th Edition, the development length, applied to straight, hooked and headed bars, can be determined using.

$$l_d = 0.17 d_b \left[\frac{\Omega f_y - \frac{F_h}{A_b}}{1.97 \lambda f'^{0.25}_c} \right]^2 \lambda_{rl} \lambda_{cf} \lambda_{rc} \qquad \textit{Equation 3-45}$$

It should be noted that the excess reinforcement factor λ_{er} is not applied here because the factor is not part of the concept of capacity-based plastic design. All other modification factors refer to Section 5.10.8.2.1 in AASHTO LRFD.

3.5. Analysis for Loss of a Support

Similar to vehicular collision, sudden loss of one of the columns causes dynamic impact and stress re-distribution on multi-column bents. However, the analysis of such scenarios involves complex non-linear dynamic modeling. There is no explicit provisions or procedures in AASHTO LRFD for scenarios of column removal from bridge structures.

To overcome the challenges, "General Services Administration: Alternate Path Analysis & Design Guidelines for Progressive Collapse Resistance (2013)" (GSA) provides methods for prevention of progressive collapse. GSA (2013) provides three major methods for analysis of progressive collapse of buildings: linear static analysis (LSA), nonlinear static analysis (NLSA), and nonlinear dynamic analysis (NDA). Studies revealed the NDA generates sophisticated outcomes, while the LSA yields simple but conservative results. The NLSA, on the other hands, falls in between. The research team suggests employing the methods with a few necessary modifications. Here, the research team focuses on the introduction of NDA and LSA to the prevention of progressive collapse of multi-column bents.

Due to the complexity of the analysis, commercial engineering software, such as SAP2000, can be used to build the numerical models. The overall procedures are presented in Figure 3-16.

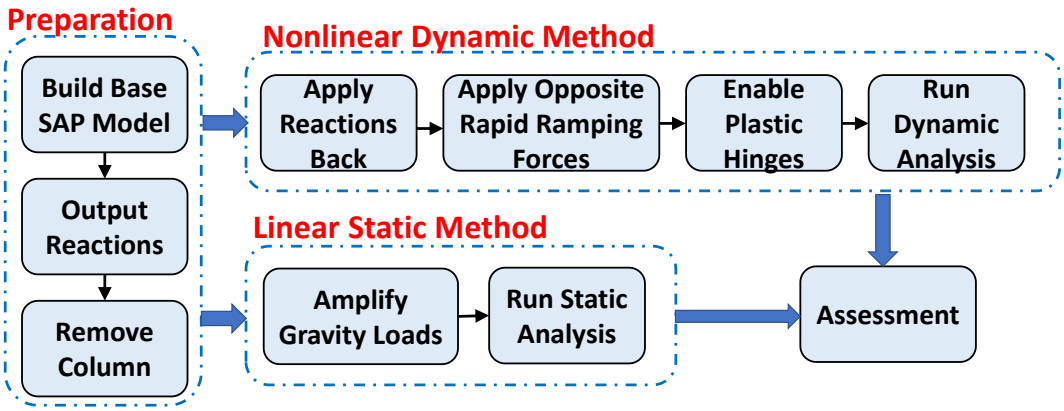

Figure 3-16. General procedure of analysis for loss a support

3.5.1. SAP2000 Numerical Model Preparation

To conduct nonlinear dynamic analysis for the evaluation of progressive collapse after losing a support, a SAP2000 numerical model of multi-column bent should be first constructed. The overall configuration is determined according to the target structure as shown in Figure 3-17(a) for example. All members are then assigned sectional properties based on the actual design and material. In SAP2000, the function "Section Designer" is recommended if it is desired to make customized longitudinal reinforcement pattern for the bent cap, as shown in Figure 3-17(b). After assigning the structural configuration and sectional properties, girder loads are assigned to the corresponding positions according to the target standard design. It is recommended to separate girder live load and girder dead load for potentially different load combinations.

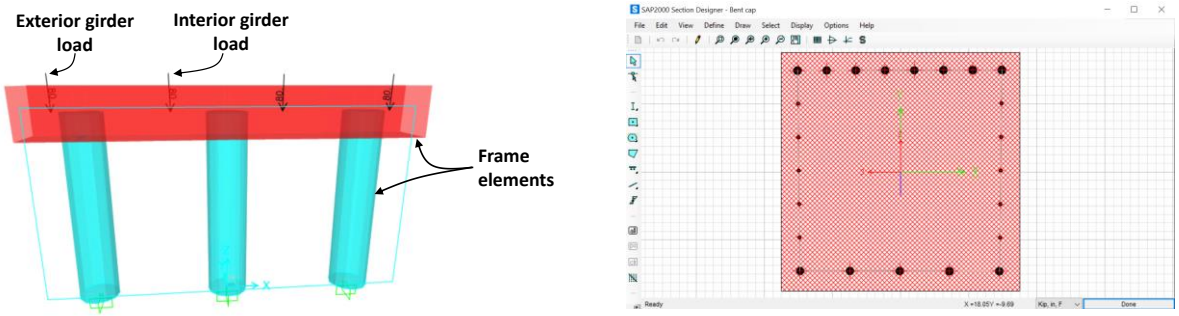

(a) Structural configuration and loads (b) Section designer

Figure 3-17. SAP2000 base model

Once the girder loads are assigned, one can set up an analysis case in order to determine reactions in each of the columns as the initial condition for later use. This initial condition takes care of

forces and moments that exist in the bent cap and columns before the event of losing a column occurs. For example, the load combination here is prescribed as 1.1DL+1.1LL. To apply the load combination here, for example, an analysis case “Reaction” in which self-weight (DEAD), girder dead load, and girder live load are included is created, and the corresponding multiplier is specified as shown in Figure 3-18.

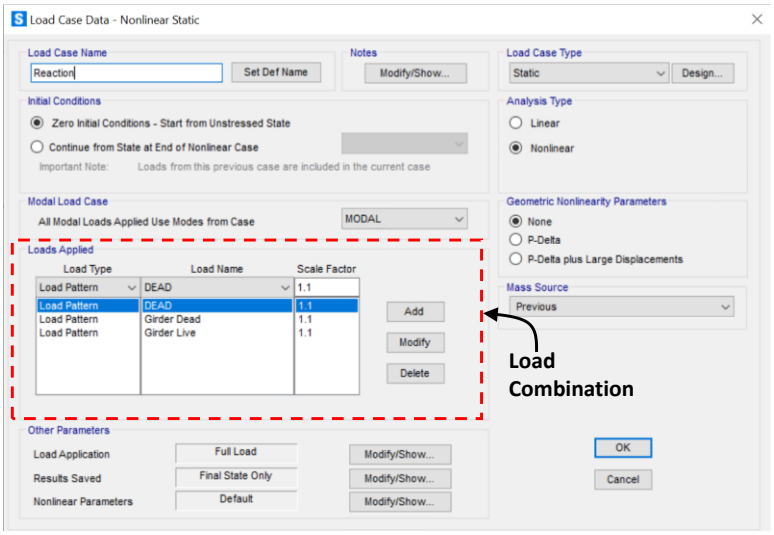

Figure 3-18. Assigned Load case for reactions

Once the settings of the analysis case “Reaction” is ready, it is ready to run the analysis case and determine member forces and moments using the function “Run Analysis.” SAP2000 is able to output all internal forces as shown in Figure 3-19. It is essential to record the end moment, the axial load, and the shear force at the column-to-bent connection of the exterior column, which is at risk of losing function. The next step is to remove the column from the original structural model and the preparation is finished.

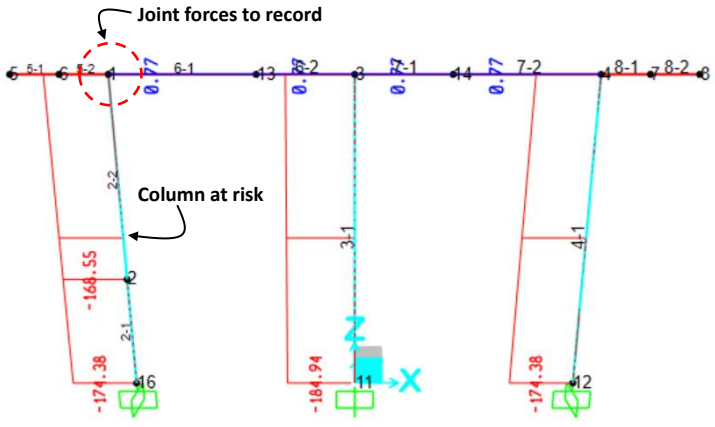

Figure 3-19. Determination of joint forces before losing a column

3.5.2. Nonlinear Dynamic Analysis

To continue with the nonlinear dynamic analysis, four more steps, as shown in Figure 3-16, are followed. First, the reactions at the top of the removed column should be re-applied to create the initial condition as load case "Initial," as shown in Figure 3-20(a).

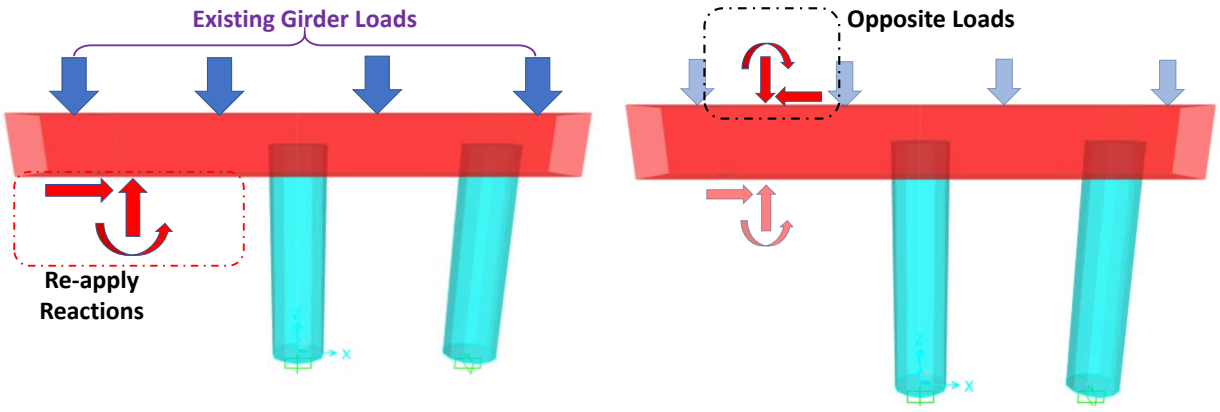

(a) Reapplying reactions at the top joint (Load case "Initial")

(b) Applying opposite loads (Load case "Dynamic Loss")

Figure 3-20. Modeling loads for loss of a support

The loss-of-a-support scenario can be modeled as a rapid diminishing of reactions in the removed column. This can be achieved by applying loads with the same magnitude as the reactions but in the opposite directions to counterbalance the reactions (as load case "Dynamic Loss"), as shown in Figure 3-20(b). The loads should increase from zero to its full magnitude within an infinitesimal period of time to reflect the instantaneous loss of the column. As suggested per GSA 2013, the time t_d can be selected as less than 1/100 of the natural vibration period of the mode of the bent cap in-plane vibration. In SAP2000, it can be defined in "Time History Function Definition" as shown in Figure 3-21.

(a) SAP2000 setup

(b) Ramping force time history example

Figure 3-21. Definition of ramping force

It is required that plastic hinges be assigned for nonlinear dynamic analysis in SAP2000. Plastic hinges should be assigned where moments are locally highest. In this case, the end of each span of the bent cap, the top of the columns, and the bottom of the columns potentially take the locally highest moment when the structure loses one of the columns.

The properties of plastic hinges should be also input using the function “Hinge Properties” as shown in Figure 3-22. Key properties for a plastic hinge include the idealized moment curvature curve and the plastic hinge length. In SAP2000, the idealized moment curvature consists of yield strengths in both negative and positive moments as well as ratios to the yield strengths that define the post-yield behavior (point B, C, D, and E in the Figure). The moment curvature behavior of members under consideration can be generated using SAP2000 or other sectional analysis methods. The software Response-2000 can be used to define the moment curvature of each member.

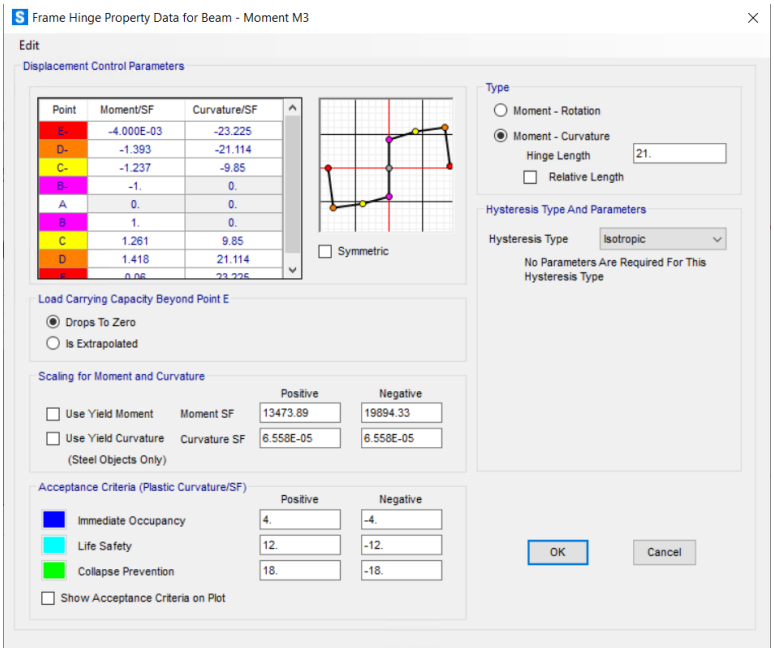

Figure 3-22. Example of plastic hinge properties

The other important property is the plastic hinge length, which is related to the member dimensions and axial load level. A simple choice for the value of plastic hinge length can be half the member depth for beams. Also, there are equations available for columns. The plastic hinge length of each member also affects the exact position of the plastic hinge on the member. Specifically, a plastic hinge is recommended to be located at a distance of half the plastic hinge length away from the joint face or the column base.

After the assignment of plastic hinges is finished, one should specify dynamic parameters before running the analysis. The most important parameter is the inherent damping ratio. The value is usually specified as 3% to 6%, which is within the range for typical concrete structures.

The analysis case "Dynamic Loss" is to start after the case "Initial." After the "Dynamic Loss" is complete, one can evaluate the hinge status of all members and displacement at the end of the bent cap with regard to time. Engineering judgements can be made based on the outputs and will be introduced in the analysis example in later sections.

3.5.3. Linear Static Analysis

The procedure of the NLDA is admittedly complicated and therefore an alternative approach based on linear static analysis is recommended. The LSA does not need to involve the assignment of plastic hinges nor dynamic properties. The same model with a column removed as introduced previously can be used.

The concept of the LSA is to simplify dynamic effects on loads as a single amplification factor, quantifying material nonlinearity by introducing a demand factor. In particular, the factored gravity loads $\Sigma\gamma_i Q_i$ are further amplified by a factor Ω to consider the dynamic effects of losing a column rapidly. The Ω-value is related to material and the structural behavior of the member, and it can be 2.0 in most cases according to GSA. On the other hand, the ductility of the members allows for energy dissipation during stress re-distribution after the loss of a column. That is, the capacity R of each member can be increased by a factor, m, which is related to its ductility and other relevant factors. Typically, the m-factor can be three for doubly reinforced beams. However, if shear failure is anticipated to happen or inadequate anchorage is provided, lower m-values should be used. Detailed determination of the m-factor refers to Section 4.4 of GSA. As a result, the structure is considered safe if the amplified demand is lower than the factored capacity of each member with the ϕ-factor, which can be expressed as Equation 3-46.

$$\Omega\Sigma\gamma_i Q_i \leq \phi m R_i \qquad \textit{Equation 3-46}$$

Applying the amplified gravity loads onto the model generates demand to each of the members of the multi-column bents. It is then possible to compare the factored demand to the factored capacity for each member. Analysis examples are provided in the following sections.

3.6. Analysis Example

This section presents two analysis examples. The first example is the standard three-column bent BIG 24 under stream or collision. The second example is the same bent subjected to loss of a column.

3.6.1. Multi-Column Bent in Consideration

The TxDOT standard interior bent BIG-24 was selected for the example analysis. The bent BIG-24 is compatible with Tx-girder type TX28 through TX54 with a 24-ft roadway. As shown in the plan view in Figure 3-23, this type of bent has three columns spaced at 8 ft and four girders spaced

at 6.667 ft. The distance from the edge to the first column and the first girder is 4 ft and 2 ft, respectively. The clear height of the columns in the example was chosen as 12 ft.

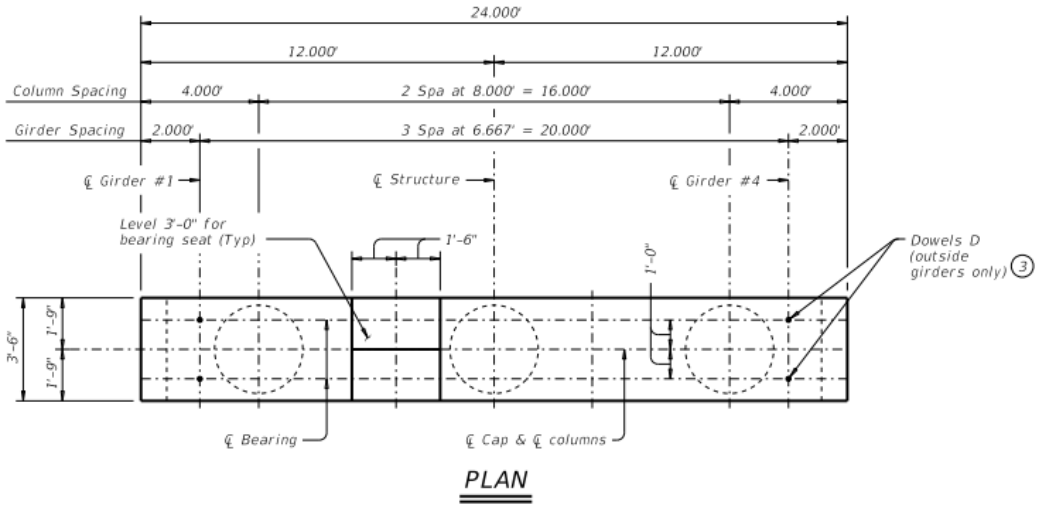

Figure 3-23. Plan view of BIG 24 (TxDOT Bridge Division Standards)

Figure 3-24 shows the elevation view and cross-sections of the bent cap and the column. The joint detail is also presented. Each column is reinforced with ten No. 9 longitudinal bars and No. 4 spiral with a pitch of 3 inches and a clear cover of 3 inches. The bent cap, on the other hand, is reinforced with six No. 11 longitudinal reinforcing bars on the top and four No. 11 bars longitudinal reinforcing bars on the bottom. Five No. 5 skin reinforcement is distributed on both sides. No. 5 stirrups are distributed at a spacing of 6 inches with a clear cover of two inches; however, no stirrups are provided in the joints.

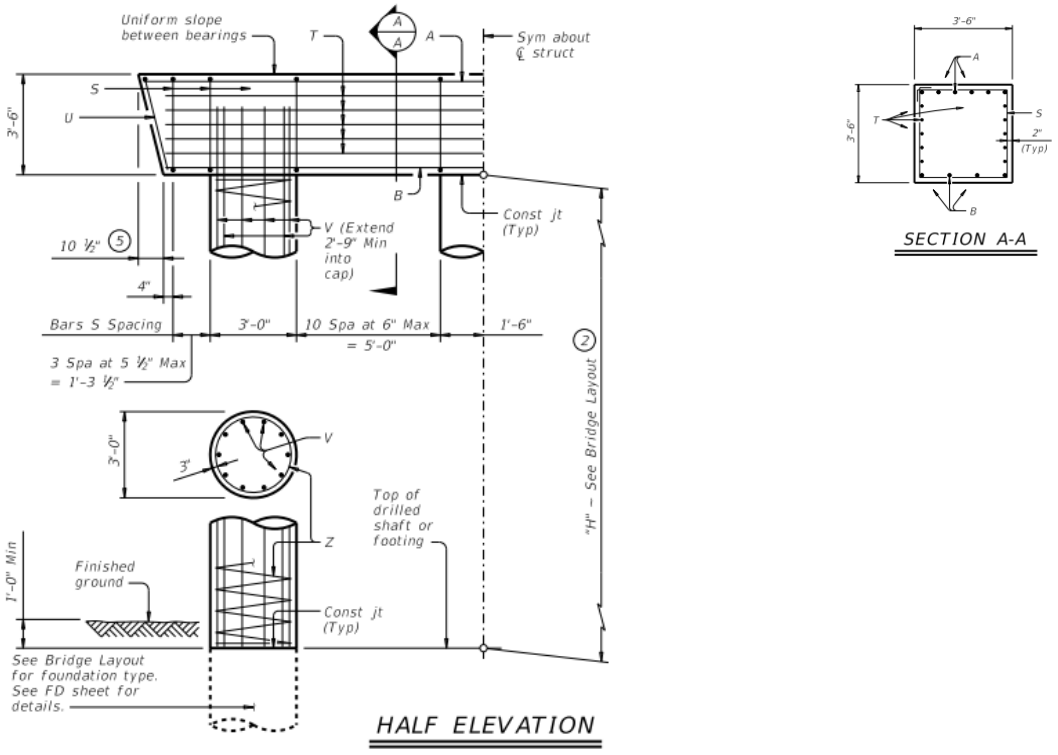

Figure 3-24. Elevation view and cross-sections

The concrete compressive strength of the columns was specified as 4 ksi, and that of the bent cap was 5 ksi. The yield strength of the reinforcement was 60 ksi for both longitudinal and transverse reinforcing bars. The elastic moduli of the concrete for the columns and the bent cap were calculated as 3605 ksi and 4030 ksi, respectively based on the relation $57000\sqrt{f'_c}$.

3.6.2. Example 1: Subjected to Stream and Collision

3.6.2.1. Base Structural Model

According to the structural configuration considered in the previous section, a base structural model was constructed as shown in Figure 3-25. Essential dimensions were determined and denoted in the figure. It should be noted that the overall height of the model is the clear height plus half the depth of the bent cap.

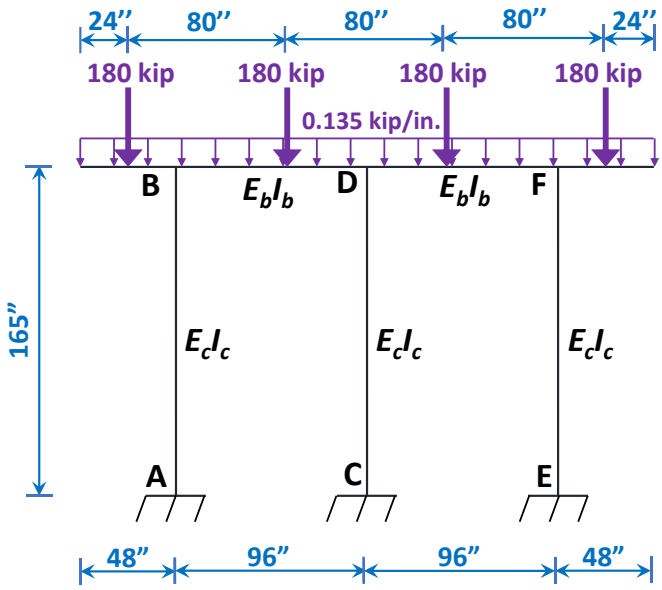

Figure 3-25. Base structural model of three-column bent under consideration

The second moment of inertia of the columns and the bent cap were calculated per gross properties. In other words, contributions of the reinforcement were not considered. Therefore, each of the columns had an E_cI_c of 2.972×10^8 kip-in.^{2} while the bent cap had an E_bI_b of 1.045×10^9 kip-in.^{2}, as denoted in the Figure 3-25. The load of each girder line was assumed 180 kips, and the self-weight was assumed 0.135 kip/in. in this case.

3.6.2.2. Analysis for Stream Load

Water profile was taken from the flood event Tropical Storm Imelda 2019 recorded in TxDOT project 5-9054-01. The peak water velocity during the streamflow was 6 ft/sec. The water pressure, according to Equation 3-1, was calculated to be 0.35 psi with C_D factor being 1.4. The water pressure was applied over the full height of the first column, corresponding to an evenly distributed stress of 0.0126 kip/in, as shown in Figure 3-26.

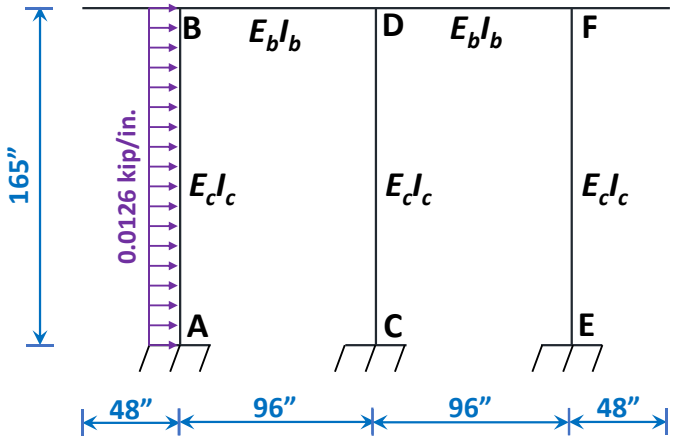

Figure 3-26. Structural model of base bent under flood load

With the determined water load and the structural model, the internal forces were solved by expressing the structure as a matrix form per Equation 3-3 through Equation 3-5. The result is shown in Equation 3-47.

$$\begin{bmatrix}0\\0\\0\\0\end{bmatrix}=\begin{bmatrix}5.075\times10^{7} & 2.177\times10^{7} & 0 & -6.550\times10^{5}\\ 2.177\times10^{7} & 9.430\times10^{7} & 2.177\times10^{7} & -6.550\times10^{5}\\ 0 & 2.177\times10^{7} & 5.075\times10^{7} & -6.550\times10^{5}\\ -6.550\times10^{5} & -6.550\times10^{5} & -6.550\times10^{5} & 2.382\times10^{3}\end{bmatrix}\begin{bmatrix}\theta_B\\ \theta_D\\ \theta_F\\ \Delta_B\end{bmatrix}+\begin{bmatrix}28.586\\0\\0\\-1.040\end{bmatrix} \quad \textit{Equation 3-47}$$

Solving Equation 3-42 obtained nodal displacement as shown in

$$\begin{bmatrix}\theta_B\\ \theta_D\\ \theta_F\\ \Delta_B\end{bmatrix}=\begin{bmatrix}-7.083\times10^{-8}\ \text{rad}\\ 2.180\times10^{-7}\ \text{rad}\\ 4.924\times10^{-7}\ \text{rad}\\ 4.540\times10^{-4}\ \text{in.}\end{bmatrix} \quad \textit{Equation 3-48}$$

Then, moments acting on the column at the upstream were determined using Equation 3-11, shown as

$$\begin{bmatrix}V_{bot}\\ M_{bot}\\ V_{top}\\ M_{top}\end{bmatrix}=1.801\times10^{6}\begin{bmatrix}4.408\times10^{-4} & -3.636\times10^{-2} & -4.408\times10^{-4} & -3.636\times10^{-2}\\ -3.636\times10^{-2} & 4 & 3.636\times10^{-2} & 2\\ -4.408\times10^{-4} & 3.636\times10^{-2} & 4.408\times10^{-4} & 3.636\times10^{-2}\\ -3.636\times10^{-2} & 2 & 3.636\times10^{-2} & 4\end{bmatrix}\begin{bmatrix}0\\0\\4.540\times10^{-4}\\-7.083\times10^{-8}\end{bmatrix}+\begin{bmatrix}-1.040\\-28.586\\-1.040\\28.586\end{bmatrix}=\begin{bmatrix}-1.405\ \text{kip}\\ -58.580\ \text{kip-in.}\\ -0.674\ \text{kip}\\ -1.663\ \text{kip-in.}\end{bmatrix} \quad \textit{Equation 3-49}$$

It can be seen that the maximum moment acting on the column was 58.580 kip-in., which is far lower than the nominal flexural capacity. Indeed, the column was anticipated to remain elastic under the storm event. The result indicates that flooding hardly causes multi-column bents to collapse only by water loads. Linear static analysis can be sufficient for analysis of water loads under flood events.

On the other hand, if the front column was assumed to have a pinned connection on the top, the matrix form was reduced according to Equation 3-6, shown as

$$[0] = [595.491][\Delta_B] + [-1.040] \quad \textit{Equation 3-50}$$

Solving Equation 3-50 obtained

$$[\Delta_B] = [1.746 \times 10^{-3}\ \text{in.}] \quad \textit{Equation 3-51}$$

Using Equation 3-13 obtained moment and shear demands to the first column, shown as

$$\begin{bmatrix} V_{bot} \\ M_{bot} \\ V_{top} \end{bmatrix} = \begin{bmatrix} -198.497 \\ -6.550\times10^{4} \\ 198.497 \end{bmatrix} \left[1.746\times10^{-3}\right] = \begin{bmatrix} -1.646 \text{ kip} \\ -100.052 \text{ kip-in.} \\ -0.433 \text{ kip} \end{bmatrix} \qquad \textit{Equation 3-52}$$

Therefore, for the case with pinned connections, the maximum moment demand occurred at the bottom with a magnitude of 100.052 kip-in. The moment demand was once again lower than the nominal flexural capacity of the column. Using linear structural analysis is appropriate for flood loading regardless of multi-column bents with pinned connections or rigid connections. Also, flood loading was not considered critical from the example. Instead, scouring effect might be more critical, and severe scouring possibly causes loss-of-supports scenarios.

3.6.2.3. Analysis of Vehicular Collision

After confirming that the stream load hardly causes collapse, assessing the structure under vehicular collision was necessary. Per Section 3.6.5 of AASHTO LRFD, a lateral load of 600 kips was added to the base structure on the first column 5 ft above the ground as shown in Figure 3-27. Again, two different cases of fixities at column tops are included. Following steps according to Section 3.4 demonstrate the analysis.

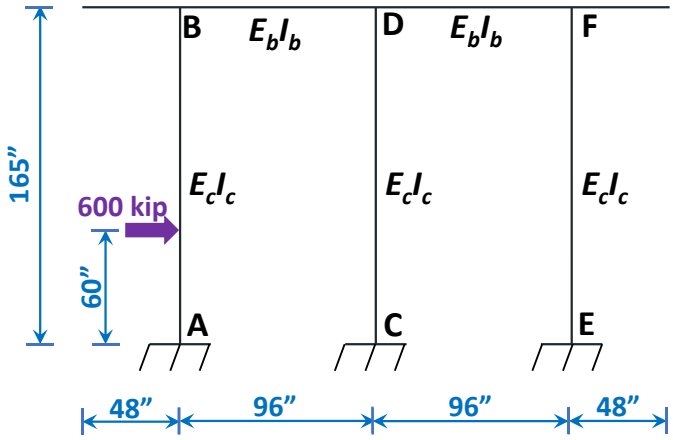

Figure 3-27. Base model under AASHTO vehicular collision load

The base structural model was transformed to a beam as shown in Figure 3-28 to determine the column axial loads. The rotational spring has a rotational stiffness K_θ of 7.204×10^6 kip-in.^{2} if well-detailed joints are present; otherwise, it has a zero stiffness if poorly-detailed joints are present.

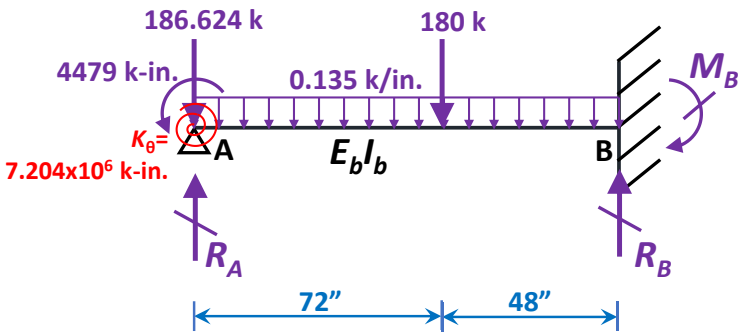

Figure 3-28. Simplified structural model for column axial loads

For either of the cases, only one degree of freedom was needed, which is the rotation at point A. Therefore, according to Equation 3-14 through Equation 3-17, the structural matrix form is expressed as Equation 3-53 for well-detailed joints and as Equation 3-54 for poorly-detailed joints.

$$[-4479] = [3.484 \times 10^7 + 7.204 \times 10^6][\theta_A] + [-2239] \qquad \textit{Equation 3-53}$$

$$[-4479] = [3.484 \times 10^7][\theta_A] + [-2239] \qquad \textit{Equation 3-54}$$

Solving Equation 3-53 and Equation 3-54 generated the rotation at point A, which is -5.327×10^{-5} rad for well-detailed joints; -6.429×10^{-5} rad for poorly-detailed joints. The negative sign indicates the rotations are counterclockwise.

Substituting the value of the rotations into the local stiffness matrix of the beam, as shown in Equation 3-55 for well-detailed joints and Equation 3-56 for poorly detailed joints, obtained end shear force V_A = 94.45 kip and 99.64 kip for well-detailed joints and poorly-detailed joints, respectively.

$$\begin{bmatrix} V_A \\ M_A \\ V_B \\ M_B \end{bmatrix} = 8.710\times10^6 \begin{bmatrix} 8.333\times10^{-4} & -0.05 & -8.333\times10^{-4} & -0.05 \\ -0.05 & 4 & 0.05 & 2 \\ -8.333\times10^{-4} & 0.05 & 8.333\times10^{-4} & 0.05 \\ -0.05 & 2 & 0.05 & 4 \end{bmatrix} \begin{bmatrix} 0 \\ -5.237\times10^{-5} \\ 0 \\ 0 \end{bmatrix} + \begin{bmatrix} 71.64 \\ -2239 \\ 124.92 \\ 3276 \end{bmatrix} = \begin{bmatrix} 94.45 \\ -4064 \\ 102.11 \\ 2364 \end{bmatrix} \qquad \textit{Equation 3-55}$$

$$\begin{bmatrix} V_A \\ M_A \\ V_B \\ M_B \end{bmatrix} = 8.710\times10^6 \begin{bmatrix} 8.333\times10^{-4} & -0.05 & -8.333\times10^{-4} & -0.05 \\ -0.05 & 4 & 0.05 & 2 \\ -8.333\times10^{-4} & 0.05 & 8.333\times10^{-4} & 0.05 \\ -0.05 & 2 & 0.05 & 4 \end{bmatrix} \begin{bmatrix} 0 \\ -6.429\times10^{-5} \\ 0 \\ 0 \end{bmatrix} + \begin{bmatrix} 71.64 \\ -2239 \\ 124.92 \\ 3276 \end{bmatrix} = \begin{bmatrix} 99.64 \\ -4479 \\ 96.92 \\ 2156 \end{bmatrix} \qquad \textit{Equation 3-56}$$

Therefore, the axial load in the impacted column P_A was determined using Equation 3-57, shown as

$$P_A = 94.45 + 180 + 6.624 = 281 \text{ kip (for well-detailed joints)} \qquad \textit{Equation 3-57}$$

and

$$P_A = 99.64 + 180 + 6.624 = 286 \text{ kip (for poorly-detailed joints)} \qquad \textit{Equation 3-58}$$

It can be seen that the axial loads were slightly different, and 281 kip was used for the rest steps.

Regarding column cross-section and the material properties, a *P-M* interactive diagram was constructed as shown in Figure 3-29 to determine column flexural and shear capacity. From the figure, the moment capacity corresponding to the axial load 281 kips is 11150 kip-in.

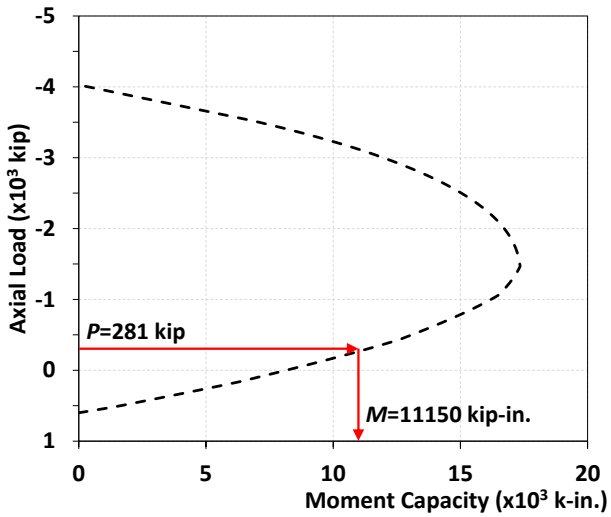

Figure 3-29. P-M interaction curve for determining moment capacity

The ratio h/H_{clear} was equal to 0.417, lower than 0.5, resulting in collapsing of the hit column (Mechanism 3). The corresponding maximum lateral load was determined by using Equation 3-35 and Equation 3-37 for well-detailed joints and poorly-detailed joints, respectively, shown as

$$\frac{11150 \text{ kip-in.}}{P\ (144 \text{ in.})} = (0.417)(1 - 0.417)\left(\frac{1}{2}\right) \text{ (for well-detailed joints)} \qquad \textit{Equation 3-59}$$

and

$$\frac{11150 \text{ kip-in.}}{P\ (144 \text{ in.})} = (0.417)\left(\frac{1 - 0.417}{2 - 0.417}\right) \text{ (for poorly-detailed joints)} \qquad \textit{Equation 3-60}$$

Solving Equation 3-59 obtained that lateral collision load *P* equals 637 kips, which is higher than the AASTHO requirement for vehicular collision (600 kips). Therefore, the three-column bent with well-detailed joints has sufficient moment capacity to sustain vehicular collision. On the other hand, solving Equation 3-60 obtains that lateral collision load *P* equals 504 kips, which is lower than the AASHTO requirement when connections are pinned to the bent cap. This observation indicates that the structure is more likely to sustain a vehicular collision if the joints are well-detailed rather than poorly-detailed.

Next step is to check shear capacity and bond strength of ductility. According to the free body diagrams in Figure 3-14, given the end plastic moment being (1.25)(11150 kip-in.) = 13938 kip-

in., shear demands to the column top and the column bottom were 332.9 kips and 466.1 for well-detailed joints; 166.5 kips and 466.1 kips for poorly-detailed joints, respectively. The results are summarized in Figure 3-30.

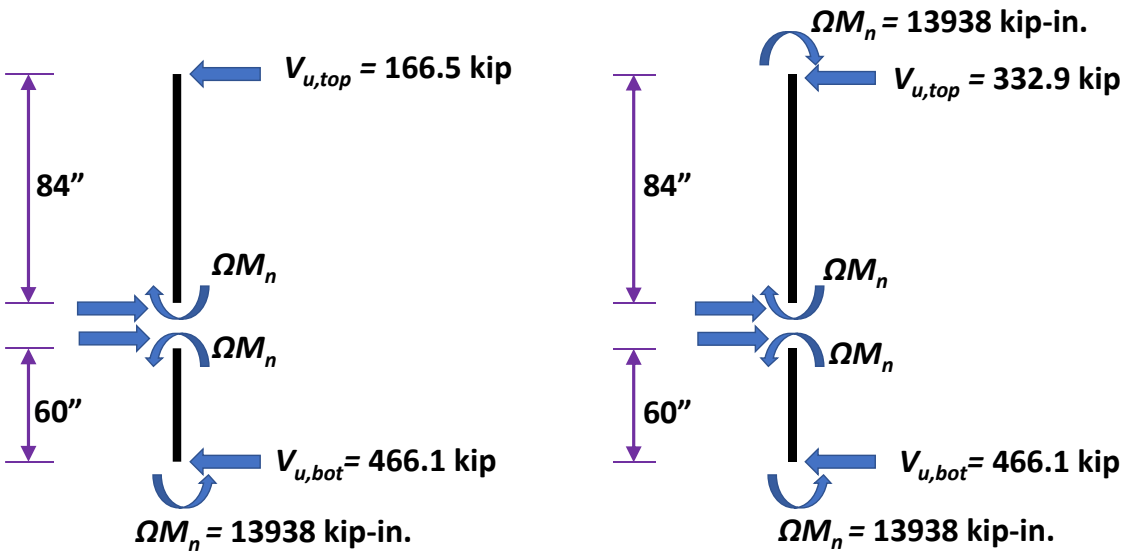

(a) Poorly-detailed joints (b) Well-detailed joints

Figure 3-30. Shear demands to the impacted column when under plastic moment

In the meantime, the shear capacities of the column at the top joint and the bottom were determined using Equation 3-38 through Equation 3-41. Using Equation 3-39 with a *k*-value of 0.6 obtained the contribution of concrete shown as

$$V_c = 0.6(\sqrt{4000}\text{psi})(0.8)\left(\frac{\pi}{4} \times 36^2\text{in.}^2\right) = 30900\text{ lb} = 30.9\text{ kip} \qquad \textit{Equation 3-61}$$

As the arrangement of the spiral was the same throughout the entire column, according to Equation 3-40 the contribution of transverse reinforcement was calculated as

$$V_s = \frac{\pi}{2}\frac{(0.2\text{in.}^2)(60\text{ksi})(30\text{in.})}{3\text{in.}}\cot 35^\circ = 291.6\text{ kip} \qquad \textit{Equation 3-62}$$

The effect of the axial load on the shear capacity was determined using Equation 3-41. The angle of the diagonal struts varies depending on the position under consideration and the fixity of the connection. For the column bottom, the term tanα in Equation 3-41 is equal to $0.8D_c/h = 0.48$ referring to Figure 3-15. For the column top, the rigid connection leads to a tanα of $0.8D_c/(H\text{-}h) = 0.343$, while the pinned connection led to a tanα of $0.4D_c/(H\text{-}h) = 0.171$. In sum, the contribution of the axial load was expressed as

$$V_p = (281\text{kip})(0.48) = 134.88\text{ kip (for column bottom)} \qquad \textit{Equation 3-63}$$

$$V_p = (281\text{kip})(0.343) = 96.34 \text{ kip (for column top, rigid connection)} \quad \textit{Equation 3-64}$$

$$V_p = (281\text{kip})(0.171) = 48.17 \text{ kip (for column top, pinned connection)} \quad \textit{Equation 3-65}$$

Taking summation of V_c, V_s, and V_n generated shear capacities at different positions, which are summarized in Table 3-1.

Table 3-1. Shear capacities at various positions

	Rigid connection	Pinned connection
Column top	418.8 kip	370.7 kip
Column bottom	457.4 kip	457.4 kip

Other than analysis of shear, the anchorage in the column-to-bent connection was evaluated by comparing the extension of the column longitudinal bars to the overstrength development length shown as

$$l_d = 2.4(1.128 \text{ in.})\frac{(1.25)(60\text{ksi})}{\sqrt{(4\ )}\text{ksi}}\left(\frac{(1.0)(1.0)(0.4)(1.0)}{1.0}\right) = 40.61 \text{ in.} \quad \textit{Equation 3-66}$$

In addition, the confinement requirement, according to Equation 3-42, is given as

$$\rho_s = \frac{4(0.2 \text{ in.}^2)}{(30 \text{ in.})(3 \text{ in.})} = 0.89\% \geq 0.12\frac{4 \text{ ksi}}{60 \text{ ksi}} = 0.8\% \quad \textit{Equation 3-67}$$

To assess and discuss the result of Example 1, the comparison between resistance to vehicular collision and the requirement of AASHTO LRFD is summarized in Table 3-2.

Table 3-2. Assessment of lateral resistance to vehicular collision

Connection type	Demand	Capacity	D/C ratio
Rigid connections	600 kip	637 kip	0.942
Pinned connections	600 kip	504 kip	1.190

It can be seen from Table 3-2 that when rigid connections are used in the three-column bent, the D/C ratio is less than one, indicating the vehicular collision load required by AASHTO LRFD would not cause the collapse mechanism of the first column. However, if pinned connections are used, the D/C ratio is higher than one, meaning the bent does not have enough resistance to vehicular collision per AASHTO LRFD. The observation also reveals that using moment connections in multi-column bents would largely increase the resistance to vehicular collision.

Although the three-column bent with rigid connections has higher possibility not to exhibit a collapse mechanism, the shear capacity for preventing brittle failures becomes a concern. Both cases do not have sufficient shear capacity to take required shear forces at the bottom. Moreover,

the results were derived with the use of arch effect. If the typical AASHTO method for shear resistance was used, a lower shear resistance could be derived.

In addition, the anchorage and confinement in the column-to-bent connections are potentially insufficient. As shown in Table 3-3, the available extension of the column reinforcing bars in the connections is 36 in., shorter than the overstrength development length 40.61 in. Moreover, no confinement is provided in the column-to-bent connections.

Table 3-3. Assessment of development length and joint confinement

Development length			Joint confinement		
Required	Available	Assessment	Required	Available	Assessment
40.61 in.	36 in.	NG	0.89%	0%	NG

3.6.3. Example 2: Subjected to Loss of Support

3.6.3.1. Base Structural Model

The same three-column bent introduced in Section 3.6.1 is used in this analysis example. That is, the base structural model had identical configurations and sectional properties. In this case, the scenario to be analyzed has girder load applied on the exterior spans assumed 121 kips; while the girder load applied on the interior spans was 165 kips. The self-weight was automatically generated by SAP2000. The base model is shown in Figure 3-31.

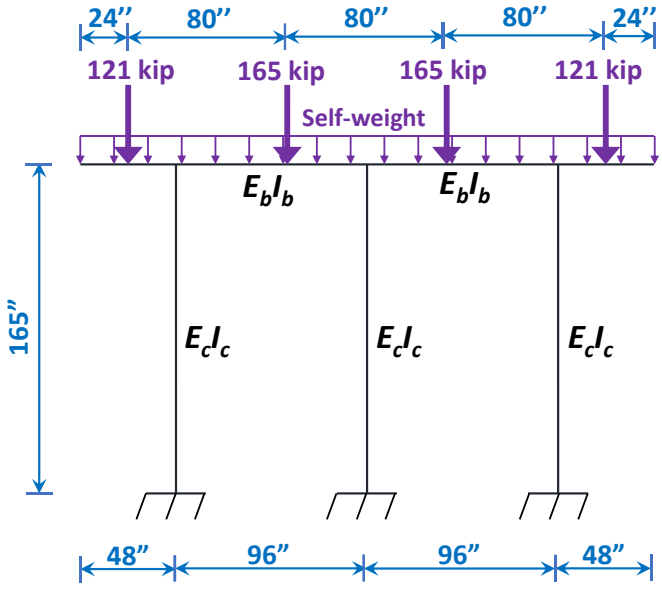

Figure 3-31. Base model of analysis for loss a support

3.6.3.2. SAP2000 Model Preparation

According to Figure 3-31, one could simply transform the structure into a numerical model based on the configuration, material, and sectional properties, as shown in Figure 3-32. Girder loads were assigned accordingly. The boundary condition at the base was assumed fixed, and column-to-bent connections were assumed rigid.

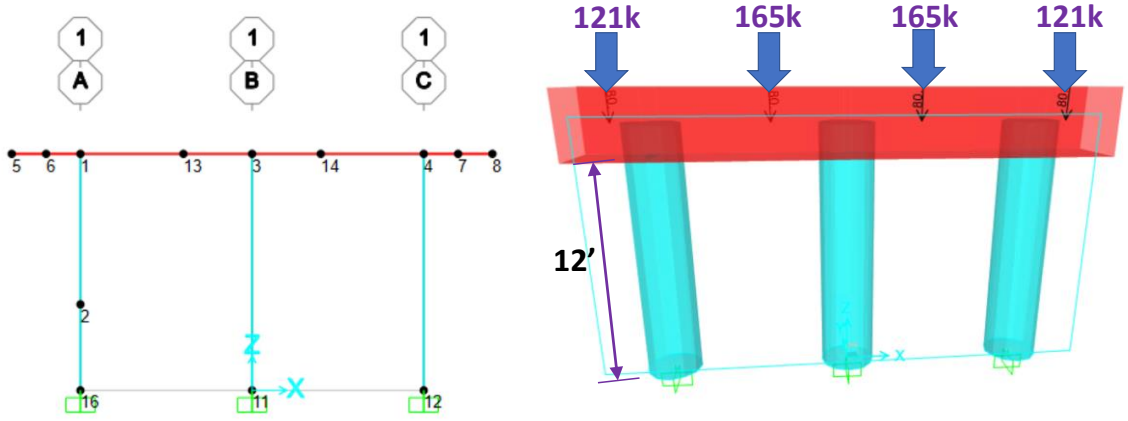

(a) Elevation view (b) Extrusion view

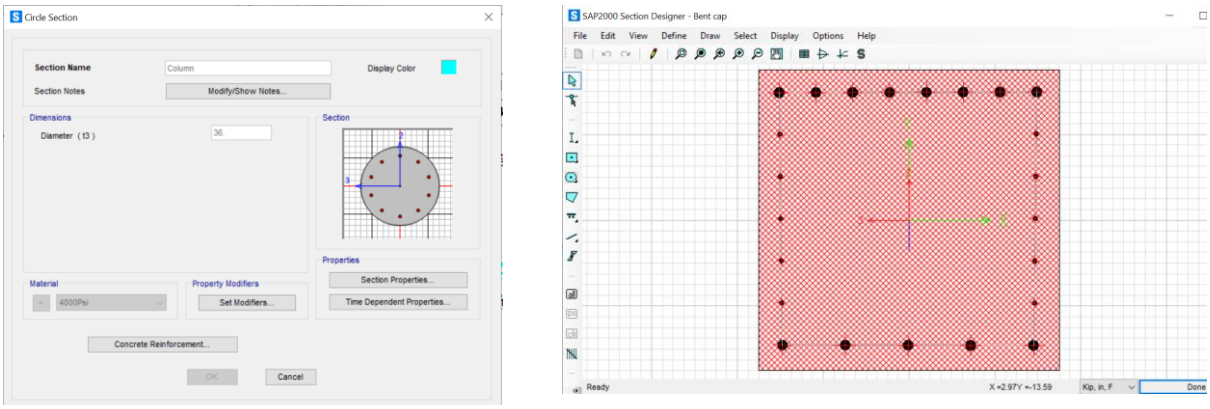

(c) Column cross-section (d) Bent cap cross-section

Figure 3-32. SAP2000 numerical model of example three-column bent

Upon the completion of the numerical model, one could determine reactions provided by the first column (i.e. the column to lose) under the current load condition. It was achieved and the results are shown in Figure 3-33. At the column top (denoted as Joint 1), the axial force was 215.4 kips, the shear force was 0.48 kips, and the moment was 54.6 kip-in.

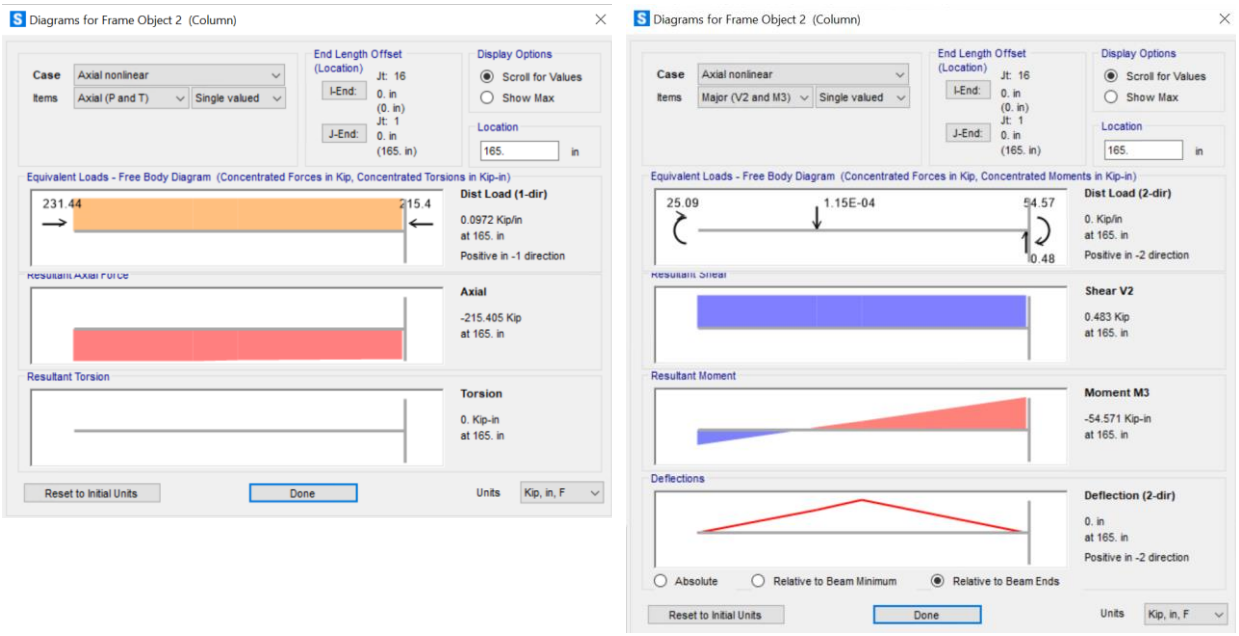

(a) Axial force (b) Shear force and moment

Figure 3-33. Output of reactions at Joint 1

After determining the reactions at Joint 1, the column was removed as shown in Figure 3-34. Everything else remained the same.

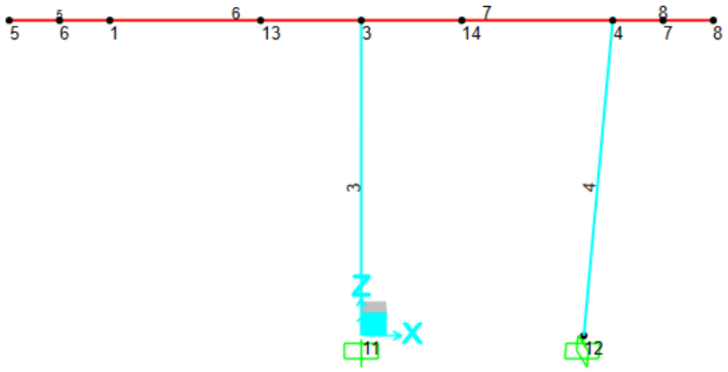

Figure 3-34. SAP 2000 model of the example bent with a column removed

3.6.3.3. Nonlinear Dynamic Analysis

The output reactions introduced in the previous section were assigned back to Joint 1 to create the initial condition, as shown in Figure 3-35.

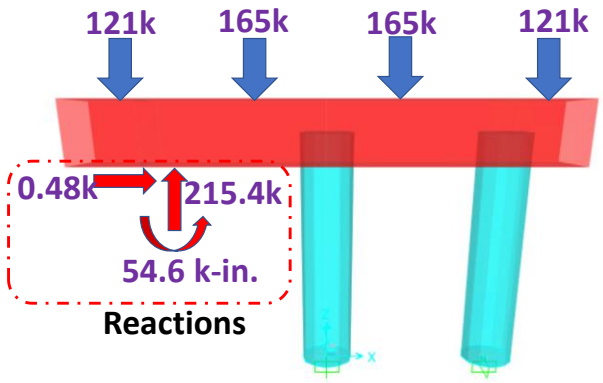

Figure 3-35. Applying reactions back to the model

As shown in Figure 3-36, loads with the same magnitude but in the opposite direction to the reactions were applied back to Joint 1.

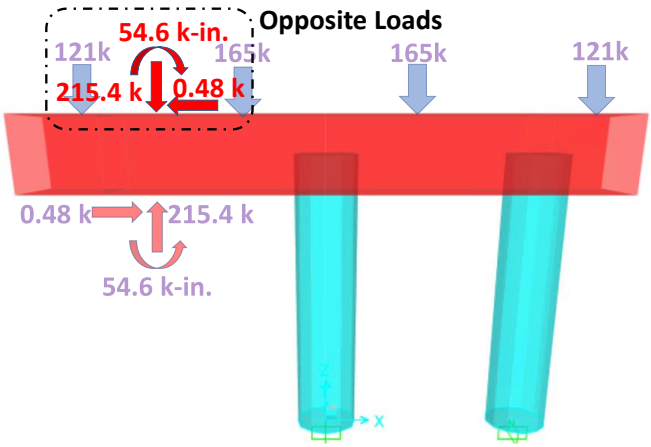

Figure 3-36. Applying loads opposite to reactions at Joint 1

Since the loads were supposed to counterbalance the reactions rapidly, a time history function of ramping was defined. The loads were set to develop to its full magnitude within a time period. To determine the time period, a modal analysis was first executed to determine the corresponding natural vibration period, and it was found that the natural period was 0.0489 seconds as shown in Figure 3-37.

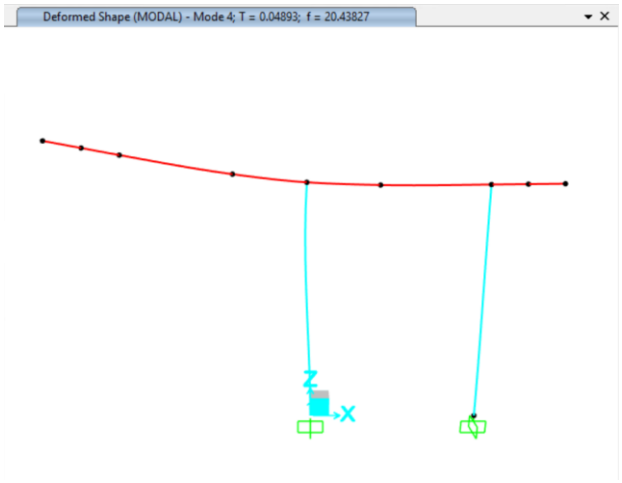

Figure 3-37. Natural period of vibration of the bent

Therefore, the ramping time was specified as 4×10^{-3} seconds, which is less than 1/100 of the natural period. The time history function was automatically generated by SAP2000 as shown in Figure 3-38. The point corresponding to a time of 10 seconds was for numerical purposes.

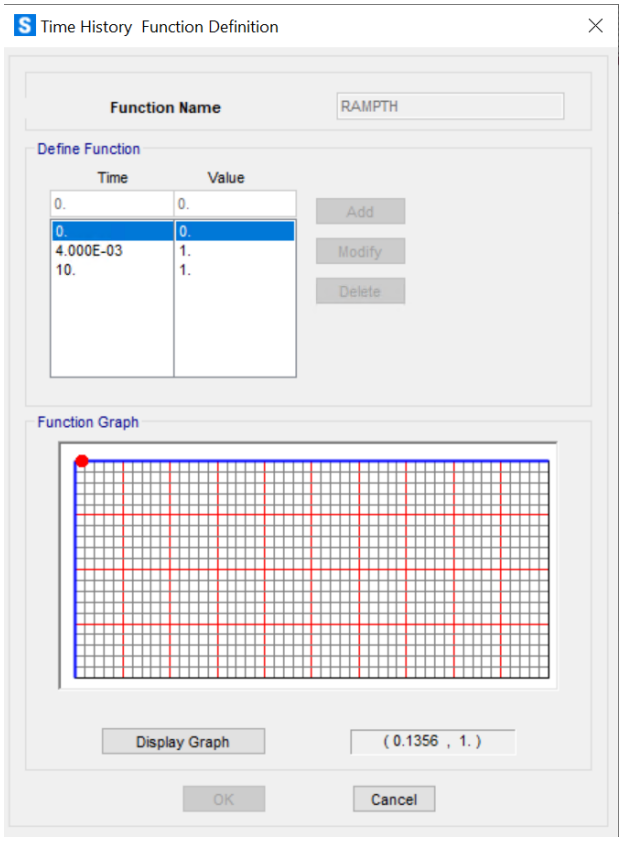

Figure 3-38. Definition of ramping function

Plastic hinge properties were defined for the bent cap as shown in Figure 3-39. Datapoints shown in the figure were derived from sectional analysis software Response-2000. The plastic hinge length was specified as 21 in., which is half the depth of the bent cap. Plastic hinges were assigned to ends of each bent cap span.

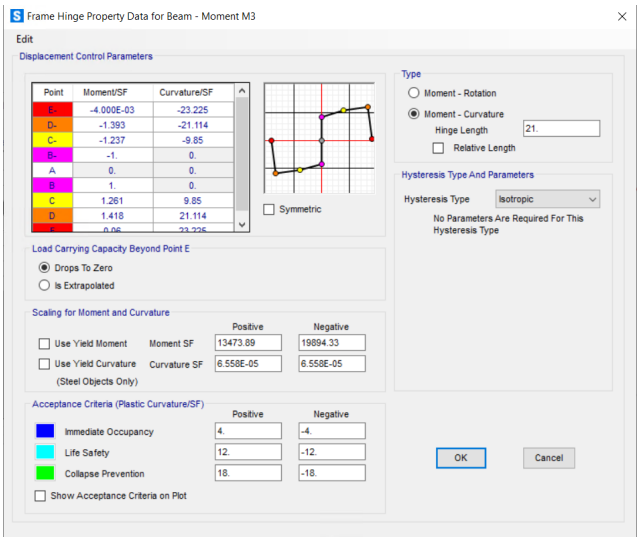

Figure 3-39. Bent cap plastic hinge properties

Figure 3-40 shows parameters specified for the nonlinear dynamic analysis. The analysis was set to start after the initial condition. The inherent damping ratio was selected as 3% and direct integration was used for iteration. The time output step size was 5×10^{-4} and the total number of steps was 20000.

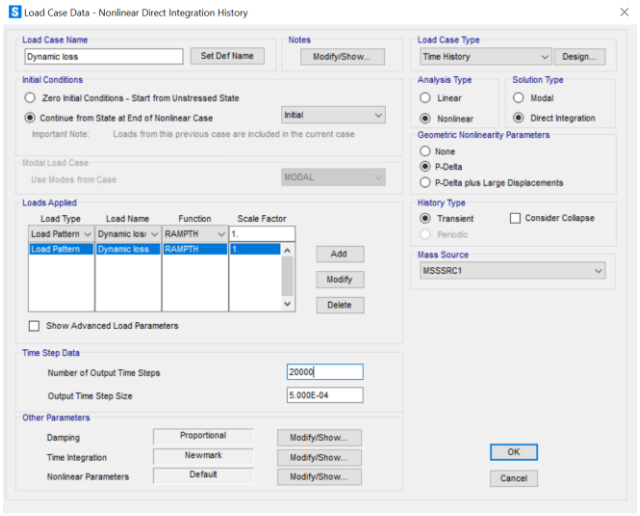

Figure 3-40. Parameters of dynamic analysis

3.6.3.4. Linear Static Method

According to Section 3.5, the gravity loads, including girder loads and self-weight, were amplified by a factor of two, resulting in a status shown in Figure 3-41(a). In SAP2000, the operation was done simply by specifying load factor as shown in Figure 3-41(b). The factor 2.2 shown in the figure includes original load factor 1.1 in the previous example and the dynamic amplification factor.

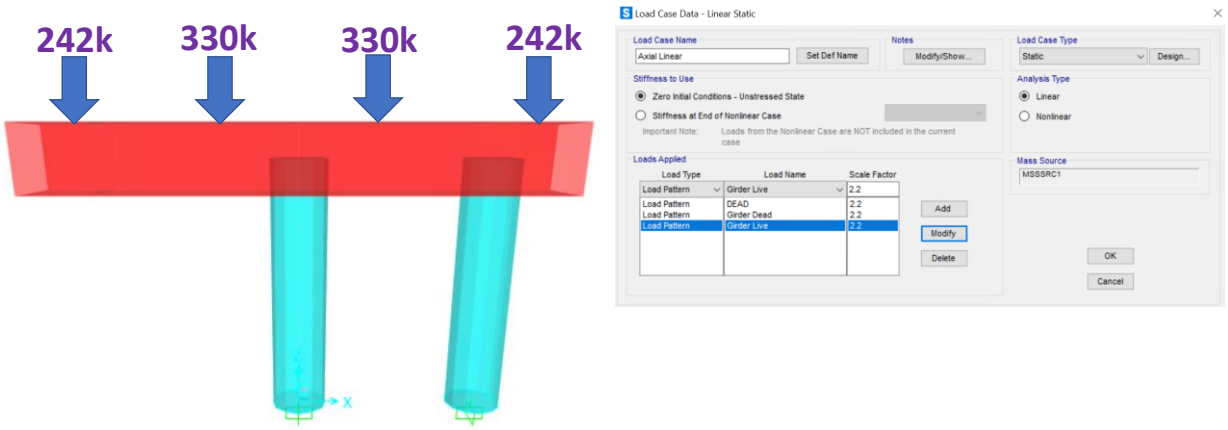

(a) Amplified gravity loads (b) SAP 2000 load case settings

Figure 3-41. Amplified gravity loads and settings

For the linear static analysis, there were not as many parameters to setup as the nonlinear dynamic analysis introduced previously. The final settings are shown in Figure 3-41(b). In addition, a linear dynamic analysis was configurated for the purpose of comparison. In this case, the load case type was specified as dynamic while other parameters remained the same.

3.6.3.5. Results and Discussions

Figure 3-42 shows the displacement time history curves derived from various methods at Joint 1, where the column was lost. The result obtained from linear dynamic method is presented in the figure for the purpose of comparison. The displacement predicted by the linear static method is a constant because it is independent of time. The peak displacements predicted by each of the methods are also presented in the figure.

Regarding the result of nonlinear dynamic method, the bent cap overhang drastically went down in the first 0.1 second after the removal of the front column. The displacement reached its peak at 0.14 second and the peak displacement was 3.42 in. After reaching the peak, the overhang bounced back and vibrated with a small magnitude. The vibration almost completely decayed in the first 0.4 second and had a residue displacement of 3.39 in. The bounce back of the overhang and

attainment of steady state indicate that no total collapse was happening. It was likely the three-column bent survived loss of the first column.

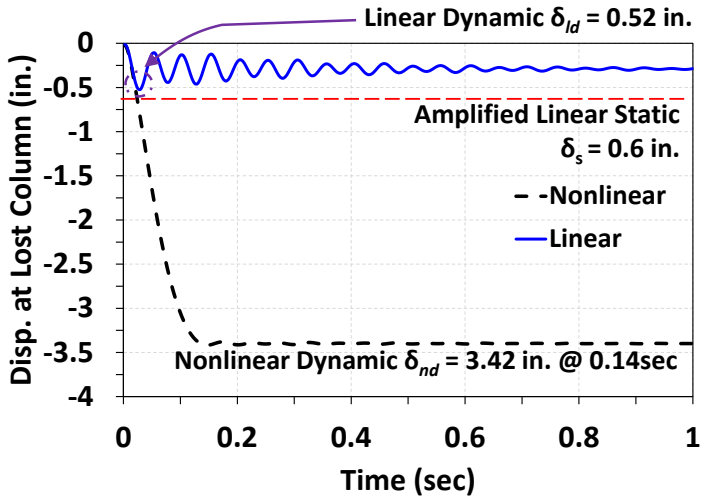

Figure 3-42. Displacement time history of different methods

The analytical plastic hinge status and the deformation of the structure, shown in Figure 3-43, also support reveal that the three-column bent would not exhibit a catastrophic collapse after losing the column. Firstly, most plastic deformation concentrated on the end of the overhang bent cap, reaching a peak rotation of 0.0263 rad. On the other side of the joint, some plastic rotation also developed, but only slightly exceeded the yield rotation. The rotational capacity of the end bent cap was 0.0291 rad, resulting in a demand-to-capacity ratio (DCR) of 0.9. Therefore, the joint was likely to sustain the rotation, although largely damaged, after losing the column, if no shear failure in the joint occurred. On the other hand, no column joints reached plastic region.

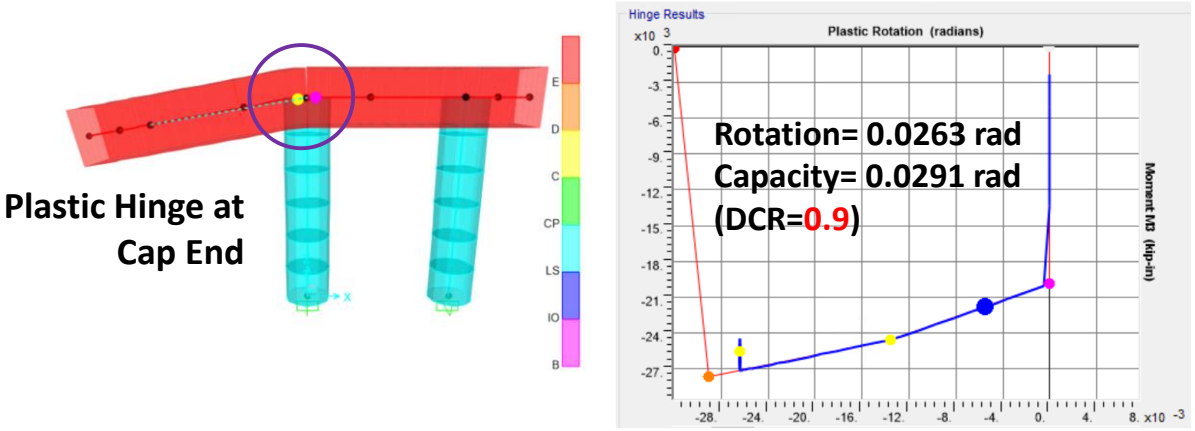

(a) Overall deformation (b) Plastic hinge status

Figure 3-43. Analytical results of plastic hinges

In addition to the nonlinear dynamic method, the linear static method also delivered promising results. First, the displacement at Joint 1 caused by the amplified gravity loads reached 0.6 in., which is close to and slightly higher than that of linear dynamic analysis. The observation indicates that an amplification factor of 2.0 reasonably accounts for dynamic effects.

Furthermore, comparing amplified moments to modified capacity also yields a similar DCR to the nonlinear dynamic method. It can be seen from Figure 3-44 that the amplified moment demands to the end of the bent cap was 44581 kip-in. and to the column top was 10103 kip-in. The modified capacity of the bend cap, on the other hand, was determined as shown in Eq. 2-68; and that of the column was calculated as shown in Eq. 2-69. The DCR for the bent cap was 0.83 and the DCR for the column was 0.38. Therefore, the linear static method also reveals that the structure was likely to survive losing the column.

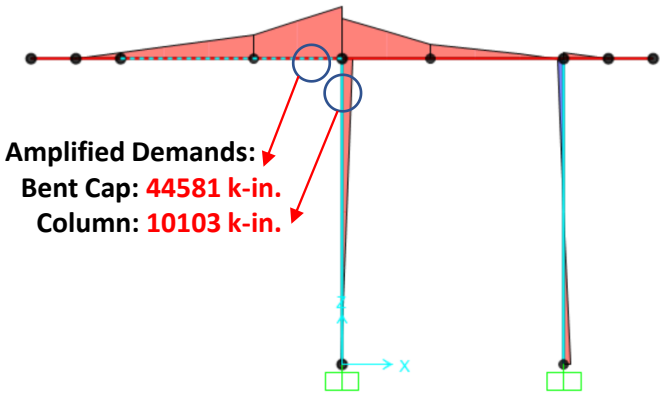

Figure 3-44. Generated moment diagram and peak moments

$$\phi m M_n = (0.9)(3)(19894 \text{ kip-in.}) = 53714 \text{ kip-in.} > 44581 \text{ kip-in} \quad \textit{Equation 3-68}$$

$$\phi m M_n = (0.9)(3)(9785 \text{ kip-in.}) = 26420 \text{ kip-in.} > 10103 \text{ kip-in.} \quad \textit{Equation 3-69}$$

In sum, both methods provide valuable insights into the response of the three-column bent when losing a column. Both methods delivered similar results, but the linear static method did not require intensive computational resources.

3.7. Summary

It has long been suggested that extreme events such as flood, vehicular collision, and loss of a support be taken into consideration when designing multi-column bents. TxDOT bridge design manual also introduces the load combination for Extreme Event III and measures for vehicular collision. However, the current method only accounts for shear forces based on an oversimplified assumption that two shear planes at the collision point can be involved. In addition, both AASHTO LRFD and TxDOT bridge design manual do not explicitly provide methods for loss of a support.

To address this, the research team proposed a holistic framework that incorporates the analysis of standard multi-column bents under all three extreme events. The methods were developed based on static analysis, upper bound theorem of plasticity, and nonlinear dynamic analysis.

Analysis examples using the proposed methods are provided. It was observed that flooding loads hardly cause multi-column bents to demonstrate nonlinear response. In addition, using moment column-to-bent connections in multi-column bents exhibits higher resistance to vehicular collision. Moreover, shear capacity, anchorage, and confinement are recommended to be taken care of to guarantee ductile behavior. Lastly, both computer-assisted linear static method and nonlinear dynamic method were proved to be effective for analysis of loss of a support.

Chapter 4. Experimental Program and Finite Element Analysis

Multi-column reinforced concrete bents are among the most commonly used bridge substructures. Their inherent redundancy due to the multiple supporting columns providing several load paths makes it highly efficient for resisting ultimate loads. Bent-to-column connections are vital for transferring loads from the bent cap to the column, especially during extreme loading events, such as collisions or flooding. In recent years, extreme events such as vehicle collisions, floods, and scouring have increased. Because of this, considerable research has focused on investigating the impact of extreme events on bridges. These extreme events are generally represented as equivalent static lateral loads. According to the TxDOT Bridge Design Manual, an Equivalent Static Force (ESF) of 600 kips is used to design the structure for vehicular collisions. Commonly used structural analysis methods for bent caps assume a simply supported continuous beam, where moments transfer between the bent cap and column is neglected. However, a basic structural analysis indicates that lateral loads, such as those from collision, induce moment at the joint between the column and bent cap.

There is limited knowledge on the behavior of the bent-to-column connection under lateral loading. Research thus far suggests that further investigation is required to better understand the response of connections. For example, Klinga & Alipour (2015) explored the behavior of bridges supported on pile-group foundations under the influence of scour. The erosion of sediment around the structure exposes the axially loaded substructure to instability and potentially larger lateral loadings, weakening the structure. Their simulation results revealed that a structure's lateral resistance reduces as scour depth increases. These findings raise a concern that the reinforcement in the bent-to-column connections may require detailing improvements because adequate detailing is essential for the overall structural response of the connection.

Some detailing practices around the US require increased confinement and shear reinforcement in the joint region, which are commonly used in seismic areas to prevent joint failure, enhance ductility, and facilitate the development of the ultimate capacity of the adjacent members. In low seismic areas, limited implementation of these practices has been seen, yet concern about other lateral loads brings forth the question of whether these details should be enacted. Multiple studies have investigated the behavior of different reinforcing detailing in the bent-to-column connection, observing the effects of confinement and bar anchorage. For example, Roeder et al. (2001) investigated the seismic performance of moment-resisting pile-wharf connections with various detailing, including different levels of confinement and bar anchorage. Overall, the connections tolerated large cyclic deformations but observed a large deterioration of resistance and stiffness. Additionally, Hoshikuma et al. (1997) investigated the effect of crossties on confinement, noting that crossties performed significantly better than the unconfined specimens, showing increased

ductility. Both of these studies lack the direct implications of a monotonically loaded column, resembling a collision loading, onto the connection.

Moreover, the bond strength of the longitudinal bars in the bent-to-column connection is a key component in the strength and ductility of these substructures. A key concern of these connections is the available length required to properly develop the bars. Research conducted by Fawaz (2021) investigated the influence of longitudinal bar bond strength on the lateral response of reinforced concrete columns. The study suggests that partial debonding improves deformation capacity but exhibits reduced lateral load resistance when compared to the specimen without debonding. This finding highlights the importance of properly bonded bars in achieving the ultimate capacity of the system. Additionally, other studies demonstrated the improvement of bond strength due to different anchorage details.

This chapter evaluates the impact of detailing improvements at the bent-to-column connection identified in previous studies, focusing on their direct effects on bent-to-column connection specimens subjected to monotonic lateral loading. The investigation extends prior work by assessing how enhanced confinement and anchorage improve structural performance. Additionally, to compare and analyze the influence of lateral load direction, tests were conducted separately for failure in the in-plane and out-of-plane directions.

4.1. Phase I: In-Plane Direction Tests

4.1.1. Specimen Design

Nine bent-to-column subassemblies were fabricated and tested to failure at Ferguson Structural Engineering Laboratory at the University of Texas at Austin as part of Phase I of the experimental program. Table 4-1 summarizes the test matrix, and Figure 4-1 illustrates the cast-in-place specimens' geometry and reinforcement details. The specimens were tested under a constant axial load and a monotonically-increasing lateral load. Self-reacting and non-self-reacting axial test frames were employed for the axial load application. This approach aimed to simulate scenarios where a girder is positioned on top of the connection, thus being a more favorable boundary condition for the strength of the connection. Figure 4-3 illustrates the real-world applications of each of the different boundary conditions investigated. Only Specimen S-NS-CIP-NH* utilized the self-reacting axial load frame, while all other specimens were tested with the non-self-reacting axial load frame, deemed as the critical layout.

The bent caps were reinforced with three #11 longitudinal bars placed at the top and bottom, and #5 closed stirrups spaced 6 in. apart throughout the beam, except in the joint region where no vertical reinforcement was provided. For the bent caps of specimens S-SK-CIP-NH, HK-SK-CIP-NH, and HD-SK-CIP-NH, two #5 bars were included as skin reinforcement, as illustrated in Figure 4-1(a), reflecting current detailing standards in Texas. No skin reinforcement was provided in the bent cap of specimens S-NS-CIP-NH* and S-NS-CIP-NH, consistent with past detailing practices.

For specimens S-SK-CIP-H2 and S-SK-CIP-H4, #3 hoop reinforcement was provided in the joint region, spaced at 2 in. and 4 in., respectively, representative of current AASHTO seismic standards and the TxDOT manual.

All columns were reinforced with ten #9 longitudinal bars placed symmetrically around the perimeter. Regarding spiral reinforcement, all columns featured #3 spiral reinforcement with a 6 in. pitch, as shown in Figure 4-1 (c), except for specimens S-SK-CIP-H2 and S-SK-CIP-H4, which had a pitch of 2 in. and 4 in., respectively. Specimens S-NS-CIP-NH*, S-NS-CIP-NH, S-SK-CIP-NH, HK-SK-CIP-NH, HD-SK-CIP-NH, S-PC, and HD-PC had identical reinforcement layouts in the columns, differing only in the method of anchorage for the longitudinal column reinforcement. Specimens S-NS-CIP-NH- NH*, S-NS-CIP-NH, S-SK-CIP-NH, S-PC, S-SK-CIP-H2, and S-SK-CIP-H4 utilized straight bar anchorage into the bent cap for longitudinal column reinforcement, while HK-SK-CIP-NH used 180-degree hooks, and HD-SK-CIP-NH and HD-PC incorporated headed bars in compliance with ASTM A970/A970 M standards.

Specimens S-NS-CIP-NH* and S-NS-CIP-NH represented the past standard details used in Texas in the ‘70s. This configuration lacks confinement reinforcement in the joint region and skin reinforcement in the bent cap. Specimen S-SK-CIP-NH was to evaluate the performance of a connection featuring straight column longitudinal bars without confinement reinforcement in the joint, but incorporating skin reinforcement in the bent cap. This setup was to reflect the current standard details used in Texas. Table 4-1 summarizes all specimen properties, including their respective material properties. The steel elastic modulus for all specimens was within 10% of 29000 ksi.

The design of precast bent caps was compatible with the TxDOT standard PPBC-RC. This design included 24 Gr. 270-0.6 in. prestressing strands spaced at 2 in. and a corrugated steel pipe at the joint, as illustrated in Figure 4-2(a). The bent cap widths in S-PC and HD-PC were scaled down from 36 in. to 32 in due to test setup constraints. To ensure the required strength, a concrete strength of 6.1 ksi was specified to ensure a capacity of 1600 kip-ft. The corrugated metal pipe was designed to extend through the entire section for ease of construction, as shown in Figure 4-2(c).

Table 4-1: Test matrix for in-plane direction testing

	Bent Cap						Column				
Specimen ID	Axial Load	Anchorage Type	Skin Reinforcement	ρ long. (%)	ρ trans. (%)	f'_c (psi)	ρ spiral. (%)	ρ long. (%)	f'_c (psi)	f_y (ksi)	f_u (ksi)
S-NS-CIP-NH*	Self-reacting	Straight		1.16	0.29	5850	0.4	2.2	5250	67.8	95.8
S-NS-CIP-NH	Non-self-reacting	Straight		1.16	0.29	3110	0.4	2.2	5580	65.9	108.0
S-SK-CIP-NH	Non-self-reacting	Straight	Y	1.16	0.29	5920	0.4	2.2	5390	67.8	95.8
S-SK-CIP-H4	Non-self-reacting	Straight	Y	1.16	0.29	4430	0.6	2.2	5120	65.9	108.0
S-SK-CIP-H2	Non-self-reacting	Straight	Y	1.16	0.29	5180	1.2	2.2	4150	68.0	109.5
HK-SK-CIP-NH	Non-self-reacting	Hook	Y	1.16	0.29	5190	0.4	2.2	4930	78.8	103.1
HD-SK-CIP-NH	Non-self-reacting	Head	Y	1.16	0.29	5370	0.4	2.2	3030	68.3	94.7
S-PC	Non-self-reacting	Straight		0.71	0.24	8350	0.4	2.2	3640	68.0	109.5
HD-PC	Non-self-reacting	Head		0.71	0.24	8960	0.4	2.2	4560	68.3	94.7

Note: *Self Reacting Testing Frame

Specimen Label Key

Anchorage:	S = Straight Bar	HK = Hooked Bar	HD = Headed Bar
Reinforcement:	NS = No Skin Reinforcement	SK = Skin Reinforcement	
Cast:	CIP = Cast-in-place	PC = Precast	
Hoop Confinement:	NH = No Hoop	H2 = Hoop 2 in. Spacing	H4 = Hoop 4 in. spacing

ρ = Reinforcing Steel Ratio
f'_c = Day of Testing Compressive Strength of Concrete
f_y = Steel Yield Strength
f_u = Steel Ultimate Strength

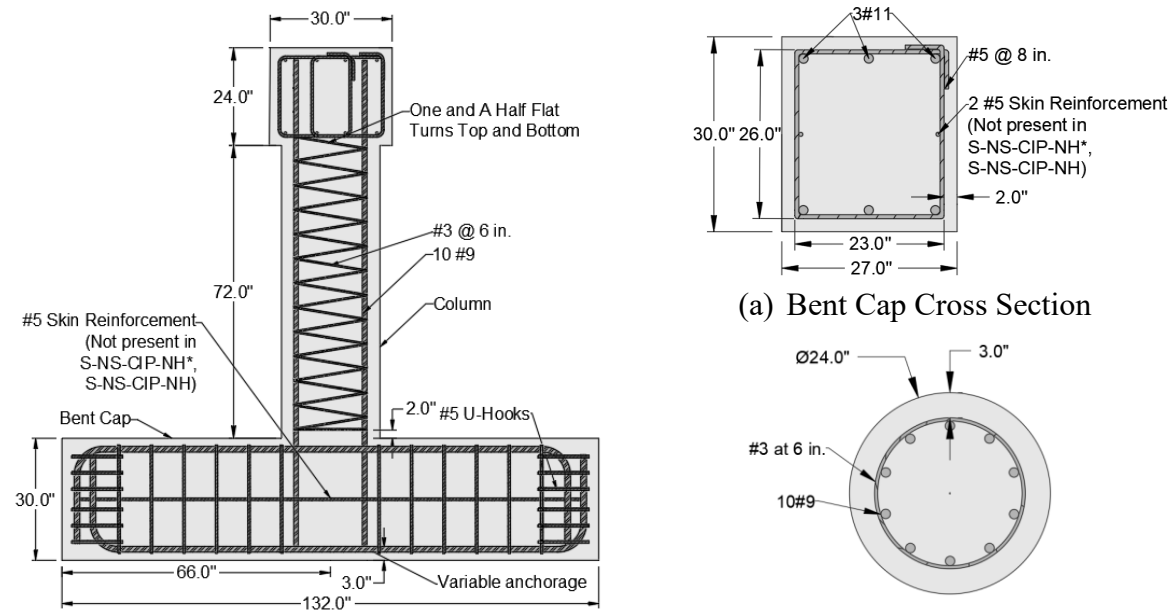

(a) Bent Cap Cross Section

(b) General Reinforcement Layout

(c) Column Cross Section

Figure 4-1. Cast-in-place specimen reinforcement details

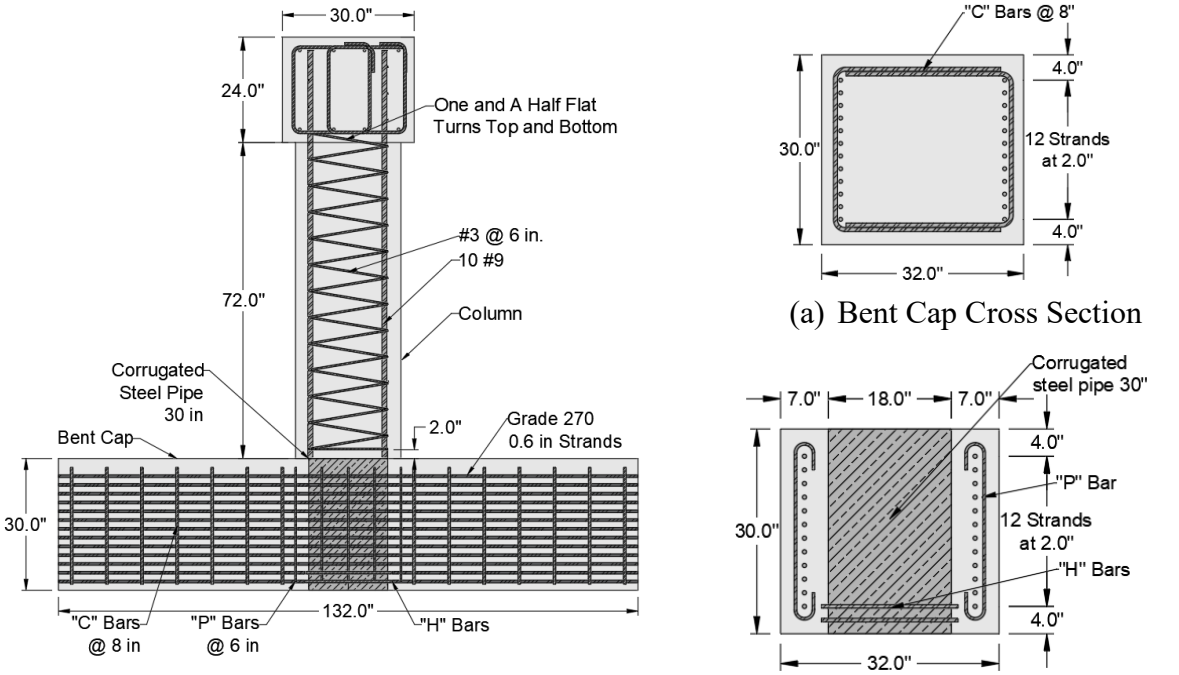

(a) Bent Cap Cross Section

(b) General Reinforcement Layout

(c) CMP Bent Cap Cross Section

Figure 4-2. Precast specimen reinforcement details

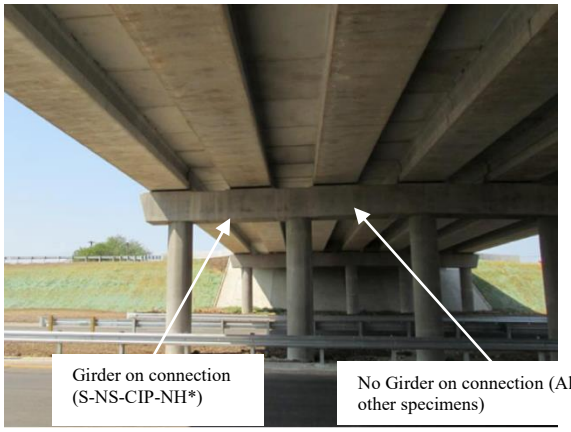

Figure 4-3. Bridge substructure

All specimens were fabricated using reinforcing bars conforming to ASTM A615/A615M Gr. 60 steel specifications. Strain gauges were installed along the compressive and tension bars in both the column and bent cap, with 12 in. spacing, as shown in Figure 4-4 (a). Additional gauges were applied along the skin reinforcement, the spiral, and the hoop reinforcement. For the precast bent caps, strain gauges were instrumented on the corrugated metal pipe in the vertical and horizontal positions at quarter turns, and on the P bars at 6 in. spacing demonstrated in Figure 4-4 (b).

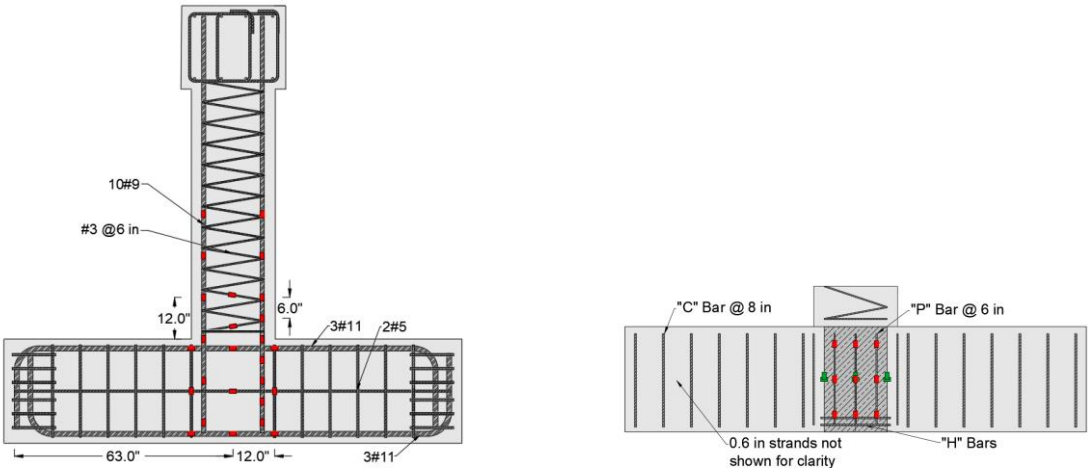

(a) Typical placement of strain gauges for cast-in-place specimen

(b) Typical placement of strain gauges for the precast bent cap

Figure 4-4. Strain gauge instrumentation

The reinforcement cages for the column and bent cap were constructed separately. After installing the strain gauges and tying the reinforcement cages, the assemblies were placed into the steel formwork, first the bent cap followed by the column. Examples of the hooked, headed, and hoop

bars positioned in the bent are displayed respectively in Figure 4-5(a), Figure 4-5(b), and Figure 4-5(c). The bent and column were cast in two different concrete placements to replicate real-world conditions, resulting in a cold joint at the interface between the column and the bent cap.

The concrete mix design consisted of class C concrete with fly ash, designated to achieve 3600 psi strength at 28 days, a water-cement ratio of 0.45, and air entrainment of 1.5%. The casting of the bent cap involved three pours, with vibration after each layer as depicted in Figure 4-5(d). During casting, this interface between the bent cap and the column was intentionally roughened to enhance the bond for subsequent layers. Surface roughening was achieved by creating an orthogonal pattern of 0.25 in. deep ruts spaced every 3 in. After casting the bent, the column formwork was installed, and the column was subsequently cast using similar techniques to those of the bent cap but with four pours for the column and two for the top block, including vibration in between each new layer. The specified concrete compressive strength was 3600 psi, with a maximum aggregate size of 1 in. The complete cast-in-place specimen is illustrated in Figure 4-5(e). The precast bent caps were fabricated at a local prestressing plant, as shown in Figure 4-5(f). The 24 strands were jacked to $0.75f_u$ (202.5 ksi) prior to the concrete being poured. The column was fabricated and cast using similar techniques to the cast-in-place columns, with two additional pours before the interface exemplified in Figure 4-5(g). The complete precast specimen is shown in Figure 4-5(h).

(a) Hooked bars (HK-SK-CIP-NH)

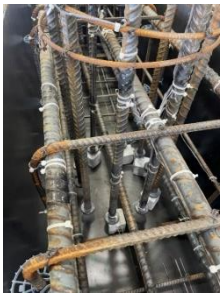

(b) Headed bars (HD-SK-CIP-NH)

(c) Hoop bars (S-SK-CIP-H4

(d) Cast bent cap

(e) Complete specimen

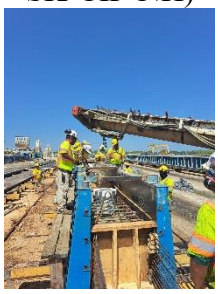

(f) Precast bent cap cast

(g) Precast column cast

(h) Complete precast specimen

Figure 4-5. Specimen construction

4.1.2. Test Setup, Instrumentation, and Loading Procedure

Figure 4-6 illustrates the test setup, including the axial load frame and major instrumentation. The self-reacting frame shown in Figure 4-6(a) was used to provide external confinement to simulate a girder on the connection. The non-self-reacting frame, illustrated in Figure 4-6(b) was used for the remainder of the tests because it was determined to represent the critical scenario for the connection. A 330-kip MTS hydraulic actuator was used to apply the lateral load, measured with a load cell in the MTS actuator. The axial loading system is depicted in Figure 4-6(d), which illustrates the clevises, rams, and load cells located at the top of the green beam. The string potentiometer and linear potentiometer presented in Figure 4-6(c) respectively were installed to measure the lateral displacements and the bar slip.

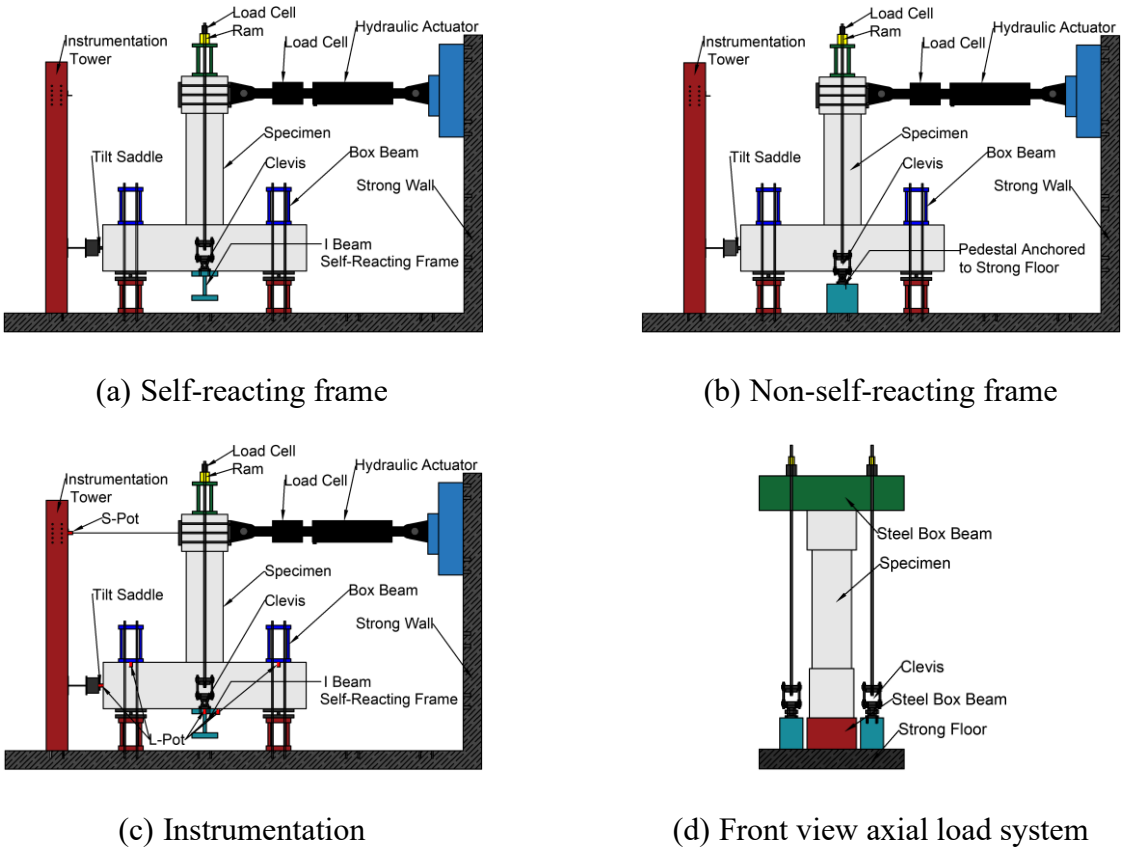

(a) Self-reacting frame

(b) Non-self-reacting frame

(c) Instrumentation

(d) Front view axial load system

Figure 4-6. Test setup and instrumentation

During the test, the specimens were subjected to a monotonically-increasing lateral load and constant axial load. The magnitude of the axial load for all specimens was chosen as $F = 0.08\, A_g f_c'$, where f_c' represents the specified compressive strength of the concrete and A_g denotes the gross cross-sectional area of the column. The corresponding load was 130 kips for all specimens.

After applying the axial load, the column was subjected to lateral loading using a hydraulic actuator. The lateral load was applied as a displacement-controlled pushover test and applied at 7 ft from the base of the column. Initially, the load was applied at a constant rate of 0.08 in./min. Upon reaching its peak, the loading rate was increased to 0.16 in./min. The test was paused at drifts of 0.1%, 0.15%, 0.25%, 0.4%, 0.5%, 0.75%, and 1.0% to measure the crack widths. The test concluded either when the lateral load decreased to 80% of its peak value or when the specimen was unable to maintain the axial load, whichever occurred first.

4.2. Phase I: In-plane Direction Test Results

Prior to discussing experimental results, it is important to describe the mechanisms of the testing apparatus as related to the applied load and the corresponding deformations of the specimens. As the specimen experienced lateral displacement, the angle (θ_2) between the rod and the vertical axis began to increase, resulting in the axial load having both vertical and horizontal components, as illustrated in Figure 4-7. This resulted in the load cell measuring both the lateral load and the horizontal component of the axial load. Equation 4-1 demonstrates the lateral load correction where F represents the lateral load measured by the actuator, P denotes the axial load, and F_c signifies the corrected lateral load. Throughout the test, the angle (θ_2) was monitored with direct angle measurements and found to have a negligible difference from the calculated angle θ_1; with that assumption, similar triangles are used for Equation 4-4. The lateral load used in data analysis is the corrected load resisted by the column. The displacement is the deflection of the column measured from the center of the top block. The drift ratio is calculated by taking the displacement and dividing it by the height of the column-bent interface to the application of the lateral load.

$$F_c = F - P_x \qquad \text{Equation 4-1}$$

$$P_x = P \ sin \ sin \ \theta_2 \qquad \text{Equation 4-2}$$

$$\theta_2 = \frac{\Delta_2}{H_2} \qquad \text{Equation 4-3}$$

$$\Delta_2 = \frac{H_2 \Delta_1}{H_1} \qquad \text{Equation 4-4}$$

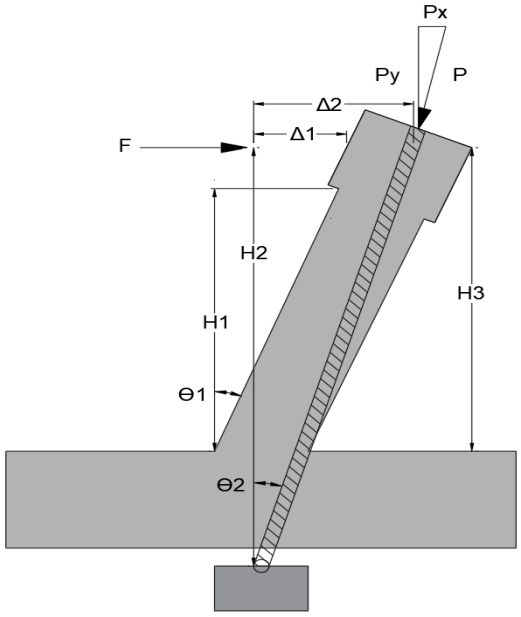

Figure 4-7. Applied load and corresponding deflections

4.2.1. Description of Specimen's Behavior

To conduct the comparison of multiple bent-to-column specimen configurations, the following performance indicators were considered: the peak lateral load and corresponding displacement, yielding of longitudinal column bars, progression of cracking in both the bent cap and column, failure mechanism of each specimen, and the post-peak ductility.

Under the axial load only, Specimen S-NS-CIP-NH* (straight bars, no skin reinforcement, cast-in-place, with no hoop confinement, and external confinement) did not develop cracks. When the lateral load reached 18 kips, the first 0.003 in. flexural cracks appeared in the column, corresponding to 0.1% drift. Two additional 0.004 in. flexural cracks emerged at a drift of 0.25% with a corresponding lateral load of 33.7 kips. At a drift ratio of 0.4% and a lateral load of 40.5 kips, the first shear crack formed in the joint region at a 45-degree angle, with a crack width of 0.006 in. At this stage, the flexural cracks in the column had widened to 0.008 in., and a splitting crack initiated in the bent cap, aligning with the column's longitudinal reinforcement. Both flexural and shear cracks continued to propagate until the longitudinal reinforcement in the column began yielding at a lateral force of 68.1 kips and 1.08% drift. The development of the crack pattern is illustrated in Figure 4-10. It is important to note that the crack widths for the test at failure were not measured due to safety considerations. Subsequently, the loading rate was increased to 0.16 in./min, and the specimen was loaded until failure, peaking at 809 kips at a 2.0% drift before starting to decrease steadily. Crushing of the concrete in the compression region of the column was observed at a drift of 2.17%, followed by concrete spalling. The test continued until the specimen could no longer sustain the axial load, reaching a final drift of 10%. Specimen S-NS-CIP-NH* experienced a ductile flexural failure without significant damage to the connection region. Upon removal of the spalled concrete, buckling of the longitudinal reinforcement in the column was noted in Figure 4-8(a).

The configuration of Specimen S-NS-CIP-NH was the same as that of Specimen S-NS-CIP-NH*. However, Specimen S-NS-CIP-NH represented the most unfavorable scenario in terms of connection strength because of no girder placed on top of the connection to provide external confinement. Specimen S-NS-CIP-NH exhibited 0.003 in. flexural cracks in the bent cap due to the axial load application. Upon lateral loading, the first 0.003 in. flexural cracks in the column developed at 0.1% drift, corresponding to a lateral load of 19.6 kips. At 0.25% drift, two new flexural cracks formed in the column, one 0.003 in. crack at the column interface, and the first crack widened to 0.004 in. Existing cracks in both the column and bent cap widened, reaching widths of 0.006 in. in the bent cap and 0.004 in. in the column. At 0.5% drift and 40 kip lateral load, the flexural cracks in the bent cap transitioned into shear cracks, with the main shear crack progressively widening throughout the test illustrated in Figure 4-11. Vertical splitting cracks developed in the bent cap at 0.75% drift and 46.5 kips lateral load. Yielding of the longitudinal reinforcement in the column was observed at 61.8 kips at a 1.25% drift. The load peaked at 70.8 kips at a 2.1% drift. Crushing of the concrete in the column was observed at 70.6 kips at 2.2% drift, followed by spalling. Post-peak, the load decreased at a constant rate, while the cracks in the

column widened, and the shear crack at the connection elongated and widened. The test ended at 8.0% drift when the load reached 80% of its peak. Specimen S-NS-CIP-NH experienced a ductile flexural failure, although substantial shear deformation was observed as shown in Figure 4-8 (b).

(a) Column long. bar buckling (S-NS-CIP-NH*)

(b) Shear cracks in connection (S-NS-CIP-NH)

Figure 4-8. Extent of damage at failure

Specimen S-SK-CIP-NH exhibited its initial cracks under axial loading, with three flexural cracks measuring 0.002 in. in width observed in the bent cap. Upon lateral loading, small cracks began forming in the column at 17.5 kips at a 0.1% drift. At 0.25% drift, a larger crack began forming at the column interface, and the column's flexural cracks reached a maximum width of 0.004 in. Further flexural cracks formed, and existing ones enlarged as the longitudinal bars in the column began yielding at a 1% drift, coinciding with a lateral load of 63.0 kips. The crack development can be noted in Figure 4-12. Subsequently, the load began to plateau until peaking at 74.6 kips, at a drift ratio of 1.9%. At this point, concrete crushing was observed on the compression face of the column, followed by spalling of the column's cover. Post-peak, the specimen experienced a rapid decline in lateral load, followed by stabilization to a gradual decline. The test concluded when the lateral load decreased by 20%, reaching a maximum drift of 4.4%.

Specimen HK-SK-CIP-NH examined the influence of hooked bars on the performance of the bent-to-column connection. Like Specimen S-SK-CIP-NH, Specimen HK-SK-CIP-NH incorporated skin reinforcement in the bent cap. Specimen HK-SK-CIP-NH exhibited its initial cracks under axial loading, with four flexural cracks measuring 0.002 in. in width observed in the bent cap. Upon lateral loading, a small flexural crack formed in the column at 20.2 kips at a 0.1% drift. As the drift ratio increased, new flexural cracks developed in the column, reaching a maximum width of 0.004 in. at 0.25% drift. At 0.4% drift, the flexural crack in the bent cap expanded into a shear crack, with a width of 0.003 in. Further flexural cracks formed, and existing ones enlarged as the longitudinal bars in the column began yielding at a 0.96% drift, coinciding with a lateral load of 69.2 kips. The crack development can be seen in Figure 4-13. Subsequently, the load began to plateau until peaking at 82.1 kips at a drift ratio of 1.7%. At this point, concrete crushing was observed, followed by spalling of the column's cover. Post-peak, the specimen experienced a

gradual decline in lateral force. The test concluded when the lateral load decreased by 20%, reaching a maximum drift of 5.38%.

Specimen HD-SK-CIP-NH investigated the impact of headed bars on the performance of the bent-to-column connection. Similar to Specimen S-SK-CIP-NH and HK-SK-CIP-NH, the specimen included skin reinforcement in the bent cap. Specimen HD-SK-CIP-NH exhibited its initial cracks under axial loading, with two flexural cracks measuring 0.002 in. in width observed in the bent cap. Upon lateral loading, a small crack formed in the column at 19.1 kips at a 0.1% drift. As the drift ratio increased, new cracks developed in the column, reaching a maximum width of 0.004 in. at 0.25% drift. At 0.75% drift, a shear crack with a width of 0.002 in. formed in the connection. Further flexural cracks formed, and existing ones enlarged as the longitudinal bars in the column began yielding at a 1% drift, coinciding with a lateral load of 58.9 kips. The crack development can be noted in Figure 4-14. Subsequently, the load began to plateau until peaking at 72.4 kips, at a drift ratio of 1.7%. At this point, concrete crushing was observed on the compression face of the column, followed by spalling of the column's cover. Post-peak, the specimen experienced a gradual decline. The test concluded when the lateral load decreased by 20%, reaching a maximum drift of 8.3%. The specimen at failure is displayed in Figure 4-9 (a). Observations of the crack pattern in the joint provided insight that the addition of anchorage and skin reinforcement reduced the shear cracking. Minimal shear cracks can be noted for Specimens HD-SK-CIP-NH and HK-SK-CIP-NH.

(a) Specimen S-SK-CIP-NH (b) Specimen S-SK-CIP-H4 (c) Specimen HD-PC

Figure 4-9. Photos of specimens at failure

Specimen S-SK-CIP-H4 shifted focus from the anchorage type to the confinement reinforcement in the joints. The variable subjected to change from S-SK-CIP-NH is the addition of #5 rebar at 4 in hoop spacing in the joint. Under the initial axial load, the bent cap had multiple flexural cracks, with the largest of 0.01 in. The first flexural cracking in the column occurred at 17.5 kips at 0.1% drift. Furthermore, flexural cracks continued throughout the progression of drift percentage, bringing about the yielding of the tensile bars at 1.1% drift. The noted maximum crack width in the column of 0.04 in. occurred at 1.5% drift. The development of shear cracks in the bent cap

occurred at 1.0% drift with an applied load of 60.9 kips. The cracking pattern can be demonstrated in Figure 4-15. After the peak lateral load of 75.5 kips at 2.0% drift, the applied load gradually dropped by 9 kips post-peak, where the load then plateaued at 66.5 kips for the remainder of the test. The damage at failure for the specimen is presented in Figure 4-9 (b). The test concluded at the 6 in., 7.2% drift, the displacement limit for safety precautions, with only an 11.9% decrease in the sustained load.

Likewise, Specimen S-SK-CIP-H2 resembles a seismic design of the connection, which requires hoop spacing and a spiral pitch of both 2 in. Two flexural cracks in the bent cap were observed, measuring 0.006 in. after the application of axial load. After loading, the first flexural crack in the column occurred at 15.6 kips at 12 in. from the interface. A flexural crack in the bent cap transitioned to a shear crack at 39.1 kips for 0.5% drift, which further extended with the increasing displacement. The first yield of the longitudinal bars was noted at 1.05% drift or 0.9 in. The crack development can be better observed in Figure 4-16. The lateral load peaked at 65.9 kips at 1.7% drift; post-peak, the lateral load plateaued at 64.7 kips for the remaining displacements, concluding at 6 in. A trivial difference between the peak load and the sustained load of 1.7%, far lower than the 20% failure criteria and even the 11.9% discerned in Specimen S-SK-CIP-H4. The cracking in the column for the hoop confinement saw a noticeable increase in crack widths at 1.0% drift. The interface crack was measured as 0.04 in. for the two-inch spacing and 0.03 in. for the four-inch spacing, compared to 0.025 in. for S-SK-CIP-NH. Internal confinement reduced cracking in the joint, but not at the level of the improved anchorage.

Lastly, shifting the focus to the precast specimens, the anchorage was varied between straight bars and headed bars. Specimen S-PC used straight bars in the column. It exhibited no cracking under the axial load, and the first flexural cracks of 0.004 in. in both the bent cap and column were noted at 0.1% drift after 19.1 kips. New flexural cracks developed in the column, and a minor expansion of the bent cap flexural crack at 0.25%. Interface cracking occurred at 0.4% drift with a load of 33.5 kips, and the maximum flexural crack width reached 0.01 in. The bent cap cracking began developing a flexural-shear crack at 1.0% drift and a new shear crack at 1.25% drift due to the 65.4 kips applied load. The crack map for S-PC can be observed in Figure 4-17. The peak lateral load measured was 70.9 kips at 1.5% drift, followed by concrete crushing of the column's cover and a gradual decline in strength until the test concluded at 20% decrease in the sustained load at 7.2% drift.

The precast specimen with headed bars, Specimen HD-PC, behaved similarly to the straight bar alternative, observed to have no cracking at the application of axial, and the first flexural cracks in both the column and bent cap occurred at 0.1% drift with 16.1 kips applied. As the loading increased, cracking in the specimen continued to extend, with the interface crack developing at 37.0 kips at 0.4% drift and a shear crack in the bent cap at 52.2 kips at 0.75% drift. The crack pattern is illustrated in Figure 4-18. The specimen reached a maximum load of 76.6 kips at 1.5% drift, which subsequently saw a decrease in load to 71.7 kips, which then gradually decreased until the 20% threshold was reached. Concrete crushing in the column's cover was noted as the

sustained load diminished, as displayed in Figure 4-9(c) an ultimate drift of 5.3%. The bent cap for the precast experienced the least cracking in the joint region.

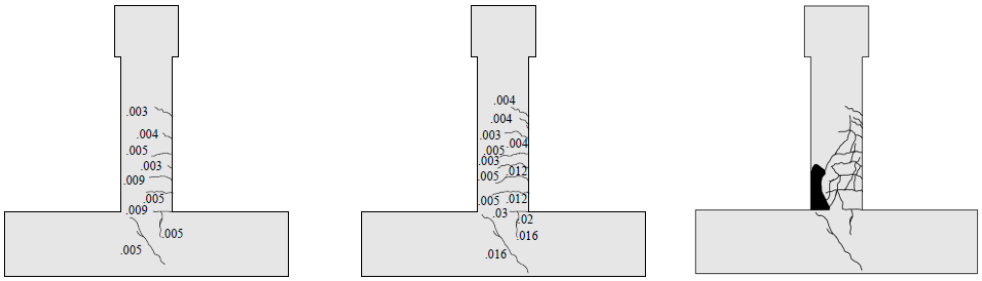

(a) S-NS-CIP-NH* 0.50% drift

(b) S-NS-CIP-NH* 1.00% drift

(c) S-NS-CIP-NH* end of test

Figure 4-10. Specimen S-NS-CIP-NH crack patterns (in.)*

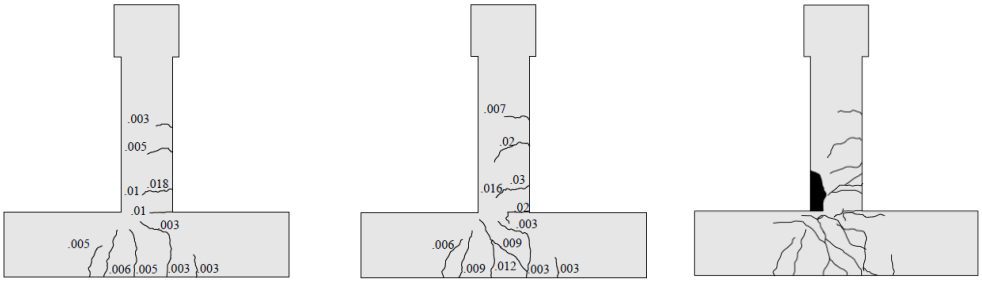

(a) S-NS-CIP-NH 0.50% drift

(b) S-NS-CIP-NH 1.00% drift

(c) S-NS-CIP-NH end of test

Figure 4-11. Specimen S-NS-CIP-NH crack patterns (in.)

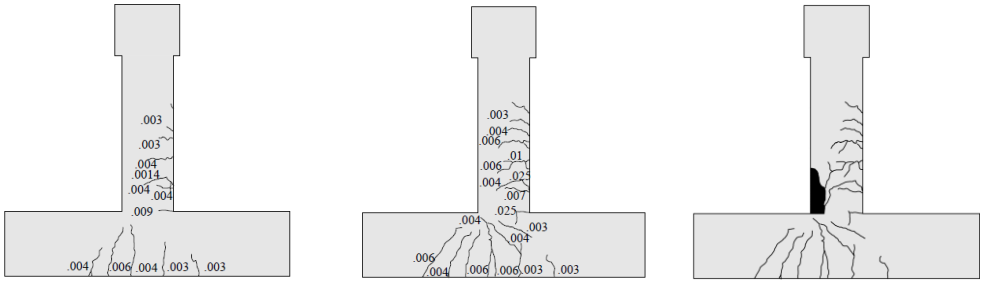

(a) S-SK-CIP-NH 0.50% drift

(b) S-SK-CIP-NH 1.00% drift

(c) S-SK-CIP-NH end of test

Figure 4-12. Specimen S-SK-CIP-NH crack patterns (in.)

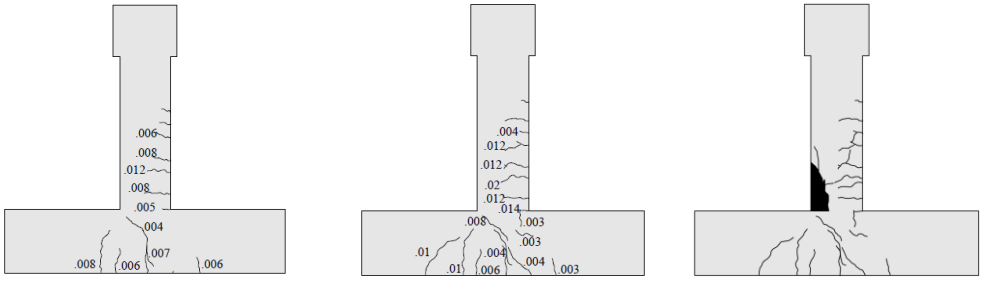

(a) HK-SK-CIP-NH 0.50% drift (b) HK-SK-CIP-NH 1.00% drift (c) HK-SK-CIP-NH end of test

Figure 4-13. Specimen HK-SK-CIP-NH crack patterns (in.)

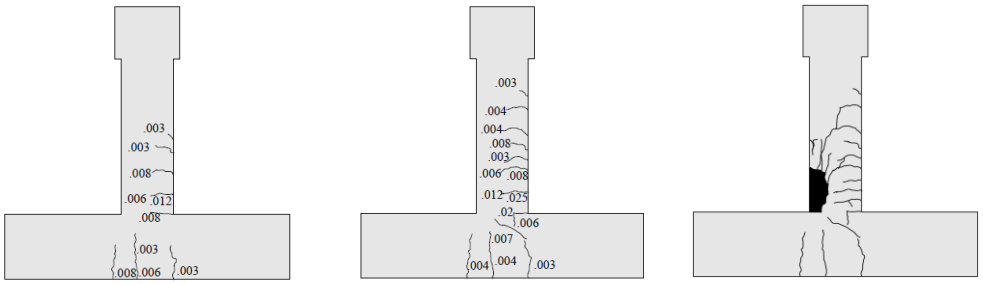

(a) HD-SK-CIP-NH 0.50% drift (b) HD-SK-CIP-NH 1.00% drift (c) HD-SK-CIP-NH end of test

Figure 4-14. Specimen HD-SK-CIP-NH crack patterns (in.)

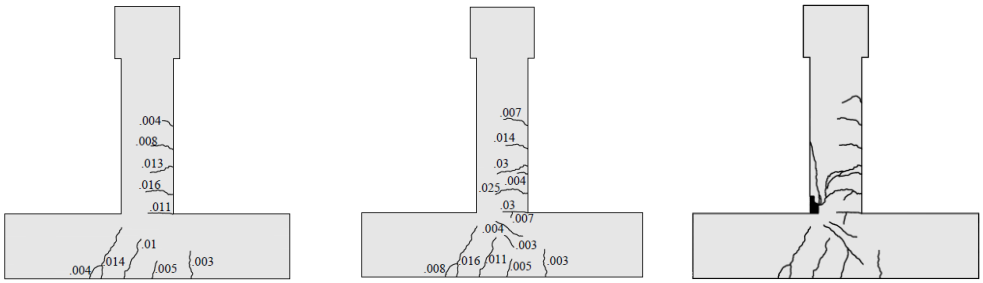

(a) S-SK-CIP-NH-CIP-H4 0.50% drift (b) S-SK-CIP-H4 1.00% drift (c) S-SK-CIP-H4 end of test

Figure 4-15. Specimen S-SK-CIP-H4 crack patterns (in.)

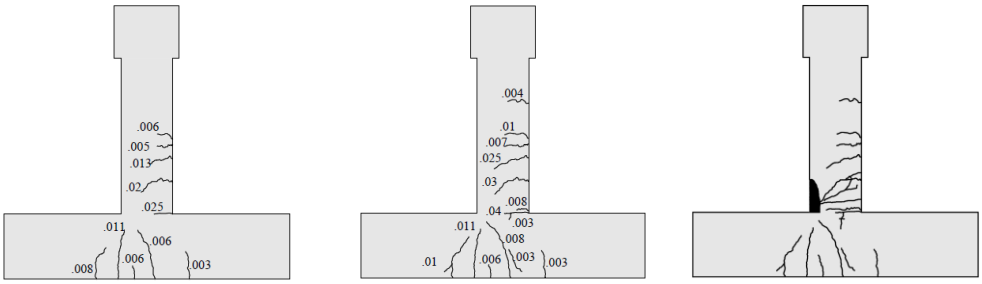

(a) S-SK-CIP-H2 0.50% drift (b) S-SK-CIP-H2 1.00% drift (c) S-SK-CIP-H2 end of test

Figure 4-16. Specimen S-SK-CIP-H2 crack patterns (in.)

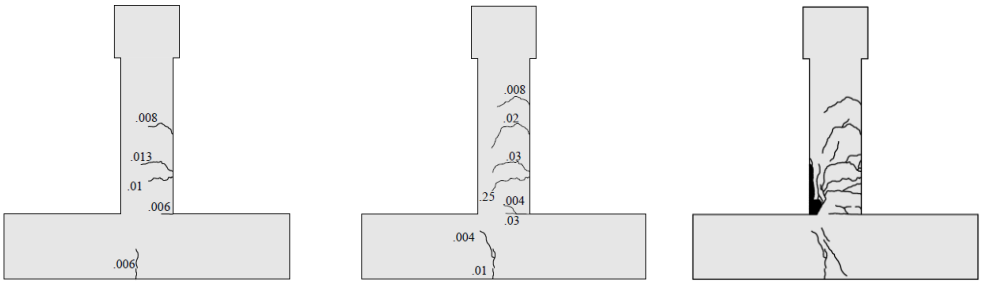

(a) S-PC 0.50% drift (b) S-PC 1.00% drift (c) S-PC end of test

Figure 4-17. Specimen S-PC crack patterns (in.)

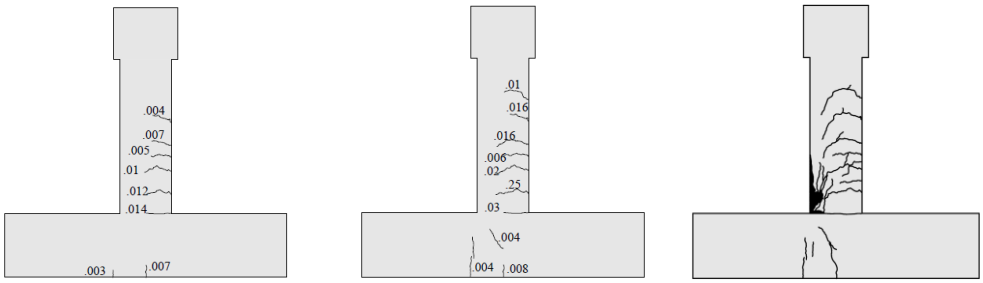

(a) HD-PC 0.50% drift (b) HD-PC 1.00% drift (c) HD-PC end of test

Figure 4-18. Specimen HD-PC crack patterns (in.)

The performance of all the bent-to-column connections exhibited flexural failure within the column, influencing the overall behavior. Shear cracking appeared in the joint after a minimum drift of 0.4%, but none of the shear deformations resulted in a failure mode. The maximum crack width in the bent cap was recorded at 0.016 in. for Specimens S-NS-CIP-NH* and S-SK-CIP-H4, but the bent cap with the most cracking was S-NS-CIP-NH.

4.2.2. Moment-Displacement Response

Moment-displacement responses for all tested specimens are depicted in Figure 4-19. All specimens demonstrated comparable structural behavior, initially exhibiting linear elastic response up to the onset of first cracking. This was followed by a post-cracking elastic phase until yielding of the column reinforcement occurred. Subsequently, each specimen reached its peak strength, after which the strength plateaued while undergoing significant deformation. Depending on the reinforcement configuration, certain specimens exhibited more rapid strength degradation; however, all specimens sustained lateral drift levels of at least 4.4%. Moreover, the enhancements in anchorage and confinement within the joint region are directly associated with the improved structural behavior demonstrated in Figure 4-19. Specimen HK-SK-CIP-NH showed a moment capacity increase of 13.9% and 9.1% relative to Specimens S-NS-CIP-NH and S-SK-CIP-NH, respectively. In contrast, the precast bent cap Specimen S-PC experienced a decrease in peak moment capacity by 1.7% and 5.9% when compared to the same specimens. Replacing straight bars with headed bars in the precast bent caps led to a 7.9% increase in peak moment capacity. Regarding joint confinement, externally confined Specimen S-NS-CIP-NH* showed a 13.3% increase in peak moment compared to its unconfined counterpart, Specimen S-NS-CIP-NH. Internally confined specimens, illustrated in Figure 4-19(c), showed limited improvement: Specimen S-SK-CIP-H4 showed a marginal 0.9% increase, while Specimen S-SK-CIP-H2 experienced an 8.7% decrease in peak lateral load compared to S-SK-CIP-NH. Despite the lack of improvement in the peak moment capacity, the post-peak capacity saw improvements of 3.7% and 14.8% respectively for S-SK-CIP-H4 and S-SK-CIP-H2, compared to the 7.3% decrease in sustained moment for S-NS-CIP-NH at the same displacement of 6 in. On similar notes, the post-peak behavior observed for Specimen S-SK-CIP-NH is attributed to two reasons: first, to maintain the axial load, the application of lateral load was paused to reduce the axial load to counter the P-delta effects, exacerbating the sustained load post-peak; second, a mechanical issue with the pump of the hydraulic actuator occurred before the peak load of the specimen at 0.42 in., resulting in unloading to 0 kips and reloading of the specimen until failure at 541 kip-ft, contributing to the premature crushing of the concrete cover. Neither of these issues occurred in the other tests. Similarly, Specimen HD-SK-CIP-NH experienced an 11.4% decrease in capacity compared to HK-SK-CIP-NH shown in Figure 4-19 (b). These lower strength responses can be attributed to variation in material properties, such as reduced compressive strength in the columns of Specimens HD-SK-CIP-NH, S-SK-CIP-H2, and S-PC, as noted in Table 4-1. The underperformance of headed bars contradicts the expected improvements from enhanced anchorage and confinement. To isolate the effects of the detailing strategies from material property variability, a normalized moment-displacement response analysis was conducted.

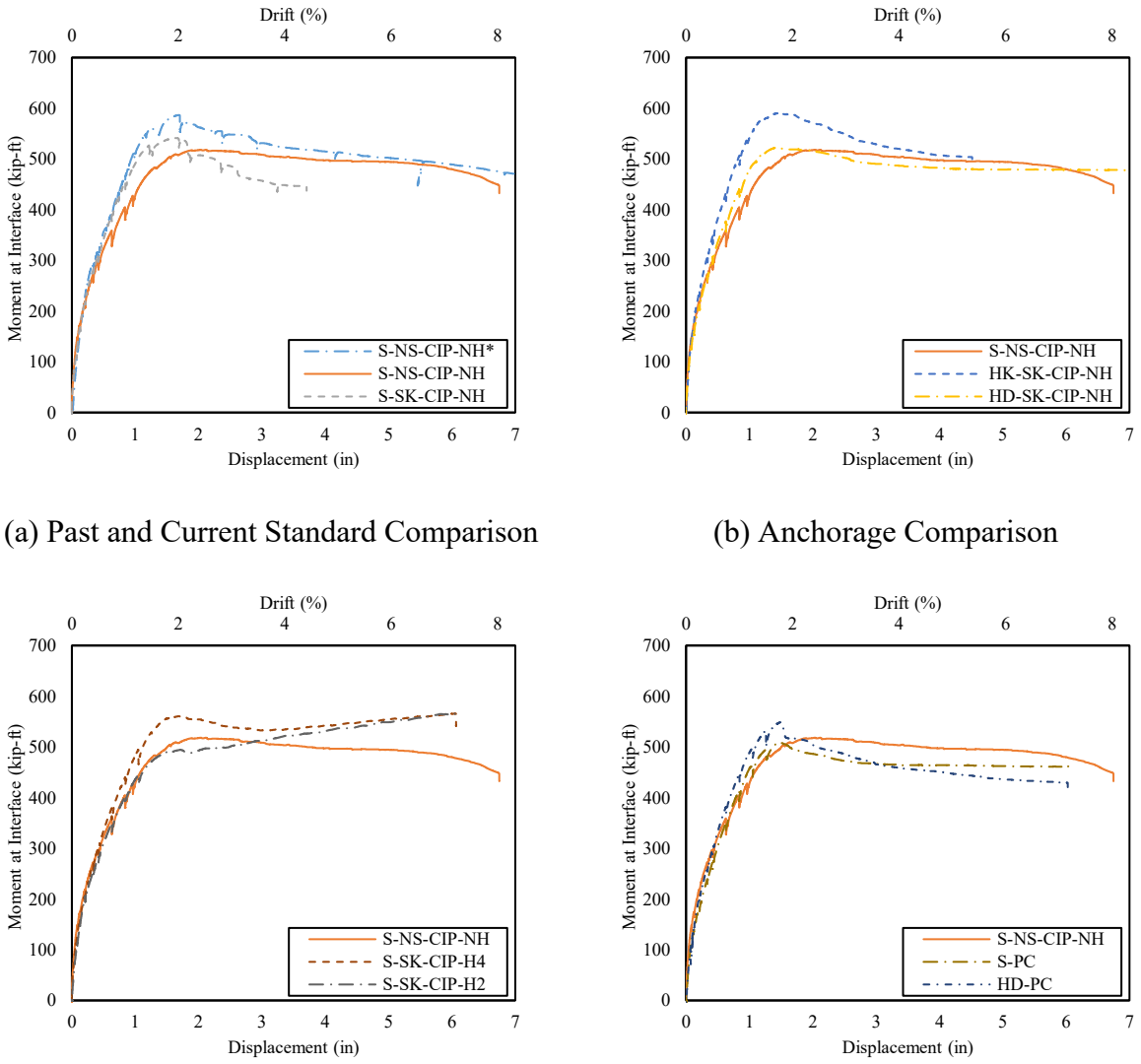

(a) Past and Current Standard Comparison

(b) Anchorage Comparison

(c) Internal Confinement Comparison

(d) Precast Comparison

Figure 4-19. Moment-displacement response for all specimens

4.2.3. Normalized Moment-Displacement Response

Despite identical specified material properties, inherent variations of the actual material properties exist across all specimens. To facilitate a meaningful comparison of specimen performance, the moment-displacement responses were normalized to the ultimate capacity of the critical section, located at the column-bent interface, where the highest moment demand is located. In addition, the moment at the section was determined to include the second-order P-Delta effects introduced by the axial load:

$$M_{test} = F_c \times H_1 + P_y \times \Delta_2 \qquad \textit{Equation 4-5}$$

where M_{test} is the moment at the critical section, calculated in kip-ft, F_c is the adjusted lateral load considering axial contribution in kip, and H_1 is the height from the intersection to the point of load application, in this case 84 in. P_y is the vertical component of the axial load in kip, and Δ_2 is the lateral displacement of the column, measured from the point of load application. Refer to Figure 4-7 on how the lateral load was corrected.

The ultimate moment measured at the critical section ($M_{u.test}$) is subsequently normalized by the calculated ultimate moment (M_{calc}) given from a nonlinear sectional analysis, considering axial loading, material properties, and reinforcement configuration summarized in Table 4-1. The nonlinear sectional analysis software used was Response 2000 [31]. The numerical approach used Popovic's model for concrete in compression, the Collins & Benz model for compression softening, and the Bentz model for tension stiffening. The experimental yield ($M_{y.test}$) and ultimate moment capacity can be summarized in Table 4-2, as well as the calculated ultimate moment capacity for the specimens. Additionally, the yield and ultimate deflections were reported in Table 4-3**,** and the ductility was calculated as the ratio of the yielding and ultimate deflections. The ultimate deflection was calculated either at a twenty percent decrease in the lateral load or at the end of the test. The normalized moment-displacement responses of all specimens are depicted in Figure 4-20.

Table 4-2. Summary of specimen capacity

Specimen ID	$M_{peak,test}$ (k-ft)	$M_{u,test}$ (k-ft)	$M_{cc,test}$ (k-ft)	$M_{y,test}$ (k-ft)	M_{calc} (k-ft)	*Maximum lateral load* (kip)
S-NS-CIP-NH*	587	521	469	489	508	81.0
S-NS-CIP-NH	518	486	432	451	509	72.3
S-SK-CIP-NH	541	468	437	450	510	74.7
S-SK-CIP-H4	567	565	545	409	486	75.5
S-SK-CIP-H2	546	>567	492	473	505	65.9
HK-SK-CIP-NH	590	523	500	453	539	82.1
HD-SK-CIP-NH	523	480	474	439	463	72.4
S-PC	509	464	459	440	475	70.4
HD-PC	549	481	439	311	491	76.1

Table 4-3. Summary of specimen displacement

Specimen ID	Yield Deflection (in.)	Concrete crusing deflection (in.)	Ultimate deflection (in.)	Displacement ductility ratio
S-NS-CIP-NH*	587	521	469	489
S-NS-CIP-NH	518	486	432	451
S-SK-CIP-NH	541	468	437	450
S-SK-CIP-H4	567	565	545	409
S-SK-CIP-H2	546	>567	492	473
HK-SK-CIP-NH	590	523	500	453
HD-SK-CIP-NH	523	480	474	439
S-PC	509	464	459	440
HD-PC	549	481	439	311

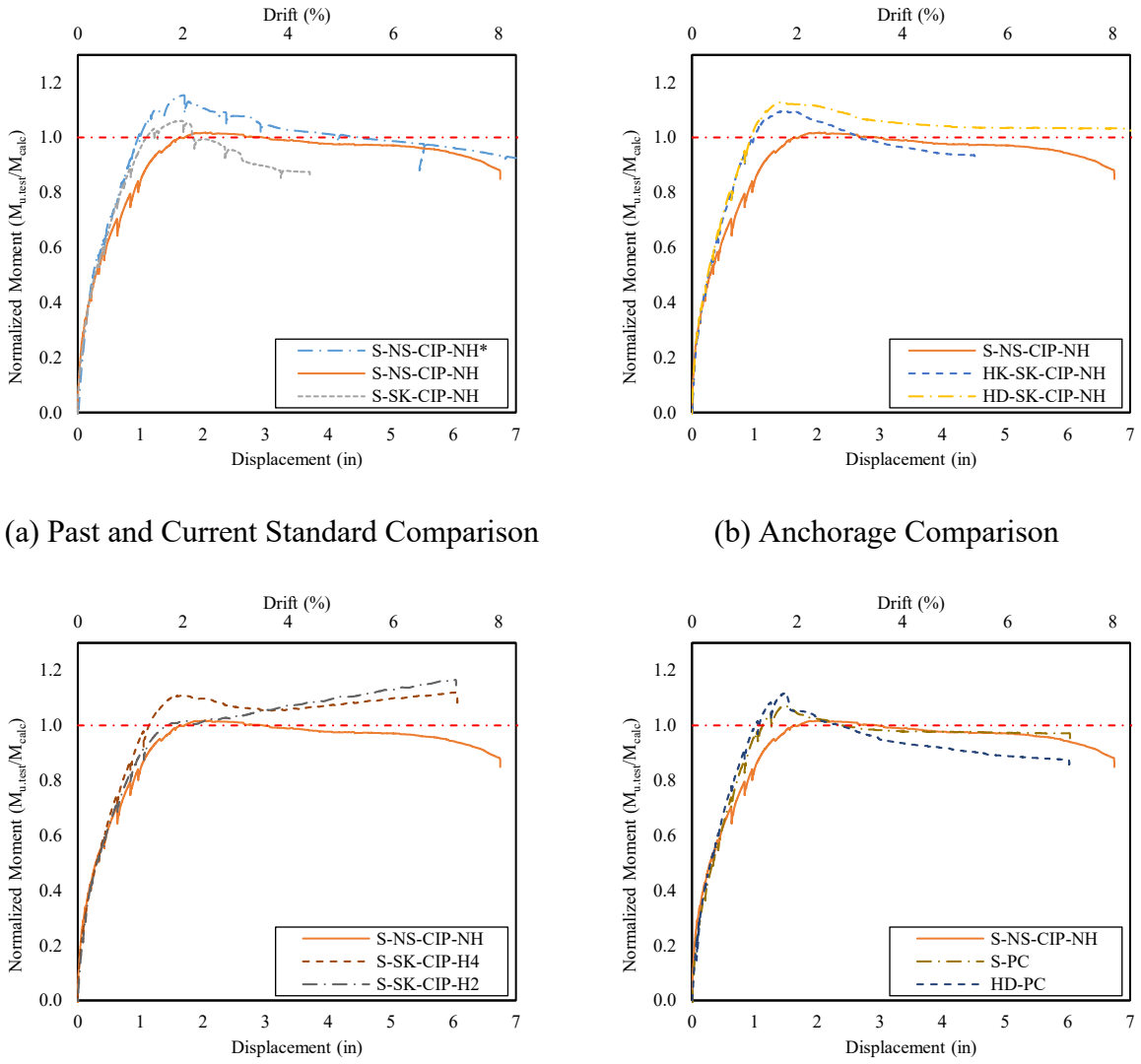

(a) Past and Current Standard Comparison

(b) Anchorage Comparison

(c) Internal Confinement Comparison

(d) Precast Comparison

Figure 4-20. Normalized moment-displacement response of tested specimens

The normalized moment-displacement responses provide valuable insights into the overall performance of the specimens because they minimize the effects of varied material properties. As anticipated, Specimen S-NS-CIP-NH exhibited the lowest moment capacity. Nevertheless, it exceeded its ultimate moment capacity calculated by the sectional analysis, achieving a maximum moment of 1.02 M_u, despite the lack of detailed connection reinforcement for such loading conditions. Specimen S-SK-CIP-NH peaked at 1.06 M_u but experienced significant deterioration shortly thereafter, failing to sustain that level of loading. Both are demonstrated in Figure 4-20(a).

Specimens HK-SK-CIP-NH and HD-SK-CIP-NH shown in Figure 4-20(b) showcased higher ultimate capacities and exhibited highly ductile behavior. Their maximum moments reached 1.10 M_u and 1.13 M_u, respectively. When compared to Figure 4-19(b), the improvements to the

anchorage better indicate the anticipated behavior with headed and hooked bars, both increasing the capacity of the specimens. Lastly, Specimen S-NS-CIP-NH* boasted the highest normalized moment capacity among all specimens and demonstrated exceptional ductility. It sustained a maximum moment of 1.15 M_u.

Specimen S-NS-CIP-NH* exhibited in Figure 4-20 (a) had a 13% higher capacity than Specimen S-NS-CIP-NH, despite having identical detailing. This discrepancy highlights the significant contribution of external confinement to the increased capacity. The presence of external confinement effectively prevented the development of shear cracks in the bent cap. Furthermore, the failure mechanism differed, as Specimen S-NS-CIP-NH* was unable to sustain the axial load after the test.

Specimens HK-SK-CIP-NH and HD-SK-CIP-NH exhibited very similar ultimate capacities, with Specimen HD-SK-CIP-NH demonstrating a 3% higher capacity than Specimen HK-SK-CIP-NH. However, Specimen HK-SK-CIP-NH experienced a much more rapid deterioration post-peak compared to Specimen HD-SK-CIP-NH. Specimen HK-SK-CIP-NH failed to sustain its peak load, experiencing a near-constant decrease in sustained moment. The normalized moment decreased to 1.0 M_u at a 3.18% drift ratio. On the other hand, Specimen HD-SK-CIP-NH managed to sustain most of the load throughout the test, with its moment never dropping below 1.0 M_u, even at high drift ratios. Overall, the normalized moment of each specimen demonstrated both the improvement of the maximum moment capacity with headed and hooked anchorage and the improvement with external confinement in the joint.

Specimens S-SK-CIP-H4 and S-SK-CIP-H2 both displayed a maximum normalized moment at 7.1% drift, where the test was concluded illustrated in Figure 4-20(c). When observing the normalized moment at peak lateral load, both at 2.0% drift, Specimen S-SK-CIP-H4 outperformed S-SK-CIP-H2 by 48%, despite having a lower hoop confinement spacing. Albeit, S-SK-CIP-H2's maximum normalized moment was 4.5% higher than S-SK-CIP-H4 by the end of the test. This constitutes an increase of 56% from the moment of peak lateral load and the end of the test, compared to a minimal increase of 9% seen in S-SK-CIP-H4. As the spacing of the hoop confinement decreases, an improved ductility can be noticed in the increase of normalized moment capacity during post-peak behavior. This can be attributed to the post-peak plateau in lateral load noted in the load-displacement responses in Figure 4-19(c), with the P-delta effects increasing, allowing the moment to increase. Additionally, the decreased spiral spacing in the column provides improved confinement, allowing for more of the inner core to be available to hold stress, thus preventing the decrease in the level arm between the concrete and steel.

Specimen S-PC's maximum normalized moment was 1.07 M_u; compared to the cast-in-place, the difference between them was less than 1%, depicted in Figure 4-20 (d). The same trend is noticed between HD-PC and HD-SK-CIP-NH. As for ductility, no significant improvements are examined with the use of precast bent caps. Therefore, demonstrating no improvements or defects to the overall behavior. Cast-in-place and precast bent caps can be implemented interchangeably based

on the needs of the project. Furthermore, the improved moment capacity from the headed bars is also noted in the precast specimens with an increase of 4.7%.

4.2.4. Strain Profile of the Column Longitudinal Bars

Axial strains along the outermost longitudinal bars in the column are reported for all specimens at various drift ratios. Figure 4-21 displays the tensile strain profiles of each specimen alongside the corresponding loads at each drift ratio. The strain was averaged between the two column bars in tension at the location of each strain gauge.

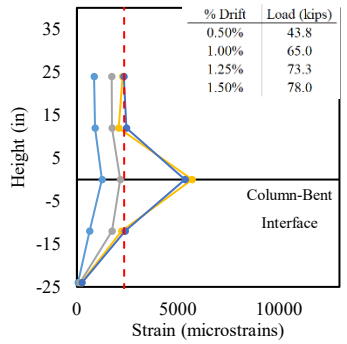

(a) Strain Profile S-NS-CIP-NH*

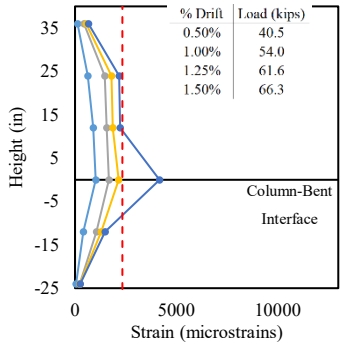

(b) Strain Profile S-NS-CIP-NH

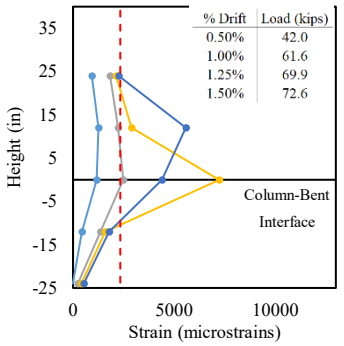

(c) Strain Profile S-SK-CIP-NH

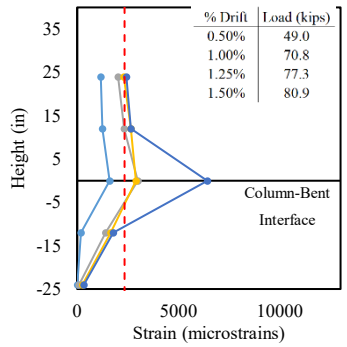

(d) Strain Profile HK-SK-CIP-NH

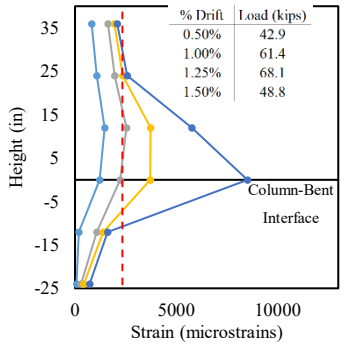

(e) Strain Profile HD-SK-CIP-NH

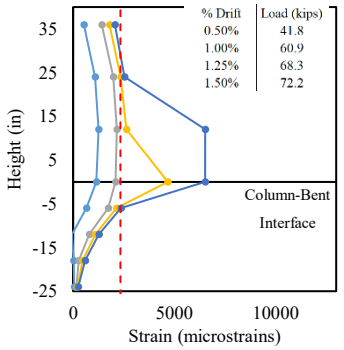

(f) Strain Profile S-SK-CIP-H4

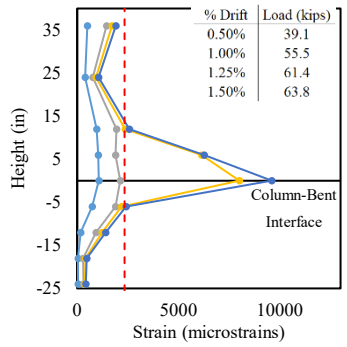

(g) Strain Profile S-SK-CIP-H2

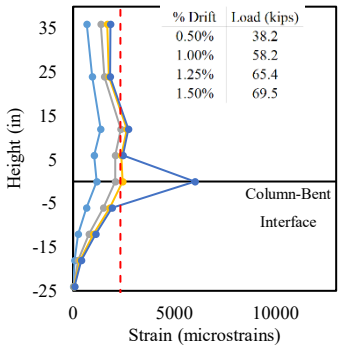

(h) Strain Profile S-PC

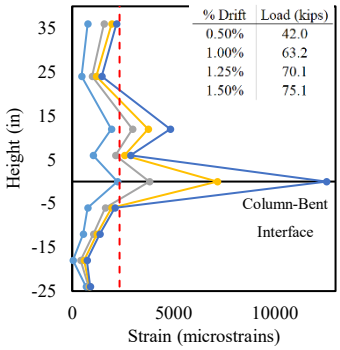

(i) Strain Profile HD-PC

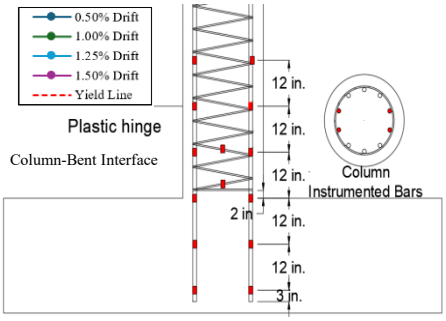

(j) Legend

Figure 4-21. Strain profiles

At the critical section located at the column-bent interface, a height of 0 in. in Figure 4-21, all specimens fully developed the yield strength of the column's longitudinal rebar. The extent of strain penetration is evident across all specimens, with bar yielding extending well into the joint region. The trends of the strain profiles are similar for all specimens, with strain remaining close to zero until the interface, where large strain is measured. The large strains at 12 in. in S-SK-CIP-NH, HD-SK-CIP-NH, and S-SK-CIP-H4 can be attributed to the large crack at that location. The larger strain at 18 in. below the interface is associated with the larger crack widths observed in the bent cap noted in Figure 4-15. Particularly noteworthy is the significantly higher strain penetration observed in Specimen S-NS-CIP-NH* than in Specimen S-NS-CIP-NH, where the bars yield up to 12 in. into the bent cap.

To facilitate a comparison of strain profiles among different specimens, a procedure similar to the one used in section 4.2 was implemented. The strains were normalized based on their respective yield strains. Figure 4-22 illustrates the comparisons between S-NS-CIP-NH* and S-NS-CIP-NH, S-SK-CIP-NH, and HD-SK-CIP-NH, as well as HK-SK-CIP-NH and HD-SK-CIP-NH.

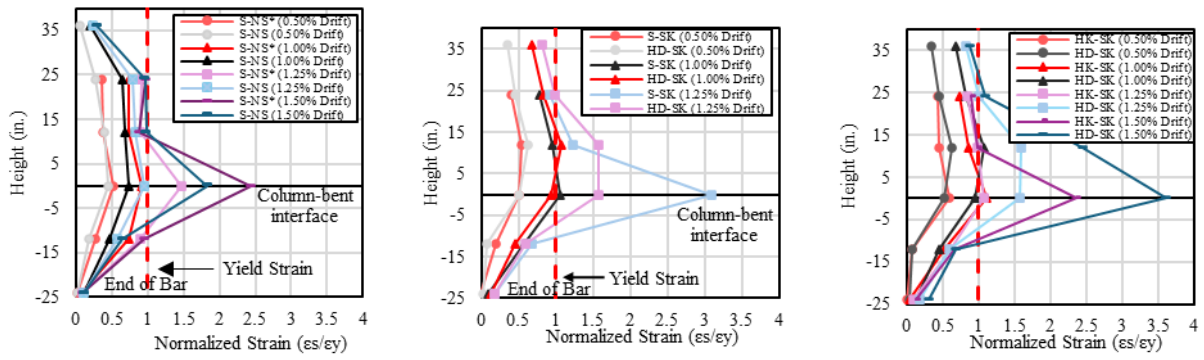

(a) Specimen S-NS-CIP-NH* vs Specimen S-NS-CIP-NH strain profile

(b) Specimen S-SK-CIP-NH vs Specimen HD-SK-CIP-NH strain profile

(c) Specimen HK-SK-CIP-NH vs Specimen HD-SK-CIP-NH strain profile

Figure 4-22. Normalized strain profiles comparison between specimens

Figure 4-22 (a) shows the comparison between the normalized strain profiles of specimens S-NS-CIP-NH* and S-NS-CIP-NH. The strains within the connection in the column bar of specimen S-NS-CIP-NH* surpass those of specimen S-NS-CIP-NH at each drift ratio. This indicates that external confinement aids in bar development and that strain penetration is greater when external confinement is present in the joint region. The rebar in specimen S-NS-CIP-NH* nearly yielded ($0.95\varepsilon_y$) 12 in. into the joint region, with only 15 in. of development length, compared to the 34 in. of development length denoted by AASHTO.

Similar to Figure 4-22 (a), Figure 4-22 (b) and Figure 4-22 (c) display the comparison between the normalized strain profiles of specimens S-SK-CIP-NH and HD-SK-CIP-NH, and HK-SK-CIP-NH and HD-SK-CIP-NH, respectively. Regarding strain penetration and rebar development, it is evident that headed and hooked bars do not exert a significant influence. However, at higher drift ratios, headed bars enhance the development of the bar end compared to hooked bars. Specifically, at 3 in. from the end of the bar, the strain in the headed bars was 2.5 times higher than in the specimen with hooked bars.

The critical section at the interface demonstrated yielding for most specimens at 1.0% drift, as shown in Figure 4-23. Additionally, the strain at the interface of each specimen increased as the drift increased. This trend was especially pronounced in the two specimens with headed bars, where the first and third largest strains occurred at the interface at 1.5% and 2.0% drift. It should be noted that some strain data is missing in the later stages of the figure, post-yielding, the strain gauge data for those specimens became unreliable. Comparing interface strains at 1.5% drift, an increase of 28% can be noted when external confinement is provided. Additionally, the strain at the interface at 1.5% drift when the headed bars are implemented in the cast-in-place and precast increased by 104% and 201%, respectively, when compared to S-NS-CIP-NH. The decreased spacing in the hoop confinement from four inches to two inches increased the strain at the interface

by 119%. As for the precast bent caps, an increase of 44% for straight bars and 47% for headed bars was found.

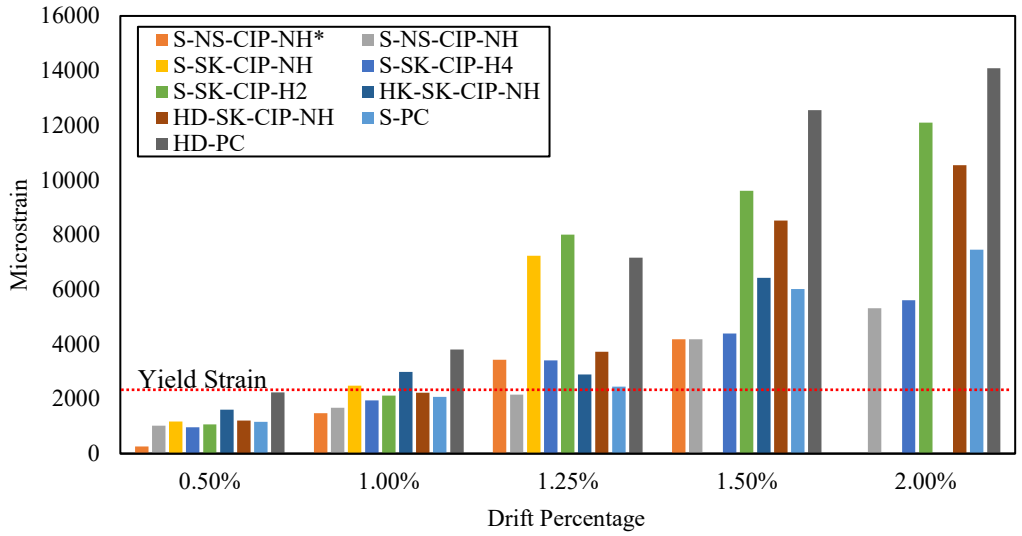

Figure 4-23. Tensile Strain at Interface

4.2.5. Crack Width

The crack width values were plotted against the percentage of the maximum applied load for each specimen, as shown in Figure 4-24. Two benchmark crack widths are presented in the graphs. The benchmark crack width was chosen as 0.006 in. and 0.012 in., aligning with the ACI 224R committee report for reasonable crack widths for concrete exposed to seawater and seawater spray, wetting and drying, and concrete exposed to humidity, moist air, and soil under service loads. The maximum crack width specified in AASHTO provides a more conservative limit than the ACI guidelines. Table 4-4 shows the percentage of ultimate load at which the ACI 224R benchmark crack widths were reached in the bent cap and column. Additionally, it can be observed that specimens with hooked (HK-SK-CIP-NH) and headed bars (HD-SK-CIP-NH) exhibited better crack control in the column. Conversely, for the bent cap, all specimens performed very similarly, as there were no major cracks in the connection until 70% of the maximum applied load, except for S-SK-CIP-H4. The hoop confinement specimens (S-SK-CIP-H4 and S-SK-CIP-H2) both reached the benchmark cracks earlier than the majority of the specimens. As for the precast specimens, the column saw significant cracking earlier in the loading stages but reached the 0.012 in. benchmark at similar levels as the cast-in-place specimens. The larger cracks noted in the column demonstrate that the failure was dictated by flexure in the column, thus, the connection performs satisfactorily.

Table 4-4. Percent of ultimate applied load at benchmark crack widths

Specimen ID	Column flexural cracks		Connections cracks	
	0.006 in.	0.012 in.	0.006 in.	0.012 in.
S-NS-CIP-NH*	43%	51%	49%	74%
S-NS-CIP-NH	45%	55%	33%	72%
S-SK-CIP-NH	43%	52%	58%	N/A
S-SK-CIP-H4	34%	45%	20%	41%
S-SK-CIP-H2	31%	45%	17%	88%
HK-SK-CIP-NH	34%	43%	21%	N/A
HD-SK-CIP-NH	44%	54%	42%	75%
S-PC	31%	52%	47%	87%
HD-PC	27%	52%	37%	79%

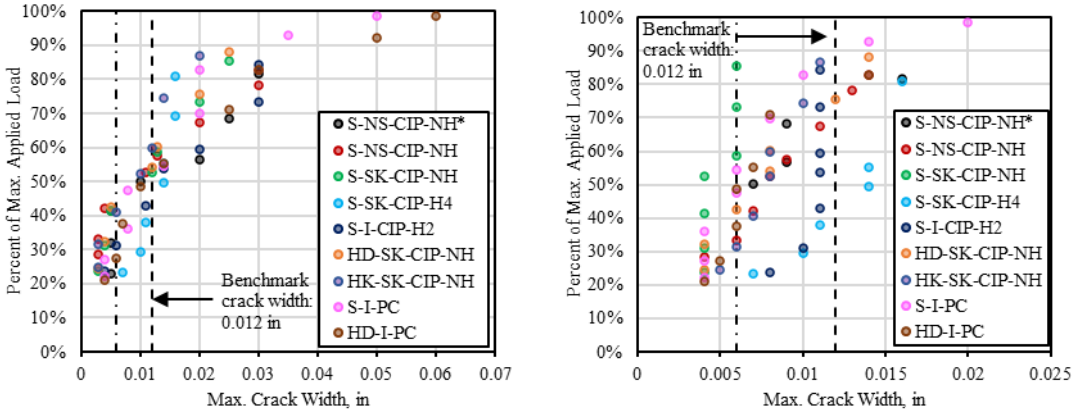

(a) Column flexural cracks (b) Connection cracks

Figure 4-24. Crack width behavior of specimens

4.2.6. Bar Slip

Figure 4-25 illustrates the comparison of bar slips between multiple specimens. First, focusing on headed bars (HD-SK-CIP-NH) and straight bars without confinement detailing (S-NS-CIP-NH). In Specimen S-NS-CIP-NH, bar slip was initially observed when the load reached 49.9 kips, before the bar yielded. The slip gradually increased beyond the peak lateral load of 70.8 kips and reached a maximum of 0.15 in. by the end of the test. Despite this, the bar eventually yielded, achieving the full moment capacity of the column. Conversely, in Specimen HD-SK-CIP-NH, no slip was observed until the specimen reached its peak lateral load. At a drift of 1.74%, there was a sudden increase in slip to around 0.006 in. Following this increase, the slip continued to rise at a steady rate, reaching 0.012 in. by the end of the test. Likewise, HD-PC noted minimal slip in the bar of

0.009 in. Overall, the use of headed bars proved effective in reducing rebar slip. The only other specimens that recorded more than a 0.03 in. of slip were S-SK-CIP-H4 with 0.05 in. The improved internal confinement improved the slip of the bar with a reduction of 67% for four inches spacing and 92% for two inch spacing. Moreover, the precast specimens had minimal slip.

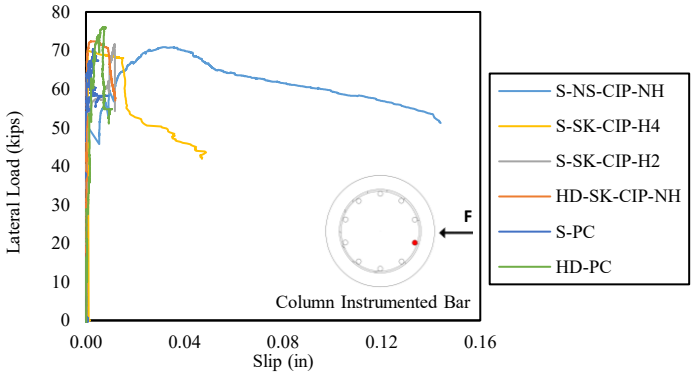

Figure 4-25. Bar slip Specimens S-NS-CIP-NH and HD-SK-CIP-NH

4.3. Phase II: Out-of-Plane Direction Tests

4.3.1. Specimen Design

Four bent-to-column connection specimens were constructed and tested in the out-of-plane direction at the Ferguson Structural Laboratory. A summary of the testing program is provided in Table 4-5, and the geometry and reinforcement layouts for the cast-in-place units are depicted in Figure 4-1. Specimens S-O-CIP and HD-O-CIP consisted of cast-in-place bent caps reinforced with three #11 longitudinal bars placed at both the top and bottom. Throughout the beam span, #5 closed stirrups were spaced at 6 in., while no vertical reinforcement was installed within the joint. Additionally, two #5 skin reinforcement bars were included, as shown in Figure 4-1(a), in accordance with current detailing practices in Texas. The precast bent cap configuration followed the TxDOT standard PPBC-RC. This layout incorporated 24 Gr. 270 strands with a diameter of 0.6 in., spaced at 2 in. intervals, as illustrated in Figure 4-2(a). For specimens S-O-PC and HD-O-PC, the original bent cap width of 36 in. was reduced to 32 in. to accommodate the laboratory test setup. A target concrete strength of 6.1 ksi was selected to provide a flexural capacity of 1600 kip-ft. For constructability, the corrugated metal pipe was extended continuously across the section, as indicated in Figure 4-2(c).

All columns contained ten #9 longitudinal reinforcing bars arranged symmetrically around the perimeter. The spiral reinforcement consisted of #3 spirals with a 6 in. pitch, beginning 2 in. above the bent-column interface, as shown in Figure 4-1(c). The only variation among the columns was the anchorage detail: straight bar anchorage was used for S-O-CIP and S-O-PC, whereas headed bars conforming to ASTM A970/A970M were used in HD-O-CIP and HD-O-PC. All reinforcement met the ASTM A615/A615M Gr. 60 specifications. Instrumentation included strain

gauges installed along both compressive and tensile longitudinal bars in the column and bent cap at 12 in. and 6 in. intervals respectively, as illustrated in Figure 4-26(a). Additional strain gauges were placed on the spirals within the column. In the bent cap, strain gauges were positioned on longitudinal bars, skin reinforcement, and stirrups to capture torsional behavior. In the precast bent caps, the corrugated metal pipe was instrumented with gauges at quarter turns in both vertical and horizontal directions, while P bars were monitored at 6 in. spacing, as shown in Figure 4-26(b). The fabrication and casting procedures mirrored those used for the in-plane specimens described in Section 4.1.1.

Table 4-5: Test matrix for out-of-plane direction testing

Bent Cap					Column				
Specimen ID	Anchorage Type	ρ long. (%)	ρ trans. (%)	f'_c (psi)	ρ spiral. (%)	ρ long. (%)	f'_c (psi)	f_y (ksi)	f_u (ksi)
S-O-CIP	Straight	1.16	0.29	4760	0.4	2.2	4640	68.0	109.5
HD-O-CIP	Head	1.16	0.29	4460	0.4	2.2	4740	68.3	94.7
S-O-PC	Straight	0.71	0.24	8430	0.4	2.2	4310	68.0	109.5
HD-O-PC	Head	0.71	0.24	8430	0.4	2.2	4200	68.3	94.7

Specimen Label Key
Anchorage: S = Straight Bar HD = Headed Bar
Cast: CIP = Cast-in-place PC = Precast
ρ = Reinforcing Steel Ratio
f'_c = Day of Testing Compressive Strength of Concrete
f_y = Steel Yield Strength
f_u = Steel Ultimate Strength

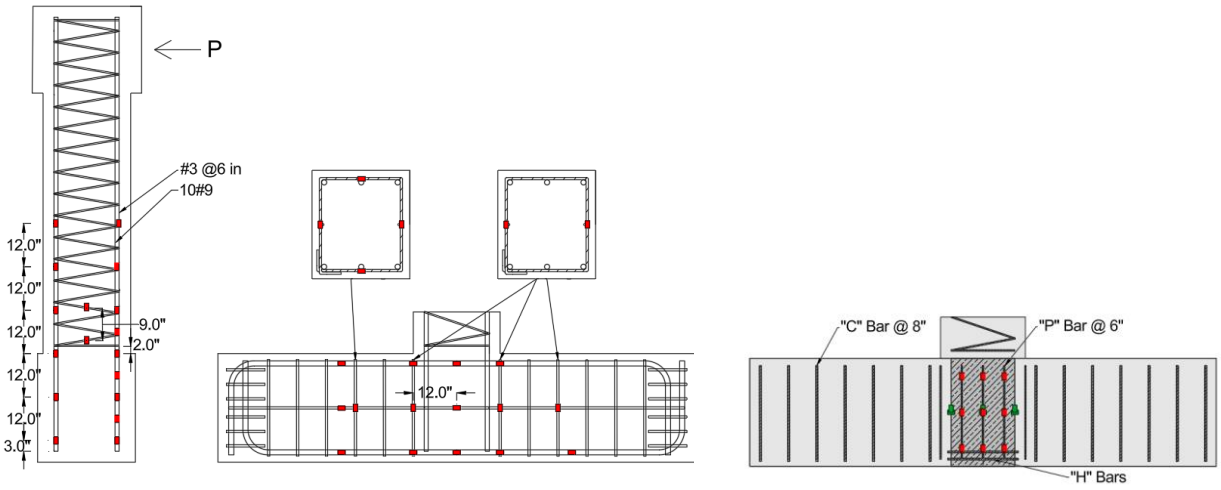

(a) Typical placement of strain gauges in cast-in-place

(b) Typical placement of strain gauges in precast

Figure 4-26. Strain gauge instrumentation

4.3.2. Test Setup, Instrumentation, and Loading Procedure

The specimens were tested under monotonically-increasing lateral load. Axial load, used to simulate scenarios where a girder is positioned on top of the connection, was not employed due to

the limited space around the test setup. A 330-kip MTS hydraulic actuator was used to apply the lateral load, measured with a load cell in the MTS actuator. The lateral load was applied as a displacement-controlled test and applied at 7 ft from the base of the column. Initially, the load was applied at a constant rate of 0.08 in./min. Upon reaching its peak, the loading rate was increased to 0.16 in./min. The test was stopped to measure the crack widths when load reached 10 kips. 17 kips, 24 kips, 31kips, and 45 kips for the cast-in-place specimens, and 13 kips, 23 kips, 33 kips, 43 kips, and 53 kips for the precast specimens, because of the higher expected peak load for the precast specimens.

The bent caps of the specimens were clamped with two pairs of steel plates spaced 8 feet apart. The steel plates were not on the same plane to enable the specimen to experience torsion. Two Teflon sheets were placed behind each steel plate to prevent non-axial load transfer into the test frame. The detailed test setup is shown in Figure 4-27. String potentiometer was used to accurately measure the displacement of the top block, while many linear potentiometers were placed at various locations around the specimen to record any rigid body movements during the test, as shown in Figure 4-28.

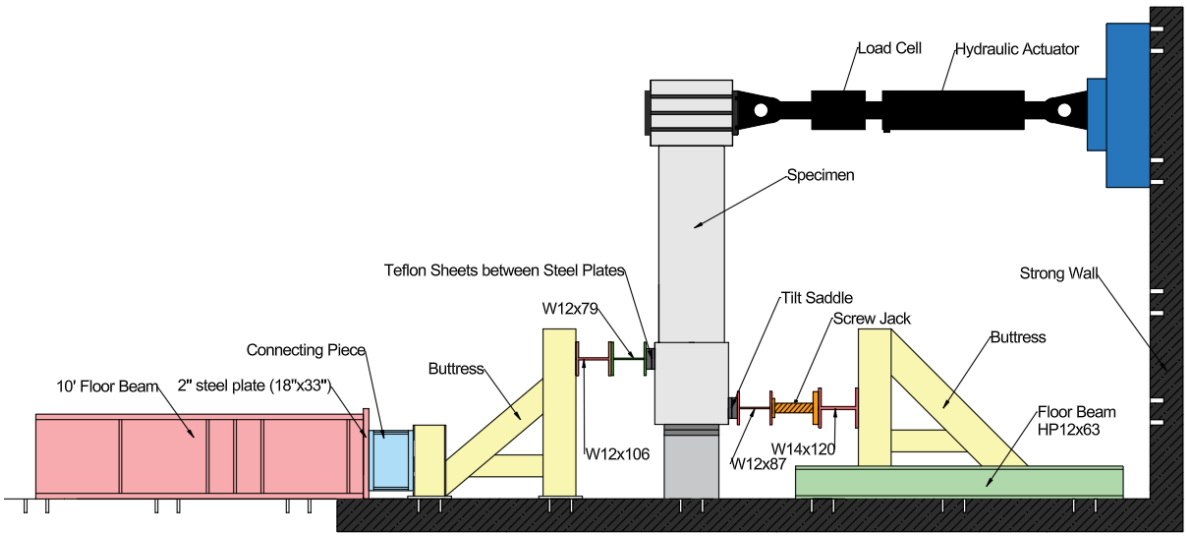

(a) Side View

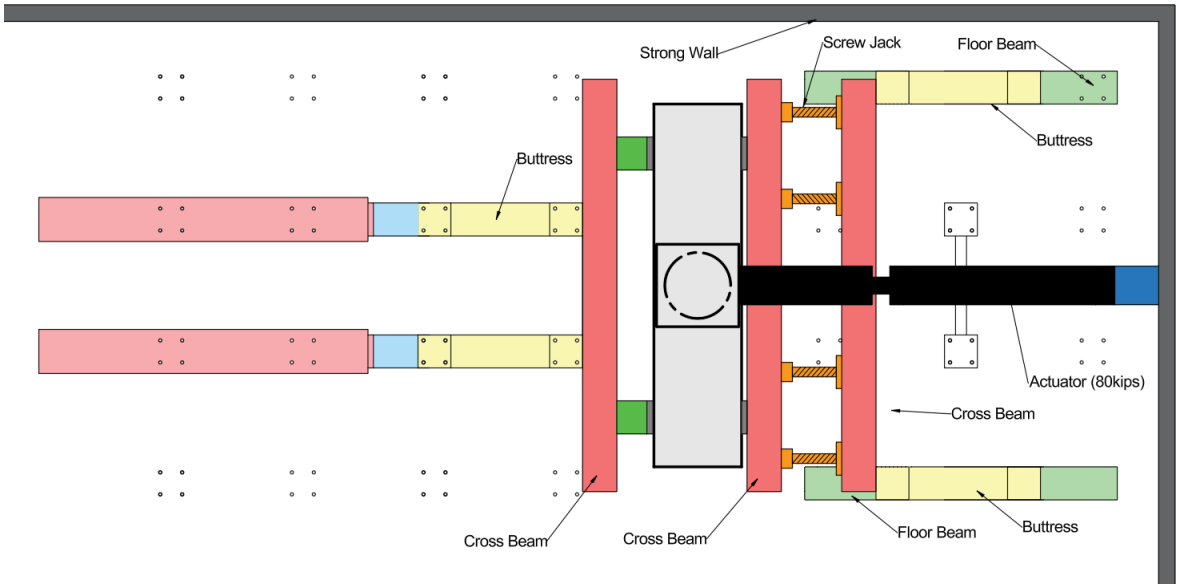

(b) Top View

Figure 4-27. Test setup

(a) External instrumentation (b) HD-O-CIP in the test frame

Figure 4-28. Test frame and instrumentation

4.4. Phase II: Out-of-Plane Direction Test Results

4.4.1. Description of Specimen's Behavior

After the load applied to specimen S-O-CIP reached 10 kips, the first 0.004 in. crack appeared in the column. As the load increased to 17 kips, two additional flexural cracks formed in the column, with the maximum crack width recorded at this stage being 0.006 in. At 24 kips, these column cracks widened to 0.01 in. and lengthened, while new cracks developed at the bent-column interface and higher up the column. The interface crack at this point remained short and measured 0.006 in. in width. The first torsional cracks, approximately 0.004 in. wide, formed on the compression side and top surface of the bent cap, propagating toward the column base. When the load reached 31 kips (0.5 % drift), existing cracks in the column continued to widen, with the interface crack reaching 0.02 in. Cracks on the compression face of the bent cap extended through its full height and widened to 0.016 in. At 38 kips, column flexural cracking intensified, and the interface crack widened to 0.03 in. Additional torsional cracks appeared on the compression face, while those on the top face expanded to widths of up to 0.04 in. The first torsional crack also appeared on the tension face, showing the characteristic torsion crack pattern. At 45 kips (1 % drift), column cracks exhibited slight additional widening and elongation, and multiple new cracks developed on all faces of the bent cap. A few asymmetrical cracks were observed on the tension face; additional cracks formed as the load increased further. At 48 kips (1.35 % drift), both the column's longitudinal reinforcement and the bent cap stirrups yielded. The test continued until the specimen reached a peak load of 52.6 kips. The experiment was terminated when concrete crushing at the interface became evident, and when the bent cap had reached its maximum torsional capacity. Extent of the damage at failure is shown in Figure 4-29. For safety reasons, full post-peak behavior was not investigated.

(a) Concrete crushing (b) Torsional cracks adjacent to joint region

Figure 4-29. Extent of damage at failure (S-O-CIP)

Specimen HD-O-CIP, which incorporated headed bar anchorage for the column longitudinal reinforcement, exhibited a response similar to that of S-O-CIP. The first flexural cracks were recorded at 10 kips, followed by two new column cracks at 17 kips, while the bent cap remained

uncracked. At 24 kips, the interface crack appeared, with a measured width of 0.012 in., and other column cracks were narrower than 0.01 in. No bent cap cracks were observed at this stage. At 31 kips (0.5 % drift), column flexural cracking progressed, and the interface crack reached 0.02 in. Cracks also appeared on all faces of the bent cap, mainly on the compression side, spanning its full height. Additional top face cracks connected these to the column base, but their width remained limited to 0.016 in. When the load reached 38 kips, both column and bent cap cracks widened, and new cracks formed on the top and compression faces of the bent cap. The interface crack reached 0.03 in. At 45 kips (1 % drift), numerous new cracks developed, linking existing cracks around the bent cap. The torsional capacity of the bent cap was visibly being approached. Column cracks elongated downward toward the base, and the interface crack widened to 0.04 in. At this load level, the column longitudinal bars and bent cap stirrups were yielding. The specimen reached a peak load of 54.8 kips. Unlike the previous test, post-peak behavior was recorded up to 9 % drift. The specimen maintained 92 % of its peak capacity when the test was stopped due to excessive displacement. Due to the increase displacement reached during the test, greater damage is shown in Figure 4-30.

(a) Interface crack (b) Torsional cracks and crushed concrete

Figure 4-30. Extent of damage at failure (HD-O-CIP)

The first loading stage for specimen S-O-PC occurred at 13 kips, at which three flexural cracks were recorded in the column, all narrower than 0.006 in. At 23 kips, new column cracks formed, and existing ones widened to 0.01 in. and lengthened. A small interface crack was also observed. At 33 kips (0.5 % drift), the interface crack extended and widened to 0.02 in., and additional flexural cracks formed in the column, following a similar crack propagation pattern to that of the previous specimens. At 43 kips, the bent cap remained intact with no visible cracking; the interface crack reached 0.03 in., and column cracks widened to 0.02 in. At 53 kips (1 % drift), the tension-side interface crack widened to 0.06 in., while other column cracks widened with minimal elongation. A 0.08 in. crack developed on the top face of the bent cap and connected to new torsional cracks on the compression side. The tension face remained uncracked, and the column longitudinal bars were approaching yield. When the load reached 65 kips, an issue was encountered with the test frame and the test had to be stopped. Based on the data, the specimen was only a few kips below its peak flexural capacity, primarily governed by flexural failure of the

column. Crushing of concrete was observed on the compression side of the interface, and longitudinal bar yielding was significant. Bent cap cracking remained less extensive than in the cast-in-place specimens, as shown in Figure 4-31.

(a) Concrete crushing (b) Torsional cracks

Figure 4-31. Extent of damage at the end of the test (S-O-PC)

After repairs, specimen HD-O-PC was loaded to 13 kips, at which point initial column flexural cracks formed, measuring less than 0.006 in. in width. At 23 kips, existing cracks widened and lengthened to under 0.016 in., and additional cracks appeared, including the first interface crack. At 33 kips (0.5 % drift), the maximum crack width of 0.025 in. was recorded approximately 1 ft above the column base. The interface crack propagated along the base, and new cracks formed higher up. A rare vertical crack between the base and a point 0.5 ft above emerged. At 43 kips, the interface crack as well as one other flexural crack widened to 0.03 in., while other column cracks showed slight growth. A 0.008 in. torsional crack developed on the top face of the bent cap, not spanning its full width. At 53 kips (1 % drift), the interface crack widened to 0.06 in., and other column cracks expanded significantly as longitudinal bar yielding began. Symmetrical diagonal and a single vertical crack formed on the compression face of the bent cap, connecting with existing top-face cracks that widened to 0.025 in. The tension face remained uncracked at this stage. The specimen was then loaded to failure, reaching a peak of 68.3 kips when concrete crushing and reinforcement yielding became critical. Thanks to the test frame improvement, it was able to obtain the post peak behavior of the specimen. It was recorded that the specimen retained 91% of its peak capacity at 7.5% drift. At that point, large pieces of concrete spalled off at the bent-column interface. The magnitude of the concrete spalling compared to the damage of the bent cap is shown in Figure 4-32.

(a) Concrete crushing

(b) Torsional cracks

Figure 4-32. Extent of damage at failure (HD-O-PC)

Based on the experiments, we saw little difference when the anchorages are compared. Both cast-in-place specimen behaved similarly, as did both precast specimens. However, we saw a big difference when cast-in-place specimens are compared to the precast specimens. While torsional mode of failure was predominant in the cast-in-place specimens, the precast specimens were able to contain the spread and widening of the torsional cracks. It needs to be noted that the precast specimens were slightly wider than the cast-in-place specimen; however, the prestressing force in the strands was also a significant positive factor. This stiffer response of the of the precast specimens enabled more concrete crushing before severe torsional cracks occurred. It is important to note that in all of these tests, whether we were able to see the post peak behavior or not, the longitudinal bars yielded significantly, showing adequate development length within the bent cap. Figures below show the crack patterns and crack widths from all views at different drift ratios.

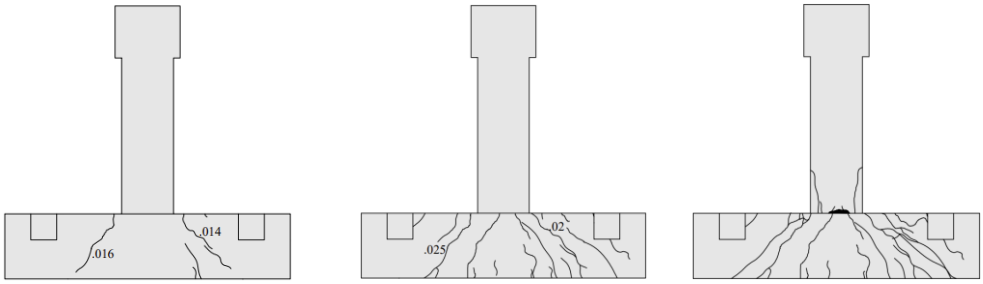

(a) S-O-CIP 0.5% drift compression side

(b) S-O-CIP 1% drift compression side

(c) S-O-CIP test end compression side

Figure 4-33. Specimen S-O-CIP crack patterns (in.)

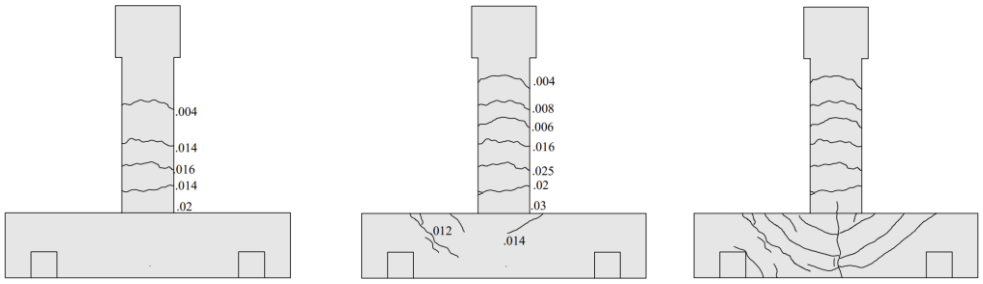

(a) S-O-CIP 0.5% drift tension side

(b) S-O-CIP 1% drift tension side

(c) S-O-CIP test end tension side

Figure 4-34. Specimen S-O-CIP crack patterns (in.)

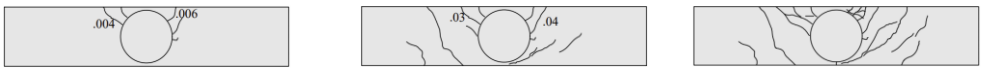

(a) S-O-CIP 0.5% drift top view

(b) S-O-CIP 1% drift top view

(c) S-O-CIP test end top view

Figure 4-35. Specimen S-O-CIP crack patterns (in.)

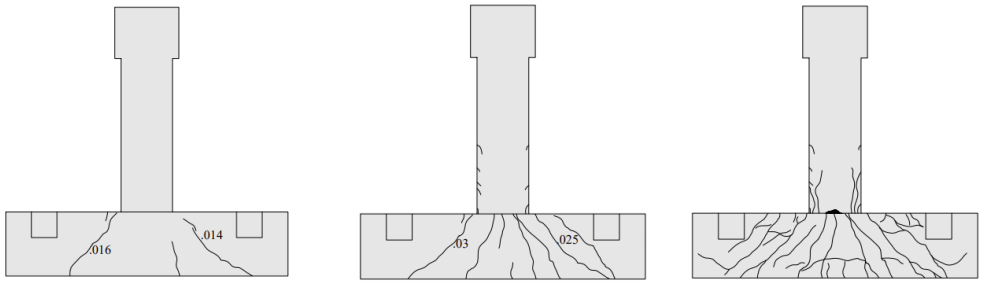

(a) HD-O-CIP 0.5% drift compression side

(b) HD-O-CIP 1% drift compression side

(c) HD-O-CIP test end compression side

Figure 4-36. Specimen HD-O-CIP crack patterns (in.)

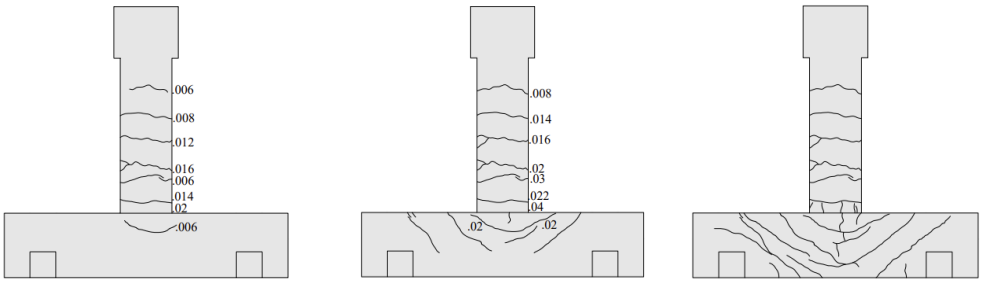

(a) HD-O-CIP 0.5% drift tension side

(b) HD-O-CIP 1% drift tension side

(c) HD-O-CIP test end tension side

Figure 4-37. Specimen HD-O-CIP crack patterns (in.)

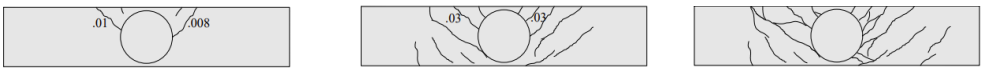

(a) HD-O-CIP 0.5% drift top view

(b) HD-O-CIP 1% drift top view

(c) HD-O-CIP test end top view

Figure 4-38. Specimen HD-O-CIP crack patterns (in.)

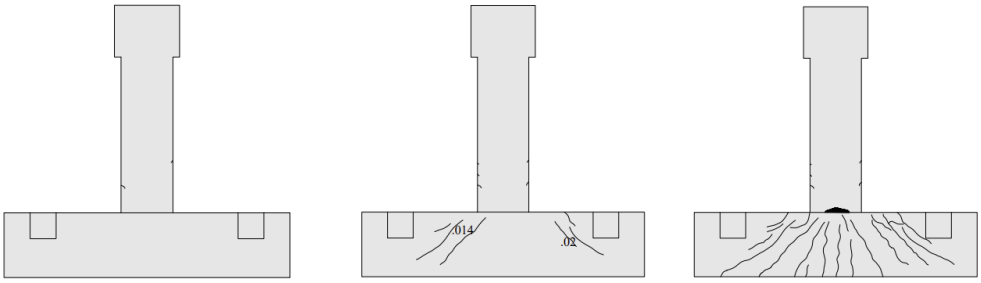

(a) S-O-PC 0.5% drift compression side

(b) S-O-PC 1% drift compression side

(c) S-O-PC test end compression side

Figure 4-39. Specimen S-O-PC crack patterns (in.)

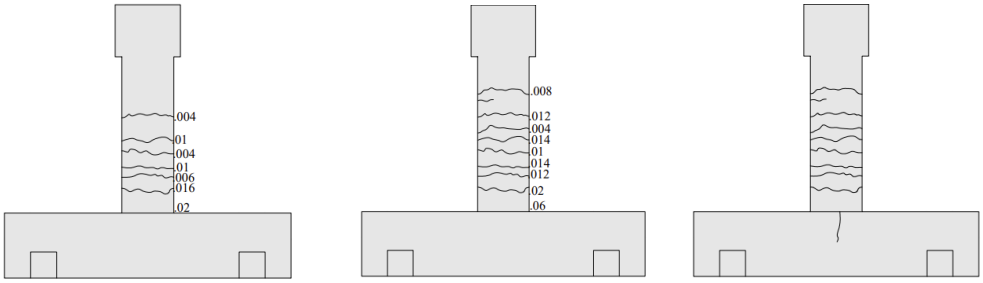

(a) S-O-PC 0.5% drift tension side

(b) S-O-PC 1% drift tension side

(c) S-O-PC test end tension side

Figure 4-40. Specimen S-O-PC crack patterns (in.)

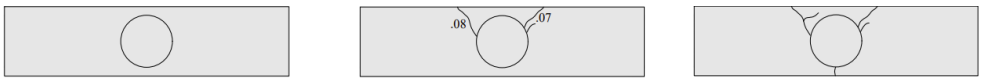

(a) S-O-PC 0.5% drift top view

(b) S-O-PC 1% drift top view

(c) S-O-PC test end top view

Figure 4-41. Specimen S-O-PC crack patterns (in.)

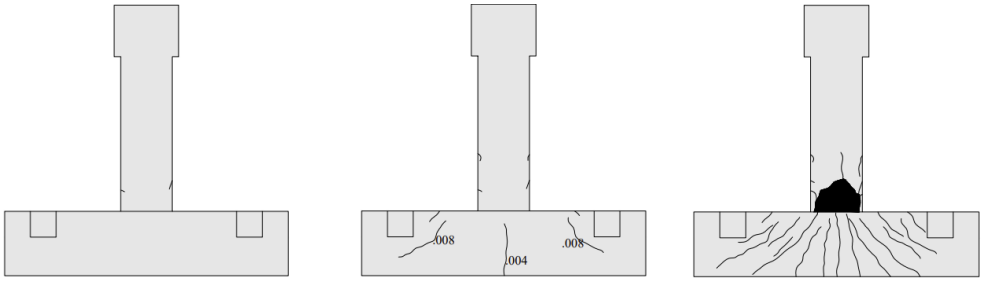

(a) HD-O-PC 0.5% drift compression side

(b) HD-O-PC 1% drift compression side

(c) HD-O-PC test end compression side

Figure 4-42. Specimen HD-O-PC crack patterns (in.)

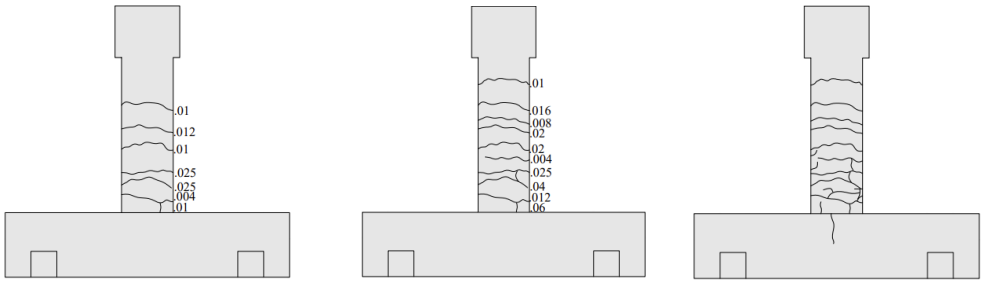

(a) HD-O-PC 0.5% drift tension side

(b) HD-O-PC 1% drift tension side

(c) HD-O-PC test end tension side

Figure 4-43. Specimen HD-O-PC crack patterns (in.)

(a) HD-O-PC 0.5% drift top view

(b) HD-O-PC 1% drift top view

(c) HD-O-PC test end top view

Figure 4-44. Specimen HD-O-PC crack patterns (in.)

4.4.2. Moment Displacement Response

The moment–displacement curves for all specimens are shown in Figure 4-45. Across all tests, the structural response followed a consistent pattern. At the beginning of loading, the specimens exhibited a linear relationship between moment and displacement, indicating elastic behavior prior to any visible cracking. Once the first cracks formed, the response transitioned into a post-cracking phase, during which the stiffness gradually decreased until the column reinforcement reached its yield point. Following this, the specimens continued to deform while sustaining their peak strength, resulting in a relatively stable plateau in the load–deformation curve. The influence of anchorage on this overall response was found to be minimal. In contrast, clear distinctions emerged between the cast-in-place and precast specimens. Although the initial stiffness was comparable—because cracking originated only in the columns, which were identical for all four specimens—their behavior began to diverge once cracks developed in the bent cap. The precast specimens preserved their stiffness for a longer period, up to the stage when the column longitudinal bars began to yield and the bent cap experienced cracking. This behavior can be attributed to the greater concrete strength of the precast bent caps, their increased section size, and the benefits of prestressing. A 24.7% increase in peak moment capacity was recorded when comparing HD-O-CIP with HD-O-PC. When the out-of-plane and in-plane responses were compared, the out-of-plane specimens demonstrated lower capacity. This reduction can be linked to torsional capacity being exceeded in the bent cap, combined with the lack of axial load that would otherwise confine the column, a factor that had the greatest impact on the precast specimens.

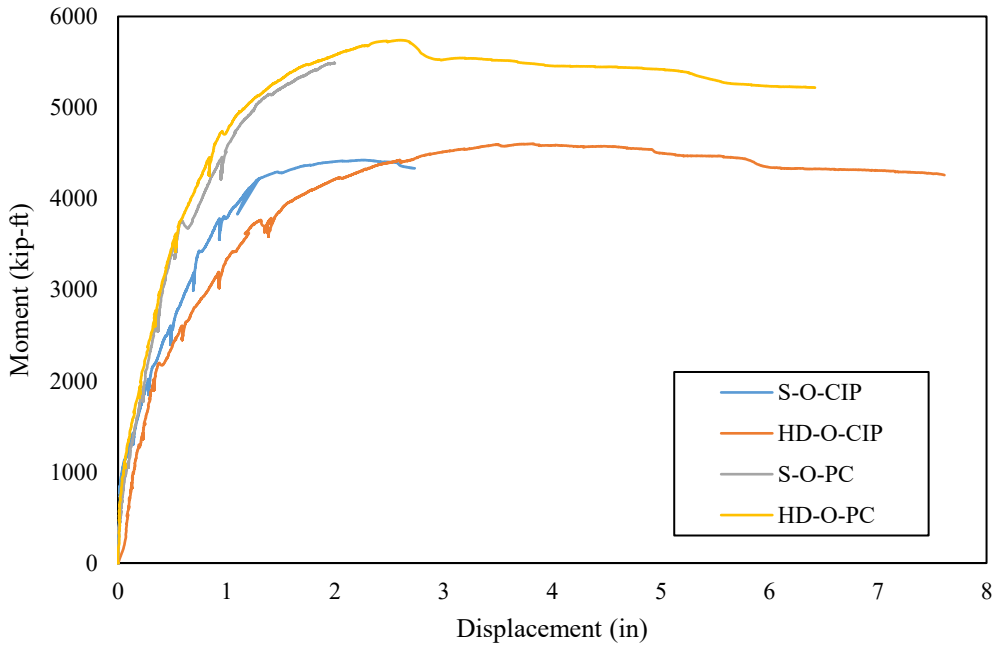

Figure 4-45. Moment-displacement response for out-of-plane specimens

4.4.3. Strain Profile on the Column Longitudinal Bars

Axial strain measurements were collected along the outermost longitudinal reinforcement in the column for all specimens at different drift ratios. Figure 4-46 illustrates the distribution of tensile strains for each specimen, plotted as a function of height above the bent-column interface. For each gauge position, the reported strain represents the average of the two tensile bars on the column's tension side. At the critical section, located at the interface, the longitudinal reinforcement reached its yield strain in all tests. Clear evidence of strain penetration was observed in every specimen, indicating that bar yielding extended well into the joint region. Despite slight variations in magnitude, the overall shape of the strain profiles was consistent across all tests. The onset of yielding occurred between 1 % and 1.5 % drift, with the highest strain values concentrated near the interface. The gradual increase in strain at different elevations is associated with crack formation both above and below the column base. Above the base, this is linked to flexural crack development in the column, while below the base, the increase results from torsional cracking in the joint region. This pattern is comparable to the higher strain observed in specimens subjected to in-plane testing, where larger shear cracks developed. Because all four specimens exhibited similar yield stress values for their longitudinal reinforcement, no normalization of strain profiles was required.

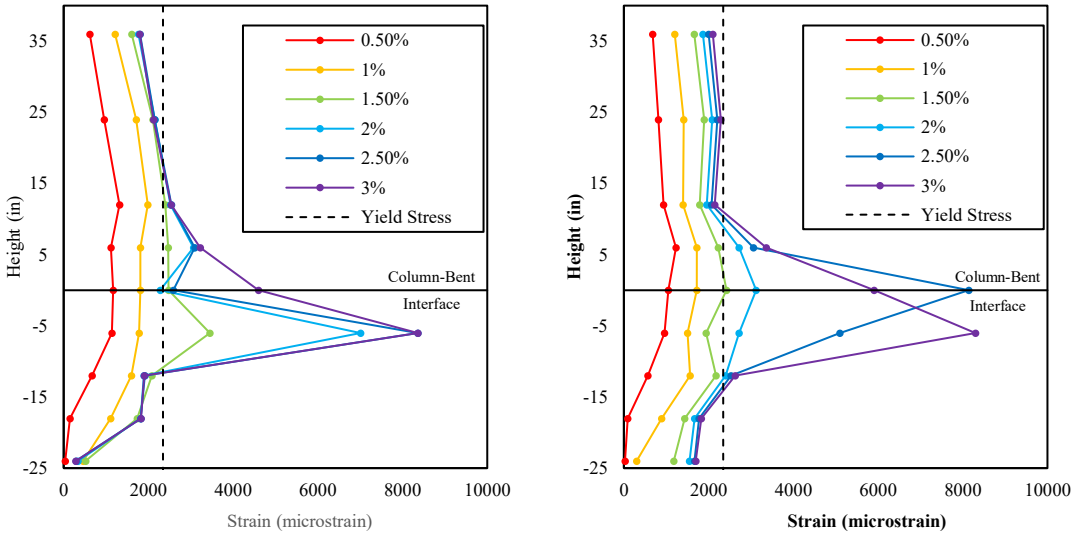

(a) S-O-CIP

(b) HD-O-CIP

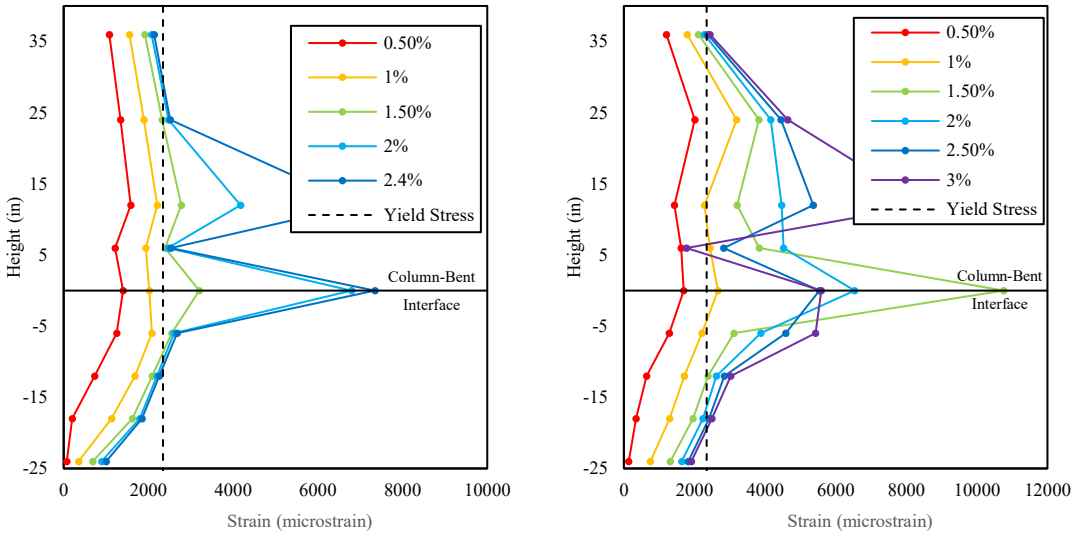

(c) S-O-PC (d) HD-O-PC

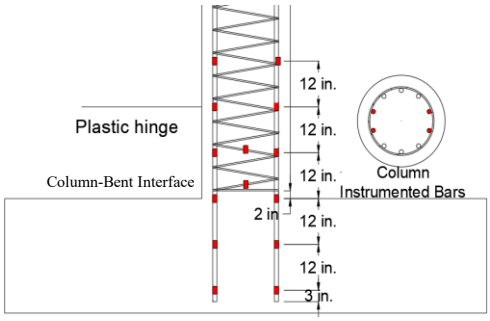

(e) Legend

Figure 4-46. Strain profiles

4.4.4. Crack Width

Crack width evolution was evaluated by plotting measured crack widths against the percentage of the maximum applied load for each specimen, as illustrated in Figure 4-47. To provide reference points, two benchmark crack widths were selected: 0.006 in. and 0.012 in., corresponding to the limits recommended by the ACI 224R committee for concrete exposed to aggressive environments such as seawater, seawater spray, wetting and drying cycles, humid air, and soil under service load conditions. Table 4-6 summarizes the percentages of the ultimate load at which the ACI 224R benchmark crack widths were reached in both the column and the bent cap. The results indicate that anchorage type had minimal influence on crack control in the column. In contrast, the use of

precast bent caps delayed the development of larger cracks, increasing the percentage of peak load required to reach the benchmark crack widths by approximately 10–19 %.

Table 4-6. Percent of ultimate applied load at benchmark crack widths

Specimen ID	Column flexural cracks		Connections cracks	
	0.006 in.	0.012 in.	0.006 in.	0.012 in.
S-O-CIP	37%	50%	48%	54%
HD-O-CIP	27%	48%	49%	53%
S-O-PC	20%	40%	67%	68%
HD-O-PC	19%	28%	59%	66%

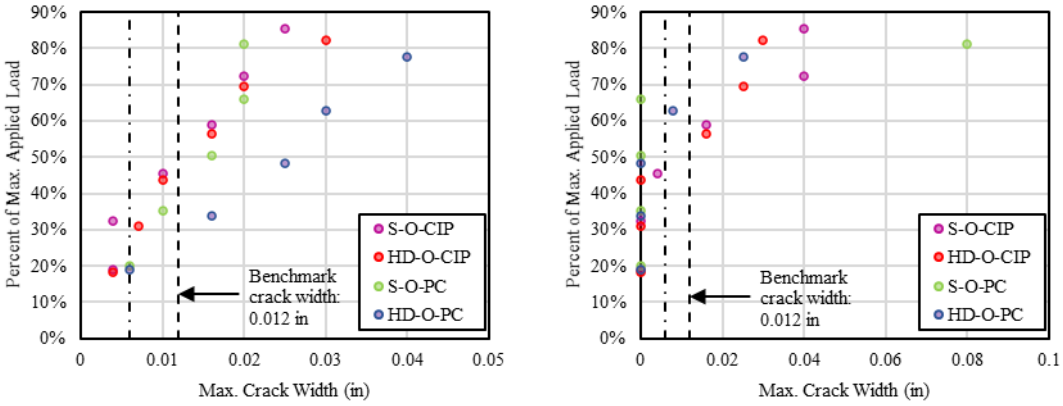

(a) Column flexural cracks (b) Connection cracks

Figure 4-47. Crack width behavior of specimens

4.5. Finite Element Analysis

Finite element analyses were conducted to gain deeper insight into the response of the specimens which are failed under in-plane direction. The nonlinear finite element analysis software VecTor2 was utilized to analyze the specimens. The program's theoretical foundation is the Disturbed Stress Field Model (DSFM), a smeared crack model, which represents a hybrid formulation that combines elements of a fully rotating crack model and a fixed crack model. Built upon the principles of the Modified Compression Field Theory by Vecchio and Collins, the DSFM takes into account equilibrium, compatibility, and constitutive relationships by analyzing average stresses and strains over a gauge length that spans multiple cracks.

VecTor2 is well-suited for analyzing members with primarily two-dimensional behavior. Its application to elements such as circular columns, where aspects of the response are inherently

three-dimensional, is made possible by defining an appropriate out-of-plane equivalent geometry and incorporating behavioral models that account for out-of-plane effects, such as concrete strength enhancement due to confinement. As such, the column was discretized as shown in Figure 4-48 (a).

To address nonlinear geometry and the secondary P-Δ effects, the structure was entirely modeled using quadrilateral elements. The longitudinal reinforcement in both the bent cap and the column was modeled discretely, with link elements assigned to the column longitudinal bars to facilitate the analysis, including the imperfect bond between concrete and reinforcement. The transverse reinforcement was modeled as smeared due to its uniform distribution throughout the specimen, including the hoop confinement and the corrugated metal pipe in the precast bent cap. The FE model had boundary conditions and the loading protocol similar to those of the experimental setup. Figure 4-48 (b) illustrates the VecTor2 model utilized for the cast-in-place specimens' analyses, and Figure 4-48 (c) illustrates the precast specimens.

4.5.1. Load-Displacement Response

The load-displacement responses of the finite element models and the experimental results for all specimens are depicted in Figure 4-48 (d-l). Across all specimens, the calculated stiffness closely matched the experimental results. However, the calculated load capacity tended to be underestimated in all models except for S-NS-CIP-NH, albeit within 20% of the experimental results. For Specimens S-SK-CIP-NH and HK-SK-CIP-NH, the NLFEA models accurately captured the overall shape of the load-displacement curve, showcasing high levels of ductility with failure primarily attributed to rebar yielding before concrete crushing on the column. Moreover, the NLFEA models effectively captured post-peak deterioration for S-SK-CIP-NH and HK-SK-CIP-NH. In contrast, the model for Specimen S-NS-CIP-NH accurately estimated stiffness and capacity, with the ultimate capacity only marginally higher than the experimental counterpart. Nonetheless, it exhibited a more rapid deterioration post-peak, underestimating the specimen's overall ductility. illustrates the comparison of calculated versus observed crack patterns for Specimen S-SK-CIP-NH, demonstrating a strong correlation between NLFEA results and experimental behavior. The S-SK-CIP-H4 and S-SK-CIP-H2 models accurately simulated the stiffness but failed to reach the peak lateral load seen in the experiment. The post-peak response in the model depicted a gradual increase in the lateral load that was not observed in the experimental behavior, but it achieved an ultimate load within a 6% error. Neither the experimental behavior nor the NLFEA demonstrated a significant loss in the sustained load. Furthermore, the precast specimens S-PC and HD-PC also did not achieve the maximum lateral load, but the stiffness of the specimens resembles that of the experimental data, and the post-peak demonstrates the gradual loss in strength and plateau.

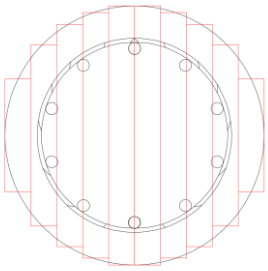

(a) Cross-sectional discretization

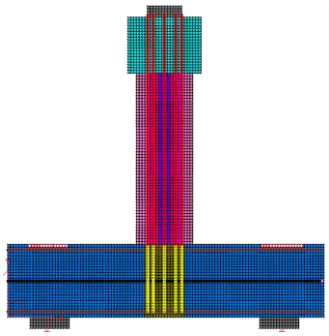

(b) Cast-in-place VecTor2 model

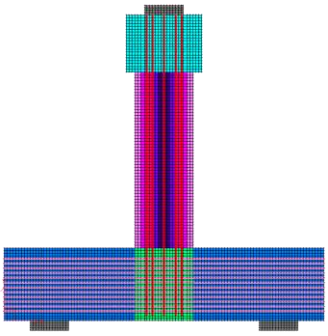

(c)Precast VecTor2 model

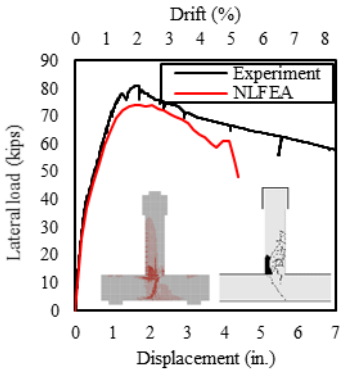

(d) Specimen S-NS-CIP-NH*

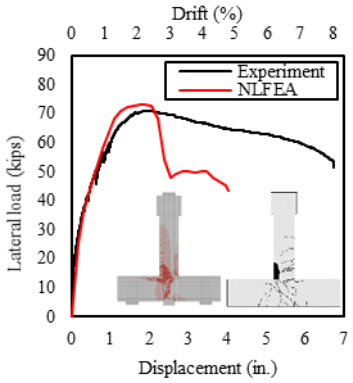

(e) Specimen S-NS-CIP-NH

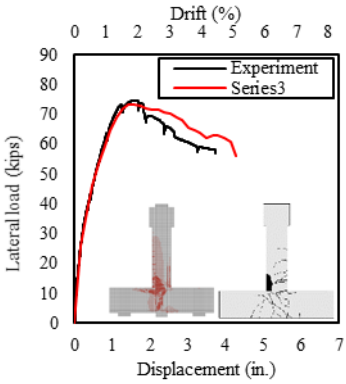

(f) Specimen S-SK-CIP-NH

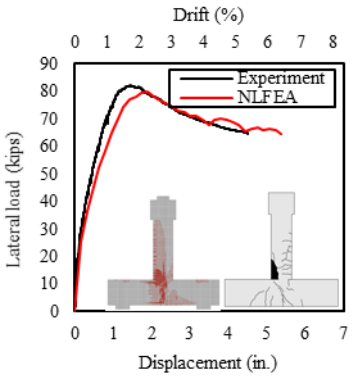

(g) Specimen HK-SK-CIP-NH

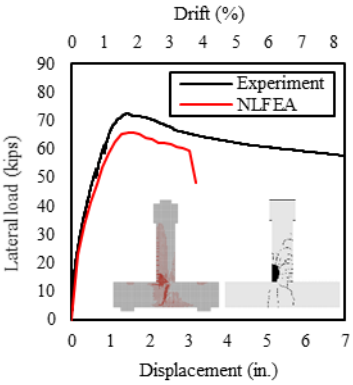

(h) Specimen HD-SK-CIP-NH

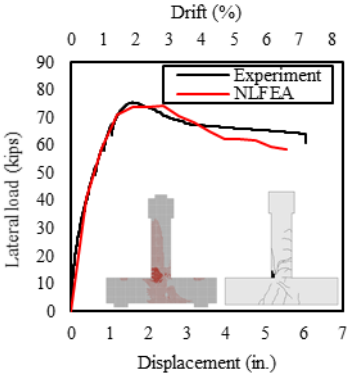

(i) Specimen S-SK-CIP-H4

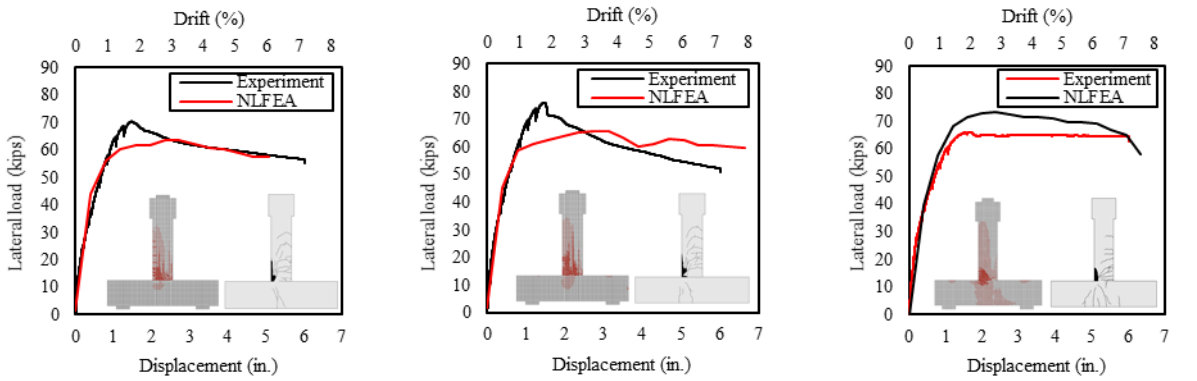

(j) Specimen S-PC (k) Specimen HD-PC (l) Specimen S-SK-CIP-H2

Figure 4-48. Experimental versus analytical behavior

4.5.2. Strain Profiles

To compare the experimental and analytical strains in the longitudinal column rebar, strain diagrams were generated at 1.5% drift, corresponding to the peak load for all specimens. For Specimen S-SK-CIP-NH, however, the strain gauges were out of range, necessitating data collection at 1.25% drift. These diagrams were instrumental in determining the theoretical and experimental development length of the longitudinal bars. Figure 4-49 illustrates the strain diagrams of the NLFEA models compared with the corresponding experimental results.

Reasonably good agreement can be observed between the analytical and experimental measured strains. However, certain discrepancies arise, particularly at the interface, where a significant jump in strain is observed in Specimens S-NS-CIP-NH*, S-NS-CIP-NH, and S-SK-CIP-H4. Despite these disparities, the models offer a precise method for estimating the anchorage and development of the reinforcement. The difference in the development lengths found for experimentally and NLFEA all have variations less than 10% demonstrated by Table 4-7. The NLFEA can be used in other loading configurations to estimate the expected development length.

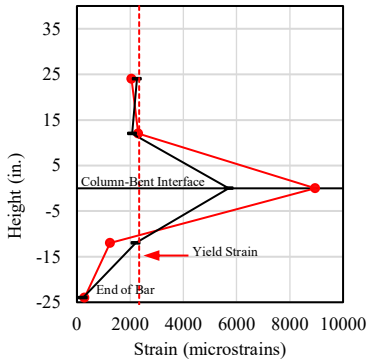

(a) Specimen S-NS-CIP-NH* (1.50% drift)

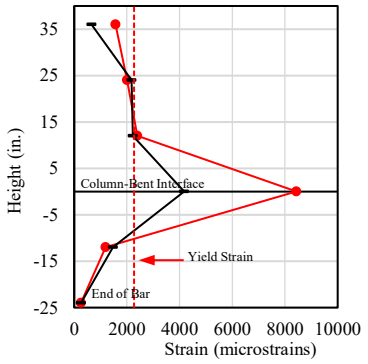

(b) Specimen S-NS-CIP-NH (1.50% drift)

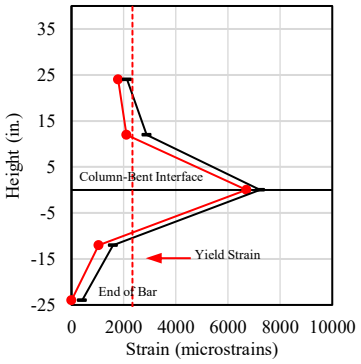

(c) Specimen S-SK-CIP-NH (1.25% drift)

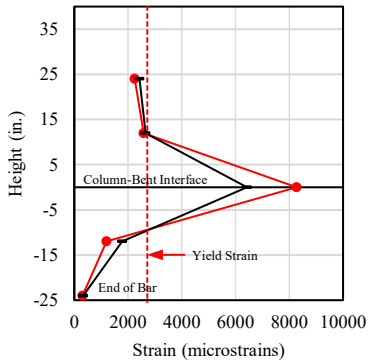

(d) Specimen HK-SK-CIP-NH (1.50% drift)

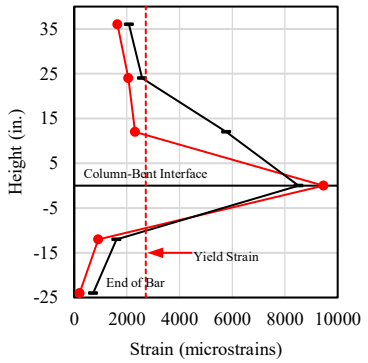

(e) Specimen HD-SK-CIP-NH (1.50% drift)

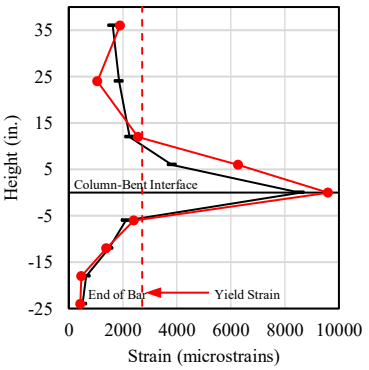

(f) Specimen S-SK-CIP-H2 (1.50% drift)

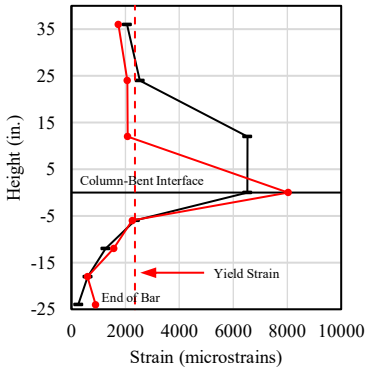

(g) Specimen S-SK-CIP-H4 (1.50% drift)

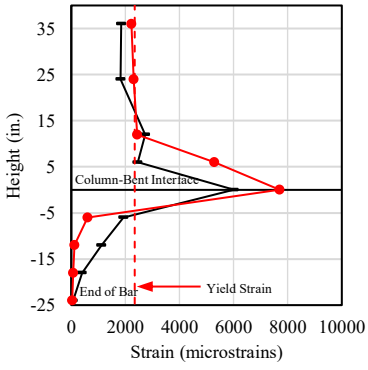

(h) Specimen S-PC (1.50% drift)

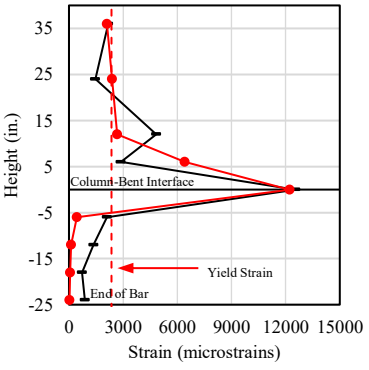

(i) Specimen HD-PC (1.50% drift)

Figure 4-49. Experimental versus analytical strain profiles

4.5.3. Column Longitudinal Reinforcement Development Length

The development length of the column's longitudinal reinforcement extending into the bent cap is evaluated to assess the effectiveness of moment transfer at the connection. The development length was calculated according to the expressions in ACI 318-19, ACI 318-25, AASHTO LRFD 2020, and the updated provisions introduced in AASHTO LRFD 2024. These calculated values were then compared with the development lengths derived from the experiments and nonlinear finite element analysis (NLFEA), as summarized in Table 4-7 and Table 4-8.

To determine the development length of the rebar in the different specimens, the strain profiles presented in the previous sections were utilized. The change in strain between two strain gauges was assumed to vary linearly, enabling the determination of the yield point through interpolation. The development length was then considered as the distance from the end of the bar to the location where the strain in the bar intersects the yield is first encountered at 1.5% drift. A drift level of 1.5% was selected because it corresponds to the minimum drift associated with the peak lateral loads observed in all specimens, ensuring that the evaluation captures the maximum moment demand at the connection without the inconsistency of strain data that occurs post-peak, and therefore, the ultimate limit state. This approach provides a consistent basis for comparing development lengths across specimens with different reinforcement details and confinement conditions. A similar procedure was employed to determine the development length calculated via the NLFEA.

Table 4-7. Development length comparison between experiment, NLFEA and design codes

Specimen ID	Exp. (in.)	NLFEA (in.)	ACI 318-19 (in.)	ACI 318-25 (in.)	AASHTO 2020 (in.)	AASHTO 2024 (in.)
S-NS-CIP-NH*	15.4	16.7	30.0	30.0	34.2	29.8
S-NS-CIP-NH	18.5	16.8	40.0	40.0	30.5	38.6
S-SK-CIP-NH	16.5	17.7	29.8	33.5	40.5	29.6
S-SK-CIP-H4	21.0	21.3	33.5	33.5	24.3	30.6
S-SK-CIP-H2	21.3	21.5	32.0	32.0	30.2	30.1
HK-SK-CIP-NH	17.4	17.6	36.2	18.3	24.7	30.9
HD-SK-CIP-NH	16.3	17.0	22.9	17.2	N/A	26.0
S-PC	21.6	22.5	38.1	38.1	29.4	35.9
HD-PC	21.1	22.0	23.4	22.0	N/A	27.2

Table 4-8. Development length ratio between experiment and NLFEA or design codes

Specimen ID	$\frac{NLFEA}{Exp.}$	$\frac{ACI\ 318\_19}{Exp.}$	$\frac{ACI\ 318\_25}{Exp.}$	$\frac{AASHTO\ 2020}{Exp.}$	$\frac{AASHTO\ 2024}{Exp.}$
S-NS-CIP-NH*	1.08	1.94	1.94	2.22	1.93
S-NS-CIP-NH	0.91	2.16	2.16	1.64	2.08
S-SK-CIP-NH	1.07	1.81	2.03	2.46	1.79
S-SK-CIP-H4	1.01	1.60	1.60	1.16	1.46
S-SK-CIP-H2	1.01	1.50	1.50	1.42	1.41
HK-SK-CIP-NH	1.01	2.08	1.05	1.42	1.78
HD-SK-CIP-NH	1.04	1.40	1.06	N/A	1.60
S-PC	1.04	1.76	1.76	1.36	1.66
HD-PC	1.04	1.11	1.04	N/A	1.29

The development length calculations appeared to be conservative regardless of the specification used. While the effect of concrete and steel reinforcement strength on the development length is evident in the experimental results (e.g., Specimen S-NS-CIP-NH had a lower compressive strength and higher development length than Specimen S-SK-CIP-NH), it is not as severe as suggested by specifications. For instance, the reduction in the experimental development length between Specimen S-NS-CIP-NH and Specimen S-SK-CIP-NH was 12.4%, whereas the ACI 318-19 indicates a decrease of 34%. Moreover, the use of headed or hooked bars did not significantly reduce the experimental development length. Specimen HD-SK-CIP-NH demonstrated only a 1.3% reduction in the development length compared to Specimen S-SK-CIP-NH. As for the precast specimens, the headed bar had a 0.5% increase in development length when headed bars were introduced. Notably, external confinement provided the most significant improvement in terms of development length, with Specimen S-NS-CIP-NH* exhibiting the shortest development length at 15.4 in., which was 16.7% lower than Specimen S-NS-CIP-NH. As for internal confinement, development length noticeably increased for both hoop confinement and the precast specimens, and S-SK-CIP-H2 saw the lowest increase in development length by 30.5% when compared to S-SK-CIP-NH. Finally, the NLFEA models produced very close estimates of the actual development length observed during the test. Overall, the comparison of experimental, NLFEA, and design specifications development length was conducted to evaluate if the design specifications were adequate in estimating these lengths. As noted, both AASHTO and ACI are conservative compared to what was found in both the experimental and NLFEA.

4.6. Summary

This study investigates the behavior of bent-to-column connections under lateral loading through a comprehensive experimental program and validated nonlinear finite element analyses. The following conclusions can be drawn:

- Despite traditional design assumptions treating the bent-to-column connection as a pinned support, the tests confirmed significant moment transfer at the joint. All specimens developed measurable moments at the interface and strain penetration into the bent cap

further supported this conclusion. Design models should account for this behavior to better reflect structural demand during extreme events.

- Connections detailed according to current Texas standards performed comparably to those with enhanced detailing under monotonically increasing lateral loads. All failures were governed by flexural yielding in the column, not by deficiencies in the joint, indicating that for flexure-critical columns, the connection detailing does not limit capacity.
- The presence of external confinement, simulating a girder on the connection, increased moment capacity by 13.6% and significantly improved ductility and strain development in the connection region. This configuration also delayed shear cracking in the joint and reduced bar development length.
- Headed and hooked bars improved structural response, increasing the moment capacity by 6.8% and 3.5%, and resulting in a stable and ductile post-peak response.
- Hoop reinforcement in the joint enhanced ductility, especially with tighter hoop spacing (two inches). This highlights the role of confinement in controlling damage progression and residual capacity.
- Normalized moment capacities and load-deflection behavior of precast and cast-in-place specimens were nearly identical. However, precast specimens showed slightly increased development lengths, likely due to differences in construction sequence and confinement effectiveness.
- In addition to in-plane tests, four specimens were tested in the out-of-plane direction to evaluate the connection's response to combined flexure and torsion. The failure mode in these tests shifted from pure flexure to one involving significant torsion in the bent cap.
- Torsional failure modes were more predominant in the cast-in-place specimens. The precast specimens, benefiting from prestressing and higher-strength concrete, exhibited a stiffer response and better-controlled torsional cracking, allowing for more flexural yielding in the column before significant torsional damage occurred.
- Despite the different failure modes and the introduction of torsion, all out-of-plane specimens demonstrated that the column's longitudinal reinforcement could be fully developed.
- Experimental and numerical results show that current design provisions for development length (ACI 318-19, AASHTO 2020/2024) are conservative, AASHTO 2024 overestimates development length by approximately 38%, AASHTO 2020 by approximately 36%, ACI 318-25 by approximately 31%, and ACI 318-19 by approximately 39%.
- The FE models effectively captured the behavior of the connections, including stiffness, crack patterns, moment capacity, and strain distribution. The numerical results were in

good agreement with the experimental outcomes and provided a valuable tool for extending the study to complex scenarios such as column removal or multi-hazard conditions.

- Regardless of connection detailing, all specimens exhibited flexural failure in the column. This suggests that the connection detailing is not the limiting factor; however performance can be optimized by improving anchorage and confinement to control crack widths, bar slip, and post-peak behavior.

Chapter 5. Design Guidelines

5.1. Introduction

The resilience of transportation infrastructure is of paramount importance, and bridge substructures are a critical component of this system. The design of these structures must account for a range of loading scenarios, including low-probability, high-consequence extreme events. While analysis in Chapter 3 has shown that direct flood loading is unlikely to cause structural failure, the threats of vehicular collision and the potential loss of a column due to scour or impact remain critical concerns. Such events demand a plastic design philosophy that prioritizes ductility and energy dissipation, ensuring load redistribution to prevent catastrophic collapse. This section presents a comprehensive set of design recommendations for bridge bent-to-column connections specifically tailored to enhance performance under these extreme conditions.

Chapter 3 has already established the potential vulnerabilities of certain conventional designs, including the Texas standard multi-column bents, when subjected to vehicle collision loads. Analysis has shown that design methodologies rooted in traditional elastic theory may require unrealistically high flexural and shear capacity to resist lateral vehicle collision. In addition, elastic design does not concentrate on the necessary ductility to absorb the significant energy imparted during an impact or to adequately redistribute loads following the sudden loss of primary vertical supports. This finding underscores the urgent need for a fundamental shift toward a more resilient design framework.

Chapter 3 also suggests the systematic adoption of a plastic design concept. In contrast to elastic methods, which aim to prevent yielding, plastic design strategically anticipates inelastic action. By designing for the formation of stable, ductile plastic hinges at predetermined locations within the structure, a bridge bent can be engineered to undergo large deformations and dissipate immense amounts of energy. The foundational principle of this approach is to guarantee that a ductile mechanism governs the response, while precluding brittle failure modes such as shear failure and bond failure before the full plastic capacity of the system is achieved.

The successful implementation of plastic design, however, is critically dependent on meticulous reinforcement detailing. The theoretical ductility and rotational capacity of a plastic hinge can only be achieved if the reinforcing steel is adequately anchored to develop its full tensile strength and the concrete core is properly confined. The development length of column longitudinal bars embedded into the bent cap and the foundation is therefore a parameter of primary importance, and the detail of transverse confining reinforcement in the column and the connections is essential, as they directly control the rotational capacity of the member and the connections and the overall ductility of the bent system.

To address this critical detail, an experimental program (Chapter 4) was undertaken to examine the flexural and shear behavior of bent-to-column connections with TxDOT standard and other

feasible details. The test results assisted in quantifying the required embedment length for column longitudinal reinforcement to achieve various levels of drift and rotational capacity, providing valuable insights into the implementation of plastic design concepts.

This section serves as the bridge between analytical and experimental findings and practical engineering applications. It synthesizes the principles of plastic design with the key takeaways from experimental testing to provide engineers with a clear, rational, and actionable design methodology. To this end, a detailed design workflow and a recommended reinforcement detail are provided for a representative bent-to-column connection.

5.2. Review of Findings from Experiment and Analysis

This section summarizes the key findings from two preceding chapters that provide the technical basis for the proposed changes. The following sections will detail the insights gained from both the analytical investigations and the subsequent experimental program, which together form a comprehensive understanding of connection behavior under extreme loads.

5.2.1. Findings of Analytical Investigations

An analytical study, detailed in Chapter 3, was conducted to evaluate the performance of standard multi-column bents under extreme event loading, with a specific focus on vehicle collision and the sudden loss of a column. This analysis moved beyond traditional elastic methods to assess the ultimate capacity of these structures through the application of plastic design principles.

A key component of the analytical work was the use of plastic collapse mechanism analysis, based on the upper bound theorem of plasticity. This method determines the ultimate lateral load capacity of a multi-column bent by identifying the most likely failure mechanism, which typically involves the formation of plastic hinges in the columns and connections. The analysis identified that for most realistic collision scenarios, the governing failure mode is a single-column mechanism, where plastic hinges form at the top and bottom of the impacted column and at the point of impact. Other potential failure mechanisms can be overall structural collapse and combined mechanisms. A visual representation of these mechanisms can be seen in Figure 5-1.

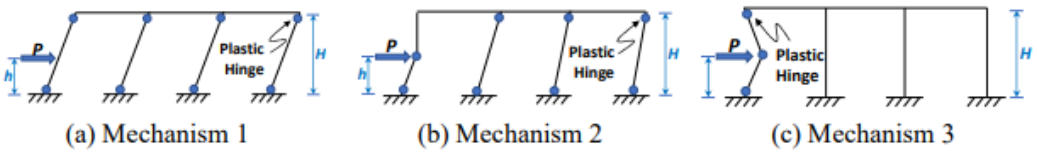

Figure 5-1 Potential failure mechanisms

By equating the external work done by the collision force to the internal energy dissipated by the plastic hinges, the analysis provides a direct method for calculating the required flexural strength (M_p) of the columns in association with a given lateral impact loading and structural dimensions.

The investigation revealed that conventional standard designs, particularly those with connection details that behave as pins (i.e., unable to transfer significant moments), possess inadequate capacity to resist the 600-kip equivalent static force for vehicle collision as specified by AASHTO. The analysis in Chapter 3 showed that bents modeled with these "poorly-detailed" joints were predicted to fail under the design collision load. In contrast, bents modeled with rigid, moment-resisting connections demonstrated sufficient capacity resisting vehicle collision. This finding underscored the critical importance of the bent-to-column connection's ability to transfer moment for the overall system's survivability.

Under the plastic design framework, the formation of plastic hinges with sufficient ductility factor is acceptable and desired, but this ductile behavior can only be achieved if premature brittle failures are prevented. The analysis in Chapter 3 further demonstrated that even when a bent has sufficient flexural strength, it may still be vulnerable to brittle shear failure. A formal procedure was established to ensure ductility by calculating the shear demand based on the flexural overstrength of the column's plastic hinges. As illustrated in the free-body diagram in Figure 5-2, the shear force is determined from the moments required to form a full plastic mechanism, amplified by an overstrength factor (Ω, typically 1.25) to account for material strength gain and strain hardening. This capacity-based approach ensures that the column has sufficient shear strength to allow the ductile plastic hinges to form and rotate.

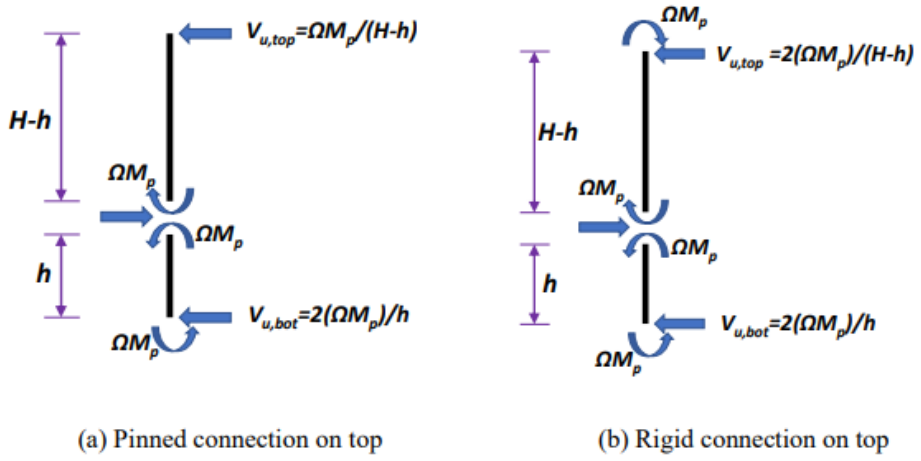

Figure 5-2 Shear demand due to overstrength flexural capacity

A critical outcome of this capacity-based shear analysis was the finding that a standard TxDOT bent design (BIG-24) lacks the shear capacity required to develop its overstrength flexural capacity and ductility. The analysis in Chapter 3 showed that when shear demands were calculated based on the column's flexural overstrength, the demand-to-capacity ratios exceeded 1.0 at both the top

and bottom of the column. This indicates that under a severe collision event, the column would likely experience a brittle shear failure before the plastic hinges could fully form and dissipate energy, preventing the intended ductile failure mechanism from occurring. This vulnerability highlights a significant deficiency in current standard details.

In addition to vehicle collision, Chapter 3 also investigated the scenario of a sudden loss of a support column. Using both sophisticated Nonlinear Dynamic Analysis (NDA) and a more straightforward Linear Static Analysis (LSA), the study confirmed that the sudden removal of a column induces significant load redistribution. Regardless of the analytical method used, the results showed that the bent cap and the remaining columns experience a rapid increase in moment and shear demands. To accommodate these high demands and prevent a progressive collapse, the structure must possess sufficient ductility to deform inelastically. This necessitates the formation of plastic hinges in the bent cap and at the top of the remaining columns. The ability of the structure to successfully form these plastic hinges is entirely dependent on robust detailing, further highlighting the critical need for proper reinforcement anchorage and joint confinement.

5.2.2. Findings of Experimental Program

A comprehensive experimental investigation into the physical behavior of various connection details was conducted as detailed in Chapter 4. The experimental program involved testing thirteen large-scale cast-in-place and precast bent-to-column specimens under monotonic lateral loading, quasi-statically simulating a vehicle collision event. The test matrix was designed to systematically evaluate the influence of key detailing parameters, including anchorage type (straight, hooked, and headed bars), joint confinement (none, skin reinforcement, internal hoops, and external confinement), and loading directions (in-plane and out-of-plane). So far, nine specimens under in-plane loading have been tested, and the remaining four specimens have been cast and scheduled to be tested.

A fundamental outcome of the testing was the definitive confirmation of significant moment transfer at the joint. All specimens, regardless of their detailing, developed substantial moment at the column-bent cap interface and exhibited significant strain penetration of the column's longitudinal bars into the bent cap. Test results, shown in the moment-displacement responses in Figure 5-3, disagrees the pinned-connection assumption often used in simplified design and reinforces the analytical finding that the joint's fixity and integrity is essential to the system's performance.

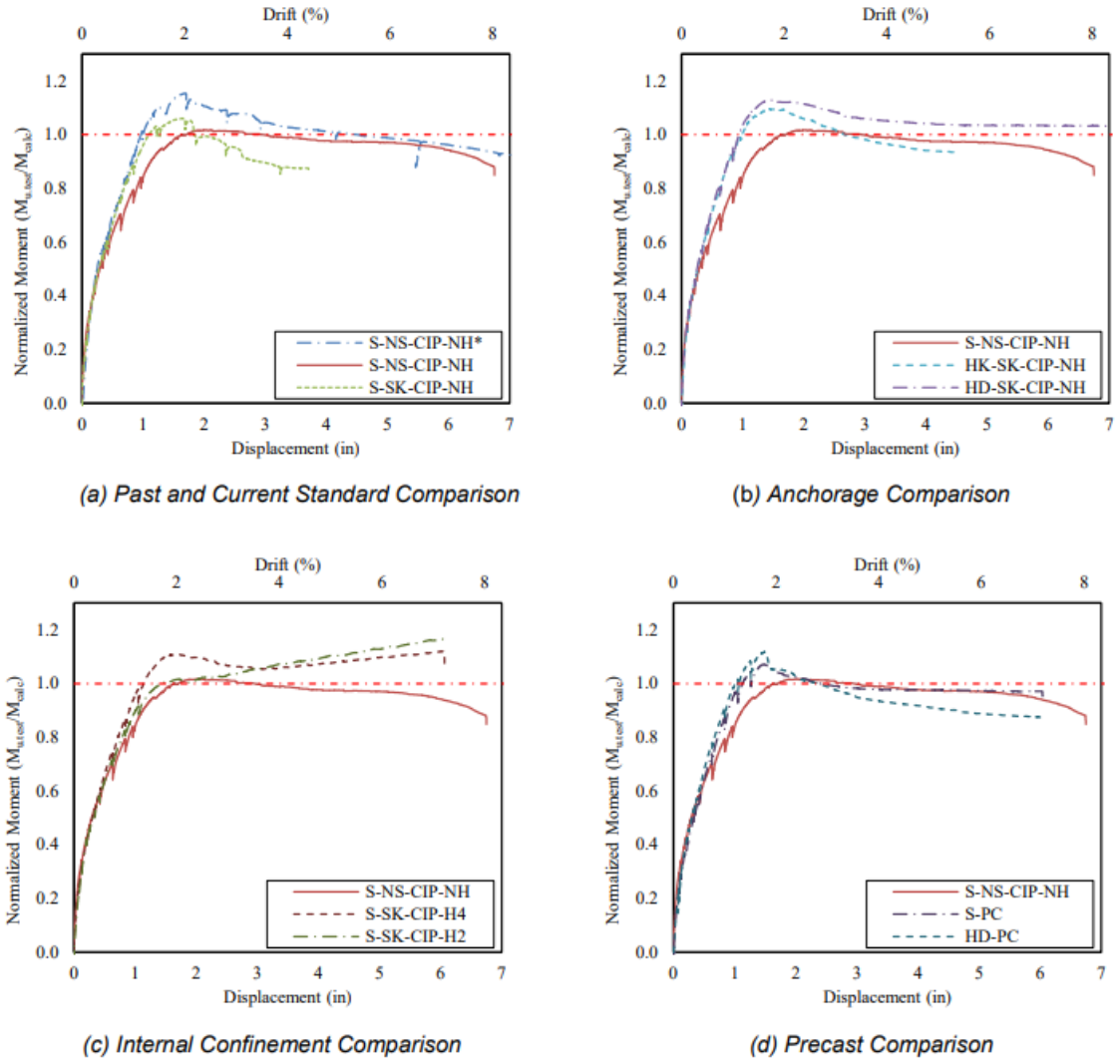

Figure 5-3 Normalized moment-displacement response of tested specimens

The experimental results demonstrated that all tested connection details had ductile post-yield behavior, achieving ductility ratios ranging from at least 3.2 to 6.7. In addition, superior performance of improved anchorage details was also observed. Specimens utilizing hooked and headed bars (HK-SK-CIP-NH and HD-SK-CIP-NH) exhibited higher moment capacities compared to specimens with standard straight bars. Furthermore, as shown in Figure 5-4, details with improved anchorage and joint confinement were effective at controlling bar slip.

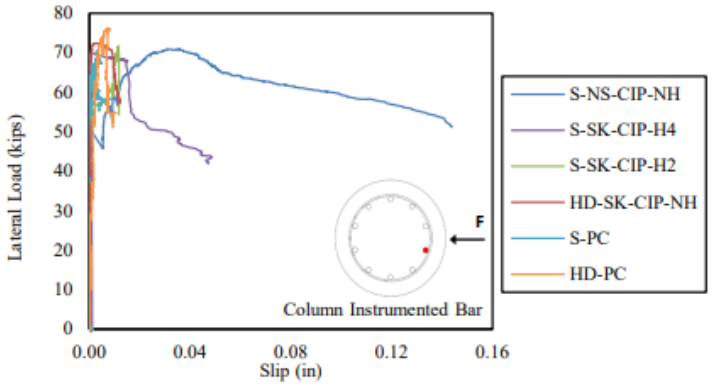

Figure 5-4 Measured bar slip versus lateral load

The benefits of joint confinement were also clearly demonstrated. The externally confined specimen (S-NS-CIP-NH*), simulating the presence of a girder over the joint, showed a 13.6% increase in moment capacity and superior ductility compared to its unconfined counterpart. Similarly, specimens with internal hoop reinforcement (S-SK-CIP-H2 and S-SK-CIP-H4) exhibited enhanced post-peak ductility and damage control, improving connection integrity.

A finding from the strain gauge data was that current AASHTO and ACI provisions for the development length of reinforcing bars are notably conservative for these connection types. In all tests, the experimentally measured development lengths were substantially shorter than those calculated by code equations. In particular, code provisions can overestimate the required length by 12%-40% or more. This suggests that there is an opportunity to refine design provisions for more efficient and economical detailing without compromising safety. It was also implied that even though not applying the overstrength factor, the column longitudinal reinforcement can be sufficiently developed for plastic design purposes.

The experimental program confirmed that the desired post-yield behavior, stable plateauing and plastic deformation, is achievable to satisfy the ductility need for plastic design concept. All nine specimens ultimately failed in a ductile, flexural manner within the column's plastic hinge region.

5.2.3. Remarks on Findings

The combined findings from the analytical and experimental investigations provide insights into revising current design practices for bent-to-column connections. The analyses in Chapter 3 established the reason why a plastic design philosophy is necessary for extreme events, while the experiments in Chapter 4 demonstrated how to achieve the requisite performance through improved detailing.

The experimental program confirmed that providing anchorage that meets or exceeds AASHTO development length requirements, whether enhanced with hooks or heads, is essential for the column bars to develop their full capacity and transfer moment into the bent cap. Concurrently,

the use of hoop reinforcement was proven to be highly effective at confining the joint, maintaining its integrity under high stress, and enhancing the post-yield behavior of the connection. These two elements further ensure that the connection remains intact, allowing a stable plastic hinge to form and rotate in the column. This synergy between robust detailing and predictable plastic behavior forms the critical link between the background studies and the design recommendations that follow.

5.3. Plastic Design Method

This section establishes the principles guiding the design recommendations, translating the analytical and experimental findings into specific, actionable design guidelines. The proposed recommendations are on the basis of the capacity-based plastic design approach. Plastic design embraces the inherent post-yield ductility of reinforced concrete members. The primary goal is to design the structure to form a ductile failure mechanism by detailing specific locations to behave as "plastic hinges." These hinges are designed to yield in flexure and undergo large rotations, thereby dissipating the extreme event's energy in a controlled manner.

Achieving this ductile behavior requires actively preventing other potential brittle failure modes, typically including shear and anchorage failures. These protected components include the shear capacity of the column, the integrity of the joint, and the anchorage of the longitudinal bars, and regions where plastic hinges form. Protection is achieved by designing these components to have a higher capacity than the maximum forces that can be generated by the plastic hinges, as well as providing sufficient anchorage and/or extra confinement following AASHTO provisions, as confirmed in the previous experimental program.

5.3.1. General Procedure

The following step-by-step procedure, illustrated in Figure 5-5, outlines the recommended workflow for designing bridge bent-to-column connections and columns of multi-column bents under vehicular collision in accordance with the capacity design philosophy.

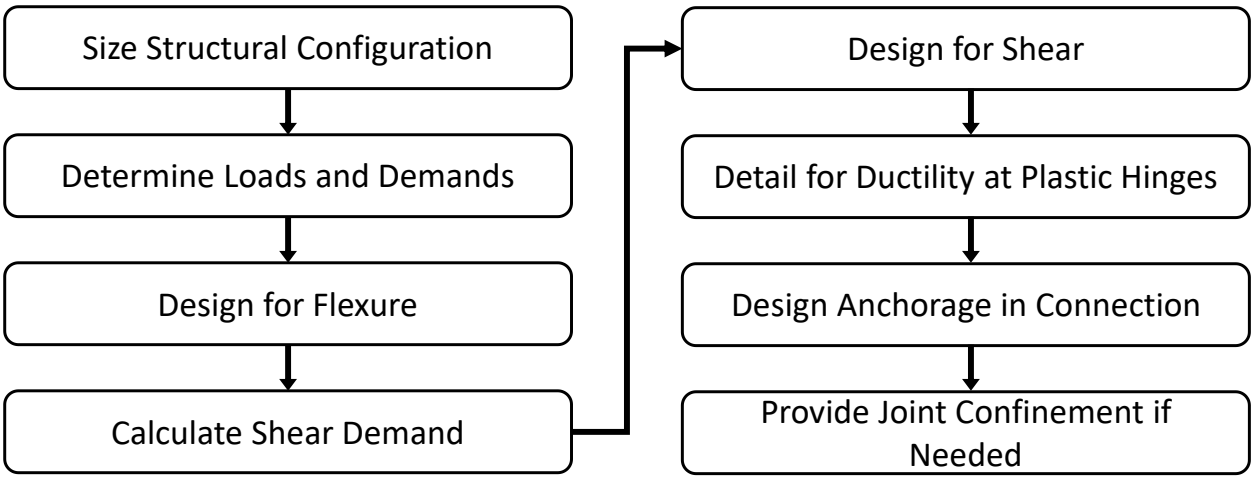

Figure 5-5 Recommended workflow for multi-column bents under vehicular collision

- **Size Structural Configuration:** Based on project requirements, establish the preliminary overall geometry of the multi-column bent, including column spacing, column dimensions, bent cap dimensions, clear height, girder load points, etc.

- **Determine Loads & Demands:** Determine governing load combinations per Extreme Event II. With a specified height of collision (h), column height (H), and equivalent static collision force (P), use plastic collapse mechanism analysis, detailed in Chapter 3, to identify the locations where plastic hinges are expected to form and calculate the required plastic moment capacity (M_p). Design charts for three-column bents and four-column bents refer to Figure 5-6. The design moment capacity must fall into the green region marked with "safe."

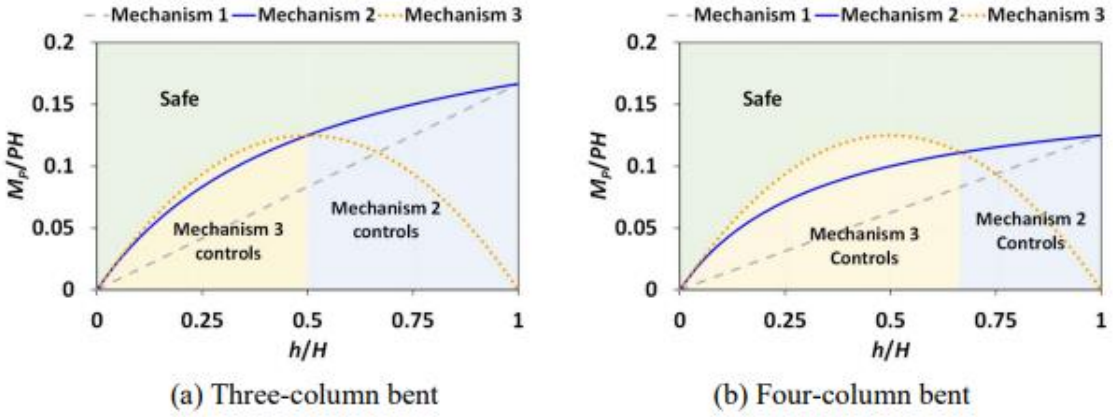

Figure 5-6 required plastic moment capacity for resisting lateral collision load

- **Design for Flexure:** Design the column's longitudinal reinforcement to provide a nominal flexural capacity (M_n) such that the design flexural strength (ϕM_n) is greater than or equal to the required plastic moment capacity (M_p) per AASHTO LRFD BDS 10th Article 5.6.3. The resistance factor ϕ can be taken as 1.0 for this extreme event.

- **Calculate Shear Demand:** Based on the column's nominal moment capacity (M_n), calculate the design shear demand (V_u) associated with the formation of plastic hinges at their flexural overstrength (ΩM_p) according to the free body diagrams in Figure 5-2(b). the overstrength factor Ω can be taken as 1.25.

- **Design for Shear:** Provide transverse reinforcement (spirals/ties) along the column such that the design shear strength (ϕV_n) is greater than or equal to the shear demand (V_u) per AASHTO LRFD BDS 10th Article 5.7.3.3. The resistance factor ϕ may be taken as 1.0 for the extreme limit state per AASHTO LRFD BDS 10th Article 1.3.2.1.

- **Detail Plastic Hinge Regions for Ductility:** At all identified plastic hinge locations, ensure the transverse reinforcement meets requirements for sufficient confinement to provide the necessary rotational ductility, as detailed in Section 5.3.2.1.

- **Design Anchorage in Connection:** Detail the anchorage of column longitudinal bars into the bent cap. The provided embedment length must be sufficient to fully develop the column reinforcing bars, as detailed in Section 5.3.2.2.

- **Provide Joint Confinement if needed:** If extra post-yield capacity and damage control are desired, provide transverse reinforcement within the joint region using hoops, as detailed in Section 5.3.2.3.

5.3.2. Design Parameters and Recommendations

5.3.2.1. Detail for Ductility at Plastic Hinges

For a plastic hinge to achieve its full rotational capacity, the concrete core within the hinge region must be adequately confined to prevent crushing and to restrain the longitudinal bars from buckling. Despite extreme events like vehicle collision are not seismic in nature, the mechanics of plastic hinging are identical. Therefore, the recommendations provided are based on the detailing provisions of **AASHTO LRFD Article 5.11.4.1.3 through Article 5.11.4.1.5**, summarized as follows:

- Potential plastic hinge regions near bent-to-column connections are recommended to extend from the face of the connections to a distance of the greater of:
    - the maximum cross-sectional dimension of the column or pile;

- one-sixth of the clear height of the column or pile; or
- 18.0 in.

- Potential plastic hinge regions at the bottom of pile bents shall be considered to extend from three pile diameters below to one pile diameter above the calculated point of maximum moment, but shall not extend less than 18.0 in. above the mud line.
- Potential plastic hinge regions near the collision point are recommended to extend above and below to a distance of the maximum cross-sectional dimension of the column.
- Over the length of plastic hinge regions near bent-to-column connections, transverse reinforcement is recommended to:
  - be sufficient to carry shear demand (V_u) determined from the last step;
  - have a volumetric ratio of spiral or hoop reinforcement per Eq.

$$\rho_s = \frac{4A_{sp}}{d_c s} \geq 0.12 \frac{f'_c}{f_{yh}} \qquad \textit{Equation (5-1)}$$

where:
A_{sp} = cross-sectional area of spiral or hoop (in.^{2})
d_c = core diameter of column measured to the outside of transverse reinforcement (in.)
s = pitch or vertical spacing of transverse reinforcement (in.)
f'_c = compressive strength of concrete for use in design (ksi)
f_{yh} = specified minimum yield strength of transverse reinforcement (ksi)

5.3.2.2. Column Longitudinal Bar Anchorage and Embedment

The ability of the bent-to-column connection to transfer moments is fundamental to the capacity design approach. This moment transfer is dependent on the proper anchorage and embedment of the column's longitudinal reinforcement into the bent cap. To ensure robust anchorage and full development of column longitudinal reinforcement, it is recommended to comply with the provisions of AASHTO LRFD Article 5.10.8.2.1. The experimental program in Chapter 4 observed that straight bars, hooked bars, and headed bars are all able to be fully developed as long as the embedment length in the connection is code-compliant. The development length is summarized as follows:

$$l_d = l_{db} \lambda_{rl} \lambda_{cf} \lambda_{rc} \qquad \textit{Equation (5-2)}$$

in which:

$$l_{db} = 0.17 d_b \left[\frac{f_y - \frac{F_h}{A_b}}{1.97 \lambda f'^{0.25}_c} \right]^2 \qquad \textit{Equation (5-3)}$$

where:

ℓ_{db} = basic development length (in.)
λ_{rl} = reinforcement location factor per AASHTO LRFD
λ_{cf} = coating factor per AASHTO LRFD
λ_{rc} = reinforcement confinement factor per AASHTO LRFD
d_b = nominal diameter of reinforcing bar or wire (in.)
f_y = specified minimum yield strength of reinforcement (ksi)
F_h = force developed by hooks or heads (kip), per AASHTO LRFD
A_b = nominal area of reinforcing bar or wire (in.^{2})
f'_c = compressive strength of concrete for use in design (ksi)
λ = concrete density modification factor per AASHTO LRFD
It should be noted that the excess reinforcement factor λ_{er} is not applicable in this case.

5.3.2.3. Column Connection Confinement and Shear Capacity Check

The experimental results from Chapter 4 demonstrated no compromise in connection integrity under high drift ratio despite not having additional joint confinement. Nevertheless, the experimental program also revealed benefits of adding joint confinement. Specimens with internal hoop reinforcement (S-SK-CIP-H2 and S-SK-CIP-H4) exhibited increased post-peak moment capacity and damage control to the joint. If extra post-peak capacity and damage control are desired, transverse reinforcement can be provided per **AASHTO LRFD Article 5.11.4.1**. Particularly, hoop reinforcement of at least No. 4 bars with spacing not greater than 4 in. can be provided and extended from the face into the connection by one-half the column's diameter but not less than 15 in. When precast bent caps are to be used, transverse reinforcement in the joint is not needed if the bent caps are following standard precast bent details (PPBC-RC).

5.4. Evaluation of Loss of a Column

While the capacity design procedure outlined above focuses primarily on the vehicle collision event, further evaluation is needed in case collision impact being overly severe or scouring being serious enough to cause a loss-of-column scenario. The methods detailed in Chapter 3, based on GSA guidelines, are recommended for evaluation.

Two primary methods are available:

1. **Linear Static Analysis (LSA):** This simplified, conservative method is suitable for preliminary design and evaluation. It involves analyzing the structure with the critical column removed and applying amplified extreme load combinations ($\Omega\Sigma Q_i$) to approximate the dynamic effects of the sudden column removal. The resulting amplified demands are then checked against the modified design flexural and shear capacities of the remaining members, expressed generally as:

$$\Omega \sum Q_i \geq m\phi R_n \qquad \textit{Equation (5-4)}$$

where: Ω is dynamic amplification factor, taken as 2.0;
Q_i is force effect
m is demand modification factor, taken as 3.0 for beam flexure and 1.0 for beam shear;
ϕ is resistance factor, taken as 0.9 for beam flexure and 1.0 for beam shear;
R_n is the nominal resistance of the member to examine.

2. **Nonlinear Dynamic Analysis (NDA):** This is a more sophisticated and accurate method suitable for final design verification. The analysis involves modeling the time-history response of the structure as the column's reactions are rapidly reduced to zero. This requires defining the nonlinear plastic hinge properties of the members to capture the inelastic deformation and energy dissipation, which is detailed in Chapter 3.

5.5. Column and Connection Detailing Example

This example demonstrates the application of the capacity-based plastic design procedure for a typical three-column bent subjected to a vehicular collision load.

Given:

- **Geometry:** Three-column bent with 36-in. (D) diameter columns spaced at 8 ft. Bent cap is 42 in. deep by 42 in. wide by 24 ft long. Clear column height (H) is 12 ft. Girder lines are spaced at 6.667 ft.
- **Load:** Girder reactions are assumed 180 kips each. AASHTO equivalent static collision force (P) is 600 kips, applied at a height (h) 5 ft.
- **Materials:** Concrete compressive strength (f'_c) is 4 ksi. Reinforcement yield strength (f_y) is 60 ksi.

Procedure:

Step 1: Size Structural Configuration

The structural configuration is given as shown in the figure below.

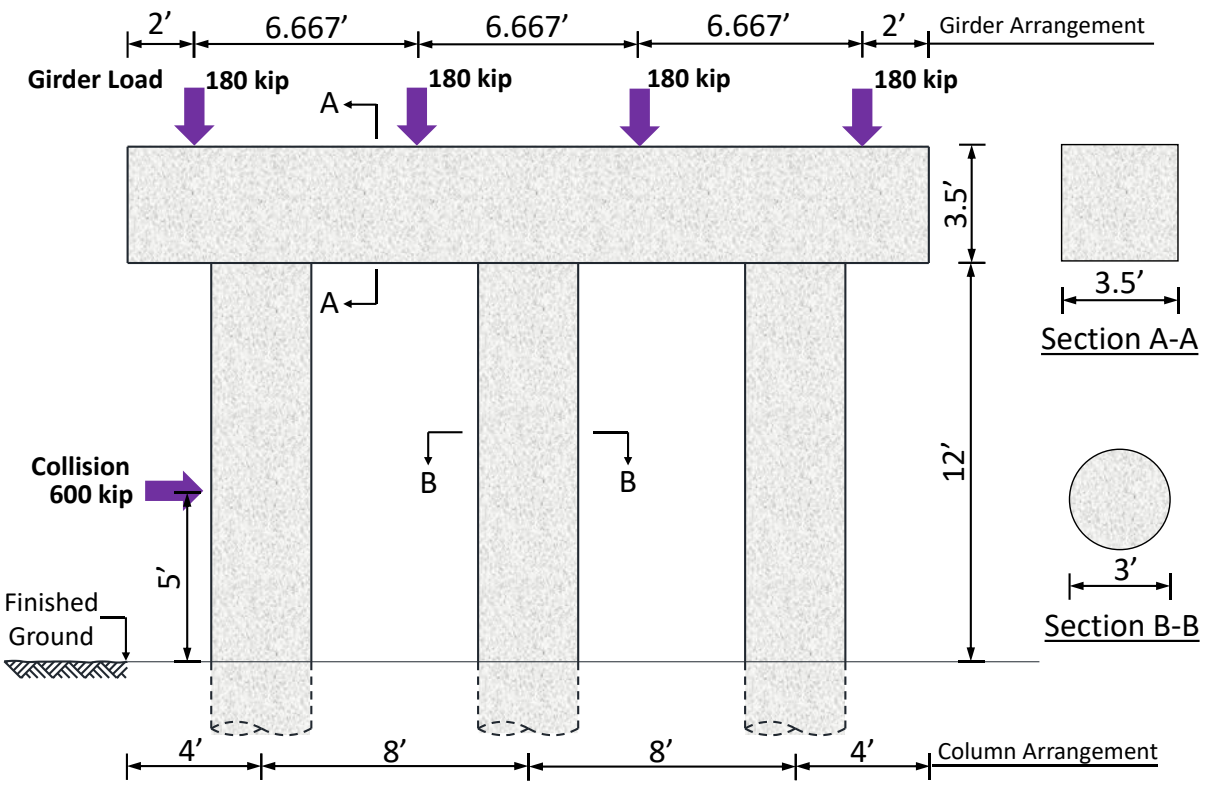

Step 2: Determine Loads & Flexural Demand (M_p)

A linear elastic structural analysis is performed first and it is found the column under collision is carrying an axial load of 281 kips.

The ratio of collision height to column height is h/H=5′/12′=0.417. Using the design chart for a three-column bent, a height ratio of 0.417 falls in the region where Mechanism 3 (single column collapse) controls. The required plastic moment capacity is calculated as

$$M_p \geq \left(\frac{Ph}{2}\right)\left(1-\frac{h}{H}\right) = \left(\frac{(600\text{kip})(5')}{2}\right)\left(1-\frac{5'}{12'}\right) = 875 \text{ kip-ft} = 10{,}500 \text{ kip-in.}$$

Step 3: Design for Flexure

The column section must provide a design flexural strength $\phi M_n \geq 10{,}500$ kip-in. Using column design charts for a 36-in. diameter column with an axial load of 281 kips, a reinforcement ratio of approximately ρ=1.0% is required. $A_{s,req}$ = (0.01)(π/4)(36 in.^{2})=10.18 in^2. Therefore, **select ten No. 9 bars** (A_s=10.0 in.^{2}).

The nominal capacity (ϕM_n) of this section is then determined to be (1.0)(11,112 kip-in), greater than the target (10500 kip-in.).

Step 4: Calculate Shear Demand (V_u)

The shear demand is based on the flexural overstrength, ΩM_n=1.25×11,150 kip-in.=13,890 kip-in. According to the free body diagram below, it can be determined that

- Segment above collision point (length = 144 in. − 60 in. = 84 in.): $V_{u,top}$ = 2(13,890 kip-in.)/(84 in.) = 331 kips
- Segment below collision point (length = 60 in.): $V_{u,bot}$ = 2(13,890 kip-in.)/(60 in.) = 463 kips

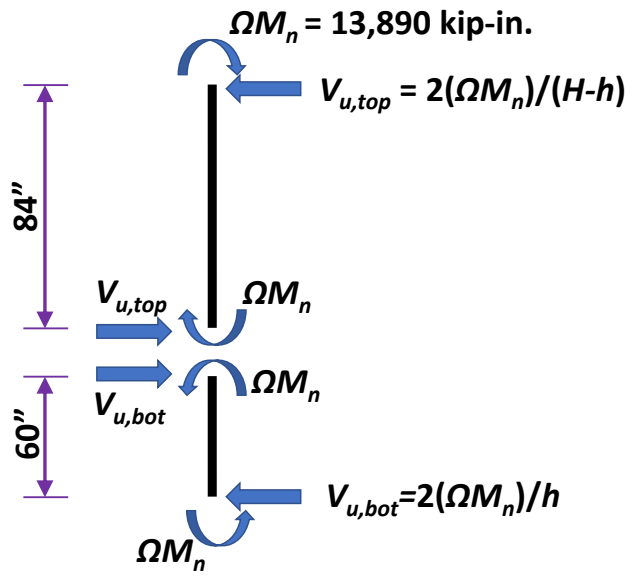

Step 5: Design for Shear

Design the transverse spiral reinforcement. Per AASHTO 5.7.3.3 (no prestress involved),

$$V_n = V_c + V_s$$

$$V_c = 0.0316\beta\lambda\sqrt{f'_c}b_v d_v$$

where:
λ = 1.0 (not light weigh concrete)
β = 2.0 (per AASHTO simplified method)
b_v = 36 in. (column diameter)
d_v = 0.9(D/2-D_r/π) = 24.1 in. (per AASHTO effective shear depth)

therefore, V_c = 0.0316(2.0)(1.0)($\sqrt{4}$ ksi)(36 in.)(24.1 in) = 109.7 kips. Required shear reinforce is therefore determined accordingly:

- For the top segment, $V_{s,req}$=V_u−ϕV_c = 331 kip − 109.7 kips = 221.3 kips. Required spacing for No. 5 spiral is

$$s \text{ (for top segment)} = \frac{A_v f_y d_v}{V_{s,req.}} = \frac{(2 \times 0.31 \text{ in.}^2)(60 \text{ ksi})(24.1 \text{ in.})}{221.3 \text{ kip}} = 4.05 \text{ in.}$$

Therefore, **use #5 spiral with 4-in. pitch.**

- For the bottom segment, $V_{s,req}=V_u-\phi V_c$ = 463 kips −109.7 kips=353.3 kips. Required spacing for No. 5 spiral is

$$s \text{ (for bottom segment)} = \frac{A_v f_y d_v}{V_{s,req.}} = \frac{(2 \times 0.31 \text{ in.}^2)(60 \text{ ksi})(24.1 \text{ in.})}{353.3 \text{ kip}} = 2.54 \text{ in.}$$

Therefore, **use #5 spiral with 2.5-in. pitch.**

Step 6: Detail Plastic Hinge Regions for Ductility

The plastic hinge length near the connection is the greater of *D*, *H*/6, and 18 in., which is 36 in.; near the ground is *D* (36 in.) above the mud line and 3*D* (108 in.) below the mud line; near the collision point is *D* (36 in.) above and below.

Check volumetric ratio for the 4-in. pitch:

$$\rho_s = \frac{4A_{sp}}{d_c s} = \frac{4(0.31 \text{ in.})}{(30 \text{ in.})(4 \text{ in.})} = 0.01$$

Required

$$\rho_{s,req} = 0.12 \frac{f'_c}{f_{yh}} = 0.12 \frac{4 \text{ ksi}}{60 \text{ ksi}} = 0.008$$

Provided reinforcement ratio (0.01) is greater than the required (0.008), so the confinement is adequate. No extra confining reinforcement is needed within the plastic regions.

Step 7: Design Anchorage in Connection

Per AASHTO Article 5.10.8.2.1, the development length for No. 9 bars is determined using

$$l_d = 0.17 d_b \left[\frac{f_y - \frac{F_h}{A_b}}{1.97 \lambda f'^{0.25}_c} \right]^2 \lambda_{rl} \lambda_{cf} \lambda_{rc}$$

$$= 0.17(1.128 \text{ in.})\left(\frac{60 \text{ ksi}}{1.97(1.0)(4^{0.25}\text{ksi})}\right)(1.0)(1.0)(0.3) = 26.7 \text{ in.}$$

Providing a TxDOT standard detail that extends the bars 33 inches into the bent cap is ample.

Final Design Summary:

- **Longitudinal Steel:** 10 - No. 9 bars.
- **Anchorage:** Use straight bars, extending 33 in. into the connection.
- **Joint Confinement:** No. 4 hoops at 4 in. spacing.
- **Top Plastic Hinge (36 in. below the connection):** No. 5 spiral at 4 in. pitch.
- **Bottom Plastic Hinge (36 in. above ground):** No. 5 spiral at 2.5 in. pitch.
- **Near Collision Point (36 in. above and below the collision point):** No. 5 spiral at 2.5 in. pitch.
- **Remaining Column Lengths:** No. 5 spiral at 4 in. pitch.

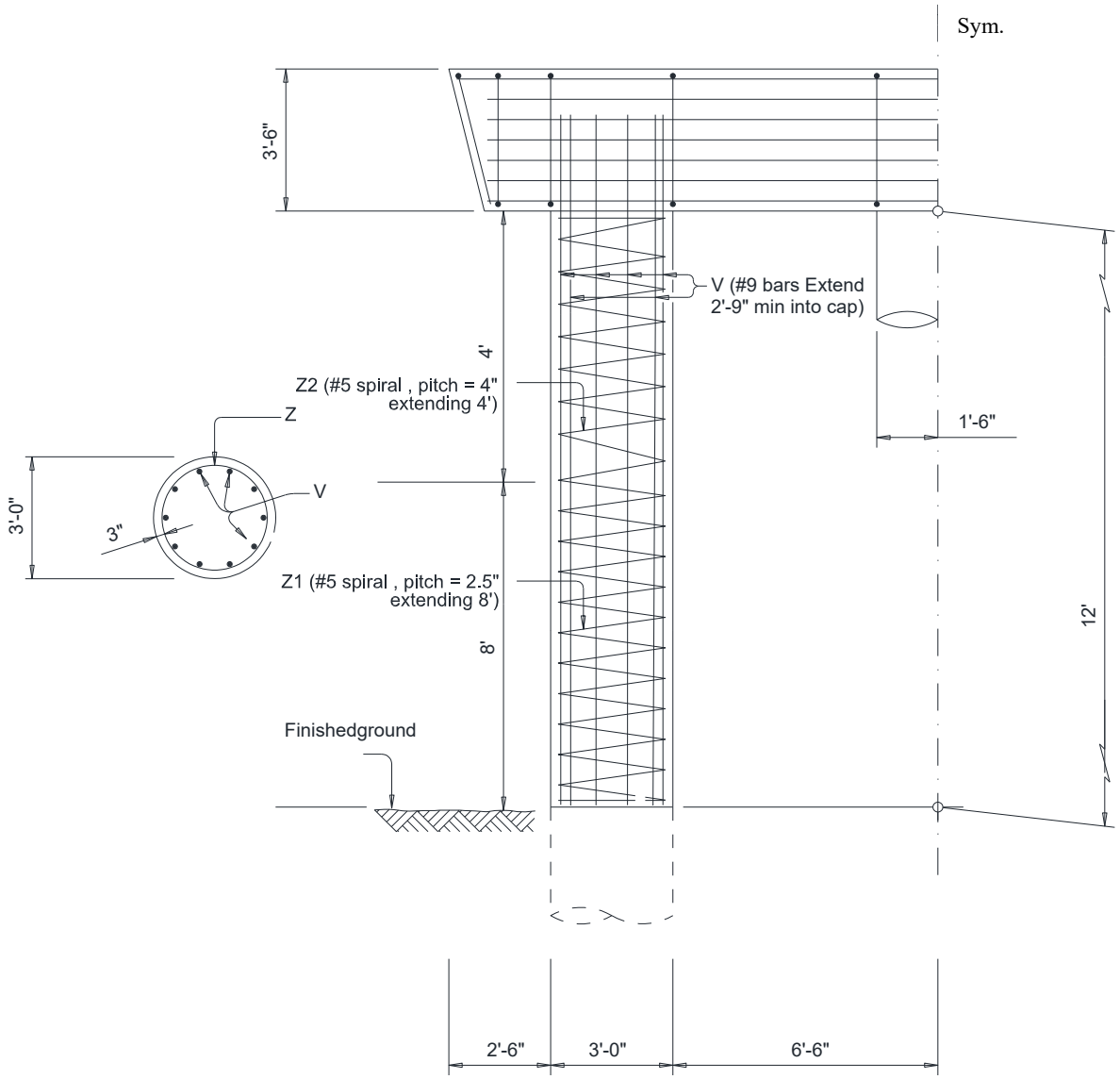

Chapter 6. Summary and Conclusion

This chapter summarizes the key findings of the research project and provides overall conclusions and recommendations for improving the design and detailing of bent-to-column joints in TxDOT bridge substructures. The research was motivated by the recognition that current standard bent-to-column joint details may be inadequate under extreme loading events and aimed to develop practical guidance for ensuring reliable and ductile joint performance. This research project was structured to build a comprehensive understanding of bent-to-column joint behavior, from fundamental principles to practical application.

Chapter 2 (Literature Review): A comprehensive review of existing literature confirmed that bent-to-column joints have traditionally been designed assuming primarily axial load transfer, without explicit consideration for the significant moment and shear demands that arise during extreme events like vehicular collisions or loss of a column. The review identified a critical need for a design philosophy focused on ductility. It also established the state-of-the-art in joint confinement techniques, reinforcement anchorage methods (straight, hooked, and headed bars), and potential retrofitting strategies, providing a foundation for the analytical and experimental work to follow.

Chapter 3 (Development of Bent-to-Column Joint Details): This phase of the research established the analytical framework for the project. Using plastic collapse mechanism analysis, it was demonstrated that multi-column bents rely on the formation of ductile plastic hinges to resist extreme lateral loads. A critical finding was that standard TxDOT bent details possess insufficient shear capacity to develop their full flexural overstrength, making them vulnerable to premature, brittle shear failure. Furthermore, analyses for a loss-of-column scenario confirmed that this event generates immense flexural and shear demands that can only be sustained through ductile, inelastic deformation of the remaining structure. This chapter established the clear analytical need for a capacity-based design approach.

Chapter 4 (Experimental Program and Finite Element Analysis): The experimental program, which included large-scale tests in both the in-plane and out-of-plane directions, provided physical validation for the analytical findings. For specimens loaded in-plane, all properly detailed connections resulted in a ductile, flexural failure in the column, validating the capacity design philosophy. Specimens loaded out-of-plane exhibited more complex behavior involving torsion of the bent cap, with precast specimens showing superior performance in controlling torsional damage compared to their cast-in-place counterparts. A key finding across all test configurations was that the connections successfully transferred moment and provided adequate anchorage for the column's longitudinal reinforcement to yield before joint failure. Current AASHTO LRFD provisions for reinforcement development length were found to be conservative. The experimental results were successfully replicated using nonlinear finite element models, validating them as a reliable tool for further analysis.

Chapter 5 (Design Guidelines): This chapter synthesizes all analytical and experimental findings into a practical, implementable design methodology. It formally presents the capacity-based plastic design philosophy, where ductile flexural yielding in plastic hinges is the intended mechanism, and all brittle failure modes (shear, anchorage) are protected. A step-by-step procedure was developed to guide engineers through the design process for vehicular collision, from initial sizing to final detailing. The chapter provides specific, evidence-based recommendations for key design parameters, including anchorage, joint confinement, and shear design based on flexural overstrength.

Chapter 7. Value of Research

The behavior of bent-to-column joints in reinforced concrete bridge substructures plays a critical role in ensuring the structural integrity of transportation infrastructure, especially during extreme events such as vehicular collisions, scour, and column loss. However, conventional TxDOT design practices have historically treated these joints as pinned, with minimal moment transfer, leading to a lack of mechanical detailing and a potential vulnerability during service and ultimate loading conditions. TxDOT Project 0-7113 addresses this gap by developing improved joint detailing strategies through a combination of analytical studies, full-scale experimental testing, and advanced finite element modeling. The outcomes of this project provide both qualitative advancements and economic benefits across multiple domains of bridge design and maintenance.

7.1. Qualitative Benefits

7.1.1. Full-Scale Experimental Validation

Thirteen full-scale bent-to-column specimens were tested under simulated collision-type loading to observe moment capacity, crack propagation, bar slip, and reinforcement strain development. The experimental matrix systematically varied anchorage types (straight, hooked, headed) and joint confinement, allowing for direct performance comparisons. These tests confirmed that even standard TxDOT joints could provide significant moment resistance. Modified connection details demonstrated comparable or better ductility and post-yield behavior.

7.1.2. Enhanced Design Clarity and Implementation Readiness

Based on experimental and computational findings, the research delivers step-by-step design procedures, reinforcement detailing guidelines, and a worked example for practical application. These outputs are compatible with AASHTO LRFD design principles and can be directly implemented into TxDOT design manuals. The findings reduce ambiguity for engineers, promote uniform application across projects, and support safe, capacity-based plastic design practices.

7.1.3. Improved Understanding of Anchorage and Confinement Requirements

The research critically evaluates current code-based development length equations and demonstrates their conservatism when applied to bent-to-column joints transferring moments. Finite element analyses calibrated to full-scale tests offer accurate predictions of development lengths and confinement effects.

7.2. Economic Benefits

7.2.1. Increased Structural Resilience

By preventing brittle failure modes and enabling controlled, ductile response during extreme loading events, the enhanced design strategies reduce the likelihood of catastrophic damage. This increases bridge survivability during vehicular collisions or loss-of-support scenarios, potentially avoiding costly repairs, emergency interventions, or total bridge replacement.

7.2.2. Material Optimization

The findings support the use of headed and hooked bars in place of extended straight bars, which require longer development lengths and may introduce construction challenges. Reducing development length through enhanced anchorage can lead to shorter bent caps, improved bar layout, and material savings during construction.

7.2.3. Reduced Life-Cycle Costs

Improved joint detailing not only enhances initial safety but also minimizes long-term deterioration risks. By controlling crack widths, limiting bar slip, and preventing joint degradation, the refined details contribute to longer service life and lower maintenance frequency, benefiting TxDOT's long-term asset management strategies.

References

AASHTO LRFD Bridge Design Specifications (2020), Washington, D.C., American Association of State Highway and Transportation Officials.

Abdelkarim, O. I., & ElGawady, M. A. (2017). Performance of bridge piers under vehicle collision. *Engineering Structures*, 140, 337-352.

ACI Committee 318 (2019). "ACI CODE-318-19: Building Code Requirements for Structural Concrete and Commentary." American Concrete Institute, Farmington Hills, Michigan.

Ajaam, A. H., Yasso, S., Darwin, D., O'Reilly, M., & Sperry, J. (2018). Anchorage strength of closely spaced hooked bars. *ACI Structural Journal*, 115(4), 1143-1152.

American Society of Civil Engineers (2014). "ASCE standard ASCE/SEI 41-13: American Society of Civil Engineers: seismic evaluation and retrofit of existing buildings." Reston, Virginia: American Society of Civil Engineers.

ASTM A978-18 (2018). "Standard Specification for Headed Steel Bars for Concrete Reinforcement." ASTM International.

Bae, S. and Bayrak, O. (2008). "Plastic hinge length of reinforced concrete columns". *ACI Structural Journal*, 105(3), 290-300.

Bentz, E. (2000). *Sectional analysis of reinforced concrete members*. University of Toronto, Toronto, ON, Canada.

Brantschen, F., Faria, D.M.V., Fernández Ruiz, M., & Muttoni, A. (2016). Bond behaviour of straight, hooked, U-shaped and headed bars in cracked concrete. *Structural Concrete*, 17, 799–810.

Brenes, F. J., Wood, S. L., & Kreger, M. E. (2006). *Anchorage requirements for grouted vertical-duct connectors in precast bent cap systems: A summary*. (Report No. 0-4176). Center For Transportation Research, Austin, TX.

Canadian Standards Association (2019). *A23.3:19 Design of Concrete Structures*.

CEB-FIP (2010). *fib Model Code for Concrete Structures 2010*.

Chen, G., Anderson, N., Luna, R., Stephenson, R., Engebawy, M., Silva, P., & Zoughi, R. (2005). *Experimental Study on Seismic Retrofit Techniques for Cap Beams, Columns and Their Connections of Highway Bridges* (No. UTC R89).

Chen, W.F. (2007). *Plasticity in Reinforced Concrete*. McGraw-Hill, New York.

Chun, S. C., Lee, S. H., Kang, T. H., Oh, B., & Wallace, J. W. (2007). Mechanical anchorage in exterior beam-column joints subjected to cyclic loading. *ACI Structural Journal*, 104(1), 102-113.

Cook, W. (2014). *Bridge failure rates, consequences, and predictive trends*. PhD dissertation, Utah State University.

David Maidment, et al. (2019). "Streamflow Measurement at TxDOT Bridges: Final Report." FHWA/TX-19/5-9054-01-1, Center for Transportation Research, The University of Texas at Austin.

Deng, Y. (2001). *Confinement of columns using headed bars*. Master's thesis, McGill University.

Fan, W., Shen, D., Huang, X., & Sun, Y. (2020). Reinforced concrete bridge structures under barge impacts: FE modeling, dynamic behaviors, and UHPFRC-based strengthening. *Ocean Engineering*, 216, 108116.

Fawaz, G., & Murcia-Delso, J. (2021). Three-dimensional finite element modeling of RC columns subjected to cyclic lateral loading. *Engineering Structures*, 239, 112291.

Gallegos, D., & McPhee, M. (2007). *Two truckers die in fiery I-70 crash*.

General Services Administration (2013). "Alternate Path Analysis & Design Guidelines for Progressive Collapse Resistance." Washington, D.C.

Gergely, J., Pantelides, C. P., & Reaveley, L. D. (2000). Shear strengthening of RCT-joints using CFRP composites. *Journal of composites for construction*, 4(2), 56-64.

Ghimire, K. P., Shao, Y., Darwin, D., & O'Reilly, M. (2019). Conventional and High-Strength Headed Bars—Part 1: Anchorage Tests. *ACI Structural Journal*, 116(3), 255-264.

Hamad, B. S., Jirsa, J. O., & De Paulo, N. D. A. (1993). Anchorage strength of epoxy-coated hooked bars. *Structural Journal*, 90(2), 210-217.

Hanson, N. W., & Connor, H. W. (1967). Seismic resistance of reinforced concrete beam-column joints. *Journal of the Structural Division*, 93(5), 533-560.

Haroun, M. A., Pardoen, G. C., Shepherd, R., Haggag, H. A., and Kazanjy, R. P. (1994). *Assessment of Cross-Tie Performance in Bridge Pier Walls*. Final Report to the California Department of Transportation.

Heng, K., Li, R., Li, Z., & Wu, H. (2021). Dynamic responses of highway bridge subjected to heavy truck impact. *Engineering structures*, 232, 111828.

Hoshikuma, J., Kawashima, K., Nagaya, K., & Taylor, A. W. (1997). Stress-strain model for confined reinforced concrete in bridge piers. *Journal of Structural Engineering*, 123(5), 624-633.

Hwang, S.J., Lee, H.J., Liao, T.F., Wang, K.C., & Tsai, H.H. (2005). Role of hoops on shear strength of reinforced concrete beam-column joints. *ACI structural journal*, 102(3), 445.

Ingham, J. M., Priestley, M. J. N., & Seible, F. (1998). Cyclic response of bridge knee joints with circular columns. *Journal of Earthquake Engineering*, 2(3), 357-390.

Jirsa, J. O., & Marques, J. L. G. (1975). A study of hooked bar anchorages in beam-column joints. *ACI Journal Proceedings*, 72(5), 210-217.

Joen, P. H., & Park, R. (1990). Simulated seismic load tests on prestressed concrete piles and pile-pile cap connection. *PCI Journal*, 35(6), 42-61.

Kang, T. H. K., Ha, S. S., & Choi, D. U. (2010). Bar Pullout Tests and Seismic Tests of Small-Headed Bars in Beam-Column Joints. *ACI Structural Journal*, 107(1), 32-42.

Kang, T. H. K., Kim, W., & Shin, M. (2012). Cyclic testing for seismic design guide of beam-column joints with closely spaced headed bars. *Journal of Earthquake Engineering*, 16(2), 211-230.

Karayannis, C. G., Chalioris, C. E., & Sirkelis, G. M. (2008). Local retrofit of exterior RC beam–column joints using thin RC jackets—An experimental study. *Earthquake Engineering & Structural Dynamics*, 37(5), 727-746.

Klein, G. J. (2008). Curved-bar nodes. *Concrete international*, 30(9), 42-47.

Klinga, J. V., & Alipour, A. (2015). Assessment of structural integrity of bridges under extreme scour conditions. *Engineering Structures*, 82, 55-71.

Larosche, A., Cukrov, M., Sanders, D., & Ziehl, P. (2014). Prestressed pile to bent cap connections: Seismic performance of a full-scale three-pile specimen. *Journal of Bridge Engineering*, 19(3), 04013012.

Lowes, L. N., & Moehle, J. P. (1995). *Seismic behavior and retrofit of older reinforced concrete bridge T-Joints* (No. UCB/EERC-95/09).

Lubiewski, M. C., Silva, P. F., & Chen, G. (2006). Retrofit of column-bent cap connections of Alaska bridges for seismic loadings: damage evaluation. *Structures Congress 2006: Structural Engineering and Public Safety* (pp. 1-13).

Mander, J. B., Dutta, A. & Goel, P. (1998). "Capacity Design of Bridge Piers and the Analysis of Overstrength." Technical Report MCEER-98-0003, State University of New York at Buffalo.

Matsumoto, E. E., Waggoner, M. C., Sumen, G., Kreger, M. E., Wood, S. L., & Breen, J. E. (2001). *Development of a precast bent cap system* (No. Report no. RR-1748-2). University of Texas at Austin, Center for Transportation Research.

McGuire, W., Gallagher, R. H., & Ziemian, R. D. (2000). *Matrix structural analysis*. New York: John Wiley.

McLean, D. I., & Shattarat, N. K. (2005). *Seismic Behavior and Retrofit of Bridge Knee Joint Systems* (No. WA-RD 601.1). Washington State Department of Transportation.

Naito, C. J., Moehle, J. P., & Mosalam, K. M. (2001). *Experimental and Computational Evaluation of Reinforced Concrete Bridge Beam-Column Connections for Seismic Performance*. Berkeley: Pacific Earthquake Engineering Research Center.

Orangun, C. O., Jirsa, J. O., & Breen, J. E. (1977). A reevaluation of test data on development length and splices. *ACI Journal Proceedings*, 74(3), 114-122.

Pantelides, C. P., Gergely, J., & Reaveley, L. D. (2001). In-situ verification of rehabilitation and repair of reinforced concrete bridge bents under simulated seismic loads. *Earthquake Spectra*, 17(3), 507–530.

Papadopoulos, V., Murcia-Delso, J., & Shing, P. B. (2018). Development of Headed Bars in Slab-Column Joints of Reinforced Concrete Slab Bridges. *ACI Structural Journal*, 115(5), 1393-1406.

Park, H. K., Yoon, Y. S., & Kim, Y. H. (2003). The effect of head plate details on the pull-out behaviour of headed bars. *Magazine of Concrete Research*, 55(6), 485-496.

Pinc, R. L., Watkins, M. D., & Jirsa, J. O. (1977). *Strength of hooked bar anchorages in beam-column joints*. Civil Engineering Structures Research Laboratory, the University of Texas at Austin.

Priestley, M. J. N., Seible, F., & Calvi, G. M. (1996). *Seismic design and retrofit of bridges*. New York: Wiley.

Roeder, C.W., Graff, R., Soderstrom, J.L., & Yoo, J.H. (2001). *Seismic Performance of Pile-Wharf Connections*. Pacific Earthquake Engineering Research Center, University of California, Berkeley.

Shang, Y., Alipour, A., & Ye, A. (2018). Selection of input motion for seismic analysis of scoured pile-supported bridge with simplified models. *Journal of Structural Engineering*, 144(8), 04018099.

Silva, P. F., Ereckson, N. J., & Chen, G. D. (2007). Seismic retrofit of bridge joints in central US with carbon fiber-reinforced polymer composites. *ACI structural journal*, 104(2), 204-207.

Speicher, M. S., & Harris, J. L. III (2018). "Collapse Prevention seismic performance assessment of new buckling restrained braced frames using ASCE 41." *Engineering Structures*, Vol 164, pp. 274-289.

Sperry, J., Darwin, D., O'Reilly, M., Lequesne, R., Yasso, S., Matamoros, A., Feldman, L., & Lepage, A. (2017). Conventional and High-Strength Hooked Bars—Part 2: Data Analysis. *ACI Structural Journal*, 114(1), 267-276.

Sperry, J., Yasso, S., Searle, N., DeRubeis, M., Darwin, D., O'Reilly, M., Matamoros, A., Feldman, L., Lepage, A., Lequesne, R., & Ajaam, A. (2017). Conventional and High-Strength Hooked Bars—Part 1: Anchorage Tests. *ACI Structural Journal*, 114(1), 255-266.

Sritharan, S. (2005). Strut-and-tie analysis of bridge tee joints subjected to seismic actions. *Journal of Structural Engineering*, 131(9), 1321-1333.

Sritharan, S., Priestley, M. N., & Seible, F. (1999). Enhancing seismic performance of bridge cap beam-to-column joints using prestressing. *PCI journal*, 44(4), 74-91.

Sritharan, S., Priestley, M. N., & Seible, F. (2001). Seismic design and experimental verification of concrete multiple column bridge bents. *Structural Journal*, 98(3), 335-346.

Thewalt, C. R., & Stojadinović, B. (1995). Behavior of bridge outrigger knee joint systems. *Earthquake Spectra*, 11(3), 477-509.

TxDOT (2020). "Bridge Design Manual." Texas Department of Transportation.

TxDOT (2018). "Bridge Detailing Guide." Texas Department of Transportation.

Vasseghi, A., Soltani, M., & Bahrani, M. K. (2015). Seismic retrofit of a typical reinforced concrete bridge bent in Iran. *Scientia Iranica*, 22(4), 1402-1410.

Wang, H.C., Williams, C.S., & Klein, G.J. (2020). Effect of Bend Radius of Reinforcing Bars on Knee Joints under Closing Moments. *ACI Structural Journal*, 117(5), 315-326.

Wardhana, K., & Hadipriono, F. C. (2003). Analysis of recent bridge failures in the United States. *Journal of performance of constructed facilities*, 17(3), 144-150.

Wight, J.K. and MacGregor, J.G. (2012). *Reinforced Concrete: Mechanics and Design*. Pearson Education, Inc., Upper Saddle River, New Jersey.

Williams, C., Deschenes, D., & Bayrak, O. (2012). *Strut-and-tie model design examples for bridges* (No. FHWA/TX-12/5-5253-01-1). University of Texas at Austin, Center for Transportation Research.

Willis, L. K. (1975). *Bent cap program user manual*. Bridge Division Texas Highway.

Wright, T., DesRoches, R., & Padgett, J. E. (2011). Bridge seismic retrofitting practices in the central and southeastern United States. *Journal of Bridge Engineering*, 16(1), 82-92.

Wu, M., Jin, L., & Du, X. (2020). Dynamic responses and reliability analysis of bridge double-column under vehicle collision. *Engineering structures*, 221, 111035.

Zaborac, J., & Bayrak, O. (2023). Unified approach for reinforcement development length using the partly cracked elastic stage for bond strength. *Structural Concrete*, 24, 2528–2546.

Zhao, X., Wu, Y.F., Leung, A.Y., & Lam, H.F. (2011). "Plastic Hinge Length in Reinforced Concrete Flexural Members." In *Procedia Engineering*, Vol. 14, pp. 1266-1274.

Appendix A. Draft Specifications and Example Details

Draft Specifications for TxDOT Bridge Design Manual

Proposed changes in Rectangular Reinforced Concrete Caps

The following provisions are proposed for inclusion in Chapter 4 Section 4 of the TxDOT Bridge Design Manual to address the design of rectangular reinforced concrete bent caps for the extreme event limit state of loss-of-a-column scenario.

Loss of a Column

An analysis for loss-of-a-column scenarios shall be considered for bents where columns are at an elevated risk of removal, such as from scour or vehicular/vessel collision. Refer to the *Bridge Design Guidelines* for the required analysis procedure.

The bent cap, with one of the exterior columns removed, shall be analyzed for amplified loads. The amplified demands on the remaining components shall not exceed their modified design capacities, expressed as follows:

$$\Omega \sum \gamma_i Q_i \leq m\phi R_n$$

where: Ω is dynamic amplification factor, taken as 2.0;

γ_i is load factor per Extreme Event II or per project's needs.

Q_i is force effect

m is demand modification factor, taken as 3.0 for beam flexure and 1.0 for beam shear;

ϕ is resistance factor, taken as 0.9 for beam flexure and 1.0 for beam shear;

R_n is the nominal resistance of the member under consideration.

A more sophisticated nonlinear dynamic analysis is permitted to obtain the response of the bent cap under loss-of-a-column scenarios**.** A time-history analysis shall be performed simulating the instantaneous removal of the column's support reactions, assuming nonlinear behavior of the remaining elements. It is required to check all the remaining elements do not exhaust their ductility nor experience brittle failure.

Proposed changes in Columns for Multi-Column Bents

The following provisions are proposed for inclusion in Chapter 4 Section 7 of the TxDOT Bridge Design Manual and TxDOT Design Guidelines to address the design of columns in multi-column bents for the extreme event limit state of vehicular collision.

Chapter 4 Section 7 of the TxDOT Bridge Design Manual

Vehicular Collision

When the design choice is to redirect the collision load, follow the requirements given in Chapter 2 - Limit States and Loads. When the design choice is to provide structural resistance, design for the 600-kip equivalent static load as described in Chapter 2 - Limit States and Loads, Section 2 - Loads.

Design the column to withstand the collision force in shear and flexure. Consider the transfer of this force to the other elements such as bent caps, footings, piles, or drilled shafts. Utilize capacity-based plastic design principles. Design all the structural elements for collision forces. Consider the soil response when determining the boundary conditions (i.e. depth to fixity). Neglect the collision load when determining the lateral and bearing pressures for foundation design.

The design shall ensure the formation of ductile plastic hinges in the columns. All non-ductile failure modes, including shear failure and anchorage failure, shall be prevented. The prevention of shear failure shall be achieved by designing the corresponding components to resist the forces generated by the flexural overstrength of the plastic hinges. The prevention of anchorage failure shall be achieved by providing sufficient embedment length into the bent cap according to AASHTO.

Transverse reinforcement shall be provided in the bent-to-column connection extending from the column face through a distance per AASHTO. This joint confinement reinforcement shall consist of closed hoops or spirals of at least No. 4 bars at a maximum spacing of 4 inches. When precast bent caps are to be used, transverse reinforcement in the connections is not needed if the bent caps are following standard precast bent details (PPBC-RC).

Transverse reinforcement within designated plastic hinge regions in columns shall satisfy the requirements of AASHTO for plastic hinges. Plastic hinge length shall be determined according to AASHTO.

Use of a vehicular deflection wall between the columns is permitted if necessary. Design vehicular deflection wall assembly (columns plus wall) for the 600-kip equivalent static load as described in Chapter 2 - Limit States and Loads, Section 2 - Loads.

No further analysis is required for columns with a gross cross-sectional area no less than 40 sq. ft., a minimum thickness of 5 ft. and column transverse reinforcement is composed of at least No. 4 ties at 12 in. maximum spacing or a No. 4 spiral at 9 in. maximum pitch.

Chapter 4 Section 10 of the TxDOT Bridge Design Guidelines

Structural Analysis

For typical bridges only:

- For analysis, the designer should consider predicted scour when determining column heights.
- Moments can be magnified to account for slenderness (P-delta) effects by using <Article 5.6.4.3> or other analytical methods. <Article 5.6.4.3> is typically considered highly conservative.
- Column size may change within the bent height, producing a multi-tiered bent. Consider multi-columns bent tiers with web walls to be braced in the transverse direction. Column capacity in the longitudinal direction is not affected by the web wall.
- For multi-tier bents with square or round columns separated by tie beams, analyze as a frame, and magnify transverse and longitudinal moments separately.
- Design and model single-tier bent columns without a tie beam or web wall as individual columns with bottom conditions fixed against rotation and deflection at the location of fixity. The top-of-column should be modeled consistent with the detailing of the cap to column connection.
- In most cases, it can be assumed when determining fixity conditions for loads that columns on single drilled shafts are fixed at three shaft diameters but not less than 10 ft. below the top of the shaft. This should always be reviewed by a Geotechnical Engineer to evaluate and determine the fixity condition.
- Refine designs by limiting longitudinal deflections to the maximum movement allowed due to joint closure.
- For multi-column bent design choice to provide structural resistance, capacity-based plastic design method may be used, referring to Appendix D.

Draft Appendix D of the TxDOT Bridge Design Guidelines

Appendix D: Capacity-Based Plastic Design Method for Vehicular Collision

Section 1 – Overview

This appendix outlines the recommended procedure for designing columns for multi-column bents to resist vehicular collision forces using a capacity-based plastic design approach. This method is intended for the Extreme Event II limit state and represents a shift from traditional elastic analysis to a design philosophy that relies on the ductile behavior of the structure.

The fundamental principle is to design the bent, especially the columns and connections, to form a predictable plastic collapse mechanism, allowing it to dissipate the significant energy from a collision through ductile flexural yielding in designated plastic hinges. To ensure this ductile behavior, the procedure employs capacity design principles, meaning that all non-ductile (brittle) failure modes, such as shear and anchorage failure, are protected by providing them with a higher capacity than the maximum forces that can be generated by the flexural strength of the plastic hinges.

This procedure, shown below, ensures that in the event of a design-level collision, the structure will respond in a ductile manner, preventing catastrophic collapse and enhancing the overall safety and robustness of the bridge.

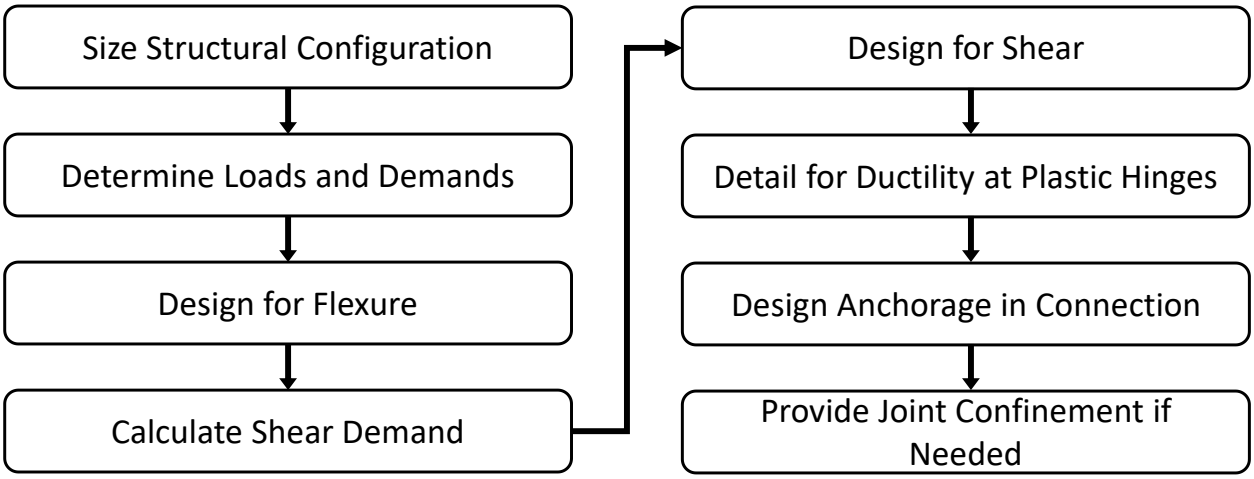

Criteria for Use of the Method

- The bent should be a multi-column bent with a rectangular bent cap and round columns.
- The grade of reinforcing bars should be Grade 60.
- Other relevant AASHTO provisions apply.

Section 2 – Procedure

Step 1: Size Structural Configuration
Based on project requirements, establish the preliminary overall geometry of the multi-column bent, including column spacing, column dimensions, bent cap dimensions, clear height, girder load points, and etc.

Step 2: Determine Loads & Flexural Demand
Determine governing load combinations per Extreme Event II. For the specified number of columns (n), collision height (h), clear column height (H), and equivalent static collision force (P), use plastic collapse mechanism analysis to determine the required plastic moment capacity, M_p. per Equation D-1. Otherwise, the design charts for three-column and four-column bents can be used to determine the controlling mechanism and the required moment capacity. The calculated point (h/H, M_p/PH) must fall within the "Safe" region.

$$M_p \geq \max\left\{\left(\frac{Ph}{2n}\right), \left[\frac{Ph}{2+2(n-1)(h/H)}\right], \left(\frac{Ph}{2}\right)\left(1-\frac{h}{H}\right)\right\} \quad \text{(D-1)}$$

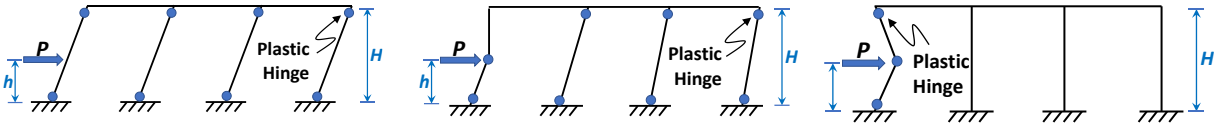

(a) Mechanism 1 (b) Mechanism 2 (c) Mechanism 3

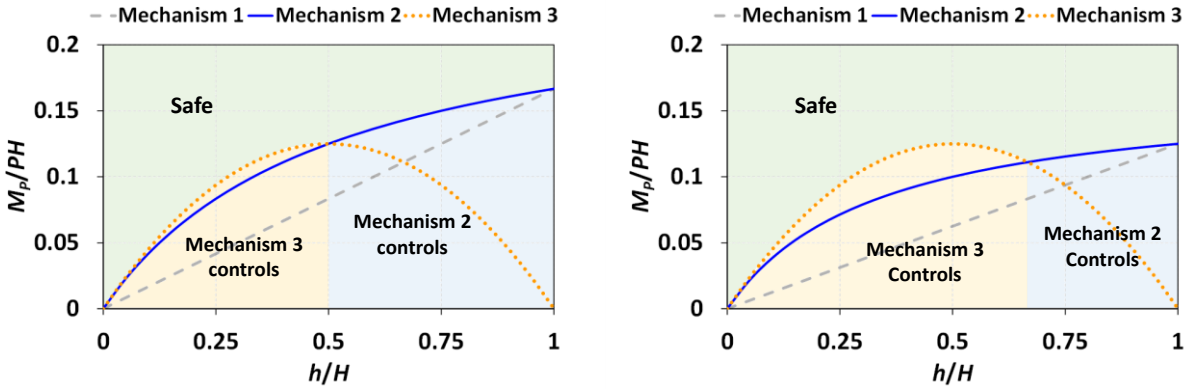

(a) Three-column bent (b) Four-column bent

Step 3: Design for Flexure

Design the column's longitudinal reinforcement to provide a nominal flexural capacity (M_n) such that the design flexural strength (ϕM_n) is greater than or equal to the required plastic moment capacity (M_p) determined in Step 2. The resistance factor, ϕ, may be taken as 1.0 for this extreme event.

Step 4: Calculate Shear Demand (V_u)

Based on the column's nominal flexural capacity (M_n) from Step 3, calculate the design shear demand (V_u) for both the top portion and the bottom that would be generated by the formation of plastic hinges at their flexural overstrength. The overstrength moment is calculated as ΩM_n, where the overstrength factor, Ω, is taken as 1.25. The shear demand is calculated using the free-body diagram for a rigid connection, as shown below.

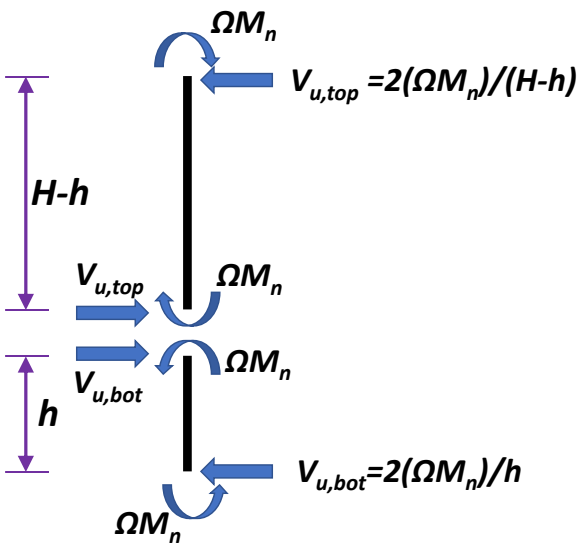

Step 5: Design for Shear

Provide transverse reinforcement (spirals or ties) along the column such that the design shear strength (ϕV_n) is greater than or equal to the shear demand (V_u) calculated in Step 4. The determination of V_n shall follow AASHTO LRFD Article 5.7.3.3, and the resistance factor, ϕ, may be taken as 1.0 for shear in the extreme event limit state.

Step 6: Detail Plastic Hinge Regions for Ductility

At all locations where plastic hinges are expected to form (typically top and bottom of the column, and at the collision point), the transverse reinforcement must meet the confinement requirements to ensure the required rotational ductility, summarized as follows.

- Potential plastic hinge regions near bent-to-column connections are recommended to extend from the face of the connections to a distance of the greater of:
    - the maximum cross-sectional dimension of the column or pile;
    - one-sixth of the clear height of the column; or
    - 18.0 in.
- Potential plastic hinge regions at the bottom of pile bents shall be considered to extend from three pile diameters below to one pile diameter above the calculated point of maximum moment, but shall not extend less than 18.0 in. above the mud line.
- Potential plastic hinge regions near the collision point are recommended to extend above and below to a distance of the maximum cross-sectional dimension of the column.
- Over the length of plastic hinge regions near bent-to-column connections, transverse reinforcement is recommended to:
    - be sufficient to carry shear demand (V_u) determined from the last step;
    - have a volumetric ratio of spiral or hoop reinforcement per Equation D-2

$$\rho_s = \frac{4A_{sp}}{d_c s} \geq 0.12 \frac{f'_c}{f_{yh}} \quad \text{(D-2)}$$

where

A_{sp} = cross-sectional area of spiral or hoop (in.^{2})

d_c = core diameter of column measured to the outside of transverse reinforcement (in.)

s = pitch or vertical spacing of transverse reinforcement (in.)

f'_c = compressive strength of concrete for use in design (ksi)

f_{yh} = specified minimum yield strength of transverse reinforcement (ksi)

Step 7: Design Anchorage in Connection

Detail the anchorage and embedment length of the column longitudinal bars into the bent cap. The provided embedment length must be sufficient to fully develop the bars, calculated in accordance Equations D-3 and D-4, based on AASHTO LRFD Article 5.10.8.2.1. Note that the excess reinforcement factor λ_{er} is not applicable in and not shown this case.

$$l_d = l_{db} \lambda_{rl} \lambda_{cf} \lambda_{rc} \quad \text{(D-3)}$$

in which:

$$l_{db} = 0.17 d_b \left[\frac{f_y - \frac{F_h}{A_b}}{1.97 \lambda f'^{0.25}_c} \right]^2 \quad \text{(D-4)}$$

where:

ℓ_{db} = basic development length (in.)

λ_{rl} = reinforcement location factor per AASHTO LRFD

λ_{cf} = coating factor per AASHTO LRFD

λ_{rc} = reinforcement confinement factor per AASHTO LRFD

d_b = nominal diameter of reinforcing bar or wire (in.)

f_y = specified minimum yield strength of reinforcement (ksi)

F_h = force developed by hooks or heads (kip), per AASHTO LRFD

A_b = nominal area of reinforcing bar or wire (in.^{2})

f'_c = compressive strength of concrete for use in design (ksi)

λ = concrete density modification factor per AASHTO LRFD

Step 8: Provide Joint Confinement if Needed

When extra post-yield capacity and damage control are desired, provide transverse confinement reinforcement from the face into bent-to-column connection by one-half the column's diameter but not less than 15 in. This reinforcement shall consist of at least No. 4 closed hoops or spirals with a spacing or pitch not greater than 4 in.